



Offshore Vertical Axis Wind Turbine with Floating and Rotating Foundation

Vita, Luca; Friis Pedersen, Troels; Aagaard Madsen, Helge

Publication date:
2011

Document Version
Publisher's PDF, also known as Version of record

[Link back to DTU Orbit](#)

Citation (APA):

Vita, L., Friis Pedersen, T., & Aagaard Madsen, H. (2011). Offshore Vertical Axis Wind Turbine with Floating and Rotating Foundation. Kgs. Lyngby, Denmark: Technical University of Denmark (DTU).

DTU Library

Technical Information Center of Denmark

General rights

Copyright and moral rights for the publications made accessible in the public portal are retained by the authors and/or other copyright owners and it is a condition of accessing publications that users recognise and abide by the legal requirements associated with these rights.

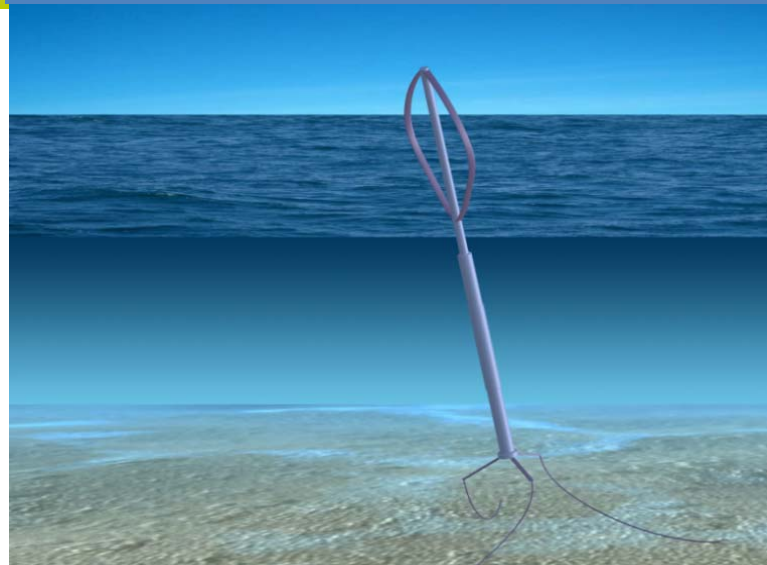
- Users may download and print one copy of any publication from the public portal for the purpose of private study or research.
- You may not further distribute the material or use it for any profit-making activity or commercial gain
- You may freely distribute the URL identifying the publication in the public portal

If you believe that this document breaches copyright please contact us providing details, and we will remove access to the work immediately and investigate your claim.

Offshore Floating Vertical Axis Wind Turbines with Rotating Platform

Risø-PhD-Report

Luca Vita
Risø-PhD-80(EN)
August 2011



Author: Vita, Luca
Title: Offshore floating Vertical Axis Wind Turbines with Rotating Platform
Division: Wind Energy Division

The fast growth of the wind energy market has increased the strategic importance of offshore wind energy, addressing the need for new offshore wind turbine concepts.

This work deals with a new offshore floating wind turbine concept, using a Vertical Axis Wind Turbine (VAWT) as rotor and a floating rotating platform as foundation. My research investigates the feasibility and the potentials of the concept.

The first step of my research is the study of the loads acting on the floating VAWT. Since the platform is rotating, a water stream generates a hydrodynamic force on the structure, known as Magnus effect. Also a friction moment acts on the platform. A CFD investigation is carried out to find out the non dimensional force coefficients at different rotational speeds of the platform.

The second step is to adapt a numerical solver, to carry out a numerical simulation of the concept. I used the software HAWC2 from Risø DTU and I added some DLLs to make it capable of investigating a floating VAWT.

I design the new concept for three different sizes:

- A 2MW size, mostly used during the code adaptation process to evaluate the code.
- A 5MW size, which I selected as the proper size for a baseline model.
- A 1kW size, which I designed as a downscaled model to use for experimental test verifications.

The last step of my investigation is a rough estimation of the economical potentials of the new concept, compared to an offshore floating HAWT concept.

(The thesis is submitted to the Danish Technical University in partial fulfilment of the requirements for the PhD degree)

Risø-PhD-80(EN)
August 2011

ISSN 0106-2840
ISBN
978-87-550-3924-7

Contract no.:

Group's own reg. no.:
1125007-01

Sponsorship:
Wind Energy Department and
DeepWind fp7 European Project

Cover :
Artistic view of the DeepWind
concept.

Pages:164
References:

Information Service Department
Risø National Laboratory for
Sustainable Energy
Technical University of Denmark
P.O.Box 49
DK-4000 Roskilde
Denmark
Telephone +45 46774005
bibl@risoe.dtu.dk
Fax +45 46774013
www.risoe.dtu.dk

Contents

CONTENTS	III
ACKNOWLEDGMENTS	VI
PREFACE	VII
NOMENCLATURE	VIII
1 INTRODUCTION	1
1.1 OBJECTIVES	1
1.2 STATE OF THE ART	1
1.2.1 <i>Background: wind power offshore market</i>	1
1.2.2 <i>Brief history of VAWT and floating wind turbines</i>	2
1.2.3 <i>Numerical tools for floating VAWTs</i>	9
1.3 THESIS OUTLINE	10
1.4 DESIGN APPROACH.....	12
2 DEEPWIND CONCEPT	16
2.1 MAIN CONCEPT DESCRIPTION	16
2.2 COMPONENTS.....	16
2.2.1 <i>Rotor</i>	16
2.2.2 <i>Blades</i>	17
2.2.3 <i>Generator</i>	17
2.2.4 <i>Anchoring</i>	18
2.2.5 <i>Safety system</i>	18
2.2.6 <i>Control strategy</i>	19
2.3 STRATEGIES FOR INSTALLATION AND OPERATION AND MAINTENANCE	19
2.3.1 <i>Installation</i>	19
2.3.2 <i>Operation and Maintenance (O&M)</i>	19
2.4 CONCEPT POTENTIALS.....	20
2.5 SPECIFIC CHALLENGES	20
2.6 METHODOLOGY FOR THE INVESTIGATION OF THE CONCEPT AND AVAILABLE CONFIGURATIONS...	21
2.6.1 <i>First Configuration (Sea bed configuration)</i>	21
2.6.2 <i>Second Configuration (Torque arm fixed configuration)</i>	22
2.6.3 <i>Third Configuration (Mooring fixed configuration)</i>	22
2.7 PROGRESS BEYOND THE VAWT STATE OF THE ART	22
3 LOADS AND DYNAMICS OF A FLOATING VERTICAL AXIS WIND TURBINE	24
3.1 FORMULATION OF THE PROBLEM	24
3.2 AERODYNAMIC LOADS ON A TWO BLADED VAWT	26
3.3 WAVE-INDUCED LOADS.....	28
3.3.1 <i>Formulation of the problem and assumptions</i>	28
3.3.2 <i>Regular waves and statistical description</i>	28
3.3.3 <i>Hydrostatic loads</i>	30
3.3.4 <i>Radiation loads</i>	31
3.3.5 <i>Diffraction loads</i>	31
3.3.6 <i>Morison's formulation and the viscous loads and damping</i>	32

3.4	EQUATION OF MOTION AND NATURAL PERIODS.....	33
4	LOADS FROM A WATER STREAM PASSING THE ROTATING PLATFORM	35
4.1	LOADS ON A ROTATING CYLINDER IN A WATER STREAM, PREVIOUS STUDIES.....	35
4.2	METHODOLOGY OF THE STUDY	37
4.3	RESULTS.....	38
4.4	DISCUSSION	40
4.5	CONCLUSIONS AND SUGGESTIONS FOR FURTHER INVESTIGATIONS	42
5	CONCEPT SCALING.....	44
5.1	POSSIBLE METHODOLOGIES.....	44
5.2	PHYSICAL SCALING OF THE PHENOMENA: MODEL SCALING	44
5.3	FEASIBILITY APPROACH: CONCEPT SCALING	46
5.4	ECONOMICAL AND PRODUCTION APPROACH: EVALUATION OF CONCEPT UPSCALING	47
6	NUMERICAL CODE TO INVESTIGATE THE CONCEPT	48
6.1	HAWC2.....	48
6.1.1	<i>Structural formulation</i>	48
6.1.2	<i>Hydrodynamic module</i>	48
6.2	ADDED DLLS	49
6.2.1	<i>VAWT aerodynamics</i>	49
6.3	FORCES ON THE ROTATING PLATFORM.....	51
6.3.1	<i>Generator module</i>	53
6.3.2	<i>Generator control</i>	53
6.4	FIXED SETUP	53
6.4.1	<i>Physical properties</i>	53
6.4.2	<i>Description of external conditions</i>	54
6.4.3	<i>Model set up</i>	55
6.4.4	<i>Reference systems</i>	55
6.5	CALCULATION POINTS	57
6.6	OTHER SOFTWARE USED FOR NUMERICAL SIMULATIONS	57
7	FIRST DESIGN: 2MW	58
7.1	DESIGN SPECIFICATIONS	58
7.1.1	<i>Rotor design</i>	58
7.2	LOAD CASES AND CODE SET UP.....	60
7.2.1	<i>Wind speed</i>	60
7.2.2	<i>Currents</i>	60
7.2.3	<i>Waves</i>	61
7.3	RESULTS.....	61
7.3.1	<i>Load case 0</i>	62
7.3.2	<i>Load case 1</i>	63
7.3.3	<i>Load case 2</i>	65
7.3.4	<i>Load case 3</i>	67
7.4	DISCUSSION	68
8	BASELINE MODEL: 5MW	70
8.1	DESIGN SPECIFICATIONS	70
8.1.1	<i>Site description</i>	70

8.1.2	<i>Rotor design</i>	72
8.1.3	<i>Platform design</i>	76
8.2	SIMULATIONS	79
8.2.1	<i>Load cases description</i>	79
8.2.2	<i>Results</i>	79
8.3	DISCUSSIONS OF THE RESULTS	85
9	DOWNSCALED MODEL: 1KW	87
9.1	DESIGN	87
9.1.1	<i>Site description</i>	87
9.1.2	<i>Downscaling considerations</i>	88
9.1.3	<i>Rotor design</i>	89
9.1.4	<i>Platform design</i>	91
9.2	RESULTS FROM NUMERICAL SIMULATIONS	95
9.2.1	<i>Natural frequencies of the rotor</i>	96
9.2.2	<i>On land configurations</i>	98
9.2.3	<i>Discussion on the results of the on land configuration</i>	100
9.2.4	<i>Offshore simulations</i>	101
9.2.5	<i>Discussion on results and recommendations on the platform design</i>	105
9.3	CONCLUSIONS	106
10	COST MODELS FOR OFFSHORE FLOATING WIND TURBINES	108
10.1	COST ANALYSIS OF WIND ENERGY	108
10.2	DEEPWIND EVALUATION	110
11	CONCLUSIONS	117
	BIBLIOGRAPHY	121
	APPENDIX A - STRUCTURAL INPUT FOR THE NUMERICAL CALCULATIONS	130
5MW		130
Tower		130
Blades		131
1kW		133
Tower		133
Blades		134
APPENDIX B – ATTACHED PAPERS		136
A NOVEL FLOATING OFFSHORE WIND TURBINE CONCEPT		136
A NOVEL CONCEPT FOR FLOATING OFFSHORE WIND TURBINES: RECENT DEVELOPMENTS IN THE CONCEPT AND INVESTIGATION ON FLUID INTERACTION WITH THE ROTATING FOUNDATION		148

Acknowledgments

My work has been carried out in the Wind Energy Division at Risø DTU, Roskilde, Denmark. The research has been supervised by Professor Troels F. Pedersen, Senior Researcher Uwe S. Paulsen and Professor Helge A. Madsen.

After three years of work, I have a broad list of people to acknowledge.

If a ranking can be made, when it comes to thank a list of people, my first thanks go to Test and Measurements program (TEM) in Wind Energy Division at Risø, which has also been my first Danish “home”. Thank to all of you to show me that outstanding work can be made with fun.

I own also some personal acknowledgment among the research community at Risø.

Special thanks go to Troels F. Pedersen, to be a reference rather than just a supervisor during these years and to Uwe S. Paulsen for always challenging me with new ideas and thoughts. And thanks to both of them for their incredibly enthusiastic way of working and for bringing me jogging under the rain in Norway.

My gratitude goes to Helge for his help in the aerodynamic part of the thesis and to Torben for his help with HAWC2. Thanks also to Frederik Zahle for the help with the CFD calculations in Chapter 4 and to Per H. Nielsen for his valuable help in dimensioning the blades and in explaining me things.

I am grateful to Poul Hummelshøj to give me the possibility of working on this project, even though there was not a project yet.

I own my gratitude to Uwe S. Paulsen, Troels F. Pedersen, Flemming Rasmussen and Helge A. Madsen to share with me their novel concept idea and let me participate in it.

Part of this work is included in the fp7 European granted project DeepWind. Thanks to all the partners in the project, for their help and contributions.

I would like to acknowledge Stefan Crstensen from DHI for the help in evaluating the met-ocean conditions at the sites, Joachim Reuder from Oceanor for the access to the met-ocean data at Sletringen, Norway and Wei He from Statoil for her suggestions and her challenging curiosity.

Thanks to all the people who have spoilt me during my “thesis lethargy”, especially to Damien, Nikolas and Braulio for their discreet moral support. I am very grateful to Gireesh for his help in reviewing the thesis and supporting me during the process.

Last but absolutely not least, thank to my little Italian world, which I always find there, every time I land in Italy. Grazie.

Eventually I own also an answer to a question I got at my very first day at Risø: yes, I really like to work on vertical axis wind turbines.

Preface

This work deals with a new concept for floating Vertical Axis Wind Turbine (VAWT), started at Risø-DTU in 2007. The concept has been later called DeepWind concept [1], taking name from the EU granted project DeepWind. In the current work, when I mention DeepWind, I refer to the concept.

During 2007-2008 Risø-DTU prepared a series of reports [2] as a result of a consultancy project for Statoil. The reports were meant to respond to Statoil's interest in new alternative designs for floating wind turbines, with emphasis in the possible use of VAWTs. In the last report [3] the new concept was presented to Statoil, as a possible candidate for a new floating VAWT design. The report included also a plan on the possible steps for a successful exploitation of the concept potential.

In 2008, the present PhD project started, aiming at exploiting the feasibility and potential of the new VAWT floating concept.

The study was meant to find out the most relevant challenges that could influence the feasibility of the concept and its advantages. Some codes (mainly HAWC2 and a BEM code for VAWT) needed some adaptation in order to reach a satisfactory accuracy for a first evaluation of the concept and of its feasibility.

From 2010 the Ph.D. project was financed, as part of the fp7 European project DeepWind (2010-2014).

Nomenclature

a_x, a_y, a_z	Components of the acceleration of the fluid particles, according the potential-flow theory	[m/s ²]
A_{ij}	Terms of the added mass matrix	[kg] - [kg m ²]
$A_{ij}^{(2d)}$	2D added mass coefficients	[kg] - [kg m ²]
A_w	Water plane area	[m ²]
B	Buoyancy	[kg]
B_{ij}	Terms of the damping matrix	[kg/s] - [kg m ² /s]
c	Chord of the blade	[m]
C_d	2D drag coefficient of the platform in oscillatory flow and of the airfoils in aerodynamics. $C_d = \frac{F_d}{0.5U^2 \rho L_r}$	[-]
C_D	Drag coefficient of the platform in oscillatory flow $C_D = \frac{F_D}{0.5U^2 \rho S}$, or drag coefficient in the Morison's equation	[-]
C_{ij}	Terms of the restoring matrix	[kg m/s ²] - [kg m ² /s ²]
C_l	2D lift coefficient of the tower in oscillatory flow and of the airfoils in aerodynamics. $C_l = \frac{F_l}{0.5U^2 \rho L_r}$	[-]
C_m	Mass coefficient in Morison's equation	[-]
C_M	Inertial coefficient in Morison's equation	[-]
C_P	Power coefficient of the rotor, $C_P = \frac{P}{0.5v_0^3 \rho S_W}$	[-]
dx, dy, dz	Displacements of the water plane section of the tower	[m]
D	Diameter of the rotor tower	[m]
DOF	Degrees of freedom of the floating system	[-]
f_{1p}	First odd frequency of the rotor, $f_{1p} = \frac{\omega}{2\pi}$	[Hz]

f_{2p}	First even frequency of the rotor, $f_{2p} = \frac{\omega}{\pi}$	[Hz]
f_p	Peak frequency of the wave spectrum	[Hz]
f_w	Wave frequency	[Hz]
F_d	Hydrodynamic drag force for length unit	[N/m]
F_D	Hydrodynamic drag force	[N/m]
f_s	Safety factor, $f_s = \frac{\sigma_{max}}{\sigma_s}$	[-]
F_D	Hydrodynamic drag force on the tower	[N]
F_i	Exiting force or exiting moment of the mode i	[N] - [Nm]
F_l	Hydrodynamic lateral force per meter	[N/m]
F_L	Hydrodynamic lateral force	[N]
Fn	Froude number, $\frac{U}{\sqrt{L_r g}}$	[-]
g	Acceleration of gravity, 9.81	[m/s ²]
h	Water depth	[m]
H	Rotor height	[m]
H_g	Height generator box	[m]
H_0	Clearance of the rotor, from the mean water level or from the ground	[m]
H_s	Significant wave height	[m]
H_{100}	Wave height with annual probability of exceedance of 10^{-2}	[m]
H_p	Length of platform (draft)	[m]
H_{tot}	Total length of the tower, $H_{tot} = H_g + H_p + H_0 + H$	[m]
I_{xx}, I_{yy}, I_{zz}	Inertia moment around the x, y and z axis	[km m ²]
k	Wave number, $k = \omega_w^2 / g$, for finite water depth is $k \tanh(hk) = \omega_w^2 / g$	[1/m]
KC	Keulegan-Karpenter number, $KC = 2\pi \frac{\zeta a}{D}$	[-]

L_r	Reference length	[m]
M	Mass	[kg]
M_{ij}	Terms of the Mass matrix	[kg] - [kg m ²]
N	Number of blades	[-]
p_D	Dynamic pressure	[kg/(ms ²)]
P	Power output	[kW]
Q	Torque on the shaft	[Nm]
R	Maximum radius of the rotor	[m]
R_p	Maximum external radius of the platform	[m]
R_T	Maximum external radius of the rotor tower	[m]
Re	Reynolds number, $Re=L_r U_r / \nu$, with L_r and U_r , characteristic length and reference velocity at the site	[-]
S_w	Swept rotor Area	[m ²]
S_{ii}	2 nd water plane moment of inertia	[kg m ² /s ²]
T_x, T_y	Lateral and longitudinal components of the aerodynamic force	[N]
T_w	Wave period	[s]
Th	Thickness of the tower	[m]
T_{ni}	Natural periods of the floating structure in the i DOF	[s]
T_p	Peak period of the wave spectrum	[s]
u_x, u_y, u_z	Water particle velocity components in oscillatory flow according the potential-flow theory	[m/s]
U	Water current speed	[m/s]
v_0	Free wind speed at the equatorial height of the rotor	[m/s]

V	Displaced volume of water	[m ³]
z _B	Vertical position of the centre of buoyancy	[m]
z _G	Vertical position of the centre of gravity	[m]
α	Speed ratio on the tower, $\alpha = \omega_r R_T / U$	[-]
β _w	Waves direction respect to wind speed direction	[deg]
β _c	Current direction respect to wind speed direction	[deg]
Φ	Potential function in potential-flow theory	[-]
φ	Tilt angle	[deg]
φ ₀	Tilt angle at the start	[deg]
λ	Tip speed ratio, $\lambda = R\omega_r / v_0$	[-]
λ _w	Wavelength, $\lambda_w = gT_w^2 / (2\pi)$, for finite depth: $\lambda_w = \tanh(2h\pi / \lambda_w) gT_w^2 / (2\pi)$	[m]
η _i	Displacements in the i DOF	[m] - [deg]
ν	Kinematic viscosity	[m ² /s]
ρ	Free stream air density	[kg/m ³]
ρ _w	Free stream water density	[kg/m ³]
σ	Solidity of the rotor, $\sigma = Nc / Rr$	[-]
σ _s	Design stress	[N/m ²]
σ _{max}	Yield stress of the material	[N/m ²]
ω _p	Peak circular frequency of the wave spectrum	[radians/s]
ω	Rotational speed of the rotor (low speed shaft)	[rpm]
ω _w	Circular wave frequency, $\omega_w = 2\pi / T_w$	[radians/s]
ζ _a	Wave amplitude, $\zeta_a = H_s / 2$	[m]

1 Introduction

1.1 Objectives

In my work, I aim at achieving the following objectives: (1) investigate the main potentials and challenges of a new concept for deep offshore wind power (DeepWind concept); (2) develop or adapt the necessary numerical tools to simulate the concept with an acceptable accuracy; (3) design DeepWind for three possible sizes; (4) have a first estimate on the feasibility of the concept in its economical and technological potential.

1.2 State of the art

1.2.1 Background: wind power offshore market

The new European targets for wind energy address a strategic role to offshore wind energy. There are some relevant reasons, to move wind energy production from land to offshore:

- Better wind resources, because of the very low roughness of the water and of the absence of obstacles.
- Offshore constructions have almost no restrictions concerning noise and visual impact.
- The limited availability of land, especially in Europe, suggests the exploitation of the sea.
- The possible involvement of new competitors, such as Oil and Gas companies (O&G), could bring new values in the market, in terms of both investments and technology.

These arguments constitute the basis for the very ambitious schedule for the European renewable energy development. According to the European annual report [4], in 2007 the annual wind energy production was 119TWh, of which only 4TWh (3%) was from offshore installations. In 2030, the same report predicts, in a neutral scenario, an annual energy production from wind power of 935TWh, with a share of offshore energy to be 50% (469TWh). This achievement will be possible with an expected growth in the new offshore power installation of 28% each year over the next 10 years.

Such high expectations are up against severe economical and logistical issues:

- In the offshore environment, the turbines experience more severe loads, due to waves and currents. Wind loads are higher as well.
- The harsh environment results in more difficult and expensive installation procedures, as well as O&M. Moreover this can affect the reliability of the machines.

- There are a few logistic problems, due to water depth and distance from shore. There is also need for a grid connection in remote offshore sites and EU seems to be aware of the issue [5].
- Transport on land of huge structures, from production to harbour, while it is not possible to manufacture the turbine near the shore.
- Dismantling can be costly and repowering has not been tried yet.
- There are still barriers caused by lack of clear regulations. In some countries the rules are still very complicated and politically dependent, in some other countries regulation is totally absent. A more uniform policy (at least at European level) may in the future solve this problem.
- The sea is not an unlimited open space, the way it looks. In fact there is plenty of restrictions and most of the waters close to shore are already booked for other purposes (i.e. military, transportation, protected wildlife areas, industries). The consequence is that often the available places are not the most logistically favourable ones: European shallow waters will probably be overcrowded quite soon.

As a result of these observations, another report from EU [6] addresses an important cost issue: in average, the cost of offshore wind energy is 2400 Euro/kW versus 1250 Euro/kW on shore (data 2008).

This discrepancy, between the very optimistic forecasts and the present cost of energy, can be more generally explained observing that offshore wind energy is not yet a mature technology. In particular, there is still a lack of integration between two mature technologies, such as O&G offshore industry and wind power production.

The production of offshore wind power began in Denmark, seeking for new space to erect wind farms and for better wind resources. The new installations were put in shallow waters and the distance from shore was limited, therefore only few adaptations were needed to move wind turbines to the sea. Nowadays offshore wind power has got new ambitions and dimensions, aiming at exploiting much more challenging sites. Therefore, it is not anymore reasonable to produce offshore wind energy just by moving wind turbine technology from land into waters.

The design of modern offshore wind turbines needs to take specific site assessment and requirements better into account. A successful design should be the result of a fully integrated study, involving different disciplines and technologies. Moreover the design could be more successful if it will focus on a specific target, selecting a range of potential offshore sites. New specific offshore concepts are also needed in order to cut off the cost (to be competitive with the onshore market) and to exploit the wind resources not affordable with current technologies.

It is finally not just a question to appoint the best concept or the best turbine, but more realistically to select the most suitable solution, for a specific available site.

1.2.2 Brief history of VAWT and floating wind turbines

In the current work, mentioning VAWT, I refer to the Darrieus concept, patented in 1926 [7], I disregard the other types of VAWTs developed in the past years.

When in the 70s, the energy crisis addressed for the first time a serious need for some new sources of energy alternative to fossil fuels, VAWT seemed perhaps to be the best candidate for wind power exploitation. After less than 20 years VAWTs was the big loser in the development of the modern wind turbines. This happened between the 70s and the 90s.

In a Darrieus rotor, since the airfoils are rotating, the relative velocity of the flow passing the airfoils is the vector addition of the wind speed and the tangential speed induced by the rotation ω . The angle of attack α of the airfoils is varying periodically during one revolution and its value depends on the tip speed ratio, $\lambda = \omega R / v_0$. In particular, α decreases as λ increases. At low λ the efficiency of the blade airfoils drops because of stall. Commonly this effect occurs in VAWT in two cases: at very high wind speed causing the stall of the rotor; at very low rotational speed, causing the turbine not to be capable of self-starting. Therefore, values of λ sufficiently large are needed: in this way α never exceeds the limit of stall during a revolution and the blade element works at high efficiency, transmitting a high torque to the rotor.

However, the values of λ cannot be increased indefinitely. Indeed for values of λ too large, α becomes very small and the airfoils has low efficiency. Moreover the projection of the lift force on the chord direction is decreasing with the decreasing of α .

Thus a blade element has low efficiency at both very low and high λ and the turbine needs to operate in a range of favourable tip speed ratios, in order to work efficiently.

An important consequence of the periodicity of the angle of attack is that the loads on each blade are also periodic, with a frequency depending on the rotational frequency of the rotor. This brings us to two conclusions:

- The blades experience periodic loads, which affect their fatigue-life.
- The forces and moments transmitted from each blade to the tower are periodical with an amplitude and a frequency dependent on the number of blades of the rotor. It is easy to demonstrate that the two bladed rotors have the maximum amplitude of the periodic oscillations.

Darrieus rotors can be generally divided in two sub-groups, depending on the rotor shape:

- Curved blades
- Straight blades, also known as giromill.

When the blades are straight, all the blade elements have the same distance from the rotational axis. Then, at a fixed time t and neglecting the variation of v_0 with the height, all the elements of one blade experience the same tip speed ratio. Thus in principle it is possible to run the rotor at a selected λ , which is the optimum for all the blade airfoils. The same is not achievable with curved blades, because λ changes along the blade. Therefore, optimizing the value of λ , giromil rotors reach higher values of maximum efficiency, measured in terms of C_p . On the other hand, the blades need support connection arms, which would produce parasite drag and reduce

the C_p . The effect of constant λ along the blade also reduces the range of tip speed ratio to have an acceptable efficiency, since in theory, all the elements would stall at the same time. Thus the peak for giromill will be higher and less broad, compared to curved blades. Straight blades have also been used, combined with cambered airfoils and pitch passive control, to increase the torque at the start in order to have self-starting capability [8].

Curved blades are characterized by having λ varying along the blades, causing each element stalling at different wind speed (at constant ω). The most significant advantage of this type of VAWT is the possibility to use a Troposkien shape (from the Greek τροπος, turning, and σχοινιον, rope), [9]. A Troposkien blade is shaped like a perfect flexible cable of uniform density and cross section, spinning around a vertical axis at constant rotational speed. In this way the stress caused by the centrifugal loads will be transferred as tensional stress in the blade direction and no flatwise moment will be acting on the blade. This characteristic is very important to increase the fatigue life-time of the rotating structures, considering the periodic aerodynamic loads acting on the blade.

Most of the VAWTs erected between the 70s and the 90s had a diameter less than 35m and used curved blades. The Sandia Laboratory in Albuquerque (NM), has been one of the most active institute in research on VAWT. There are available data for at least three of the Sandia vertical axis rotors:

- A 2m diameter [10], that was primarily built for wind tunnel test [11]. The blades had a Troposkien with NACA 0012 airfoils. The results of the experiments showed a strong influence of the Reynolds number on the power production and an optimum solidity (at fixed Re) between 0.2-0.25.
- A 5m [12] was built as a proof-of-concept machine in 1974. A maximum C_p of 0.39 was reached with a solidity of 0.22. They also calculated the value of C_{d0} of the turbine, spinning the turbine at no wind condition. The results show a decreasing of C_{d0} as the Reynolds number increases.
- A 34m 500kW [13] was erected and used as a test bed case [14]. The turbine was in operation for eleven years (1987-1998) and it has been a milestone in VAWT development, since several studies were carried out on it: an investigation was carried out on resonance response [15]; new geometric configurations were tested, such as tapered blades with 3 different chords and first laminar airfoils for wind turbines [16]; a direct-drive, variable speed generator was used to control the turbine [17].

A comparative investigation on two possible geometries was carried out by Sandia and FloWind Corp. on a 300kW machine [18]. They considered the effects of increasing the rotor ratio, defined as height over diameter, from 1.31 to 2.78. That would require an increase of the swept area and probably of the cost. FloWind also succeeded in using pultruded jointless blades, even though the level of pultrusion technology was not mature.

In 1988 EOLE, so far the largest VAWT ever erected, started operations. It was developed from Hydro-Quebec and the National Research Centre of Canada, while the rotor was manufactured by Versatile Vickers shipyard. The turbine had a height

of 96m and a maximum diameter of 64m, the chord was 2.4m ($\sigma=0.15$) and the airfoils were NACA0018. EOLE was a direct-drive, variable-speed machine and the generator was 12m large, with a rated power of 4MW at 14.5rpm. The turbine produced power up to 2.7MW and it was running at maximum 11.35rpm. Even though EOLE had a good availability (94%), it was stopped in 1993 after five years of operation, because of the failure of the bottom bearing [19].

After more than twenty years of experience on VAWTs, it was possible to estimate potentials and problems connected with a possible commercial development. The results are well summarized by Paraschiviu in his book [20].

The technological advantages in using VAWTs, compared to HAWTs, are:

- Independence from wind direction, that allows to save the cost of a yaw control system.
- Possibility of placing the electrical and mechanical components at the bottom of the structure
- Simplicity of the geometry of the blades, usually neither tapered nor twisting is present.

The disadvantages in using VAWTs and the lessons learnt from the past years are:

- For the same swept area, a VAWT needs blades which are 2-3 times longer than a HAWT.
- VAWTs are not self starting and need torque from a motor at the start. Some new concepts have overcome this problem, using pitching straight blades and cambered airfoils. [8]
- The periodical aerodynamic loads give structural problems on the tower and the bearings. To increase the stiffness of the tower at the upper bearing, the most used solution had been the use of pre-tensioned guy-wires [13]. However, these cables give other kinds of problems: their natural frequency is often in the range of the operational rotational speeds and, to avoid resonance undesired effects, a damper is needed; the tension of the cables load the rotor with a vertical component that must be absorbed by the bottom bearing. To avoid this problem, guy-wires could be replaced by other solutions, such as a structural bearing. This would add new structural costs.

On the basis of these points, the HAWTs got a large supremacy on the market in the 90s and today they are the only commercialized MW size wind turbines. In the last 20 years the use of VAWTs has mainly been restricted to a few small market spots, where their technological advantages are still considered of primary importance, i.e. urban wind energy [21] and hydropower turbines [8].

To bring back VAWT in the competition new technological developments are needed. Some economical and energetic global change may thereby give new ambitions to the wind energy industry.

The new targets for wind energy productions push the limit of the rotor size, looking for new technologies and solutions. In the second edition of “The World Offshore

Renewable Energy Report” [22], published by the British Department of Trade and Industry, VAWT has been pointed as a possible solution for large wind turbines:

“The idea of large megawatt VAWTs is an interesting one [...] Lower levels of blade stress occur on VAWTs as opposed to their horizontal counterparts, therefore allowing them be built to a higher capacity. Cost is obviously a key issue and even now it is believed that above 5 MW, large capacity VAWTs could prove to be more cost effective than their traditional tribladed horizontal cousins”

VAWT could be then a candidate for next generation offshore wind turbine, larger than 5MW.

Meanwhile, offshore wind industry is struggling to solve other logistic issues, often independent from the selected turbine. One of the most challenging problems is the erection of wind turbines in deep waters. It is commonly accepted that for offshore sites deeper than 50m, the floating platforms are more economical convenient than the monopoles, used for shallow waters [23], [24], [25].

To my knowledge, the first idea of a floating wind power device was a SPAR concept proposed by Bill Heronemus from MIT in the early 70s [26], Figure 1. Another offshore application, using a VAWT, was proposed by Olle Ljungström of FFA in Sweden, as seen in Figure 2 [2]. The end of the energy crisis of the 70s also meant the end of several pioneering ideas in the field of the energies, such as the ones of Heronemus and Ljungström.

But nowadays, following the shrinking of the fossil sources, some of those ideas are back to the attention.

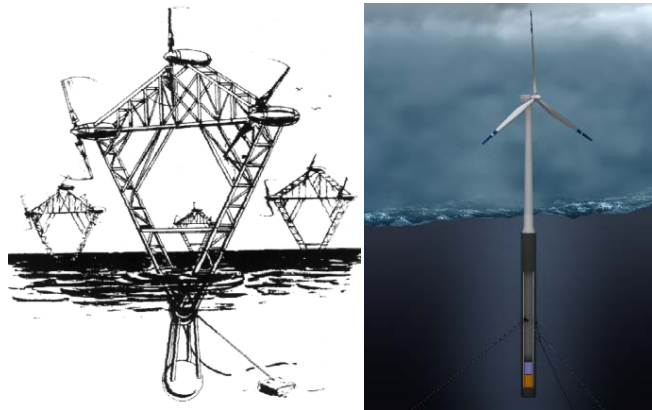


Figure 1 The futuristic idea from Bill Heronemus in 1974 [26] on the left and a modern application of his concept, HyWind¹, using the same ballast stability principle proposed by Heronemus.

The possible solutions for a wind turbine platform are derived from O&G industry. They are essentially divided in three groups, depending on the anchoring system and in the way that they reach hydrostatic stability, as described in Table 1.

¹ www.statoil.com

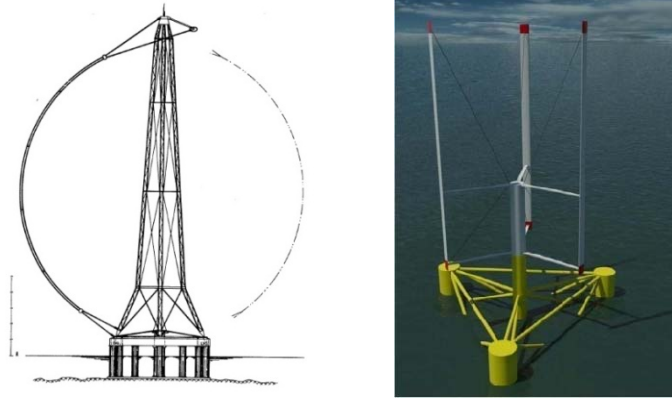


Figure 2 -180 Poseidon proposal of an offshore VAWT by O Ljungström [2] and a modern version of offshore VAWT from Vertiwind on the right².

In only a few years, several projects have been started, aiming at coupling a wind turbine with a floating platform. The most relevant projects are listed in Table 2.

Table 1 Type of platform and characteristics.
*These aspects are supported by the following sources: [27],[23], [28].

Platform	Stability system	Mooring system	depth*	Critical aspects*	Favourable issues*
TLP (Tension Leg Platform)	Anchoring	Tensioned legs (gravity anchor)	>50m	<ul style="list-style-type: none"> • Weight • Anchoring cost • Installation 	<ul style="list-style-type: none"> • Periods • Stability
Barge	Hydrostatic	Catenary lines	>50m	<ul style="list-style-type: none"> • High loads on the tower at WL • Periods and wave excitation • Stability 	<ul style="list-style-type: none"> • Installation • Weight • Anchoring cost
SPAR	Ballast	Catenary lines	>120m	<ul style="list-style-type: none"> • Periods in heave • Installation 	<ul style="list-style-type: none"> • Anchoring cost • Stability to waves

From the Table 2 it is clear that the research is in an early stage and it is still very broad, analyzing very different solutions, for both rotor and platforms.

A comparison between the three possible types of platforms has recently been carried out by Jonkman in [28] and by Henderson in [23]. Their analysis offers the following considerations:

- The barge system achieves the stability using the very large area at the water surface. It is commonly considered the easiest and cheapest solution from an installation point of view. Meantime, due to its large area at the mean water level, the barge has the largest stability problems in waves, among the three solutions. Simulations carried out by Jonkman and Matha show an increment of the loads on the tower base, exceeding four times the on shore loads. Its

² www.renewbl.com

potential seems to be mostly restricted to sites where met-ocean conditions are favourable, i.e. a bay rather than open ocean.

However some improvements seem to be possible, using a tri-floater configuration, as in the Norwegian project WindSea and in WindFloat from the US. In this project the stability is improved with a novel system of pumps, moving water between the three columns [29].

- The TLP has been, so far, the most exploited concept. The stability is obtained with tensioned cables anchored to the sea bed. Jonkman and Matha show that a turbine mounted on this platform experiences loads very close to the on-shore configuration. On the other hand, the turbine has the largest value of displaced water among the three selected configurations and installation would be challenging, especially because of the anchors. Above that Henderson and Witch notice that in case of failure of one of the wires, the turbine would flip and it would probably collapse in the water.
- The SPAR aims at exploiting deepest sites, at least 120m, as aimed by HyWind [30]. SPAR strength points are in its simple and reasonable light design and in the low wave loads due the small section at the water surface level. In their simulations, Jonkman and Matha found loads similar to the TLP platform, a part from slightly higher bending moments at the tower bottom. Henderson and Witch notice that, contrary to TLP, the failure of one of the anchors would not affect dramatically the stability of the platform. However, they emphasize the challenges connected with installation of such a platform, at sites where a vertical installation (used for HyWind prototype) would not be possible. Indeed in this case the turbine should be towed-out horizontally and then tilted up. This procedure may cause severe loads on the structure, due to the gravitational loads of the rotor and the nacelle mounted at the tower top. During analysis of HyWind concept, Larsen pointed out also a resonance problem due to the interaction of one of the floating natural frequencies (which are very low) with the pitch control of the turbine [33]. He solved the problem by using an adapted control system, whose lowest control-structure natural frequency is lower than the lowest resonance frequency of the tower. Nevertheless, this type of interaction is probable to occur in such kind of constructions and they have to take into account during the design phase.

Eventually, Henderson emphasizes also the small design space for such a turbine, due to the many restrictions on the design parameters.

An alternative SPAR design, using a tensioned leg anchoring system, was proposed and investigated with a fully coupled dynamic analysis by Withee [34].

Another comparative analysis of SPAR and TLP systems has been presented by Lee and Scлавounos in 2005 [35], who conducted a numerical stability investigation mounting a 5MW HAWT on the two platforms. The results did not show any instability and the authors believe that both the concept would have technological potentials.

Table 2 Projects on floating offshore wind turbines

Project Name	Partner Leader	Status and target of the of project	Platform	Rotor
DeepWind	Risø	Paper/ Academic	SPAR	VAWT
HyWind [30]	Statoil, NO	Demonstration / Commercial	SPAR	HAWT
MIT/NREL TLP [31]	MIT/NREL, US	Paper/ Academic	TLP	HAWT
JOIA SPAR [32]	JOIA (Japan Ocean Industries Association)	Paper and Prototype / academic and commercial	SPAR	HAWT
BLUEH ³	BLUEH, UK	Prototype/ Commercial	TLP	HAWT
VERTIWIND ⁴	Technip, FR	Paper /Commercial	TLP	VAWT
ITI Energy barge [31]	Glasgow University, UK	Paper/ Academic	Barge (squared semi-submerged platform)	HAWT
WindFloat ⁵	Principle Power, US	Paper /Commercial	Barge (tri-floater jacket)	HAWT
WindSea ⁶	Statkraft, NO	Paper /Commercial	Barge (tri-floater jacket)	HAWT
Sway ⁷	Sway, No	Demonstration/ Commercial	Spar	HAWT

1.2.3 Numerical tools for floating VAWTs

The development of numerical codes for investigation of the performances of VAWTs started in the 70s. It is possible to distinguish between two groups of numerical methods:

- The BEM codes (based on the Blade Element Momentum theory), also known as stream-tube codes. They are based on the disk actuator theory, imposing the total forces on the blade to be equal to the change in momentum of the stream flow passing through the rotor. The main advantage of this model is the very fast computational time. On the other hand, the code has low accuracy at high tip speed ratio (low rotational speeds) and high solidity.
- The vortex codes, usually based on the Biot-Savart formulation of the vorticity. Their results are commonly considered to be more accurate. Their

³ <http://www.bluehgroup.com>

⁴ <http://www.technip.com/en/press/technip-launches-vertiwind-floating-wind-turbine-project>

⁵ <http://www.principlepowerinc.com/products/windfloat.html>

⁶ <http://www.windsea.com>

⁷ <http://sway.no>

use is limited by high computational time and convergence problems at low tip speed ratio.

The first BEM codes were using a single stream tube comprehending the whole rotor. Strickland improved the accuracy with the multi-streamtube formulation, [36]. He divided the rotor into many different stream-tubes, allowing to evaluate the variation of the flow in the two direction perpendicular to the direction of the flow. A further improvement to the model has been carried out by Paravischivoiu, who added another actuator disk to the model, considering the different induced velocities in the upstream and downstream part of the rotor [20].

Another development was achieved by Madsen [37], replaced the plane actuator disk with an actuator cylinder. In this way the velocity field is dependent from the all three directions and not only the two perpendicular to the stream, as in Stricklands dissertation [36].

The BEM codes are mainly used, because of their rapidity, in development of aero-elastic codes. That is also the case for the most used software for simulating offshore floating wind turbines. There are at least a few codes, which couple the aero-hydro-dynamics of the system platform-wind turbine.

At Risø DTU, a hydrodynamic module has been integrated in the aero-elastic code HAWC2, [33], [38], [30]. HAWC2 uses a multi-body formulation, allowing the user to model each component of the turbine as a separate body. The implementation of each body is carried out adopting a finite element theory. The code will be further described in Chapter 6.

Software, currently available for the simulation of fully coupled dynamics of floating wind turbines, has been part of a comparative program under the IEA organization [39].

1.3 Thesis outline

Based on this status of the art, I outline my work to solve the proposed objectives.

First of all, in chapter 2, I describe the concept as presented in 2009 and 2010 [1], [40]. I describe the components, justifying their choice in a global design context, bearing in mind that the main goal is to investigate the concept feasibility, rather than its optimization. I dedicate the last part of the chapter to the differences with the former VAWT technology, arguing how some of the typical VAWTs limitations are overcome in this new concept.

The design of an offshore floating wind turbine involves both aerodynamics and hydrodynamics. Then in Chapter 3 I introduce the problem of the floating bodies in the time domain, as formulated by Faltinsen [27] and Newman [41]. My objective is not to have a full comprehensive set of equations, since I will later use a numerical code including an accurate formulation of the floating problem. My objective in this chapter is instead to develop a simplified model to utilize as a preliminary tool for the design of the turbine and the platform. In this model the aerodynamic loads are considered as an external force exciting the system.

The DeepWind concept has a peculiarity with respect to the other platforms so far used for wind turbines: the platform is integrated in the tower rotor and it is rotating in the water. Because of this feature, the platform will be loaded with additional external hydrodynamic loads. Indeed a cylinder rotating in a fluid stream experiences a lift force (known as Magnus effect) and a drag force, whose intensity depends on the rotational speed, the radius and the stream velocity. Additionally, a friction moment too acts on the cylinder. Due to the very high Reynolds numbers of a DeepWind MW design, there is not enough literature on this topic. In Chapter 4 I present a study on the forces, conducted with Frederik Zahle at Risø DTU and mainly based on the paper presented at the OMAE conference in 2010 [42]. The results are limited to a few data. However, the values of Cl are very high (up to 10.4) and the Magnus effect needs to be added to the loads in the floating model formulation. Eventually, another aspect needing further investigation is whether and in which magnitude the rotation would alter the flow regimes around the cylinder. This alteration may indeed affect the dependency of the platform behaviour from the no-dimensional numbers commonly used in hydrodynamics.

One of the preliminary aspects in the design and evaluation of the concept is to evaluate the right size for the wind turbine. I decided to adopt a 5MW design as a baseline model. At the present time, this would be a realistic magnitude for a new offshore wind turbine. Additionally, it is also the rated power of the NREL 5MW baseline HAWT defined in [43]. This turbine is broadly used as a reference turbine for offshore platform investigations and it has also been used on a SPAR buoy, recalling the HyWind design, [44]. Even though the size of DeepWind baseline turbine is 5MW, the concept demonstration has to pass through the design of a much smaller demonstrator, as suggested in [3]. Then in Chapter 5 I focus on the challenges connected with the downscaling of the concept from MW to kW size.

My numerical simulations of the concept are mainly conducted with the hydro-aero-elastic code HAWC2, developed at Risø DTU. The code has been used to design the HyWind concept and to simulate other floating wind turbines. HAWC2 has also been selected along with other codes, for a code-to-code verification under Subtask 2 of the International Energy Agency Wind Annex XXIII. [39]. Even though the code has been developed for HAWTs, it has a multi-body formulation, allowing in principle any type of geometry. In chapter 6, I describe the necessary additions to the code, in order to be able to simulate numerically the concept. My work has mostly regarded the development of appropriate computer codes to simulate the aerodynamic loads on each blade element, the control of the rotational speed of the generator and the hydrodynamic loads and friction due to the rotation of the platform.

The chapters 3-6 give the necessary tools to design the floating VAWT. In the chapters 7, 8 and 9 I present the study of three possible sizes, 1kW, 2MW and 5MW. The work is divided in three sections, including the design specifications, the results from numerical simulations and a discussion on the results.

As a result of my work, in Chapter 10 I present an evaluation of the concept and a rough comparison with another floating wind turbine which uses a SPAR platform. Since my study is based on several simplifications, a realistic complete comparison

between the two concepts is not possible. Therefore beyond my evaluation, I added some considerations on the possible strategy to obtain a useful tool to compare offshore floating concept.

In Chapter 11, I wrap up my work and I propose some recommendations for the further development and verifications of floating VAWTs with rotating platform.

1.4 Design approach

There are two possible approaches to start the design of a floating wind turbine:

- A floating turbine is a very robust turbine mounted on a platform, which need to be stable enough to not create problems to the turbine operations.
- A floating turbine refers to the problem of a complex type of platform, on which additional aerodynamic loads are acting.

Both the two sentences are fundamentally right and they reflect the approach to the problem commonly used by people with different backgrounds, i.e. wind energy or offshore industry.

In this work, my aim is to have an approach to the DeepWind concept that is an integration of the two philosophies above. That requires an iterative process in the evaluation of the concept, which would ideally bring us not to the best rotor neither to the best platform, but to the best integrated system. However, since the main objective of my thesis is the feasibility rather than the optimization, some of the design choices are primarily based on their proven reliability.

There are several constraints in designing a floating VAWT with a spar platform. I grouped them in three groups:

- Structural constraints, limiting the loads on the structure.
- Stability constraints, consisting in maximize the natural periods (to avoid the dominant wave periods), increase the stiffness in pitch and in heave.
- Cost constraints, addressing a general reduction in the mass of the structure.

The most relevant dependency of the design from these constraints are shown in Figure 4, following the design philosophy described by Henderson [23]. Several design parameters have a multiple dependency from different requirements, showing the necessity of an iterative and integrated design process. The conflicting requirements reduce significantly the concept design space, as shown in Figure 3, where the simplified case of the design of a spar buoy support structure with constant section is illustrated. The design space is limited by different constraints, which make not feasible many values of the draft and of the radius of the platform. The resulting blank area is the available space for designing the spar buoy. In fact the design is more complex, because of a larger number of variables and constraints and the resulting geometry of the spar buoy is more complex.

My approach to solve this problem is described in Figure 5. The process starts from the fixed external conditions at the selected site, including wind, waves and currents. I consider a shear effect for the wind and the currents but I don't consider the

turbulence effects. Linear theory for regular waves is used to model the oscillatory flow.

The external conditions are transferred to:

- The aerodynamic module, consisting of a BEM code. I used the code to select the dimensions of the rotor (chord, length and diameter) and to calculate the aerodynamic loads on the tower. Considering the bending and the torsion moment applied on the structure, I dimension the cross section of the tower at the mean water level.
- A wave module, to calculate the wave-induced loads on the structure, knowing the dimensions of the tower at the water surface.
- A current module, to compute the loads on the rotating platform, including lateral force (Magnus effect), drag and friction.

All the loads converge to the design of the SPAR platform, taking into account the stability of the system in a steady state (hydrostatic equilibrium) and the resonance frequencies of the system. The wave-induced loads are recalculated with the values of the underwater structure, using an iterative process.

The design obtained with this simplified model is used as input in the aero-elastic software. The verification on the design includes: structural strength and deformations; verification of the maximum loads; verification of the natural periods; stability of the system in terms of tilt angle and maximum displacements.

The process is iterated until the design is acceptable.

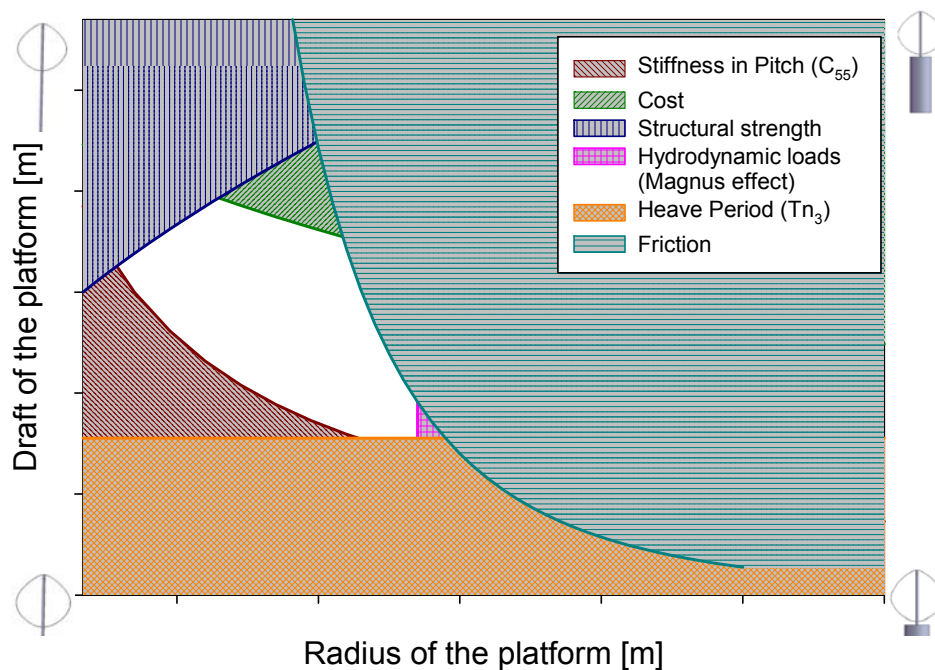


Figure 3 Design space area for the rotating supporting structure of a floating VAWT.

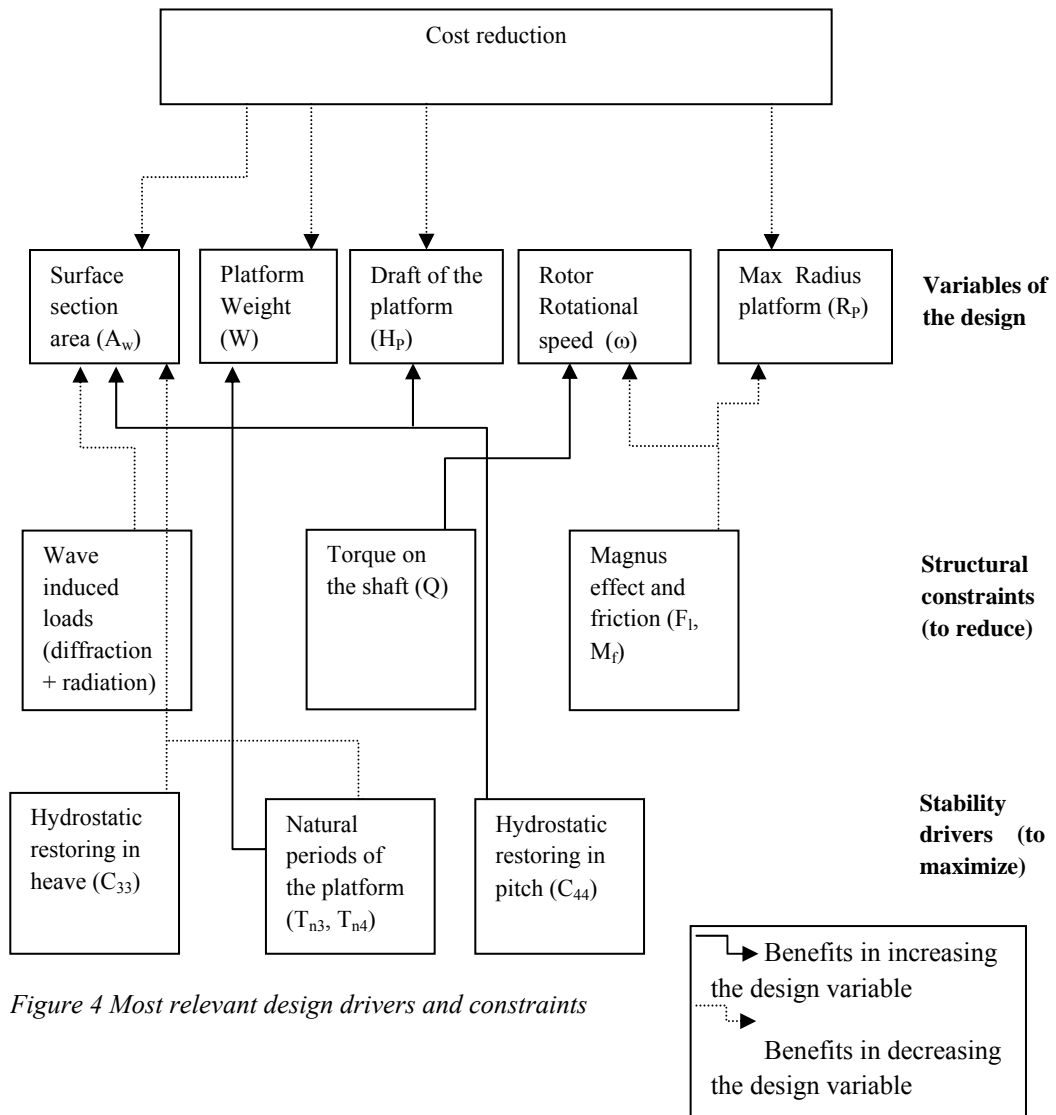


Figure 4 Most relevant design drivers and constraints

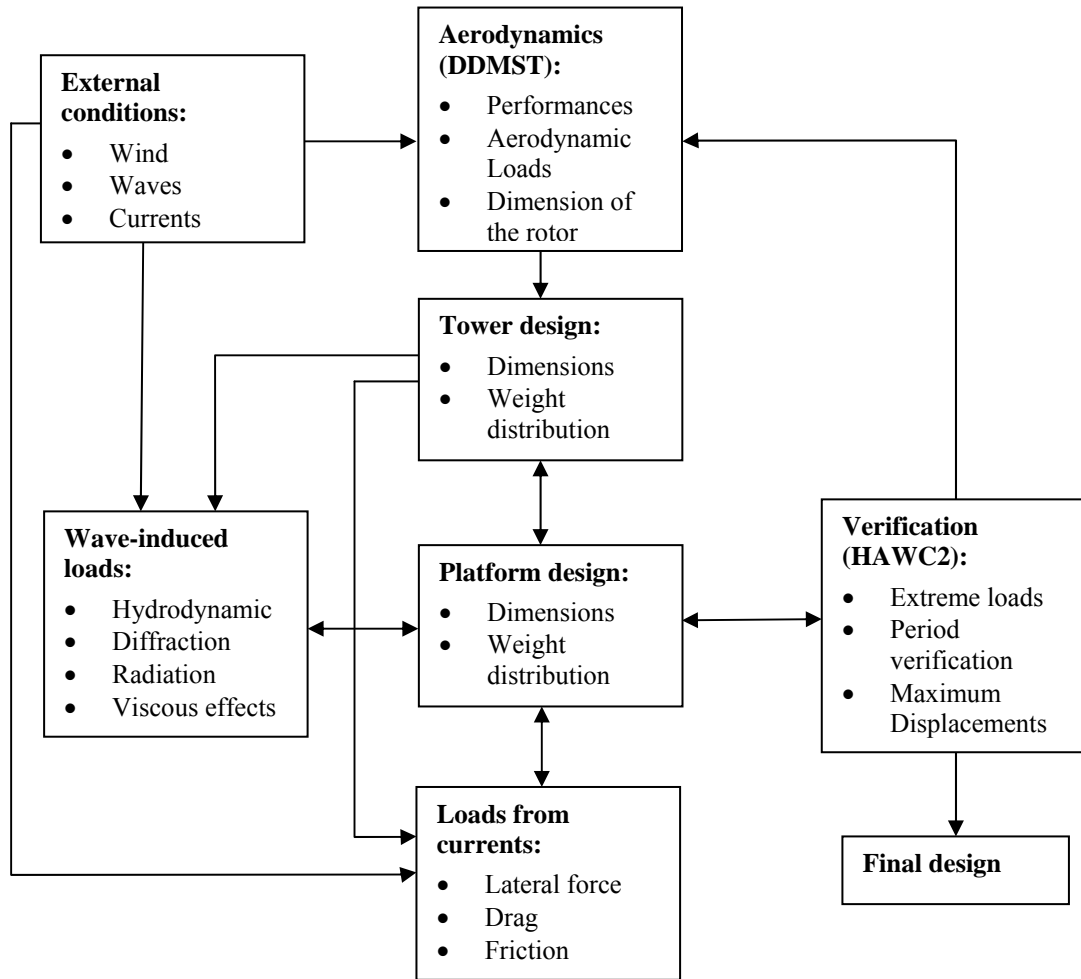


Figure 5 Design layout

2 DeepWind concept

2.1 Main concept description

This work regards the concept shown in Figure 6 and described in [1]. The design consists of a Darrieus rotor, whose tower is extended underwater, in order to act as a spar buoy. The whole system is rotating and generates power with a generator placed at the tower bottom and fixed at the anchoring system.

The water is working as a rolling bearing, damping the dynamic effects of the bending moment on the turbine.

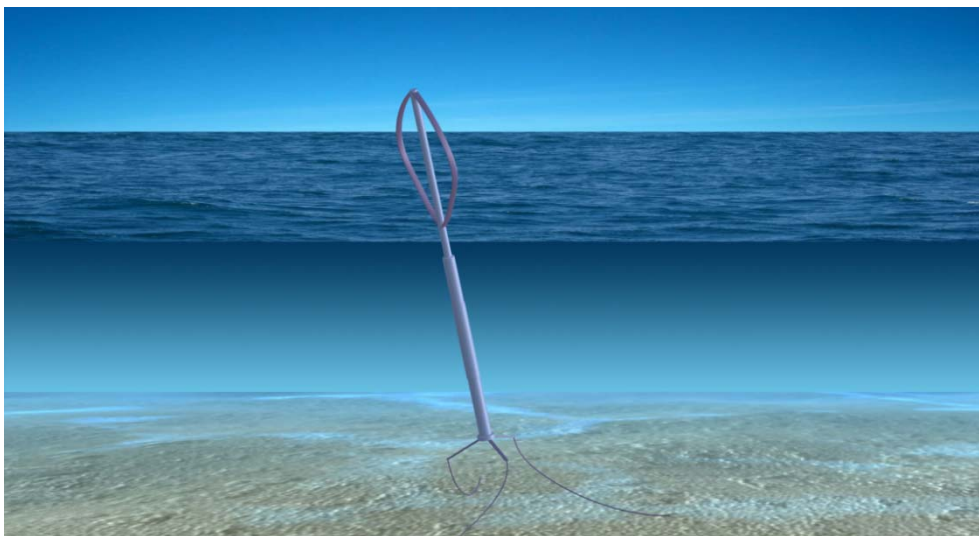


Figure 6 Artistic view of the concept

Before starting the description of the components, a clarification is needed. At the present stage the design of the concept has two purposes: demonstrate the feasibility of the concept and create a baseline model to test technological improvements. Therefore the number of uncertainties in the design has to be limited to the minimum and proven technologies should be used, when possible. This approach will justify most of the technological choices on the components described in the next paragraphs. A similar approach has been used by Hendricks [45] for the design of the baseline 6MW HAWT, included in the DOWEC project.

2.2 Components

2.2.1 Rotor

The rotor is a vertical-axis wind turbine. The Darrieus rotor has been selected among the many design solutions proposed for VAWTs in the past years. The reasons for this choice are:

- The simplicity of the concept design, that is at the basis of the entire design. Darrieus rotor gives better up-scaling potential and it matches with the other components described in the next paragraph (i.e. blades and control system).

- The possibility of using blades with Troposkien shape, which can reduce the bending moment on the blades due to the centrifugal force [9], [20].
- The reasonable efficiency of the Darrieus rotor, rated to C_p around 0.4 and close to the values reached with HAWTs [20].
- The long record of research and development in the past years, as mentioned in Chapter 1. The acquired experience on this rotor can facilitate the feasibility evaluation of the concept.

2.2.2 Blades

The blades for a Darrieus rotor, as in Figure 6, are between two and three times longer than a HAWT of the same rated power [20]. The length can be reduced using straight blades, but then the rotor would additionally need some connection arms. Eventually, curved blades have been selected also considering the possibility of Troposkien shape, as previously mentioned.

The blades for a VAWT are characterized by a simple design and in principle they can be produced with a constant geometry along the length, without tapering. This allows the use of pultrusion for the manufacturing process, that would allow a significant reduction in the costs [46]. The pultrusion process of GRP seems quite promising for large blade profiles, and the material strength of pultruded GRP is much better than for hand layed-up GRP for horizontal-axis wind turbines. Migliore estimates a reduction in the manufacturing costs around 50 and 74%, that would permit to produce blades for VAWTs at competitive cost (compared to blades for HAWTs).

2.2.3 Generator

There are a few solutions to generate power using the torque transmitted to the bottom of the platform. Some solutions are presented in the concept description in [1].

Here I will focus on three solutions using a generator placed in the bottom of the submerged structure.

The configurations are:

- The generator is mounted inside the submerged foundation at the bottom and rotates with the rotor. The shaft is extended through the foundation bottom and fixed to the torque arms, Figure 7-a.
- The generator is mounted outside the foundation and fixed to the torque arms. The shaft is fixed to the torque arms, Figure 7-b.
- The generator is fixed on the sea bed and the shaft is fixed to the rotating structure, Figure 7-c.

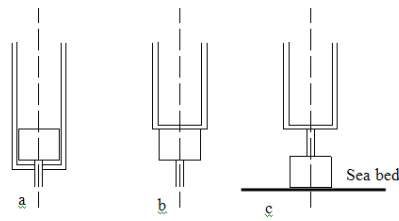


Figure 7 Possible configurations for the generator

Additionally the generator is used for two other tasks:

- it must work as a motor to start the Darrieus rotor, since this kind of turbine is not self starting.
- it has to operate at variable speed to control the turbine operations.

2.2.4 Anchoring

The torque and the thrust are transmitted through the tower to the bottom of the structure. The platform is anchored to the sea bed with a catenary mooring system. The forces are transferred through the mooring lines, but to take the torque two or more rigid arms are necessary, as seen in Figure 8.

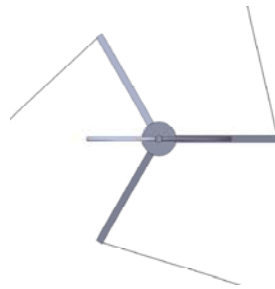


Figure 8 Torque arms to connect the rotor to the anchoring system, dimensions of the arms are exaggerated for visualization

A solution involving other types of anchoring system, such as the tensioned wires proposed by Withee [34], is not suitable due to the high values of the torque to be absorbed. Another limitation regards the point to connect the anchoring system. In a similar concept for HAWTs, i.e. Hywind [30], the mooring lines are attached on the platform above the centre of gravity. In this concept, this is not possible because the platform is rotating and this solution would require a big and expensive bearing. Therefore the mooring lines are attached at the bottom of the platform and they do not give contribution in restoring the turbine in pitch and roll.

When the generator is placed on the sea bed, as in Figure 7-c, the mooring lines are not needed and the torque is transferred directly to the ground.

2.2.5 Safety system

The VAWTs are weaker than HAWTs in avoiding overspeeding conditions. Indeed the most common HAWTs are nowadays pitch controlled and can use aerodynamic brakes in addition to a mechanical system. VAWTs need a big mechanical brake

system at the bottom of the structure, sometimes consisting of two brakes, one on each shaft (low and high speed), [2].

For a floating VAWT, water brakes can be used as overspeeding protection. The system consists of drag devices, deploying from the rotating submerged foundation in case of overspeeding conditions, Figure 9.

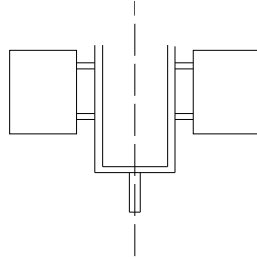


Figure 9 Sketch of the water brakes system

2.2.6 Control strategy

Compared to a HAWT, the rotor does not need a pitch neither a yaw control system. The power control is obtained by rpm control of the rotor speed [17]. Also this solution allows a simple design and it is in principle favourable for up-scaling purposes.

A control based on the rotational speed has also some limitations, bringing severe periodical loads on the generator connection.

2.3 Strategies for installation and operation and maintenance

2.3.1 Installation

The rotor and the foundation can be towed to the site. In case of a two-bladed rotor, the whole structure, without counterweight, can float and lay horizontally on the water line. Counterweight can be gradually added, to tilt down the turbine. In case that the generator is mounted inside the foundation, it can be inserted from the top of the structure. This is a typical installation in O&G industry and it would be more favourable than for HAWTs, because the lower weight at the top of the tower would reduce the bending moment on the structure during the procedure.

2.3.2 Operation and Maintenance (O&M)

Some specific solutions are available for the maintenance of the turbine.

Moving the counterweight from the bottom of the foundation upwards is possible to tilt up the submerged part for service. An outside generator can be serviced and marine growths on the rotor can be removed.

In case of internal arrangement of the generator, it is possible to place a lift inside the tubular structure to have easy access from the top of the turbine to the submerged part.

2.4 Concept potentials

The most obvious advantage of the concept is its simple design. The whole construction is simply a rotor, embedded in and supported by the water itself. Another example of the simple concept is the blades. Rather large blade sections can be pultruded in GRP by production facilities that are indeed rather small. In principle, a production facility can be put on a ship, and the blades can be produced offshore in lengths of kilometres. Otherwise the blade could be manufactured at the harbour avoiding the limitations connected with on land transportation.

Another advantage is in the control system. It needs no yawing system to position the rotor into the wind and no pitching of blades is necessary to regulate power. The Darrieus rotor is stall-regulated at high wind speeds, or the power can be down-regulated by reducing the rotor speed. Over-speeding protection can be made very efficient and small using water brakes.

An advantage of the concept is that the rotor may be tilted by moving the ballast in the tube, during installation and maintenance.

2.5 Specific challenges

In [1], the most important challenges have been pinpointed, which need to be investigated in order to validate the feasibility of the concept.

The rotating tower is subject to hydrodynamic loads, due to the interaction to a waterstream. This will create further limitations in the design and it will overload the submerged structure. Moreover there are some losses due to the friction of the platform in the water. This issue addresses special requirements on the platform maintenance, to control an excessive marine growth.

The advantage that the generator with a high mass may be put in the bottom of the rotor tube generates another challenge. The positioning of the generator in the bottom makes maintenance and exchange of the component very complicated. Methods for lifting up the generator through the tube, eventually in smaller parts, must be developed.

Even though the Darrieus rotor was developed significantly during the 70's and 80's it is still considered a challenge to make blades for this design in a cost-efficient way. The most promising method seems to be pultrusion of GRP in full blade length sections that are bent into the blade shape and glued together.

The most significant tower difference compared to the horizontal-axis wind turbine is that the rotor torque must be absorbed in the sub-sea systems. This may be through the use of torque arms connected to the anchoring system or through drag elements in the water. The torque of the Darrieus rotor varies with the position on the rotation and this varying torque will also have to be absorbed through the anchoring system.

2.6 Methodology for the investigation of the concept and available configurations

The complexity of the floating VAWT suggests the possibility to decompose the investigation in different steps, based on the number of DOF (degrees of freedom). We decided to develop the concept, investigating three configurations with different DOF. The degrees of freedom of the three configurations are summarized in the table below, the yaw motion is not considered because it is in the direction of the rotational speed of the rotor.

Table 3 Degrees of freedom of the three configurations

	Surge	Sway	Heave	Pitch	Roll
1st Configuration (Sea bed configuration)				X	X
2nd Configuration (Fixed torque arm configuration)			X	X	X
3rd Configuration (Mooring fixed configuration)	X	X	X	X	X

2.6.1 First Configuration (Sea bed configuration)

The generator is directly fixed on the sea-bed and the shaft is extended to the sea bottom, as in Figure 7-a. The shaft has two rotational degrees of freedom: it can tilt back and forth and to the sides (pitch and roll).

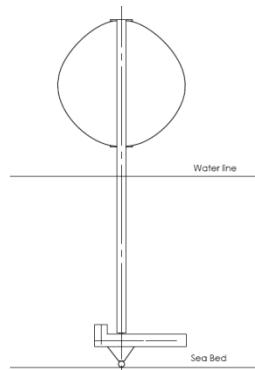


Figure 10 Schematic drawing of the first configuration (sea bed configuration)

This configuration is not fully floating, it has not translational degrees of freedom and the forces are transferred vertically between the rotor and the sea bed. However, the equilibrium in pitch and roll is achieved with the same principle of a moored anchored floating turbine. Also the equilibrium between the buoyancy and the gravity loads is equally necessary, to avoid high loads on the bottom bearings.

The sea bed configuration has been selected to be investigated first, in order to verify that the concept works without serious vibrations and instabilities. Therefore the current work is focused on the study of this configuration.

2.6.2 Second Configuration (Torque arm fixed configuration)

The generator is mounted on a torque arm. Compared to the sea-bed configuration the shaft has one more translational degree of freedom, i.e. it can move up and down (heave).

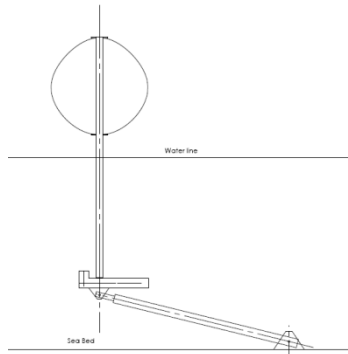


Figure 11 Schematic drawing of the second configuration (torque arm fixed configuration)

This configuration has been selected for next test in Roskilde Fjord.

2.6.3 Third Configuration (Mooring fixed configuration)

Three torque arms are mounted to the generator box. The torque arms are connected to the sea bed by a mooring system. Compared to the previous configuration the shaft has two more translational degrees of freedom (sway and surge).

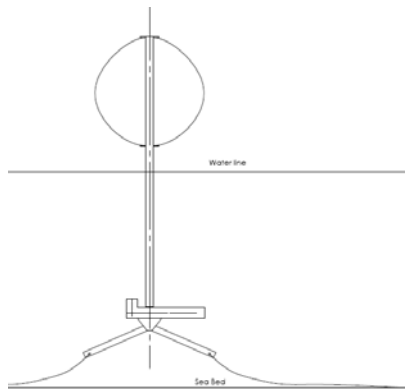


Figure 12 Schematic drawing of the third configuration (Mooring fixed configuration)

2.7 Progress beyond the VAWT state of the art

Blackwell in 1974 [47] pointed out three reasons to prefer VAWTs technology to HAWTs:

1. Independence of the VAWTs operation from the wind direction
2. Generator placed at the bottom
3. Simplicity of the tower construction.

More than 35 years after, those are the same mostly used arguments to bring VAWTs back in the market.

Thus, the question is “why those arguments, which were not good enough forty years ago, should be valid today?”

The goal of this concept is to demonstrate that those arguments can finally make VAWTs competitive, if they are combined with the right new technological development and ideas. In particular, there are two limitations concerning old VAWTs technology, which DeepWind concept aims at overcoming.

The first is the cost of blades that was a serious limitation for VAWT development. The pultrusion process had made strong progresses compared to forty years ago. Its use has already been considered for HAWTs, for the high cost reduction in the production, [46]. So far this solution has been limited by the shape of the blades for HAWTs, which need to be tapered using different airfoils. For VAWTs pultrusion represents an important improvement over one of the most relevant limitations of their design.

The second novelty concerns the use of guy wires or of costly bearings, which were affecting the cost-effectiveness of VAWTs. DeepWind design uses the water as a roller bearing, aiming at preventing severe vibration on the tower and avoiding bearings above the sea water. The idea to use the ocean as a bearing is common to another concept, developed in Sweden⁸, called SeaTwirl. The developer of this other concept claims to have conducted studies at Gothenburg University, proving the feasibility of the use of the water as a bearing.

⁸ <http://seatwirl.com>

3 Loads and dynamics of a floating vertical axis wind turbine

3.1 Formulation of the problem

The design of a floating VAWT is driven by two types of parameters:

- Structural endurance to the loads (ultimate strength and fatigue).
- Dynamic stability of the system, stability of the structure and of the motion (translational and rotational)

In this chapter I introduce the loads acting on the turbine and the corresponding dynamics. A few clarifications are needed:

- I use a simplified model, aiming at having a general insight into the concept and to identify the most relevant parameters for a pre-design of the concept, see Figure 5. I will introduce in the following paragraphs the needed assumptions for the respective simplifications.
- When it is in a water stream, the turbine experiences some specific hydrodynamic loads, due to the rotation of the foundation. Considering the novelty of these loads on a wind turbine, I have chosen to discuss the currents-induced loads in a broader way in a separate chapter (Chapter4). However these loads can be added to the equation of the dynamics as further external loads.

An offshore floating turbine is subject to higher loads than on land. Therefore more robust structures are commonly used to dimension the structure. However the real challenge in the design of these machines is to integrate the rotor design in the project of the floating platform. The sketch in Figure 13 shows the different aerodynamic and hydrodynamic loads acting on the system. The reaction forces of the anchoring are not included in the figure and I will not consider them in my further discussion.

The met-ocean conditions are described using the concept of sea state. A sea state is a statistical description of the met-ocean conditions at a site with respect to waves, and it is described with the significant height H_s , the peak period T_P and the power spectrum. Joint description of currents and wind can be added to the sea state. The sea state varies with the time, but in the formulation I will use in the next sub-chapters, the sea state is supposed to be a stationary random process. This is a reasonable assumption for the relative short periods used for averaging statistical met-ocean data (i.e. one hour) and for the length of the time series of steady state numerical simulations.

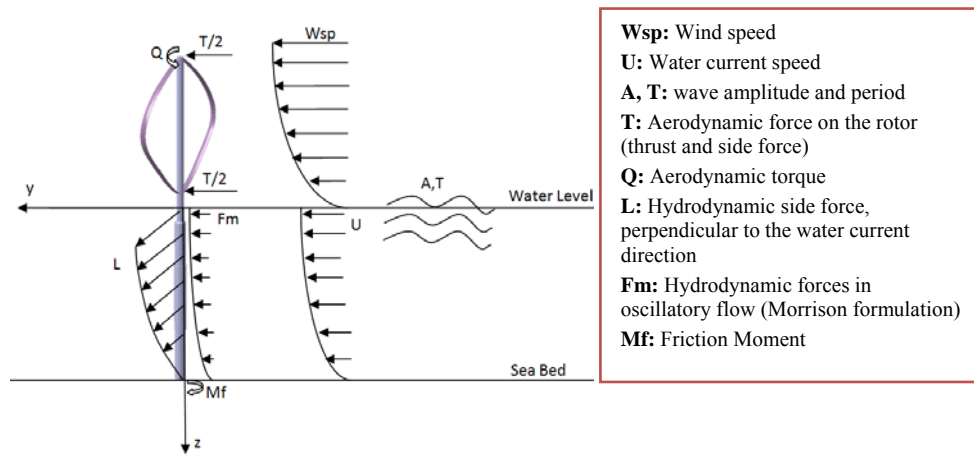


Figure 13 Simplified sketch of the loads acting of the floating VAWT. Magnitudes and directions are not fully indicative of the real loads. Wind speed is defined along the y-axis

In this chapter, I consider the floating turbine as a rigid body having six degrees of freedom, corresponding to the three rigid translations and three rigid rotations, respect to the three axes. The six types of motion are described in Figure 13 and Table 4. As emphasized in Table 4, the most critical motions for a SPAR platform are the displacement on the z axis (heave) and the rotational modes around the x and y axis (pitch and roll).

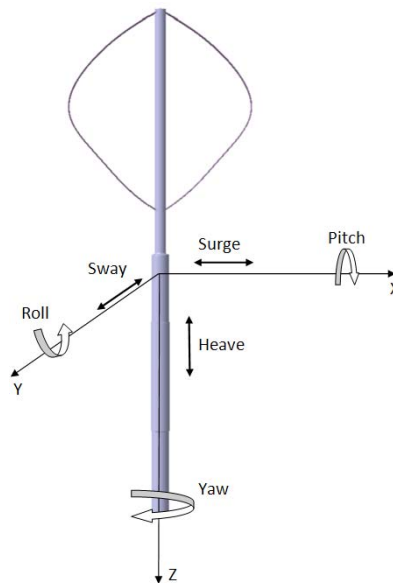


Figure 14 Degrees of freedom for a floating VAWT

In other references, as [27], the pitch motion is described as the motion around the y-axis. My choice is to select the pitch as the motion generated by the aerodynamic thrust (the wind direction is selected on the y-axis in the numerical solver).

The z-axis is often pointing upwards in other studies, also this choice is made to be consistent with the reference system of the numerical solver.

Table 4 Definition of the DOF of a floating VAWT

Index	DOF	Displacement		Critical for spar system
1	Surge	η_1 , translation on the x axis	[m]	No
2	Sway	η_2 , translation on the y axis	[m]	No
3	Heave	η_3 , translation on the z axis	[m]	Yes
4	Pitch	η_4 , rotation around the x axis	[degrees]	Yes
5	Roll	η_5 , rotation around the y axis	[degrees]	Yes
6	Yaw	η_6 , rotation around the z axis	[degrees]	No

A floating body has three main types of motion

- Wave-induced motion: Induced by the hydrodynamic loads in an oscillatory flow, as I will discuss accordingly to the linear potential theory and the Morison's formulation.
- High frequencies motion: it mainly occurs at resonance conditions. It is a common design procedure, to dimension the structure in order to have natural periods out of the range of dominant wave frequencies. However resonance conditions can occur to the second order non linear wave conditions
- Drift motion: it consists of the translational motion (main drift) and its second order components (slow-drift). It can be generated by external loads, such as from wind and currents, or by second order non linear effects.

In chapter 3 I only consider the wave-induced motion, disregarding non linear effects and supposing the displacements of the turbine to be small.

Apart from the waves, the other external loads acting on the turbine (i.e. aerodynamic and water currents loads) will be added as further external loads in the equation of the motion. The problem will then describe the *wave-induced motion of a floating VAWT, subject to aerodynamic and current loads.*

3.2 Aerodynamic loads on a two bladed VAWT

I consider the aerodynamic loads on the turbine, as the total aerodynamic forces and moments acting on the tower. In this simplified model, I will disregard the inertial loads deriving from the centrifugal force.

All the aerodynamic loads on a VAWT are periodical, as shown in the VAWT introduction in Chapter1. The amplitudes and the periods of the oscillations depend on the number of blades. A three bladed rotor is characterized by more regular loads and lower periods. The plot of the thrust force on the tower presents three low and quite broad peaks in a revolution.

On the opposite, the thrust produced by a 2 bladed rotor has 2 high and sharp peaks per revolution. In this chapter I will consider the aerodynamic loads from a 2 bladed rotor, following the design of chapter 2.

The basic aerodynamic loads to dimension a VAWT are:

- The longitudinal force in the wind direction (thrust) T_y :

$$T_y = T_{ymean} + |\sigma_{T_y}| \cos(2\pi f_{2p} t)$$

T_y is the component of the aerodynamic force in the y direction σ_{T_y} is the variation in a revolution, f_{2p} is the half rotational frequency of the rotor (corresponding to the period needed for a blade to cover an arch of 180 degrees), $f_{2p} = \frac{\omega}{\pi}$.

- The transverse force perpendicular to the wind T_x :

$$T_x = T_{xmean} + |\sigma_{T_x}| \cos(2\pi f_{2p} t)$$

- The torque

$$Q = Q_{mean} + |\sigma_Q| \cos(2\pi f_{2p} t)$$

For a two bladed rotor, which is the design considered in this work, the following applies:

$$T_{ymean} \gg T_{xmean}$$

$$T_y \sim |\sigma_{T_x}| \sim |\sigma_{T_y}|$$

$$Q_{mean} \sim |\sigma_Q|$$

Where \sim indicates the same order of magnitude.

These equations express a useful approximation, describing the relevance of the periodical components, in the loads on a 2 bladed VAWT.

The aerodynamic forces can be divided in two halves and applied on the rotor as in Figure 13, generating a moment M_b on the tower, having its maximum value on the cross section at the mean surface level. These loads are useful here, to define the external loads in the equations of the motion of the floating body.

Additionally the loads are used to calculate the maximum stress on the turbine. Compared to a HAWT, the tower of a floating VAWT is subject to a lower stress from M_b , $\sigma = \frac{M_b R_T}{I_P}$, due to the lower height of the centre of the rotor. On the other hand the tower is loaded with an additional torsion moment, generated from the reaction of the generator, corresponding to a stress $\sigma = \frac{Q R_T}{I_P}$ on the external surface of the cylinder. (With R_T external radius of the tower, I_P polar moment of inertia of the section and σ stress on the surface of the tower).

3.3 Wave-induced loads

3.3.1 Formulation of the problem and assumptions

There are different possibilities to investigate the steady-state wave-induced loads on a floating body. Here, I use the academic theories based on a frequency-domain approach and I write the resulting equations in the time domain. A more detailed description of these theories can be found in [41], [27] and [48]. An alternative approach to the wave-induced problem is reported by Jonkman [31], where he described the “true linear hydrodynamic model”.

All the references above use the linear theory of the wave propagation to solve the equations of the motion of the floating body. This means that the loads and the motions induced by the waves are proportional to the wave amplitude, ζ_a . This assumption is acceptable for sea states far from the breaking wave limit, i.e. for ζ_a/λ_w sufficiently small, where λ_w is the wavelength.

Under the linear theory it is possible to apply the superposition of the effects. The hydrodynamic loads on a platform in oscillatory flow (excluded the loads due to currents) are then composed of three contributions:

- Hydrostatic loads, which are present independently from the waves and consisting of the buoyancy and the restoring terms (excluded the restoring from external forces, such as the reaction force of the mooring lines).
- Diffraction loads, corresponding to the loads on the body, when this is supposed to be fixed in an oscillatory flow. They consist of scattering wave loads and the Froude-Krylov force and moment.
- Radiations loads, due to the waves irradiated from the body, when the body itself is forced to oscillate (in each of the six DOF) in steady water at the same frequency of the exciting waves. They are composed of added mass (inertial) and damping (viscous) loads.

In my simplified model, I calculate the diffraction and radiation loads using the potential theory. Then to estimate the viscous terms, disregarded by the potential formulation, I use the Morison's equation.

3.3.2 Regular waves and statistical description

Some additional assumptions are necessary to apply the potential theory: the fluid is supposed to be inviscid and incompressible and the motion is irrotational. Under these conditions it is possible to find a velocity potential function Φ , that satisfy the

Laplace equation:
$$\frac{\partial^2 \Phi}{\partial x^2} + \frac{\partial^2 \Phi}{\partial y^2} + \frac{\partial^2 \Phi}{\partial z^2} = 0.$$

A velocity potential is obtainable imposing four boundary conditions: the body surface is supposed to be impermeable, imposing the normal velocity equal to zero; the same conditions is applicable at the sea bottom equalizing the vertical velocity to zero; the water pressure at the sea surface is equal to the atmospheric pressure (free surface dynamic condition) and the fluid particle on the free surface will continue to belong to the same surface ($\frac{D(z-\zeta_a)}{Dt} = 0$, kinematic free surface condition).

It is possible to demonstrate, [41], that a solution of Laplace equation that satisfies the four conditions is:

$$\Phi = \frac{g\zeta_a}{\omega_w} e^{-kz} \cos(\omega_w t - kx) \quad \text{Eq.1}$$

Where $k=2\pi/\lambda$ is the wave number and ω_w is the circular wave frequency; the waves are propagating in the x direction and the z axis is oriented downwards, as in Figure 14. Here, the water depth is considered infinite, Φ represents the potential function of a two-dimensional plane progressive regular wave system, propagating along the positive x direction with the surface elevation described by the equation:

$$\zeta = \zeta_a \sin(\omega_w t - kx)$$

For finite water depth (h), the equation Eq.1 becomes:

$$\Phi = \frac{g\zeta_a}{\omega_w} e^{-kz} \frac{\cosh(-z+h)k}{\cosh kh} \cos(\omega_w t - kx), \text{ with } k \text{ satisfying the identity}$$

$$\frac{\omega_w^2}{g} = k \tanh kh$$

Integrating the potential function, it is possible to derive the equation of the free surface ζ , the velocity and the acceleration of the water particles and the dynamic pressure p_D .

The description of random irregular waves is achievable by superimposing multiple regular waves. The free surface of an irregular wave propagating on the x axis is obtainable by superimposing the amplitudes of N regular waves:

$$\zeta = \sum_{j=1}^N \zeta_{aj} \sin(\omega_{wj} t - k_j x - \varphi_{0j}),$$

With φ_{0j} the phase angle of the j wave.

The values of each amplitude ζ_{aj} are related to the wave spectrum at a particular site. The most used wave spectrum is the JONSWAP (Joint North Sea Wave Project), [48]. The IEC standards for offshore wind turbines [49], recommends the following formulation for the JONSWAP spectrum:

$$S(f_w) = 0.3125 H_s^2 T_p \left(\frac{f_w}{f_p}\right)^{-5} \exp\left(-1.25 \left(\frac{f_w}{f_p}\right)^{-4}\right) (1 - 0.287 \ln \gamma) \gamma^{\exp\left(-0.5 \left(\frac{f_w - 1}{\sigma}\right)^2\right)}$$

In the formula, f_p and T_p are respectively the peak wave frequency and period, H_s is the significant wave height, f_w the wave frequency, γ is a shape parameter defined in the standards depending on the sea state and σ is a parameter varying with the wave frequency.

For γ equal to 1, the equation above describes the Pierson-Moskowitz (PM) spectrum. This has a lower and broader peak compared to the JONSWAP spectrum. The standards recommend that PM spectrum is used for fatigue calculations and the JONSWAP to evaluate extreme sea states, as well for shallow water sites.

Eventually the IEC standards gives also indications on the calculation of the zero crossing wave periods, to evaluate the range of the significant wave periods, in which resonance is likely to occur [49].

In open-sea conditions, it is commonly used, as range of significant waves, the frequencies interval between:

$$0.04\text{Hz} < f_w < 0.2\text{Hz},$$

Corresponding to the periods:

$$5\text{s} < T_w < 25\text{s}.$$

3.3.3 Hydrostatic loads

The hydrostatic loads consist of the restoring terms, which are proportional to the displacement η_i , and of the gravitational loads acting only on the z axis (buoyancy).

$$F_{Hydrostatic,i} = -\delta_{i3}\rho_w V g - C_{ij}\eta_i \quad i = 1,6 \quad j = 1,6$$

δ_{i3} is the Kronecker-Delta function, ρ_w is the density of the water, V the displaced volume of water without considering the effect of displacement η_i , C_{ij} are the terms of the restoring matrix. The first right-hand term in the equation above is the buoyancy of the body without considering the displacements η_i of the body itself. As argued by Jonkman [31], this term is often disregarded, because it is equalized by the total weight of the structure and the anchoring system. Nevertheless to catch the dynamics of the system it is important to evaluate the relative positions of the centre of gravity and the centre of buoyancy. Therefore it is a good practice to decouple the two centers. Moreover from a design aspect, the vertical equilibrium is not given, instead it is an important parameter to adjust during the iterative design process.

The second right-hand side terms are the loads originated by the change in the hydrostatic forces and moments, subsequently to the rigid displacement η_i of the platform.

For an axial symmetric body (i.e. a cylindrical platform) the matrix has only five terms not null [27], [31]:

$$C = \begin{pmatrix} 0 & 0 & 0 & 0 & 0 & 0 \\ 0 & 0 & 0 & 0 & 0 & 0 \\ 0 & 0 & \rho_w g A_w & 0 & -\rho_w g \iint_{A_w} x ds & 0 \\ 0 & 0 & 0 & \rho_w g V(z_B - z_G) + \rho_w g \iint_{A_w} y^2 ds & 0 & 0 \\ 0 & 0 & -\rho_w g \iint_{A_w} x ds & 0 & \rho_w g V(z_B - z_G) + \rho_w g \iint_{A_w} x^2 ds & 0 \\ 0 & 0 & 0 & 0 & 0 & 0 \end{pmatrix}$$

Where, z_B and z_G , represent respectively the position on the z axis of the centre of buoyancy and of gravity.

The terms in the matrix are:

- C_{33} is the buoyancy, as argued above.
- $C_{53}=C_{35}$ is the restoring moment of the coupled motion heave-roll, due the action of the water plane area.
- C_{44} and C_{55} are the restoring terms in pitch and roll. They are composed of two terms. A moment generated by the relative positions of the centre of gravity and the centre of buoyancy; another moment related to the water plane area. For platform with $L \gg A_w$, such as a SPAR buoy, the first term is dominant over the second.

3.3.4 Radiation loads

A system of radiating waves is created by the forced oscillations of the floating body in still water. The loads on the body generated by these waves are the radiation loads:

$$F_{Radiation,i} = -A_{ij} \frac{d^2 \eta_i}{dt^2} - B_{ij} \frac{d\eta_i}{dt}$$

An exact derivation of the equation of A_{ij} is described by Jonkman in [31]. Here, I will refer to the engineered methods introduced in other references [27], [41].

Since these loads are generated by the oscillation of the body, A_{ij} and B_{ij} are dependent on the body shape and on the frequency of the oscillations.

In this paragraph I disregard the terms B_{ij} and I will consider the viscous effect using the Morison's formulation.

To calculate A_{ij} , the most used method is the strip theory. This consists of integrating the 2d coefficients A_{ij}^{2D} , calculated for a cross section, along the main length of the body (i.e. the platform length for a SPAR). Newman reports the 2D coefficients of added mass for the most common cross sections [41]

3.3.5 Diffraction loads

These are the loads acting on the platform, when it is considered fixed. They are composed of two terms:

- The Froude-Krylov force, which are the loads generated by the undisturbed pressure field, as calculated from the wave potential theory.
- The loads from wave diffraction, caused by the perturbed pressure field.

From the potential flow, for waves propagating in the x axis, the dynamic pressure of a fluid particle in the undisturbed wave field is:

$$p_D = \rho g \zeta_a \frac{\cosh(-z+h)k}{\cosh kh} \sin(\omega_w t - kx)$$

For a slender structure, whose dimension is smaller than the wavelength (for a SPAR $D \ll \lambda$), the diffraction forces are:

$$F_{diffraction,i} = \iint_{S_l} p_D n_i + A_{i1} a_1 + A_{i2} a_2 + A_{i3} a_3,$$

S_l is the lateral surface of the platform, A_{ij} are the added mass terms as discussed in the former chapter and a_{ij} are the acceleration of a fluid particle according to the potential theory.

3.3.6 Morison's formulation and the viscous loads and damping

Morison found an engineering approximation to express in-line forces induced by the waves on a slender structure, whose diameter is smaller than the wavelength.

Morison's force acts on the direction of the wave propagation and the value dF on a strip dz of a vertical cylinder, is:

$$dF = 0.5\rho_w C_D D |u| u dz + \rho_w \frac{\pi D^2}{4} C_M \dot{u} dz \quad \text{Eq.2}$$

u is the velocity of a fluid particle and \dot{u} is the acceleration.

The first right hand term is the drag force of the radiation problem and C_D is the drag coefficient.

The second right hand term is the inertial force and C_M is the inertia coefficient.

C_M can be expressed as $C_M=1+C_m$, where C_m is the hydrodynamic mass coefficient, that is equal to 1 for circular cylinders [50].

Considering the body moving relative to the flow with velocity u_r , the in-line force on a strip dz is:

$$dF = 0.5\rho_w C_D D |u - u_r| (u - u_r) dz + \rho_w \frac{\pi D^2}{4} C_m (\dot{u} - \dot{u}_r) dz + \rho_w \frac{\pi D^2}{4} \dot{u} dz$$

The last two right hand terms correspond to the hydrodynamic mass force and the Froude-Krylov force as discussed in the potential flow theory.

The non dimensional coefficients C_M and C_D can be related to some characteristic parameters of the platform. The most important values to consider to estimate C_M and C_D are:

$$\text{Keulegan-Karpenter number: } KC = 2\pi \frac{\zeta_a}{D}$$

$$\text{Reynolds number: } Re = \frac{UD}{\nu}$$

$$\text{Re/KC: } \beta = \frac{D^2}{\nu T}$$

The dependence of the Morison's coefficients has been largely investigated and it is reported in books [27], [41] and [50]. For instance, the dependence of KC states the existence of two regimes.

At $0 < KC \ll 20-30$, the inertial term of the equation Eq.2 is dominant and the cylinder is in an inertia-dominated regime.

At $KC > 20-30$, the wave amplitude is much larger than the characteristic length of the body and the fluid separate from the body's boundary. At this conditions it is

possible to observe a rapid decrease of the inertial term (inertial crisis) and the cylinder is in a drag-dominated regime.

Another important parameter is the ratio λ_w/D and, for $\lambda_w \gg D$, the first term of equation Eq.2 corresponds to the wave-induced loads calculated with the potential theory.

3.4 Equation of motion and natural periods

Applying Newton's second law and considering the loads mentioned so far, it is possible to write the equation of the motion for a floating body:

$$F_i e^{-i\xi t} = \sum_{k=1}^6 \left[(M_{jk} + A_{jk}) \frac{d^2 \eta_k}{dt^2} + B_{jk} \frac{d\eta_k}{dt} + C_{jk} \eta_k \right] \quad (i = 1, 6)$$

The left hand term is the complex amplitude of the external exciting force, i.e. the wave-induced loads. M_{ij} are the terms of the mass matrix that, considering again the symmetry around the plane x-z, is equal to:

$$M = \begin{pmatrix} M & 0 & 0 & 0 & Mz_G & 0 \\ 0 & M & 0 & -Mz_G & 0 & 0 \\ 0 & 0 & M & 0 & 0 & 0 \\ 0 & -Mz_G & 0 & I_x & 0 & -I_{xz} \\ Mz_G & 0 & 0 & 0 & I_y & 0 \\ 0 & 0 & 0 & -I_{xz} & 0 & I_z \end{pmatrix}$$

The other terms A_{ij} , B_{ij} and C_{ij} are respectively the added mass, damping and restoring coefficients.

By imposing for the displacements: $\eta_i = \check{\eta}_i e^{-i\xi t}$

And $A_{ij} = M_{ij} = B_{ij} = C_{ij} = 0$ for $i \neq j$

Dividing by $e^{-i\xi t}$, one obtains a system of six equations in the real numbers domain:

$$(A_{ii} + M_{ii}) \frac{d^2 \check{\eta}_i}{dt^2} + B_{ii} \frac{d\check{\eta}_i}{dt} + C_{ii} \check{\eta}_i = F_i \quad (i = 1, 6) \quad \text{Eq.3}$$

The simplifications above can be justified with the following additional assumptions:

- The floating body oscillates at the same wave amplitude and frequency at every instant
- The coupled effects are disregarded. In case of spar buoys this means in particular not to consider the coupling of the pitch-heave and pitch-roll motions. Once again, I emphasize that I use this simplification only in the simplified model for a pre-design of the platform. The coupled motions are fully taken into account in the aero-elastic simulations with HAWC2.

From equation Eq.3, it follows that the equation of the natural periods, for an undamped floating body, is:

$$T_{ni} = 2\pi \sqrt{\frac{M_{ii} + A_{ii}}{C_{ii}}} \quad \text{Eq.4}$$

4 Loads from a water stream passing the rotating platform

4.1 Loads on a rotating cylinder in a water stream, previous studies

In this chapter I present my studies on the loads on the rotating platform in a water stream. Most of the results are included in the paper [42].

These hydrodynamic forces occur due to the water currents and to the relative motion of the platform. A cylindrical structure rotating in a fluid experiences two forces (lift and drag) and one moment (friction). The two non-dimensional parameters governing the physics of the problem are: the Reynolds number ($Re = DU/\nu$) and the ratio of the peripheral speed and the free stream speed ($\alpha = \omega D/2U$). Where U is the water stream velocity, D the diameter of the cylinder, ω the rotational speed and ν the kinematic viscosity of the water.

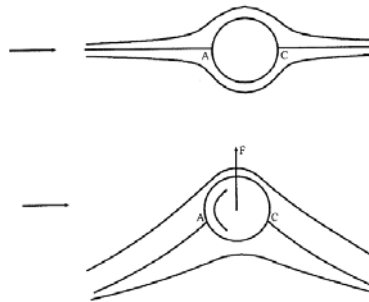


Figure 15 Genesis of the lift force on a rotating cylinder, from [51].

The lateral force (lift) acting on the rotating cylinder is also known as Magnus effect and it can be seen as a direct consequence of the Kutta-Joukowski formulation of the lift force (see Figure 15):

$$\bar{F}_l = \rho_w \bar{U} \times \bar{k} \Gamma$$

\times is the vector cross product, \bar{F}_l is the lateral force per unit length, \bar{U} is the waterstream velocity vector, \bar{k} is the unit vector perpendicular to the plane of the motion, Γ is the circulation around the cylinder. For a section of the cylinder the circulation is:

$$\Gamma = \int \bar{u} d\bar{s}$$

Γ is the integral of the scalar product between the vector \bar{u} (water velocity at the edge of the cylinder boundary layer) and the vector \bar{ds} (element of the lateral surface of the cylinder). If the cylinder is in still water, the circulation is null and there is no force on the cylinder. When the cylinder starts spinning in a viscous fluid, the viscosity creates a circulation around the cylinder and a lateral force on the surface of the cylinder:

$$\bar{F}_l = \rho_w (\bar{U} \times \frac{\bar{\omega}}{\omega} \int \bar{u} \bar{ds})$$

The magnitude of the vector \bar{F}_l per unit length can be written as proportional to the dynamic pressure:

$$F_l = 0.5 \rho_w U^2 D C_l$$

Where D is the diameter of the cylinder and C_l is the no-dimensional lift coefficient.

The first studies on a rotating cylinder were carried out by Prandtl [52]. He stated that the C_l increases linearly with α until an asymptotic value, i.e. $C_{lMax}=4\pi$, that results from integrating the pressure around the cylinder when the two stagnation points on the cylinder are coincident. In the last 50 years many numerical, theoretical and experimental studies have been carried out, as well summarized by Mittal [53] and Padrino [54].

Unfortunately most of the studies are numerical simulations at low Re ($<10^3$) and low α . The typical Reynolds values for DeepWind's platform are greater than 10^6 . The first numerical study was made by Glauert [55], who solved the two dimensional Navier-Stokes equations. Glauert's results show that the lift increases linearly and indefinitely with α , exceeding the limit of Prandtl. Other studies show different results: Chew [56] confirms in his numerical studies the results of Prandtl; however the experiments by Tokumaru [57] and the numerical model by Mittal [53] show a value of the lift higher than the limit of Prandtl, even if an asymptotic value is observed as well. The value of α when the vortex shedding ceases and the lift tends to an asymptotic value is called α_L limit (α_L). The value of α_L depends on Re. For very low Re ($Re < 160$) this value is a logarithmic function of Re, for $Re > 10^3$ it seems to be constant, i.e. $\alpha_L = 2$ [53].

Some numerical results at higher Re ($10^4 < Re < 10^6$) are presented by Chang [58]. The stopping of vortex shedding is shown and the C_l seems to decrease at high Re. Unfortunately, the numerical simulations at high Re are very limited in time because of convergence problems and it is not possible to predict a fully developed regime.

The boundary layer around a rotating cylinder is described by Padrino [54] and Wang [59] for $Re < 1000$. The friction torque coefficient is reported and it seems to decrease by the Re number. Another possibility to calculate the friction of a rotating cylinder at high Reynolds numbers is shown by Theodorsen in [60].

4.2 Methodology of the study

This study is based on a CFD investigation conducted on a rotating cylinder in a water stream. The diameter of the cylinder and the rotational speeds are consistent with the possible design of a 2MW machine. The simulation is repeated for different rotational speeds, corresponding to the operating conditions of the wind turbine at different wind velocities. The power curve used for this study is in Figure 16, along with the aerodynamic thrust force on the rotor. The dots highlighted in the chart represent the four operating conditions of the rotor presented in this chapter.

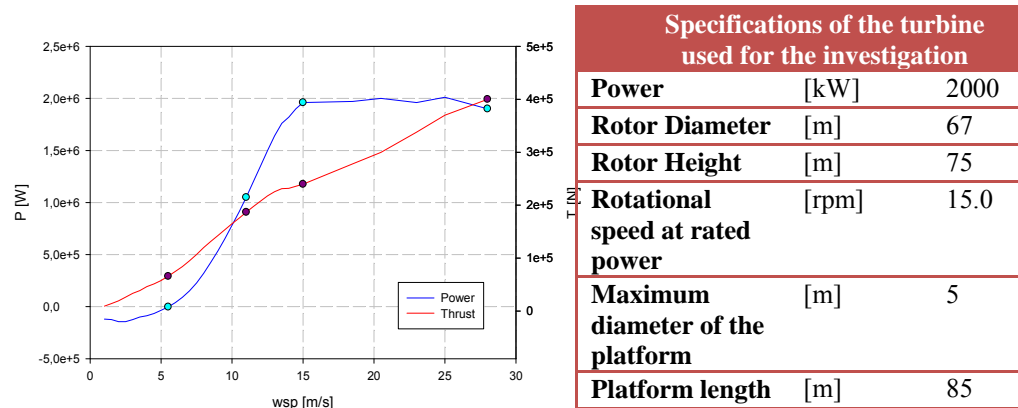


Figure 16 Power curve and Thrust curve. The dots correspond to the conditions considered for the study of the hydrodynamic forces on the structure [42]. In the table on the right, the most relevant properties of the rotor and the platform used for this study

The results are used to calculate the forces and moments acting on the structure at different operating conditions and the friction losses in terms of percentage of the nominal power.

All the computations are carried out with the EllipSys2D pressure based incompressible Reynolds averaged Navier-Stokes flow solver written by Michelsen [61,62] and Sørensen [63]. The code uses the finite volume method, solving for the primitive variables u , v , w , and p , in general curvilinear coordinates. The variables are stored in a collocated grid arrangement, and odd/even pressure decoupling is avoided using the Rhie-Chow interpolation.

The iterative PISO algorithm is used to advance the solution in time using a second-order accurate scheme. The convective terms are discretized using the Quadratic Upstream Interpolation for Convective Kinematics Scheme, QUICK, and the viscous terms are discretized using central differencing. The momentum equations are solved decoupled from each other using a red/black Gauss-Seidel point solver. To accelerate the convergence of the pressure-correction equation, a multi-grid solution strategy is implemented combined with the additive Schwarz method, where each sub-domain is solved simultaneously. To further accelerate the convergence of the solution, grid and time step sequencing is used.

The simulations were carried out using a combination of steady state and unsteady formulations. Due to the low free stream velocity, convergence was very slow, and

as such the unsteady simulations were started from an initial steady state guess. The time step used in the unsteady simulations was set to $\Delta t=0.01$ s. Fully turbulent flow was assumed over the cylinder using the k- ω SST turbulence model. The mesh corresponding to a y^+ of less than two. The outer boundary was placed 100 cylinder diameters away from the cylinder. The rotational speed was prescribed on the cylinder surface to account for the rotation.

The loads on the cylinder are estimated as 2D coefficients, defined as:

$$C_l(\alpha, Re) = \frac{F_l}{0.5 \rho_w U^2 D}$$

$$C_d(\alpha, Re) = \frac{F_d}{0.5 \rho_w U^2 D} \quad \text{Eq.5}$$

$$C_m(\alpha, Re) = \frac{2M_f}{0.5 \rho_w U^2 D^2}$$

$$\alpha = \frac{\omega D}{2U}$$

F_l , F_d and M_f are respectively the lateral force, the drag and the friction moment acting on a cylinder of unit length, rotating at rotational speed ω in a water stream of velocity U .

F_l is defined positive according to the rules of the vector cross product; F_d is positive when points against the water stream; M_f is positive when it is opposite to the rotational speed of the cylinder.

4.3 Results

The numerical simulations have been carried out at an inflow velocity of 1m/s corresponding to $Re= 5 \cdot 10^6$, based on a 5m diameter.

The calculations are repeated at four operating conditions, corresponding to different rotational speeds. The speed ratios α and the corresponding rotational speeds are listed in Table 5.

Table 5 speed ratios α corresponding to the selected rotational speeds

α	[-]	1.4	2.9	3.9	5.2
ω	[rpm]	5.5	11	15	20

Due to the variation of α (from 1.4 to 5.2) different flow regimes are expected around the cylinder at different operating conditions.

The results and the analysis of the flow regime are reported for the different speed ratios.

$\alpha=1.4$

At the lowest speed ratio, the separated shear layer becomes unstable in the wake which gives rise to some unsteadiness in the lift and drag on the cylinder due to beginning vortex shedding Figure 17. The lift coefficient was found to be equal to 3.99, the C_d to 0.180 and the C_m to 0.0307.

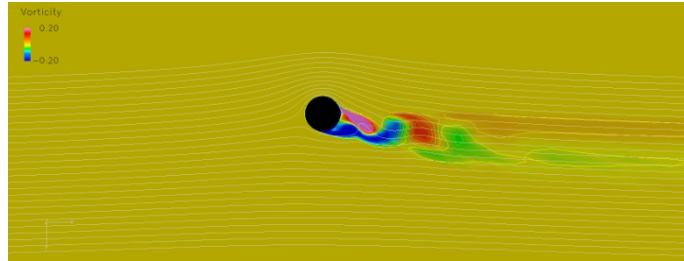


Figure 17 Vorticity contours around the cylinder at $\alpha=1.4$, $U=1\text{m/s}$.

$\alpha=2.9$

The increased rotation delays the separation of the shear layer which causes the flow to be steady in the wake of the cylinder. An approximately linear increase of lift is measured compared to α 1.4 resulting in a C_l of 9.5.

$\alpha=3.9$

This speed ratio is representative of rated power conditions ($\omega=15\text{rpm}$). Due to the relatively high rotational speed, the flow is highly influenced downstream and upstream. The high rotational speed causes the flow to be entirely steady around the cylinder, eliminating vortex shedding which would otherwise be present on a cylinder in this Reynolds number range [48]. This is illustrated in Figure 18 and Figure 19, where the vorticity magnitude and pressure coefficient contours are plotted.

The resulting forces on the cylinder are considerable with a lift coefficient C_l equal to 10.1, corresponding to a total force of 25.2 kN/m, and a drag coefficient $C_d=-0.016$ (40N/m).

C_d is negative, because the drag force changes its direction, and it acts as a thrust on the cylinder. This is an interesting aspect that is new in literature, to my knowledge. Further numerical and experimental investigation would be needed to confirm this effect. Additionally, to the physical relevance of the result, the existence of a negative drag force at rated power conditions, it would mean a negative contribution to the damping of the aerodynamic longitudinal loads.

The friction moment coefficient is equal to 0.013, corresponding to a friction moment per length unit of 324 Nm/m.

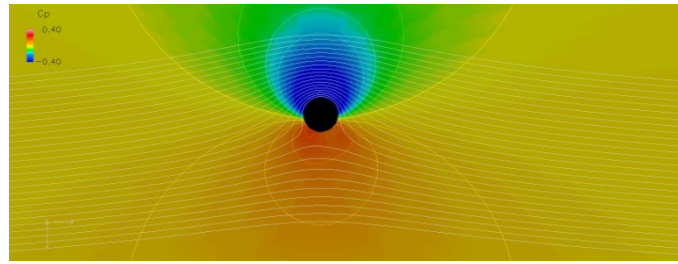


Figure 18 Pressure coefficient contours around the cylinder at $\alpha=3.9$, $U=1\text{m/s}$.

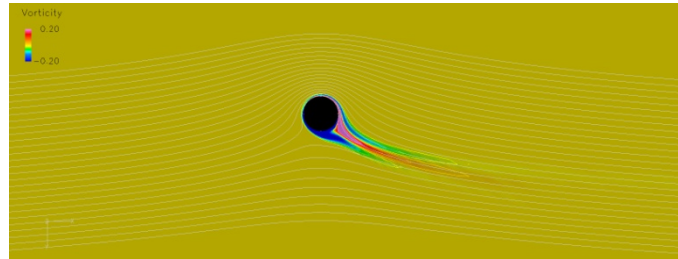


Figure 19 Vorticity contours around the cylinder at $\alpha=3.9$, $U=1\text{m/s}$.

$\alpha=5.2$

At the highest rotational speed, the flow bears the same characteristics as for $\alpha=3.9$ with a slightly increased C_L , the drag is still acting as a thrust and the C_M is the double compared to the previous conditions.

The results in terms of non dimensional coefficients are reported in Table 6.

Table 6 Non dimensional coefficients at different rotational speeds

α	C_L	C_D	C_M
1.4 (5.5rpm)	3.99	0.180	0.0307
2.9 (11rpm)	9.50	0.0009	0.06914
3.9 (15rpm)	10.1	-0.016	0.12973
5.2 (20rpm)	10.4	-0.043	0.2493

4.4 Discussion

In Figure 20, the data of C_L obtained with EllipSys2D at $Re\ 5\ 10^6$ are plotted with the data reported by Tokumaru. The C_L seems to be insensitive to the increasing of the Reynolds number for values of α between 3 and 4. At higher values of α Tokumaru achieves higher values of C_L than EllipSys2D and this can be due to 3D effects. In Figure 20, I also plotted the experimental data from Prandtl [52] and Reid [64]. The data of Tokumaru show a C_L around 10.0 at $Re\ 3.8\ 10^3$. In the experiment of Reid, C_L achieves a value between 9.0 and 10.0 at $Re\ 4.7\ 10^4$. The data from Prandtl underestimate C_L , but that is probably due to the low ratio of the cylinder span and the diameter used in Prandtl's experiment. Numerical computations for $Re < 10^3$ report C_L greater than 10 [54], [55].

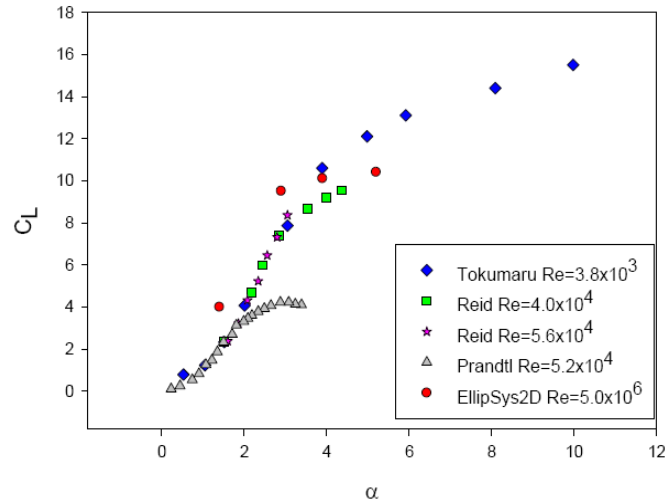


Figure 20 Values of C_l from EllipSys2D at $Re\ 5\ 10^6$ (\circ), from Reid at $Re\ 4\ 10^4$ (\square) and $5.6\ 10^4$ (\star), from Prandtl at $Re\ 5.2\ 10^4$ (\blacktriangle), from Tokumaru at $Re\ 3.8\ 10^3$ (\diamond). Data from [57].

In Table 7, the lift, the drag and the friction moment are reported for length unit. At rated power conditions, a lift of $2.52\ 10^4\text{N/m}$ acts on the submerged foundation.

Table 7 Dimensional loads per length unit, at different rotational speeds

α	Lateral force F_l [N/m]	Drag force F_d [N/m]	Friction moment M_f [Nm/m]
1.4 (5.5rpm)	9950	450	76.5
2.9 (11rpm)	23720	2.2	172.5
3.9 (15rpm)	25148	-41	323.7
5.2 (20rpm)	25860	-106	622

Assuming the current to be constant with the water depth, the total force, integrated over the whole structure would be $2.14\ 10^6\text{N}$, which is almost ten times larger than the value of the aerodynamic force.

At rated power conditions the friction moment per length corresponds to a power of 508W/m . The total power consumption from friction is 43.2kW , corresponding to a friction to the nominal power ratio of 2.2%. The same analysis has been carried out with the data suggested by Theodorsen in [60]. In his data, Theodorsen suggests to compute the friction moment per unit length on revolving cylinders using the formula $M_f = C_f \pi D^4 \omega^2 / 16$, where C_f is the skin friction factor that Theodorsen calculates with an empirical logarithmic formula:

$$\frac{1}{\sqrt{C_f}} = -06 + 4.07 \log_{10} Re \sqrt{C_f}, \quad \text{with } Re = D^2 \omega / 4\nu$$

The C_f results to be $2.22\ 10^{-3}$ at $Re\ 5\ 10^6$ and $M_f = 644\ \text{Nm/m}$. The ratio of friction to nominal power is then 4.3%.

In Figure 21, the data from Thodorsen and from EllipSys2D are compared at the four rotational speeds.

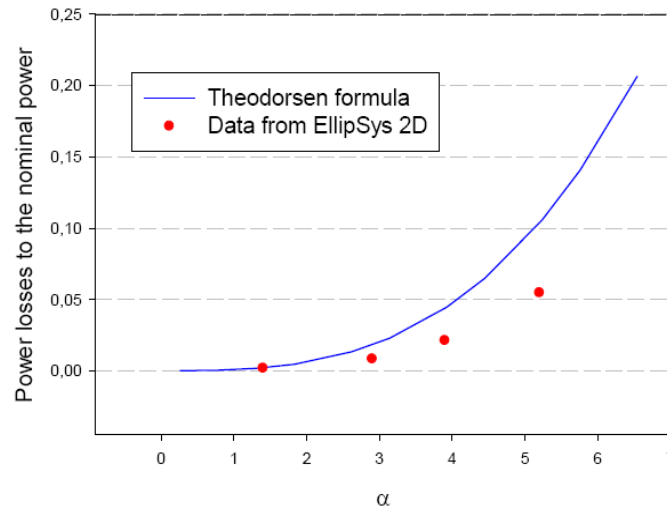


Figure 21 Power losses to the nominal power versus α . The blue line is obtained by using the formula reported in [60] by Theodorsen and the red dots are the values achieved by EllipSys2D.

Both the data seem to follow an exponential fit curve, but the Theodorsen's formula overestimates the friction moment for higher rotational speeds.

In Table 8, the forces and the friction moment acting on the turbine at the four operating conditions are summarized ($U=1\text{m/s}$ is considered). In all the conditions, the thrust is small compared to the lift force acting on the underwater foundation. The power friction is compared to the power production at the same rotational speed and not to the nominal power. The power friction has a maximum of 5.6% during operational conditions. However, for a stall-regulated rotor the rpm must be limited to a constant speed in order to develop the stall. The rotational speed for $\alpha=5.2$ is therefore perhaps overestimated for the operative conditions. On the other hand, the investigation at large values of α was relevant for the study of the Magnus effect, especially to evaluate the trend of C_1 at high α and the sign of C_d .

Table 8 Forces acting on the turbine, power production and power friction at the four operating conditions

α	Hydrodynamic lateral force F_1 [kN]	Aerodynamic thrust T_y [kN]	Hydrodynamic friction [kW]	Mechanical power [kW]	Friction /power [-]
1.4	845.7	65.81	3.71	0.00	/
2.9	2016.2	186.85	16.69	1050	0.012
3.9	2137.6	239.65	43.20	1960	0.022
5.2	2198.1	400.00	109.49	1900	0.056

4.5 Conclusions and suggestions for further investigations

The investigations, carried out in EllipSys2D, show force coefficients consistent with other results at lower Re [57]. At nominal power conditions (at $\alpha=3.9$) a C_1 of 10.1 is achieved when the solution of the flow appears steady.

Vortex shedding was observed only for the lowest rotational speed (at $\alpha=1.4$).

It has to be stressed that from these studies, the hydrodynamic forces are the most important parameters in the design of the concept. Therefore it is important to know the ocean currents before this concept can be applied.

Further investigations have to concern the variation of the forces in both time and space domain. Indeed the results of this paper concern the forces for a 1D inflow stream at $U=1\text{m/s}$. In steady water conditions, the thrust is the larger force acting on the structure.

Shear and turbulence effects need also to be taken into account in the definition of the waterstream velocity and in a 3D flow, the different sections of the platform may additionally be loaded with forces in different directions.

The influence of the rotation on the flow regimes around the cylinder is another aspect needing further investigations. Indeed from CFD computations, at relatively high rotational speed the fluid seems to be attached to the surface of the cylinder and no vortex shedding is observed. This might mean a different dependency of the loads on the structure from the classical non dimensional numbers, i.e. the dependency of C_m and C_D from KC .

The friction moment, acting in the direction opposite to the foundation rotation seems to have a limited effect on the power production, i.e. 2.2% at rated power conditions. A higher value (4.3%) is achieved by using the literature [60].

A negative drag force was recorded at the higher rotational speeds. This is not a constraint for the dimension of the structure but it could affect the damping of the aerodynamic thrust.

However it is stressed that experimental results would be needed to fully validate the numerical results. Unfortunately, to reproduce these types of flow regimes would require a quite complex experimental set up. It should reflect the high Re and the high distortion of the flow around the cylinder, which is expected from numerical simulation. Also, the ratio of the cylinder span to the diameter should be correctly reproduced, as described by Tokumaru in his experimental set up and results [57].

5 Concept scaling

5.1 Possible methodologies

Supposing that we have a baseline design of a concept, then there are at least three possible approaches in looking at the problem of scaling it.

One approach is physical and aims at reproducing the same physical phenomena in different scales. This approach is used for the design of downscaled models and prototypes, in order to investigate the dynamics of the concept baseline design in controlled conditions and eventually to prove the feasibility of the concept itself.

A second way follows a feasibility approach and tries to optimize the concept to make it feasible at different scales. This is the typical procedure to adapt the baseline design to different sizes.

A third possible approach is economical and investigates the mass and economic laws necessary to scale the baseline design. It is commonly used to estimate the cost variation linked to the upscaling of a concept either of a single sub-component.

5.2 Physical scaling of the phenomena: model scaling

The most relevant parameter to scale the physics of floating bodies is the Froude number [48],

$$Fn = \frac{u}{\sqrt{gL_r}} \quad \text{Eq.6}$$

Where g is the gravity acceleration, L_r is the reference length and u is the flow velocity and in case of absence of the currents it is equal to the velocity of a fluid particle in waves. The Froude number is the ratio of the inertial over the gravitational forces and it has to be constant, in order to scale correctly the inertia of a floating system. This condition is equivalent to keep the acceleration of the water particles constant in oscillatory flow.

The geometry of the body can be scaled with a linear function, defining a linear scale:

$$L_s = \Lambda L_b$$

Where Λ is the scale factor, the suffix s stands for *scaled* and the suffix b for *baseline model*. With the length scale factor it is also possible to scale the volume, the area and, considering a uniform density, the mass (see Table 9).

Then from the hypothesis $Fn=\text{const}$ and considering the Eq.6, the scale factor for the time unit is:

$$T_s = \sqrt{\Lambda} T_b$$

Knowing the scale factor of the mass, the time and the length, it is trivial to scale velocity, acceleration, forces and power, as reported in Table 9.

Table 9 Parameters scaled according to $F_n=cost$ and geometry similarity.

	Dimensions	Scale factor
Length	L	Λ
Wave amplitude	L	Λ
Area	L^2	Λ^2
Volume	L^3	Λ^3
Mass	M	Λ^3
Time	T	$\Lambda^{0.5}$
Wave frequency	T^{-1}	$\Lambda^{-0.5}$
Velocity of water particles	$L T^{-1}$	$\Lambda^{0.5}$
Acceleration of water particles	$L T^{-2}$	1
Wind speed	$L T^{-1}$	$\Lambda^{0.5}$
Inertial forces in wave (second term in Morison's equation)	$M L T^{-2}$	Λ^3
Power	$M L^2 T^{-3}$	$\Lambda^{3.5}$

Downscaling the baseline according to these factors, it is possible to reproduce the same inertial forces in waves described in Chapter 3 and summed in the second term of the Morison's equation. Using these scale factors the KC number is also correctly scaled:

$$KC_s = KC_b$$

In order to scale all the terms of the Morison's equation, the drag force also needs to be properly scaled. The coefficient C_D depends on the Reynolds number, which is not constant in this formulation:

$$Re_s = \frac{L_s U_s}{\nu} = \frac{L_s^2 T_s^{-1}}{\nu} = \frac{\Lambda^{1.5} L_b^2 T_b^{-1}}{\nu} = \Lambda^{1.5} Re_b$$

However from literature the Reynolds number seems not to have a relevant influence on the non dimensional parameter C_D and C_M , for Reynolds sufficiently large [48]. Then the factors in Table 9 can downscale the dynamics of a floating body in a wave flow with an acceptable accuracy.

However, the rotation of the body has not been considered yet. The loads calculated in Chapter 4 are dependent on Re and the speed ratio α . Re does not seem to be very relevant, as seen in Figure 20. Instead α has a large influence on the hydrodynamic forces related to the platform rotation.

$$\alpha_s = \frac{\omega_s R_s}{U_s} = \frac{\omega_b R_b}{U_b} = \alpha_b$$

Considering the scale factors of Table 9, the Magnus effect can be scaled considering $\omega_s = \Lambda^{-0.5} \omega_b$.

Using the same scale factors, it is possible to scale also the forces of the wind on the structure: $v_{0s}=v_{0b} \Lambda^{0.5}$.

So far, I showed that it is possible to scale properly all the dynamics of a floating body, i.e. the platform of a floating turbine. In order to scale the whole system, it is still necessary to scale the aerodynamic forces on the rotor. The tip speed ratio, $\lambda = \frac{\omega R}{v_0}$, remains constant with the scale factors defined above, allowing a proper scale of the rotor properties.

However when applied to reality this scaling approach has some limitations:

- This method can be applied only for test in controlled conditions. It is impossible otherwise to find a location which would fulfil all the required scale factors on wind, waves and current characteristics.
- The variation of the wind speed can be very large and eventually unrealistic in dimensioning a small model turbine. Therefore, in order to have a working small model, the wind speed and the rotational speed of the model wind turbine need to be adjusted.
- Changing the rotational speed would affect the proper scaling of the Magnus effect. Therefore, the flow stream velocity would also need a proper adjustment to keep $\alpha = \text{const}$.

This is a good method to study the physics of a full scale machine in a downscaled model, but it is not an option to scale a concept design.

5.3 Feasibility approach: concept scaling

The methodology described above can be useful to study the dynamics of a system with a scaled model and it can give a rough estimation of the full scale design in a new size. However it cannot be used to vary properly the design of a concept. A method with this purpose has to be capable to consider an efficiency factor rather than a length scale. To scale a VAWT rotor, a similarity approach can be used, assuming the efficiency of the rotor not varying in a limited range of Reynolds numbers. Then the maximum C_p of the rotor can be considered constant for a constant tip speed ratio $\lambda = \omega R / v_0$.

If we consider the following equation for the power of the rotor:

$$P = 0.5\rho v_0^3 A_w C_p = 0.5\rho S C_p \frac{\omega^3 R^3}{\lambda^3}$$

And assuming the swept area of the rotor proportional to R^2 ,

$$A_w = \text{const} \cdot R^2$$

Then the power at a fixed tip speed ratio is equal to:

$$P = \text{Cost} \cdot \omega^3 R^5$$

This relationship allows scaling the power of the rotor according to the radius and the rotational speed, for a fixed λ . Other similar formula can be used with the some purpose.

In design scaling, local effects of particular external conditions have to be considered. Examples are the effects of the Reynolds number on the design of small rotors which I will describe later in Chapter 9 and of the gravity in dimensioning blades for large sizes, as it will be discussed in Chapter 8.

The dimension of the platform is depending largely from the site and the location is not necessary scaled as the size. Therefore an appropriate design has to be achieved independently from any scale law.

5.4 Economical and production approach: evaluation of concept upscaling

This approach brings up new issues, such as the choice of the materials and of the manufacture process. Up -scaling studies on HAWTs are present in literature [65] and [66], and also old studies on VAWTs exist [67]. The goal of those studies is to guess the curve of the cost and mass of the components and eventually of the whole wind turbine, based on the technological learning curve and on the selection of a design with the best upscaling potential. I will discuss how this approach can be used to DeepWind in the Chapter 10.

6 Numerical code to investigate the concept

6.1 HAWC2

6.1.1 Structural formulation

For the numerical evaluation of the design, I use HAWC2, an aero-hydro-servo-elastic code developed by Risø DTU. The code is capable to simulate the structural response of a pitch controlled HAWT subject to aerodynamic and hydrodynamic loads, as in [30] and [33]. The core program has a multibody formulation, which in principle gives the possibility to describe any arbitrary geometry, including a VAWT.

The structure of the turbine is described as composed by several bodies, each one with an own reference system. The structural response of each body is implemented with finite element method (FEM), using Timoshenko beam formulation and assuming small deflections within the bodies. The bodies are coupled with algebraic constraints, which allow large rotations and translations. The use of algebraic constraints automatically adds the internal reaction forces and moments on the connected elements. Different constraints are possible, such as fixed relative position, bearings and cardanic joints. More details about code capabilities are described in [38]. Figure 22 represents the multibody formulation in a glance.

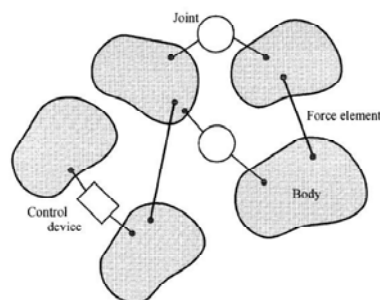


Figure 22 Sketch describing the multibody formulations and the links between the individual bodies, from [38].

The aerodynamic module for a HAWT is implemented with a BEM code but it is not used in this context.

6.1.2 Hydrodynamic module

The hydrodynamic module is part of the core program. The external conditions are implemented, including:

- Regular or irregular waves, according to the linear theory. The JONSWAP spectrum formulation is used for irregular waves, allowing directional spreading. Wheeler profile stretching is used for shallow waters.
- Unidirectional currents can be added. The direction is kept constant with the water depth, while there are a few possibilities to model the water shear profile. In my calculation I use a power law formulation, as I will describe later.

The hydrodynamic wave-induced loads are computed using the Morison's formulation and assuming slender bodies. The coefficients C_D and C_M need to be specified in the main input file for a finite number of sections of the platform.

The axial damping contributions are added at the end of the nodes, while the dynamic pressure is considered as a concentrated force and it is applied at the ends of the nodes and also distributed on conical shaped surfaces.

The hydrostatic loads are considered as concentrated forces and moments due to static pressure distributions and are distributed on the bodies.

6.2 Added DLLs

HAWC2 allows the use of DLLs (Dynamic Link Library) to transfer arrays of data and to apply external forces on specific elements.

I have added some DLLs to make the code capable of investigating the DeepWind concept.

This approach allows some flexibility in adapting and testing the added sub-routines. However there are also some relevant restrictions, such as a large quantity of data to transfer, a larger input file to adapt at each new geometry and longer computation time. A further implementation of some of these DLLs in the main program will make computation more robust and faster.

6.2.1 VAWT aerodynamics

I implemented the aerodynamic loads on the rotor with a BEM code for VAWTs connected to the main program with a DLL link.

The DLL routine takes input data from the main program: the position of the blade and the values of the wind velocity along the rotor height. Then the value of the wind velocity on each blade element is extrapolated.

The output array consists of the aerodynamic loads to apply on each element in the local coordinate system.

Other two external input files contain the geometrical data of the blade elements of the rotor and the aerodynamic coefficients of the airfoils for a given number of Re . It is possible to specify the values of the aerodynamic coefficients in the hysteresis loop, if such data are available.

The DLL routine has a double disk multistream tube (DDMST) formulation, based on the multistream tube model from Strickland [36] and with the double disk modification from Paravischivoiu [20]. The code follows the implementation of the induction calculation in Paulsen [68] at Risø DTU.

The first formulation of the stream tube theory used a single actuator disk and a single stream tube, see Figure 23.

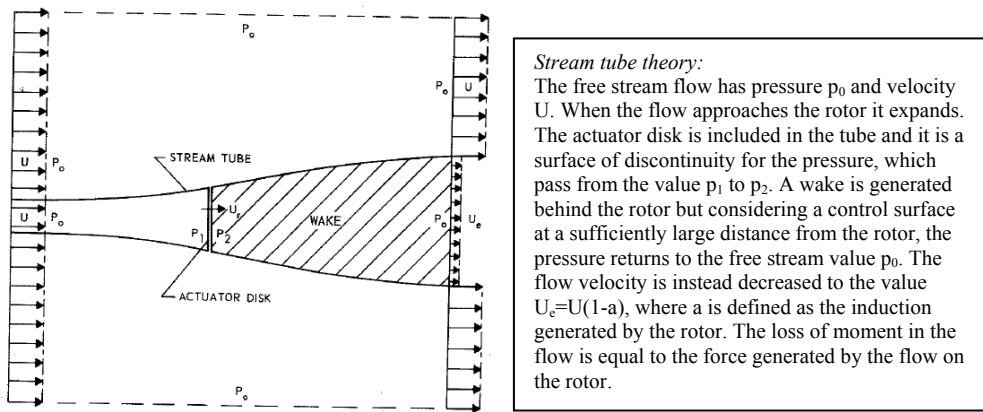


Figure 23 Sketch describing the stream tube theory, from [69].

Strickland improved the model, dividing the rotor in several stream tubes [70]. A further modification from Paravischivoiu consists of using two actuator disks in tandem instead of the single disk used by Strickland [20]. Watching the rotor from the top, the two actuator disks divide the rotor area in two parts, one upstream and another one downstream. Each of the two actuator disks describes a surface of discontinuity and in the output of the first actuator disk is the input velocity for the second one. Figure 24 clarify the physical idea of the model, compared to previous versions. Coupled with the theory of the blade element, this formulation forms a system of independent equations equal to the number of variables.

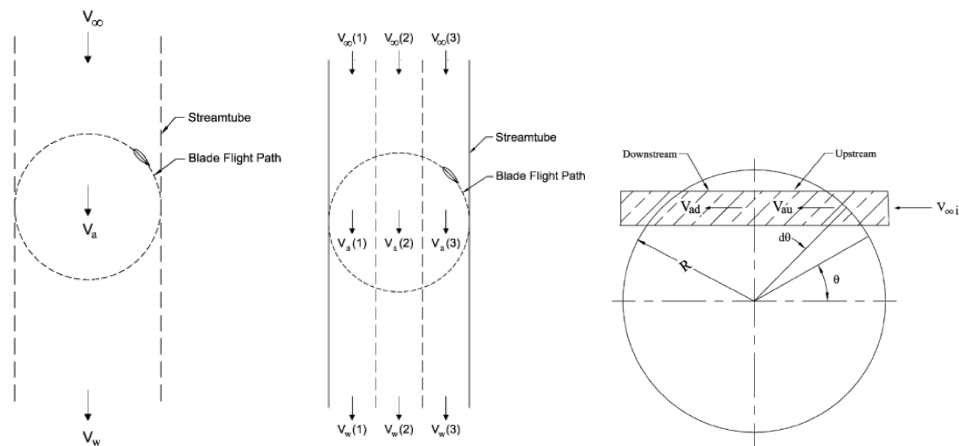


Figure 24 Sketch describing single stream tube theory (left), multi stream tubes theory (centre) and double disk theory (right)

I do not mention here the details on the derivation of the equations, broadly described in [20], but I briefly describe the way the routine is implemented:

- First the relative velocities and angle of attacks are calculated at the azimuthal (orbital) positions of the each element, by vector summation of the wind speed and the relative velocity of the blade element.
- A stream tube with two actuator disks is considered for each element of each blade.
- The induced velocity in the upstream part of the rotor is calculated and it is used to calculate the input velocity in the downstream part of the tube.
- The values of the aerodynamic coefficients, at the local values of Re and angle of attack, are interpolated.

- The total force on the tube is calculated and there is an iteration process to calculate the final values of the induction.
- The tangential and normal forces on the elements are computed and written in output.

Some additional features included in the DLL are:

- For angles of attack larger than the angle of static stall of the profiles, the hysteresis data of the airfoils can be used, if specified in the input.
- The data are interpolated on the Reynolds number to take the variability of the local Reynolds number with the azimuthal angle into account.

One of the most common issues in VAWT code development is the reliability of the airfoils data. I mostly used NACA 0018 profiles and I used different sources to collect airfoils data, depending of the Reynolds number range:

- Risø experimental data on a NACA0018, Paulsen [68]. The data from wind tunnel experiments include hysteresis loop values. The range of Reynolds number is between $5.3 \cdot 10^4$ and $3.96 \cdot 10^5$.
- Sandia data [71], from wind tunnel test on NACA0012 and NACA 0015 at limited range of Re. The data are extended to $10^4 < \text{Re} < 10^7$ and to other symmetric NACA airfoils (0018, 0021, 0025), with the use of an airfoil section characteristics synthesizer computer code.
- TU Trento experimental and interpolated data for NACA 0018 and 0015 in the range $4.14 \cdot 10^4 < \text{Re} < 2.97 \cdot 10^6$.
- Tu Delft data [72], from wind tunnel experiments on NACA 0018 and a cambered airfoil with 20% thickness, i.e. DU 06-W-200. The data are included in the range $3 \cdot 10^5 < \text{Re} < 10^6$.

6.3 Forces on the rotating platform

In this DLL routine I compute the loads on the structure discussed in Chapter 4.

The loads are expressed as functions of non dimensional coefficients, as in Eq.9. As for the aerodynamic coefficients, the hydrodynamic coefficients are tabled in an input file.

The geometry of the platform is given in an input file. From the main program I transfer the water stream velocity at different water depths and the relative speed of each element of the platform.

The water velocity on each element is calculated by interpolation. Adding the relative motion of the tower, I obtain the velocity of the water on the surface of each element.

The lateral force, the in-line force and the friction moment on each element are calculated with the hydrodynamic coefficients from the input tables and transferred in output.

Also for this DLL, the greatest limitation is on the tabled coefficients. Unfortunately, I have, so far, only few data. For small Re ($Re \sim 10^4$), values consistent with the demonstrator 1kW turbine, I use the data from the literature, [57].

For the MW sizes ($Re > 10^6$), there are no data in the literature and I have only very few data from CFD calculations. In this case I disregard the influence of the Reynolds variation and I consider the variation of the coefficients linear with α , for $\alpha < 3$.

The effect of coupling the hydrodynamic lateral force F_L with the aerodynamic loads is showed in Figure 25. Two simulations were run on a floating 2 bladed VAWT (configuration 1 in section 2.6.1), in still water and the results show the motion of the cross section of the platform at the mean water level and the tilt angle ϕ . ϕ is the inclination of the platform with respect to the inertial horizontal plane, measured at the bottom cardanic connection. In my simulations in the next chapters, I use this angle to define the inclination of the platform, rather than the pitch angle or the roll angle. The wind is in the y direction and it is increased linearly from 5m/s to 25m/s.

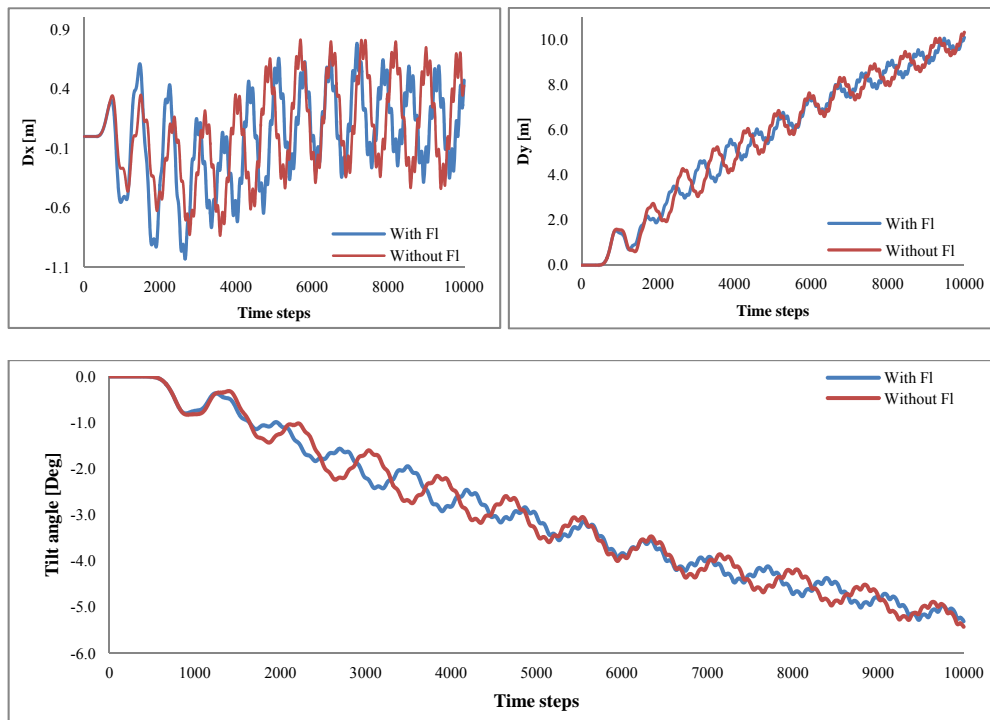


Figure 25 Effect of the Hydrodynamic force F_L , from top left in clockwise order: dx (transverse to wind direction), dy (in wind direction) and the tilt angle for a VAWT running in still water at wind speed $5 < v_0 < 25$ m/s.

In one simulation (red line) the hydrodynamic DLL is disconnected, in the second (blue line) the DLL is connected to the aerodynamic code. The motion of the platform generates a relative velocity between the platform and the still water. Therefore additional hydrodynamic forces act on the platform. At the start the forces are negligible because of the low rotational speed. After 1000 time steps, the turbine rotates fast enough to generate a force on the x axis, caused by the motion on the y axis driven by the aerodynamic thrust. In general the hydrodynamic lateral force generates another strong coupling between the two motions on the x axis and y axis (pitch/roll, surge/sway), already linked by the gyroscopic effects. From Figure 25 more specific observations can be made about the effects of the lateral force on the dynamics:

- The main period of the motion oscillations shrinks, for both the translational motions of the tower section and the tilt angle.
- The amplitude of the oscillations of the tilt angle is slightly reduced and these variations are due to damping by the effect of the hydrodynamic forces.
- The further coupling of the motions of pitch and roll creates another variation over time, which is visible in the chart of dx , where the amplitude of the oscillations is varying during the time.

6.3.1 Generator module

The generator DLL simulates a slip induction generator, based on [73]. A slip model is included, as well as a soft starter. In order to smooth the power output (considering the strong torque ripple of Darrieus turbines), a first order low pass filter is applied on the power output. It is possible to consider the losses in the generator at different values of slip.

All the input data are written in the main input and the output array includes the produced electrical power and the torque on the shaft. Eventually the generator works also as a motor to start the turbine until reaching a rotational speed fixed in input.

6.3.2 Generator control

The turbine can be controlled by regulating the rotational speed of the variable speed generator. I implemented a control based on Sandia's experience on the control of the 17m VAWT [17].

Four rotational speeds and four wind speeds can be specified through the input array. The control varies the rotational speed ω according to the wind speed v_0 and to the input variables.

Since the system has a very large inertia, I considered a limit value for the acceleration of the rotor. Mostly I used a maximum acceleration of 0.1rad/s^2 . When the acceleration is not enough to reach the expected rotational speed, the control is delayed and the turbine runs to a lower rotational speed.

6.4 Fixed setup

There are some values, hypotheses and assumptions which are essential to evaluate the results of the next chapters. Some of these values are common to all the simulations and I report them in this paragraph.

6.4.1 Physical properties

The physical properties of the fluid are kept constant. The values I considered are shown in Table 10.

Table 10 Characteristic of the fluids

Fluid	Kinematic Viscosity	Density
	[m ² /s]	[kg/m ³]
Air	1.51 10 ⁻⁵	1.21
Water	1.31 10 ⁻⁶	1025

During the design and the simulations, I used different materials to describe the components. Their characteristics are listed in Table 11. The properties of aluminium and steel are the most common used in engineering design, in particular for the steel I use the same value used in the Dutch DOWEC project [74]. To describe the properties of the fiberglass in pultrusion, I refer to the values pointed by Migliore and Chaney in their study of feasibility on pultruded blades for HAWTs [46].

Table 11 Properties of the materials used during the simulations

Material	Young Module (E)	G	Density
	[Mpa]	[Mpa]	[kg/m ³]
Steel	2.1 10 ¹¹	8.1 10 ¹⁰	7850
Aluminium	7.0 10 ¹⁰	2.8 10 ¹⁰	2700
Fiber glass	2.07 10 ¹⁰	7.59 10 ⁹	1800

6.4.2 Description of external conditions

Wind

The wind direction is always along the y axis. The vertical wind shear along the z axis is described by the power law:

$$v_0(z, t) = v_0(t) \frac{(-z_0+z)^\gamma}{-z_0} \quad \text{Eq.7}$$

v_0 : reference wind speed at the equator elevation

z : local elevation from mean water level

z_0 : the reference elevation at the half of the rotor height.

γ : power coefficient set to 0.14, as from offshore standard, [49].

The wind speed shear generated in the code is not related to the computed water currents and waves. Tubulence effects are not considered.

Currents

Water currents are computed with the water shear profile described by the equation:

$$U(z, t) = U_0(t) \left(\frac{z+h}{h} \right)^\gamma \quad \text{Eq.8}$$

Where:

z : local water depth

$U(z)$: water speed at local water depth

$U_0(t)$: water speed at the mean water surface

h : water depth

γ : power coefficient set to 0.5.

The direction of the currents is defined in input from the angle β_c , formed by the currents with the wind direction. β_c is positive for currents coming from the right when looking in the wnd direction at default conditions.

Waves

Regular waves are modelled for given ζ_a , T_p and water depth in input. Irregular waves are computed using the JONSWAP spectrum, with the shape parameter γ equal to 3.3.

The direction of the waves is described by the angle β_w , which is defined positive with the same conventions used for β_c .

6.4.3 Model set up

The numerical results included in the next chapters regard the first configuration of the concept (Figure 10), sea bed configuration. To model the floating VAWT I used different bodies:

- A cylindrical tapered tower
- 2 blades with a relative angle of 180 degrees
- A generator box
- A base.

The base is fixed to the sea bed in all the 6 DOF. This element is necessary because it is not possible to anchor the generator at the sea bed with a cardanic joint.

The generator box is instead connected to the base with a cardanic joint, fixing the three translational DOF and the yaw, around the z axis. Then the generator can rotate, with respect to the basement, back and forth and to the sides (pitch and roll).

The tower is fixed to the generator box with a bearing that allows only one rotational degree of freedom, i.e. the yaw around the vertical axis, z.

The blades are fixed to the tower in all the 6 DOF.

6.4.4 Reference systems

The model of the turbine is shown in Figure 26 along with the used reference systems. The base reference system is solidal to the inertial reference system and I neglected in the sketch.

The properties of each coordinate system respect to the inertial one are given in Table 12.

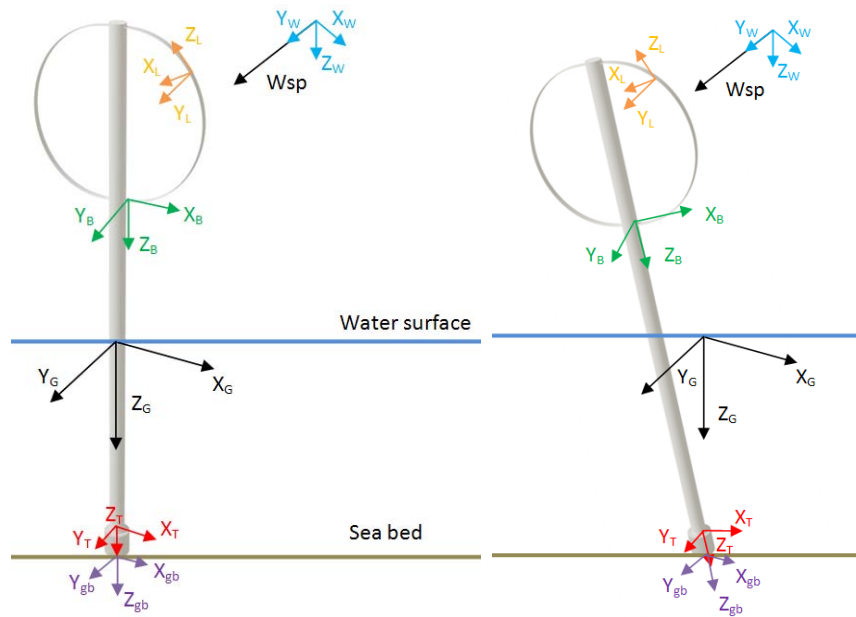


Figure 26 Reference systems used to describe the floating VAWT.

Table 12 Reference system description

Reference system	Properties
Global reference system X_G, Y_G, Z_G (g.r.s.)	<ul style="list-style-type: none"> • Inertial reference system • X_G, Y_G lay on the mean water plane • Z_G directed towards the seabed
Generator box reference system X_{gb}, Y_{gb}, Z_{gb} (gb.r.s.)	<ul style="list-style-type: none"> • The origin is on the first node of the gear box body • At $t=0$ the three axis are parallel to axis of the g.r.s. • During the simulation the system is free to rotate around X_{gb} and Y_{gb}
Tower reference system X_T, Y_T, Z_T (t.r.s.)	<ul style="list-style-type: none"> • The origin is on the first node of the tower body • Z_T rotates around Z_{gb} at ω_r • X_T and Y_T are parallel and solidal to X_{gb} and Y_{gb}
Blade reference system X_B, Y_B, Z_B (b.r.s.)	<ul style="list-style-type: none"> • The origin is on the first node of the blade body • X_B, Y_B and Z_B are solidal and parallel to X_T, Y_T and Z_T
Local reference system X_L, Y_L, Z_L (l.r.s.)	<ul style="list-style-type: none"> • The origin is on the first node of the element • Z_L is tangential to the blade centerline • X_L lays in the plane formed by the two blades; it is perpendicular to the blade centreline and it is directed towards the tower. • Y_L is parallel to Y_B.
Wind speed reference system X_w, Y_w, Z_w (w.r.s.)	<ul style="list-style-type: none"> • X_w, Y_w and Z_w are solidal and parallel to X_T, Y_T and Z_T

The direction of the wave propagation and of the water stream flow (marine currents) will be referenced to the inertial coordinate system and will always be in the horizontal plane, i.e. the currents have no vertical component.

6.5 Calculation points

During numerical simulations even though I change the design and the dimensions, I record the results at the same points on the turbine. These points are plotted in Figure 27 and described in the next table.

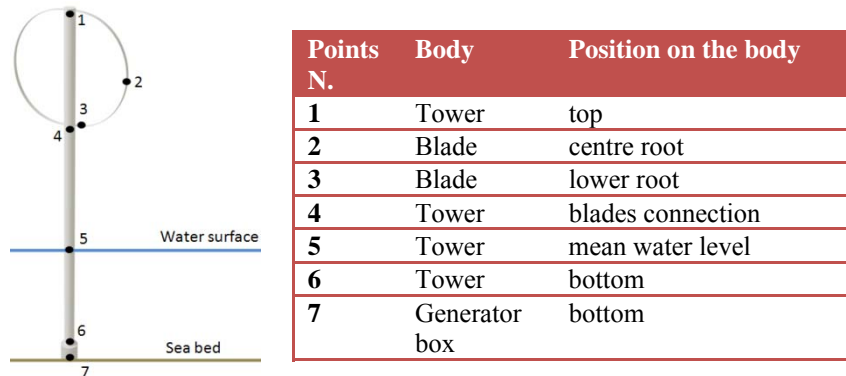


Figure 27 Position of the measurements points on the floating VAWT, dimensions are not indicative of the real design.

6.6 Other software used for numerical simulations

Other programs have been used in the current work for some dedicated tasks.

- The CFD software EllipSys2D from Risø DTU, to calculate the force and moment coefficient in currents.
- Some other routines or calculations have been implemented using other software: Matlab, Compaq Visual Fortran, Excel, Sigma plot.

7 First design: 2MW

The 2MW turbine was the first attempt to design a DeepWind concept turbine for numerical simulation and evaluation. Previously, studies had been conducted on 3 sizes (1MW, 5MW, 20MW) without fully integrating the design of the rotor with the design of the platform [75].

One reason to select a 2MW design was to have a size comparable with the Hywind concept, which was designed for 2.3MW. However the 2MW design was mostly used as a first base design to develop the code and to investigate the effects of the hydrodynamic forces on the rotating platform.

Before describing the study on the 2MW, I would like to make a few clarifications:

- The design had several changes during the time. To facilitate the understanding to the reader I have selected only the results analysis coming from one design.
- Some components and some aspects of the design have not been fully described in detail, mainly due to the purpose of the study.
- The 2MW has been used for the investigation of the Magnus effect on the rotating platform. This has eventually resulted in higher hydrodynamic loads than expected and the design is not fully tailored for those hydrodynamics forces and moments.
- The code has been developed in parallel to the design, therefore the study on the 2MW has been carried out with a preliminary and simplified version of the DLL and of the coupling with HAWC2.

7.1 Design specifications

7.1.1 Rotor design

The solidity of the rotor ($\sigma=Nc/R$), is equal to 0.19. This value is a compromise between the optimization of the rotor performances (higher values of σ) and the reduction of the cost (0.1 is the optimum σ value), [20].

The aspect ratio of the rotor, defined as ratio between height and diameter, is 1.12. Also this value is a compromise between the optimum, discussed by Paraschivoiu to be around 1.3 [20], and the reduction of the costs, obtained by reducing the height. It is useful to stress that a taller rotor in turn also requires a deeper foundation. This means higher costs in terms of: longer structure, larger forces on the submerged part and larger values of the frictional losses to the nominal power. The properties of the rotor are included in Table 13.

The turbine has a cut-in wind speed of 5 m/s, a cut-out wind speed of 25 m/s and the rated power is achieved at 14m/s, consistent with offshore environment and high wind resources. The rotational speed is regulated in order to work at the λ of maximum efficiency, i.e. considering the solidity and the Reynolds number of the rotor, $\lambda=5.2$. λ is kept equal to 5.2 until the maximum rotational speed is reached, i.e. 14rpm. Then the rotational speed remains constant and λ decreases. Meanwhile,

7. First iteration design: 2MW

the power increases until reaching the rated power of 2.35MW at 14m/s. From this condition the power is kept constant, reducing the rotational speed, until a wind speed of 17.25m/s and a rotational speed of 12.5rpm. For wind speed higher than 17.25m/s, the rotational speed is kept constant and the power is reduced until 1.63MW at 25m/s, when the turbine is stopped. The power and the corresponding rotational speeds are shown in Figure 28.

This control is different from the power curve showed in Figure 16 of chapter 4. In that case the power was kept constant while increasing the rotational speed. As discussed before, that would be a less robust control because a reduction in the wind speed can cause an increase of the power. Therefore in the study included in this chapter, I have decided to control the rotor by reducing the rotational speed as explained above.

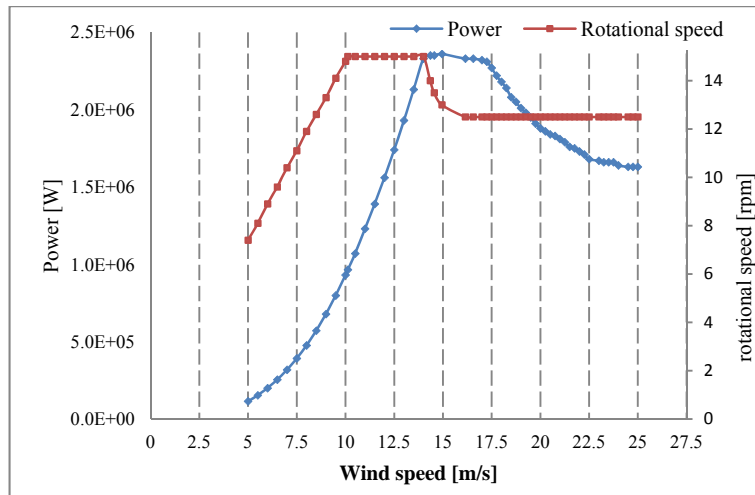
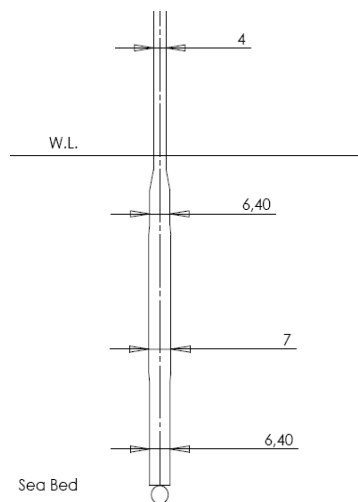


Figure 28 Power curve and rotational speed of the rotor.

The design process has followed the process described in section 1.4, although it has not been tailored to take into account very high loads due to the currents. The platform is tapered to reduce the wave-induced loads near the surface and the dimensions are reported in Table 13.

Table 13 Main design parameters of the 2MW turbine.

2MW Specifications		
Rotor Diameter	[m]	67
Rotor Height	[m]	75
Chord of the blade	[m]	3.2
Torque at rated power	[Nm]	$1.4 \cdot 10^6$
Thrust at rated power	[N]	$2.4 \cdot 10^5$
Rotational speed at rated power	[rpm]	15.0
Diameter of the tower above the water level	[m]	4.0
Maximum diameter of the platform (Tapered tower)	[m]	7
Total water displacements	[m ³]	3000
Total length	[m]	183



The design and the simulations investigate the 1st configuration (sea bed configuration) described in 2.6.1 with the bottom of the platform fixed at the sea bed and without translational degrees of freedom.

7.2 Load cases and code set up

The 2MW VAWT was not tested referring to a specific site. Instead I selected some conditions to investigate the behaviour of the turbine and to verify the code was working properly.

Here, I present the results from four simulations, corresponding to different combinations of wind, waves and currents, as summarized in Table 14. In each load case, the turbine is started up by the generator. At the time of these simulations, there were some limitations in the code:

- The aerodynamic loads are integrated on each blade and they are applied directly on the tower (i.e. no aerodynamical loads are applied on the blade elements)
- The relative speed of the platform is not considered in the calculations of the hydrodynamic lateral force F_l .

The simulations were run at constant wind speed, therefore the control showed in Figure 28 is not implemented. Instead when the rotational speed reaches the rated level of 15rpm, it is kept constant by the generator.

A summary of the load case is shown in Table 14.

Table 14 Load cases summary

	Wind	Waves	Currents
Load case 0	X		
1st load case	X		X
2nd load case	X	X	
3rd load case	X	X	X

7.2.1 Wind speed

The vertical variation of the wind speed v_0 along the z axis is described by the power law in equation Eq.7 of Chapter 6.4.2. The used values are

v_0 : 14m/s, it is constant over the time.

z_0 : 52.5m.

γ : 0.14 as for offshore standard, [49].

7.2.2 Currents

Water currents are computed, with a direction (x axis) transversal to the wind (y axis), i.e. $\beta_c=90\text{deg}$

The water velocity is constant, 1.0m/s at the water surface and zero at the sea bottom. The water shear profile is described by equation Eq.8 in paragraph 6.4.2 (see Figure 29). I used the following values:

$$U_0(t)=\text{cost}= 1\text{m/s}$$

$$\gamma= 0.5$$

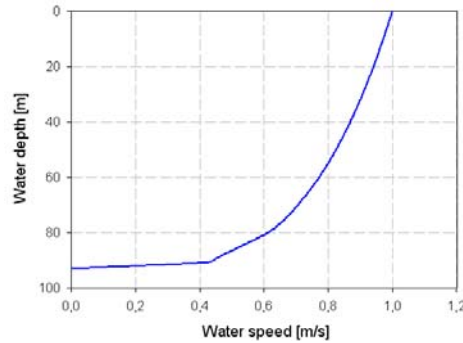


Figure 29 Water shear profile

7.2.3 Waves

The angle β_w between the wind and the waves is set equal to 90deg. Thus, regular waves are modeled on the x direction. The significant wave height is 4.0m and the wave period is 9.0s. The moderate intensity of the sea state is justified with the intention to test the effect of the hydrodynamic currents loads. Figure 30 shows plot of the velocity of waves at the surface level, including the height of the waves.

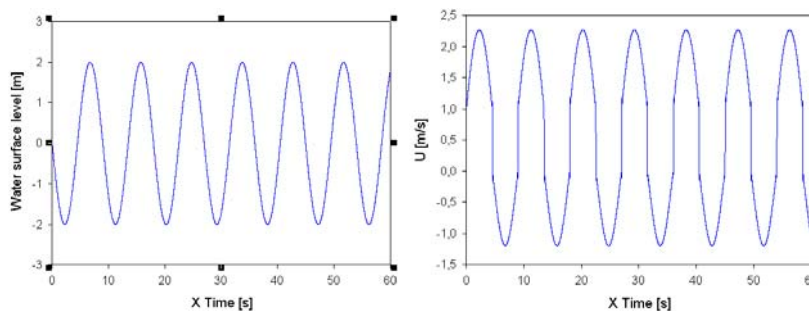


Figure 30 z coordinate of the water surface plane (left) and oscillatory flow at the water surface (right) for the wave condition used.

7.3 Results

The load cases are investigated in the time domain and in the frequency domain using an FFT transformation. In all the four cases the turbine was started from a condition of $\omega_0=0$ and $\phi_0=0$, with ω and ϕ respectively the rotational speed and the tilt angle of the floating turbine.

The results of the computations for the four load cases are presented in two sections: time domain and frequency domain. The parameters considered in the investigations are:

- Displacement dx and dy of the tower cross section at the mean water surface level, point 5 in Figure 27.
- Force F_x and F_y measured on the tower at the bottom of the blades (15m above the water surface level), point 4 in Figure 27.
- Bending moment M_x and M_y measured at the water surface cross section of the tower, point 5 in Figure 27.
- Vertical force F_z measured at the bottom of the tower, point 6 in Figure 27.

All the variables are calculated in the global reference system of Figure 26.

7.3.1 Load case 0

The turbine is tested in still water to observe the dynamic response of the turbine in absence of hydrodynamic external loads. The aerodynamic loads are present and have a large variability, as shown in Figure 31. The time series is divided into starting conditions (30s-60s) and rated conditions (300s-350s). As neither waves nor rotational speed are present, the forces are equal to zero at the starting of the turbine. At the rated conditions the forces consist of the harmonic aerodynamic side force F_x , with a null mean value; and the aerodynamic harmonic thrust force F_y with mean value of $2.39 \cdot 10^5 \text{N}$.

The displacements dx and dy of the platform at the mean surface level are plotted in Figure 32. The maximum value of the tilt angle is 1.5 degrees and it is recorded at the start of the rotor.

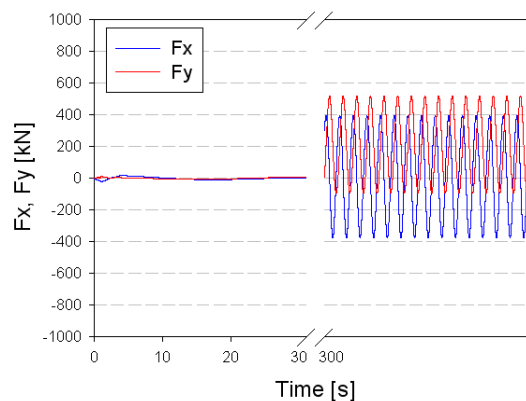


Figure 31 F_x , F_y on the tower section 15m above the sea (Point 4 in Figure 27). First time series (30-60s) with no rotation of the rotor, second time series (300-350s) at rated conditions.

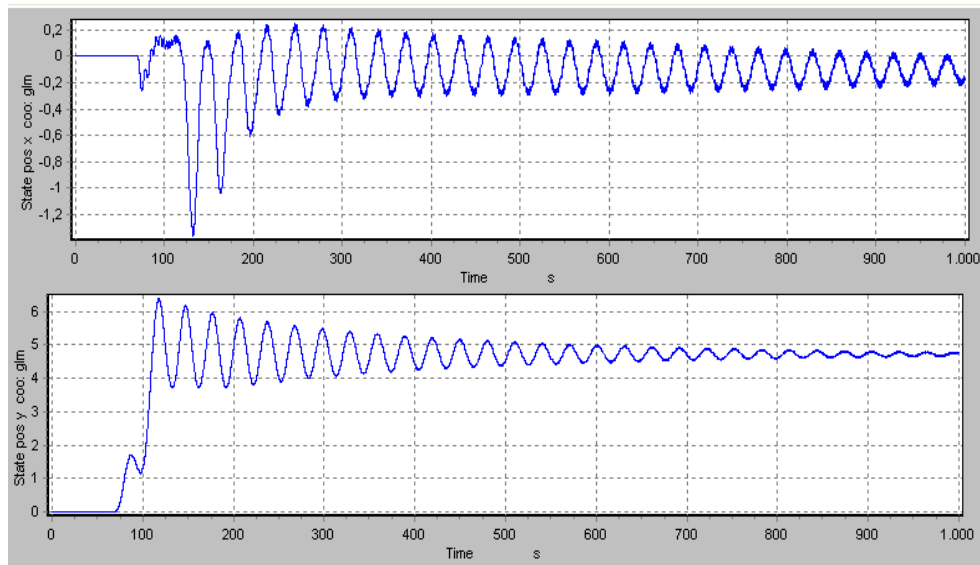


Figure 32 Displacements dx and dy (in meters) of the platform at the mean surface level, load case 0

7.3.2 Load case 1

Time domain

In load case 1 the currents are added to the input file and the water velocity is described by the shear profile of Figure 29. The water current direction lays on the x positive direction and the hydrodynamic side force acts on the y axis (positive direction). The aerodynamic loads are the same as in Figure 31.

The response of the turbine to the hydrodynamic and aerodynamic loads is show in Figure 33 in terms of displacements dx and dy . The turbine experiences first a peak at the start of the rotor and a more pronounced peak at the maximum rotational speed at 15rpm. The corresponding maximum value of the tilt angle is 13.7 degrees. However the motion is damped as the turbine is in equilibrium with the external loads at an tilt angle ϕ .

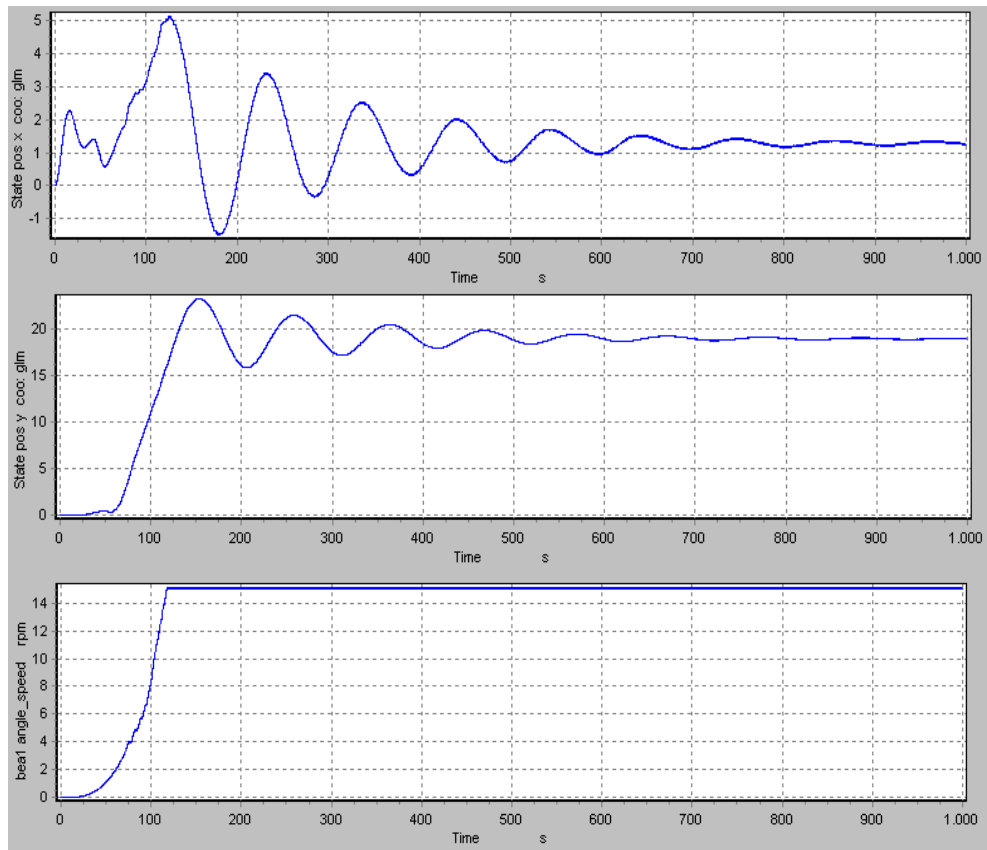


Figure 33 Displacements dx (top) and dy (middle) in meters of the platform at the mean surface level and rotational speed (bottom) - Load case 1

Frequency domain

The power spectral density (PSD) is computed for the most relevant variables recorded on the output. In Figure 34, dx reaches a peak at the f_{2p} frequency (0.5Hz), where f_{2p} is the even rotational frequency of the rotor as defined in 3.2. The same it is visible in Figure 35 for the PSD of F_z . The two components of the bending moment reach the peak at the odd rotor rotational frequencies (f_{1p} and f_{3p}), see Figure 36. Finally in Figure 37, the PSD of the component F_x and F_y is shown. The f_{2p} frequency and the higher harmonics are visible.

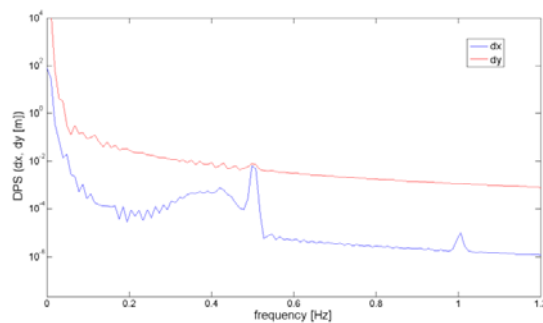


Figure 34 Density power spectrum of the displacement dx , dy

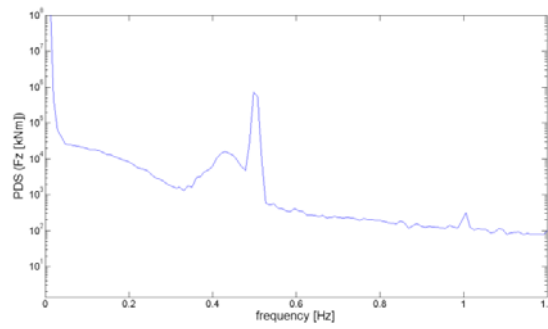


Figure 35 Density power spectrum of F_z

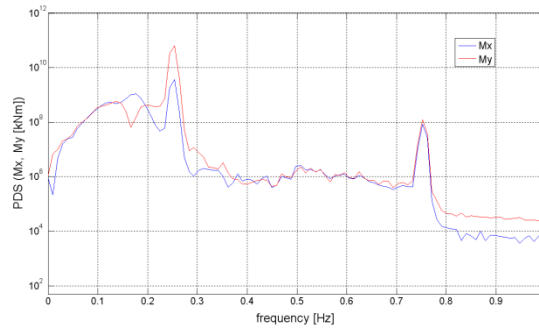


Figure 36 Density power spectrum of the bending moments M_x , M_y , at the water surface plane

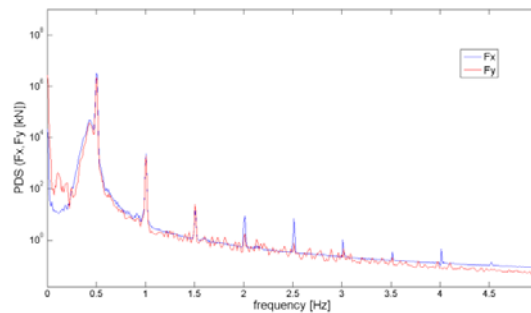


Figure 37 Density power spectrum of the force on the rotor, F_x , F_y

7.3.3 Load case 2

Time domain

Wave-induced loads introduce a force F_x on the rotor independent of the rotation of the turbine, see the first 60s of Figure 38 when the rotor is not started yet. At rated condition (Figure 38, 300s-350s) the forces are largely affected by the wave periods and the plot looks quite different from load case 1 (Figure 31).

The displacements are plotted in Figure 39, showing that the maximum displacements are due to the aerodynamic loads (y axis). The maximum value of the tilt angle is 3.0 degrees.

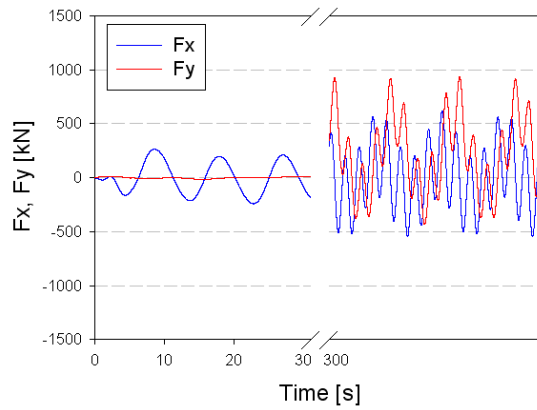


Figure 38 F_x , F_y on the tower section 15m above the sea. First time series (20-60s) with no rotation of the rotor, second time series (300-350s) at rated conditions.

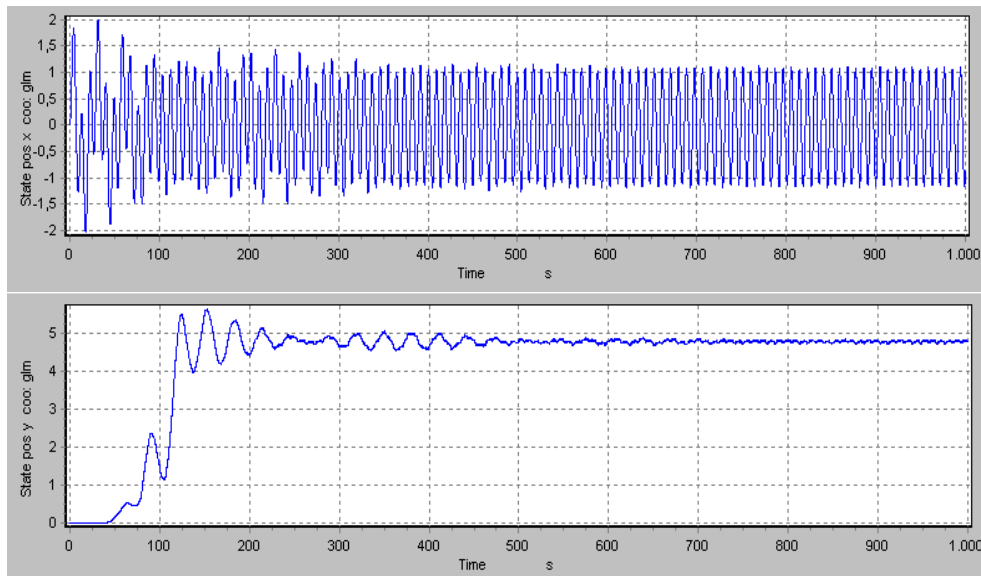


Figure 39 Displacements dx (top) and dy (bottom) of the platform at the mean surface level - Load case 2

Frequency domain

The waves effect on the displacements of the turbine is visible in Figure 40, where a peak at the wave frequency (0.11Hz) is noticeable. The same peak is achieved for the forces F_z (Figure 42) and F_x (Figure 41). However F_y still shows a stronger dependency of the rotational frequencies, see Figure 41.

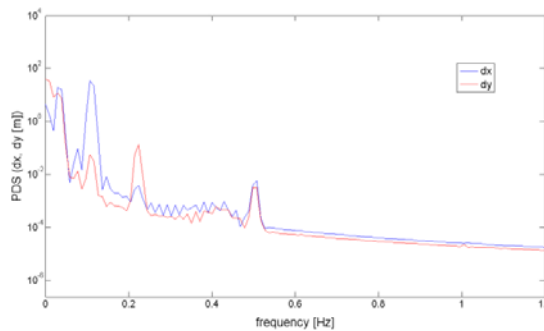


Figure 40 Density power spectrum of the displacement dx , dy

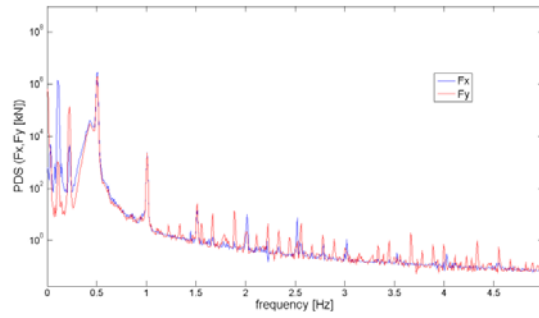


Figure 41 Density power spectrum of the force on the rotor, F_x , F_y

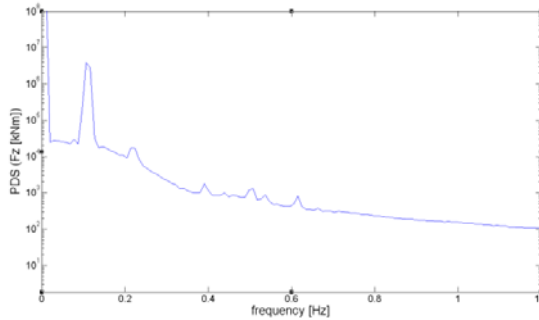


Figure 42 Density power spectrum of the vertical force F_z

7.3.4 Load case 3

Time domain

The forces acting on the tower above the sea surface with all combined loads do not show significant changes from the forces where only wave loads are added, i.e. Figure 38. Furthermore, hydrodynamic loads are added because of the currents. The displacements are larger than in the previous cases, see Figure 43. The maximum angle of tilt is 13.8 degrees, which is very close to the 1st load case.

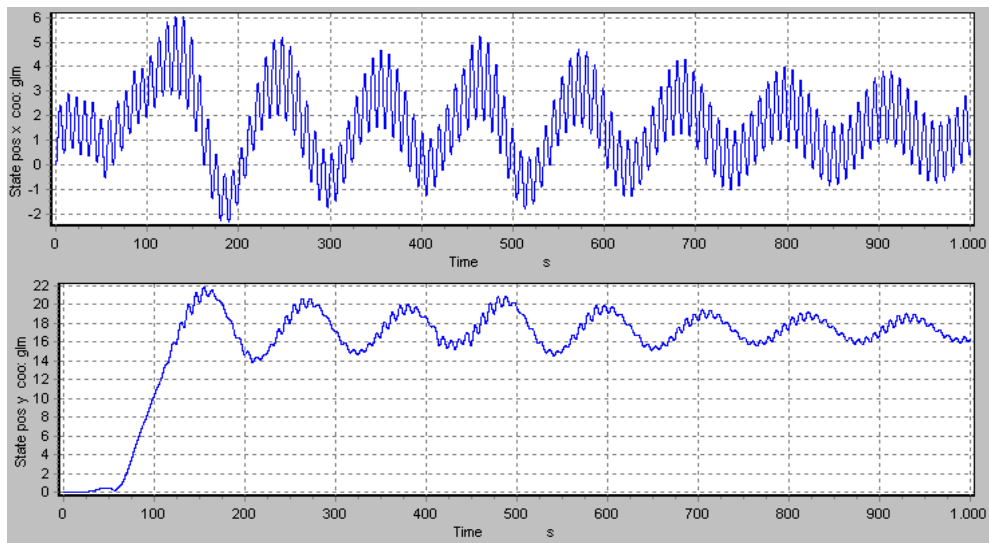


Figure 43 Displacements dx (top) and dy (bottom) of the platform at the mean surface level - Load case 3

Frequency domain

As the currents are included in the computation of this load case, the wave frequency becomes dominant also in the displacement along the y direction, see Figure 44. Meanwhile, due to the large displacements, the dominant frequency of Fz (Figure 45) is f_{2p} as in the first load case (Figure 35). Both the rotational and the waves frequencies are noticeable for Fx and Fy, in Figure 46.

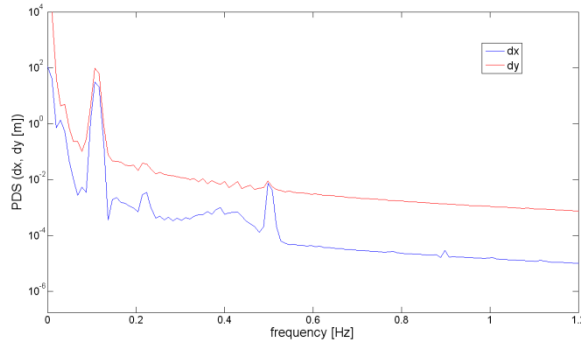


Figure 44 Density power spectrum of the displacements dx, dy

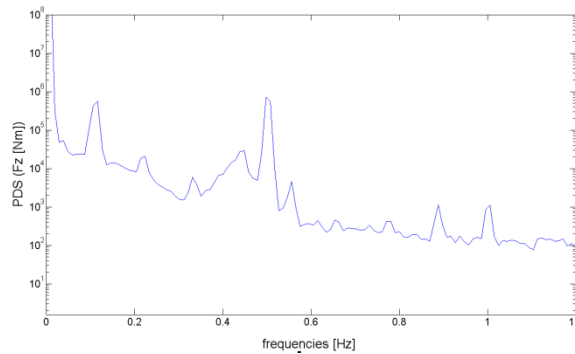


Figure 45 Density power spectrum of the vertical force on the rotor, Fz

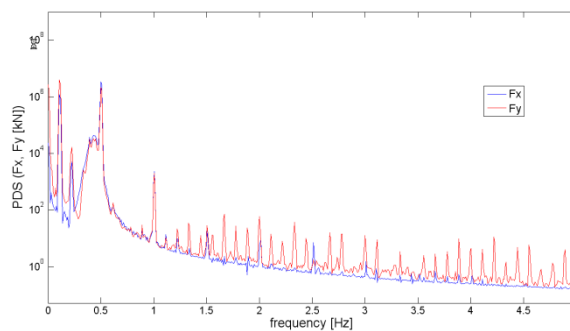


Figure 46 Density power spectrum of the force on the rotor, Fx, Fy

7.4 Discussion

The results show a strong coupling between the pitch and the roll motions of the platform. This is partially due to the fact that the turbine acts as a gyro during its

motion. This means that when the tower is turning, a moment applied on the x axis causes a reaction moment in the y axis.

The coupling of the two motions is also generated by the nature of the hydrodynamic side force, acting on the direction transverse to the currents direction. Thus a variation of the waves intensity in the x direction will affect also the equilibrium along the y direction, as seen by comparing Figure 34 and Figure 44.

Another strong coupling exists between aerodynamic and hydrodynamic loads. Indeed in wave-induced motion, the dominant period of the aerodynamic forces corresponds to the wave frequency. At the same time, also hydrodynamic forces and the friction moment are strongly dependent on the rotational speed of the rotor.

However, the hydrodynamic loads seem to be dominant on the dynamics of the system. Indeed the turbine operates with a tilt angle strongly dependent on the water currents speed. Once the turbine achieves the equilibrium, the tower experiences an elliptical motion on the water surface plane. The amplitude of the elliptical motion seems to be strongly dependent on the amplitude of the waves.

8 Baseline model: 5MW

I selected a 5MW size as the baseline model to evaluate the concept. The main reasons to motivate this choice were:

- Offshore wind energy is developing towards larger wind turbines and 5MW is a reasonable target at the present time.
- Looking at an evaluation of the DeepWind concept versus other floating concepts, most of them use as rotor the 5MW horizontal axis rotor from MIT/NREL [43]. This choice is intended to facilitate a future comparative study.
- 5MW is referred to a reasonable size, at which VAWTs can compete with HAWTs, thank to better upscaling potential, [22].

8.1 Design specifications

The design follows the iterative process of Figure 5 and takes into accounts the dependencies addressed in Figure 4. However, to help the comprehension, here the design will be presented following a straight consequential line without any feedback in the process.

There are not specific public standards for classification of floating offshore VAWTs. Then I refer to different guidelines: the IEC standard for offshore wind turbines [49], even though it is mainly focused on HAWTs and fixed bottom foundations; the standard from the French Bureau [76] is probably the most relevant one, being specifically meant for floating wind turbines; the standard from DNV [77], which is mainly thought for O&G industry, and is still the most complete guideline on the procedures for modelling waves and currents; the standard from NORSOK [78] addresses procedures and guidelines for offshore structure, with particular emphasis on North Sea conditions.

8.1.1 Site description

All the standards mentioned above agree on the need of joint met-ocean data for a correct evaluation of an offshore design. In the current study, in addition to joint statistical data describing waves and wind conditions, there is a necessity of accurate data on the sea currents at the site. A full set of data with these requirements was not available. At a first moment, I collected data from Sletringen, a location just west of Trondheim in Norway, where Oceanor is conducting a measurement campaign. The data included wind at three elevations, wave characteristic values and sea currents at several water depths. Unfortunately some technical problems occurred at the site and at present I have not enough data for a statistical evaluation of the site conditions.

An alternative solution has been proposed from DHI in a report for the DeepWind project [79]. The selected site is the test site used by Statoil for Hywind, situated off of the Norwegian coast of Stavanger, see red dot in Figure 47. Missing statistic data, a selection of the most relevant sea states can be made referring to the standards: [78], [77].

First, I selected the main objective of the design verification, which I decided should be the dynamics of the floating turbine in the most extreme external states for operation conditions of the turbine. I assume that the rotor has to work for wind speeds up to 25m/s.

The currents are composed from different terms, depending on the cause which generates them: tidal currents, wind driven currents, coast and ocean currents, local eddy currents, currents over steep slopes, currents caused by storm surge, internal waves. Here, I consider only the first two terms. Missing real data, the maximum value of the tidal currents is estimated from Figure 64 to be 0.2m/s. The wind-driven currents can be obtained as 2% of the hourly average wind speed at an elevation of 10m above the mean water level. Considering $v_0=25\text{m/s}$, as the maximum operation wind speed, the maximum value of the wind driven currents is taken equal to 0.5m/s. Therefore the total current velocity at the surface is 0.7m/s. Similar values are also available in literature, as in [80] and [81]. Additionally, these papers show that moving further from the Norwegian coast, relevant underwater currents are present and the concept design would be more challenging.

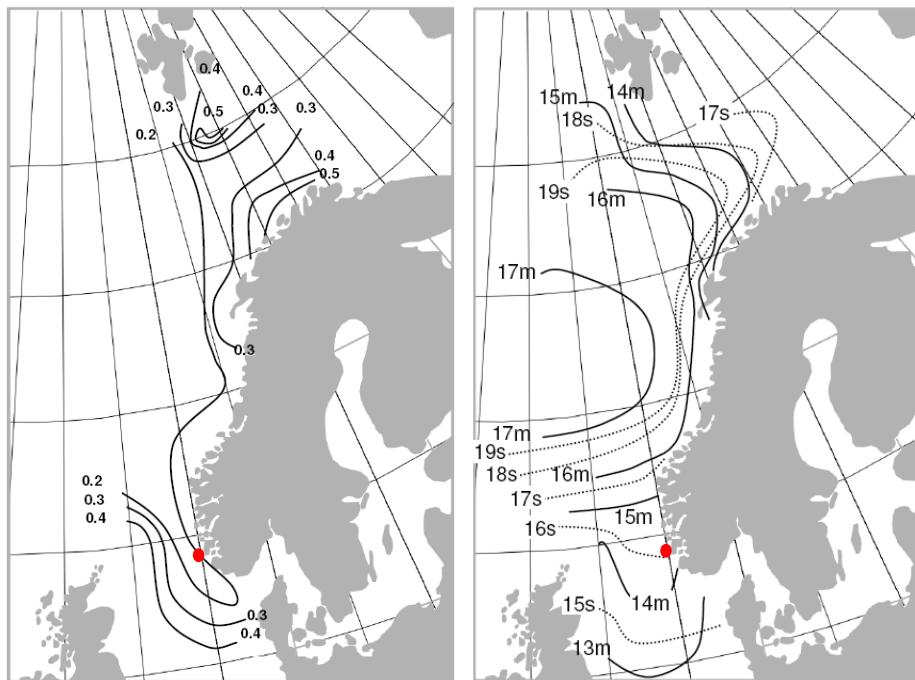


Figure 47 Maximum 100 year tidal surface current [m/s] (left). Significant wave height H_s and related maximum peak period T_p with annual probability of exceedance of 10^{-2} for sea-states of 3 h duration. ISO-curves for wave heights are indicated with solid lines while wave period lines are dotted, maps from [78]. The red dot represents the selected site.

The 100 year significant wave height H_{100} , can be estimated from Figure 47. Then I considered $H_s=14\text{m}$ and $T_p=16\text{s}$, as most critical sea state. More moderate conditions can be added for the analysis.

A list of the most critical conditions expected at the site is reported in Table 15. I disregard in my work other external factors, such as ice, snow and earthquakes.

Table 15 most critical conditions at the selected site for evaluation of the design.

Most critical external conditions		
Velocity of the water currents at the surface	[m/s]	0.7
Maximum significant wave height H_s	[m]	14
Maximum peak wave period T_P	[s]	16
Wind speed	[m/s]	<25

8.1.2 Rotor design

I used NACA 0018 symmetric airfoils for the blades of the 5MW turbine. The choice is mainly due to the large quantity of available data. The Reynolds number of the free current (calculated over the chord of the blade) is estimated at 10^7 . At similar conditions, the maximum power is extracted using a rotor solidity in the range 0.2-0.25, [70].

From a parametrical study on a rotor with solidity 0.23, I evaluated the maximum efficiency and the C_p at maximum power. Then I have chosen the solidity and the ratio height over diameter, $\sigma=0.23$ and $H/2R=1.02$. For a rotor with these specifications, the necessary swept area to produce 5MW at 15m/s is 10743m^2 . From the area, it is possible to calculate the radius and the height, i.e. $R=63.74$ and $H=129.56$. The chord and the rotational speed can be obtained from the values of the solidity and the tip speed of maximum power, respectively $c=7.45\text{m}$ and $\omega=5.25$.

The curves of the thrust aerodynamic force and the power output are plotted in Figure 48 and Figure 49 and the most relevant characteristics of the rotor are summarized in Table 16.

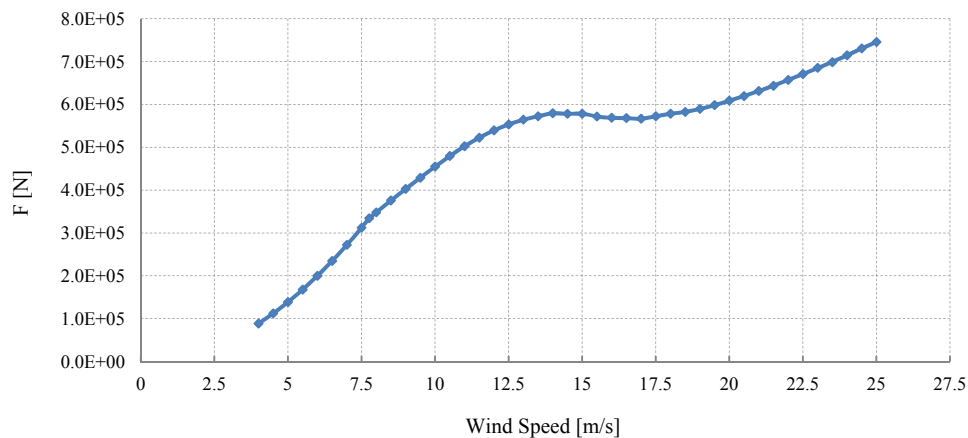


Figure 48 Thrust aerodynamic force of the 5MW turbine.

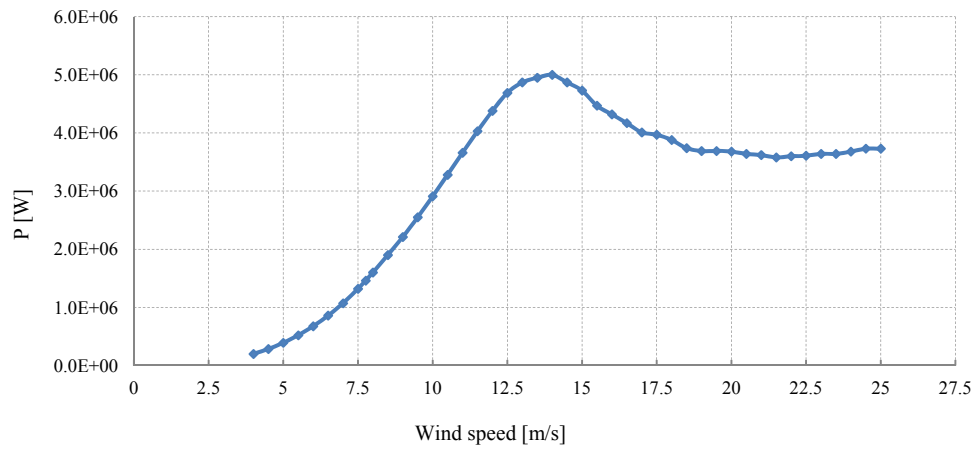


Figure 49 Power curve of the 5MW turbine.

Being the 5MW a baseline model design to evaluate the feasibility of the concept, I selected a robust control. The rotor is stall regulated and the rated power is reached at maximum power rather than at maximum efficiency (C_p). This affects the design: moving the rated power towards high wind speeds and low rotational speed, and decreasing the efficiency of the rotor. A next step will be to move the rated power towards larger value of λ and higher values of efficiency. This would require a fast regulation of the rotational speed to avoid accidents in case of large gusts. Such characteristic would depend from a detailed study of the generator and the control system, which I simply have not included so far in my research.

The design of blades for a large VAWT can be challenging, due to the inertia and the mass of the blades. In my design, the length of a single blade is 188.68m (see Table 16) and even though the pultrusion is a very convenient solution to reduce the cost of VAWT blades, there are some drawbacks as well. The most evident limitation in use of pultrusion is that the distributed properties of the blades are supposed to be constant over the length, resulting in an over dimension of some part of the blades and in a very heavy structure.

Table 16 Specification of the rotor

Geometry of the rotor			Characteristic of the rotor		
Rotor radius	[m]	63.74	Rated power	[kW]	$5 \cdot 10^3$
Rotor height	[m]	129.56	Rated rotational speed	[rpm]	5.26
Chord	[m]	7.45	Rated wind speed	[m/s]	14.0
Solidity, $\sigma = Nc/R$	[-]	0.23	Cut in wind speed	[m/s]	5.0
Swept Area	[m ²]	10743	Cut out wind speed	[m/s]	25.0
Blade length	[m]	188.68	Rated tip speed	[m/s]	35.1

To take the very high gravity load into account, I utilized a modified blade shape from the classical Troposkien, as proposed in [9] and [20]. In order to equilibrate the gravity and the centrifugal force, the shape of the blade is modified as in Figure 50 (left), deviating from the symmetric design of a classic Troposkien shape. The modification of the blade design needs to be related to the tip speed and the rotational speed. This adjustment in the design is limited by the feasibility of the

manufacture process. I considered the design blade shape in Figure 50, which is tailored for a tip speed of 36.3m/s which is very close to the one reported in Table 16 and for 30rpm that is much higher than the rated 5.26 of my design. However, the benefit of the modified shape of the blade is visible in the right picture of Figure 50, where I have plotted two time series of the moment around the local y axis (see Figure 26) at the lower root of the blade (point 3 in Figure 27). In the modified design the load is reduced and the mean value decreases with the increase of the rotational speed, by the effect of the centrifugal force. A further modification to the design is possible and it would be recommended, in order to lower the bending moment on the blade. However, it seems to be challenging to reach the full tensional equilibrium between the gravity and the centrifugal force, with a shape of the blade which is reasonable simple to manufacture. A compromise in the design could then include a possible rise in the rated rotational speed.

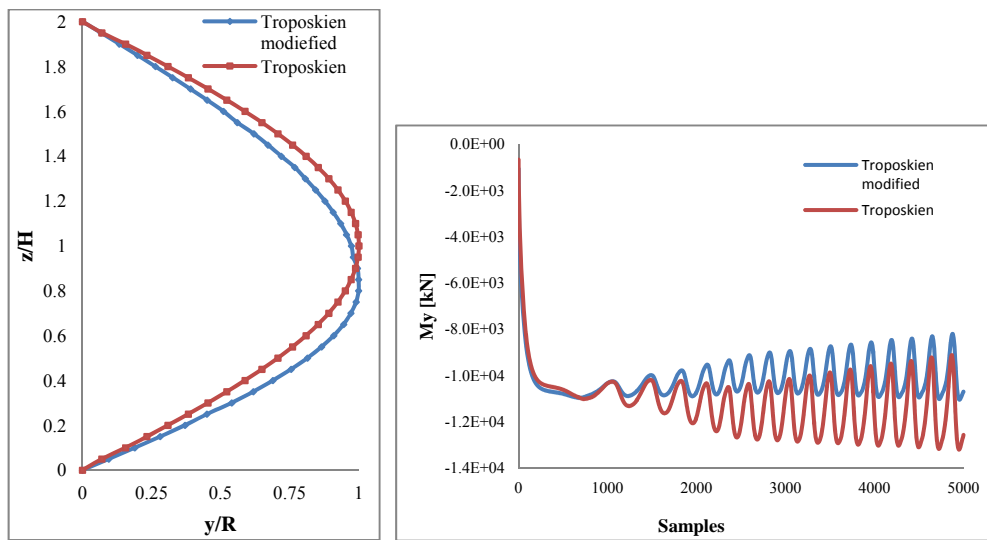


Figure 50 Blade shape for a classic Troposkien and Troposkien modified for the effect of Gravity (left). Effect of the blade shape on the bending moment at the low root of the blade (right).

I used the blade structure in Figure 51 and the distributed properties in Table 17 to describe the blade sections over the length. The properties of the material are reported in Table 11. However, in order to avoid major deformations, it has been necessary to reinforce the structure of the blade close to the connection with the rotor. Then I considered stiffer and heavier structure over the two extremities of the blade over a length of 36.7m from the top and 45.5m from the bottom. The length of the central part of the blade is 107m. The final design of the blade has a weight of $1.54 \cdot 10^5$ kg, as reported in Table 17.

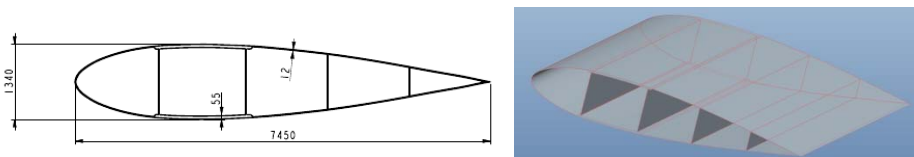


Figure 51 Section for the central part of the blade of the 5MW turbine. 2D sketch with dimensions (left) and 3D drawing (right), kindly provided by Per Hørlyk Nielsen from Risø DTU.

Table 17 Properties of the blade.

Undistributed properties of the blades		
Length 1 blade	[m]	188.68
Weight 1blade	[kg]	1.54 10 ⁵
Distance of the centre of gravity from water level	[m]	60.78
Distance centre of gravity from the centre of the tower	[cm]	33.61
I_{xx}	[kg m ²]	8.99 10 ⁸
I_{yy}	[kg m ²]	1.14 10 ⁹
I_{zz}	[kg m ²]	2.42 10 ⁸

Table 18 Sectional properties of the blades.

Distributed properties of the blades		
Linear density	[kg/m]	810.0
Area of the cross section	[m ²]	3.87 10 ⁻¹
I_x	[m ⁴]	1.06 10 ⁻²
I_y	[m ⁴]	1.19 10 ⁻¹
E	[N/m ²]	1.60 10 ¹⁰

To dimension the tower, I consider the simultaneous action of the bending moment and of the torsion moment caused by the reaction torque of the generator, and I have calculated it at the mean water level. The design stress σ_s at the external surface of the cylinder is:

$$\sigma_s = \frac{M_b R_T}{I_p} + \frac{Q R_T}{I_p} \quad \text{Eq.9}$$

Where M_b is the maximum value of the bending moment, R_T the maximum external radius of the tower, Q the maximum value of the torque and I_p the polar moment of inertia of the section, $I_p = \frac{\pi(R_{T_{ex}}^4 - R_{T_{in}}^4)}{4}$.

A HAWT experiences only the first term of the equation above, thus a floating VAWT with a rotating foundation has an additional load on the tower. On the other hand, the bending moment applied on a HAWT tower is larger, due to the higher elevation of the application point of the aerodynamic thrust. Eventually the maximum stress on the tower has similar values in the two cases, disregarding any fatigue load. To dimension the tower, I considered a safety factor of 4 defined as $f_s = \frac{\sigma_{max}}{\sigma_s}$, where σ_{max} is the material yield strength, as in the material properties of section 6.4. The wanted safety factor f_s can be achieved with a proper dimensioning of the external radius and thickness of the tower section. Also, the selection of the tower section is a result of a compromise between two solutions:

- A slender cylinder with thick walls, that would reduce the wave loads at the mean water level
- A large cylinder with thin walls, which would decrease the weight, optimising the cost.

I have selected a cross section of radius 3.15m and thickness 0.02m.

Table 19 Properties of the tower of the rotor.

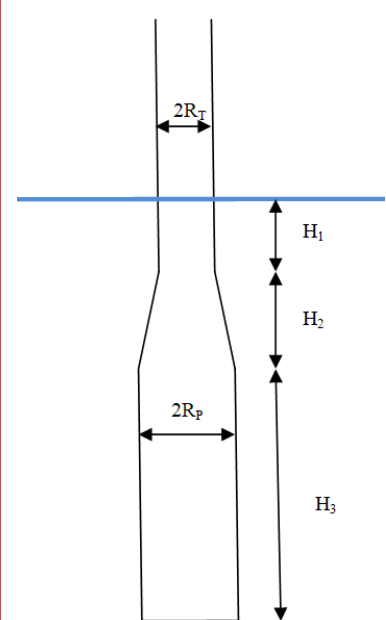
Geometry of the tower above sea level (rotor)		
Total length above sea level	[m]	145
Clearance from mean water level	[m]	15
External radius of the tower	[m]	3.15
Thickness of the tower	[m]	0.02

8.1.3 Platform design

The platform consists of a tapered structure attached to the rotor tower at the main water level. At the connection point, the radius and the thickness are equal to the properties of the tower cross section mentioned above. At 5m below the sea level the cylinder is tapered to reach the maximum diameter of the platform, i.e. 8.3m. The tapered part of the platform is 10m long and the properties are varied linearly between the top section and the bottom section. The geometry of the platform is described in Table 20.

Table 20 Dimensions of the platform.

Geometry of the tower below sea level (platform)		
Total length below sea level (H_p)	[m]	108
Depth of the slender part (H_1)	[m]	5
Radius of the slender part (R_T)	[m]	3.15
Thickness of the slender part	[m]	0.02
Length of the tapered part (H_2)	[m]	10
Length of the bottom part (H_3)	[m]	93
Maximum radius of the platform (R_p)	[m]	4.15
Thickness of the bottom part	[m]	0.05



Some ballast has to be added to the bottom to achieve the hydrostatic equilibrium of the platform. I considered the weight of the generator included in the mass of the ballast, placed at the bottom of the platform, with centre of gravity located at 4.78m from the bottom. The total mass of the cylindrical structure (tower and platform), including ballast and generator, is 5680tons with a centre of gravity located at an elevation of 27.84m from the bottom. The water displacements of the platform are 5940m³ and the centre of buoyancy is at 18.57m above the centre of gravity, as stated in Table 21.

Table 21 Undistributed properties of the tower.

Properties of the tower (rotor + platform)		
Total length (rotor + platform)	[m]	253

Weight (included ballast and Generator)⁹	[kg]	5.64 10 ⁶
I_{xx}=I_{yy}	[kg m ²]	1.87 10 ¹⁰
I_{zz}	[kg m ²]	2.12 10 ⁷
Distance of centre of gravity from tower bottom	[m]	27.84
Distance of centre of gravity from centre of buoyancy	[m]	18.57
Total water displacements	[m ³]	5.94 10 ³

The distribution of the mass and of the volumes has been designed in order to have maximum angle of inclination around 10degrees. The coefficients of hydrodynamic restoring and of the natural periods of the platform are presented in Table 22. I used the parallel axis theorem (or Huygens-Steiner theorem), to include the rotor in the calculation of the natural period of the pitch mode. As shown in the table, the pitch natural period increases considerably due to the large inertia of the rotor. I report also the coefficient and the period of the platform in heave, even though the platform is anchored to the bottom, since the system is supposed to be easily adapted to the configuration with catenary mooring lines.

Table 22 Hydrodynamic restoring coefficients and natural periods in heave and pitch.

Platform stability properties		
C₄₄=C₅₅	[kg m ² /s ²]	1.08 10 ⁹
C₃₃	[kg /s ²]	3.06 10 ⁵
T_{n3}	[s]	27.59 (0.0362Hz)
T_{n4}	[s]	25.97 (0.0385Hz)
T_{n4} (including rotor)	[s]	33.96 (0.0294Hz)

I decided to test the design for the sea states described in Table 15, and for other two more moderate sea states, described in Table 23, with maximum significant height values H_s between 4m and 14m and maximum wave peak period T_p between 9s and 16s. For the three sea states I calculated the non-dimensional parameters D/λ_w , oscillatory Reynolds number and KC number and I plotted the values over the local water depth in Figure 52, Figure 53 and Figure 54.

Table 23 Properties of the selected sea states.

	Sea states	
	H_s [m]	T_p [s]
Sea State1	4	9
Sea State2	9	13.2
Sea State3	14	16

The values of the D/λ_w are much smaller than 0.2 for all the sea states. From literature and standards the diffraction loads are therefore not relevant for the design, and potential theory can be used. The references are [77], [78], and [48].

⁹ The properties of the generator a

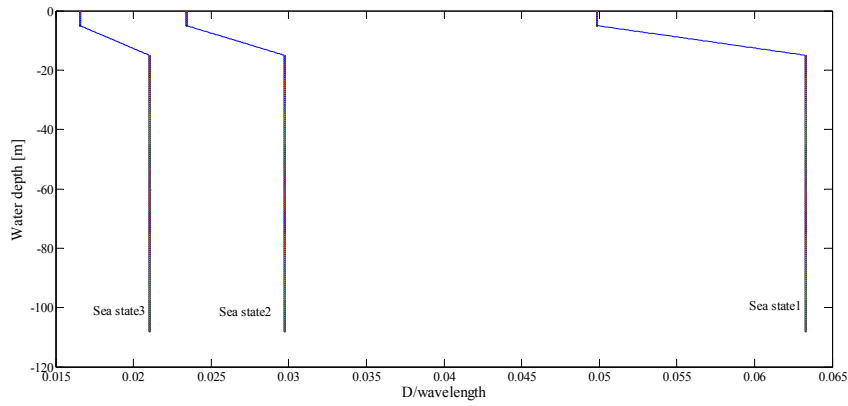


Figure 52 D/λ_w for the selected sea states.

For the most severe sea state, KC is greater than 2 for almost all the local water depths. At these conditions, the potential theory cannot be applied without taking the viscous effects into account [48]. Therefore, the correct values of C_D are calculated for the oscillatory Reynolds numbers plotted in Figure 53. For $1 < KC < 6$, the standards address $C_D = 0.65$ and $C_M = 2.0$ [78].

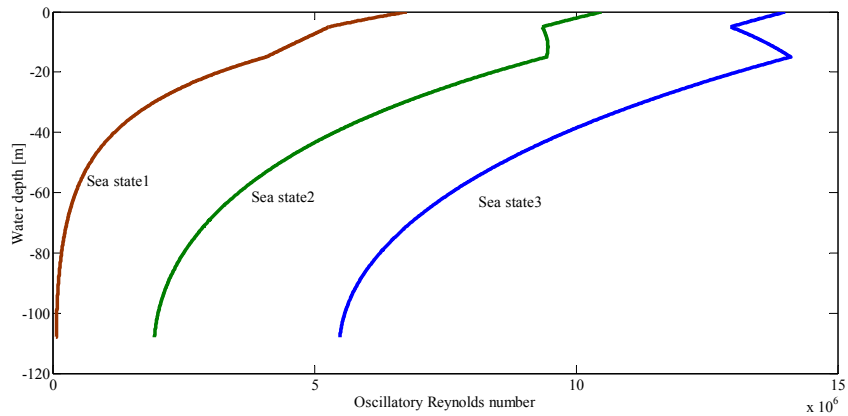


Figure 53 Oscillatory Reynolds numbers of the 5MW platform at the selected sea states.

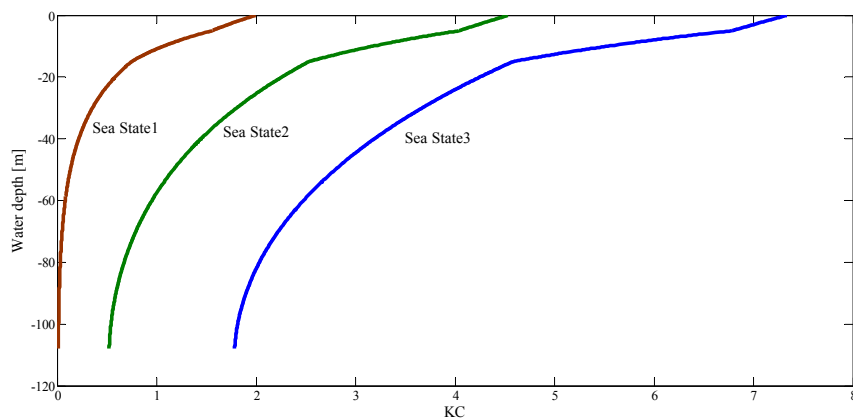


Figure 54 KC numbers of the 5MW platform at the selected sea states.

8.2 Simulations

8.2.1 Load cases description

I carried out simulations on the configuration of the system with the generator fixed at the sea bottom described in chapter 2.6.1.

The wind velocity varies linearly in the range $5\text{m/s} < v_0 < 25\text{m/s}$. The shear profile is described from equation Eq.7 in 6.4.2 with the shear factor 0.14.

The current velocity at the surface is 0.7m/s and the water shear profile varies over z , according to equation Eq.8 in 6.4.2 with the shear factor 0.5. I considered the wave properties of the three sea states in Table 23, using both regular and irregular wave formulation. The water depth is taken equal to 110m.

The Morison's coefficients are selected according to the considerations above with $C_D=0.65$ and $C_M=2$.

To handle the large number of simulations I will use a three digits number to describe each numerical time series, i.e. SimXYZ. Where X is a number describing the sea state, Y the wave direction β_w and Z the current direction β_c , according to the numbers set in Table 24. For instance, the simulations of the sea state2 with $\beta_w=90\text{degrees}$ and $\beta_c=45\text{degrees}$ is called Sim223.

Table 24 Definition of time series simulation indices

	Still water	Sea state1		Sea state2		Sea state3	
Sea state no (T_P, ζ_a)	0	1		2		3	
	No waves	180 Deg	90 Deg	45 Deg	0 Deg	-45 Deg	-90 Deg
Wave direction no (β_w)	0	1	2	3	4	5	6
	No currents	180 Deg	90 Deg	45 Deg	0 Deg	-45 Deg	-90 Deg
Current direction no (β_c)	0	1	2	3	4	5	6

8.2.2 Results

First, I carried out runs in still water and without aerodynamic loads on the rotor, i.e. no wind. In Figure 55, the results from a turbine spinning in still water and started with an tilt angle $\phi_0=10$ degrees are plotted.

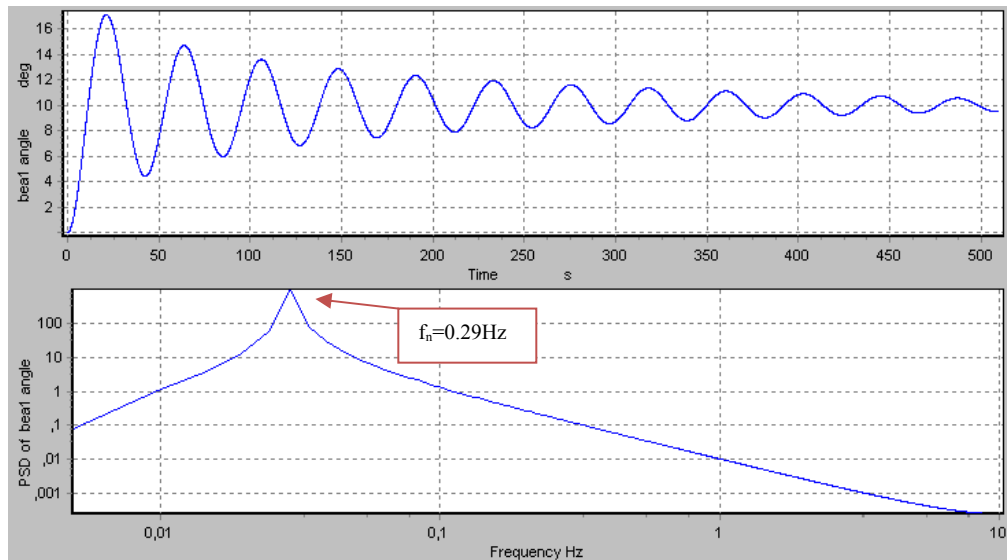
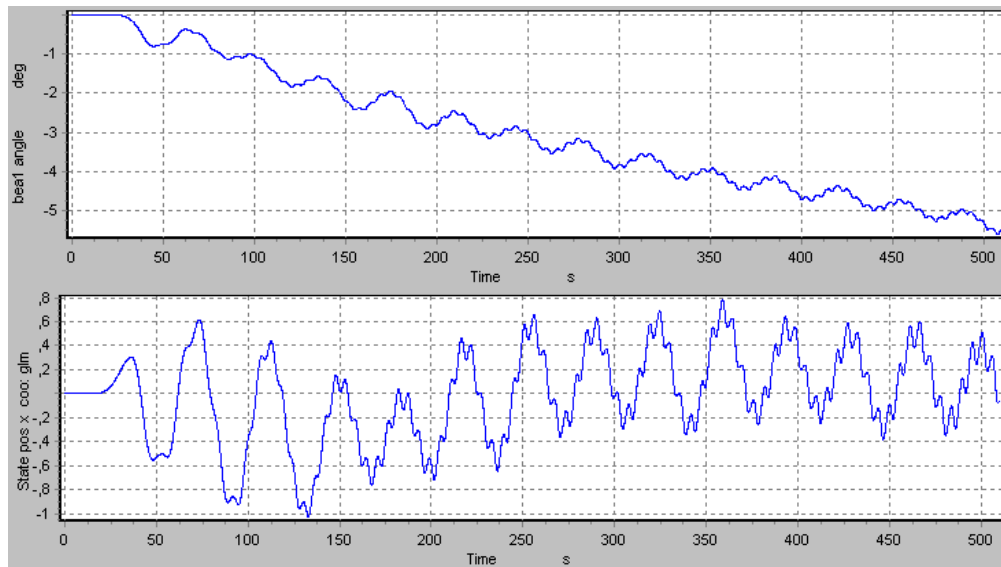


Figure 55 Turbine spinning in still water, started from an inclination angle of 10degrees. Tilt angle time series (top) and PSD of the time series using logarithmic scale (bottom). Note for the top figure: due to the tilt offset of the axis at the start, the vertical position of the turbine is achieved at 10 degrees.

The turbine goes back to the vertical position in a relatively short time and the motion seems well damped. The period of the oscillations matches with the expected natural period of the floating platform in pitch.

A second set of simulations regarded the turbine running in still water and including aerodynamic loads. Figure 56 shows the plots of: the displacements dx and dy of the cross section of the platform at the mean water level (point 5 of Figure 27); the tilt angle ϕ and the angular velocity $\dot{\phi}$ of the platform around the cardanic joint (measured at point 7).



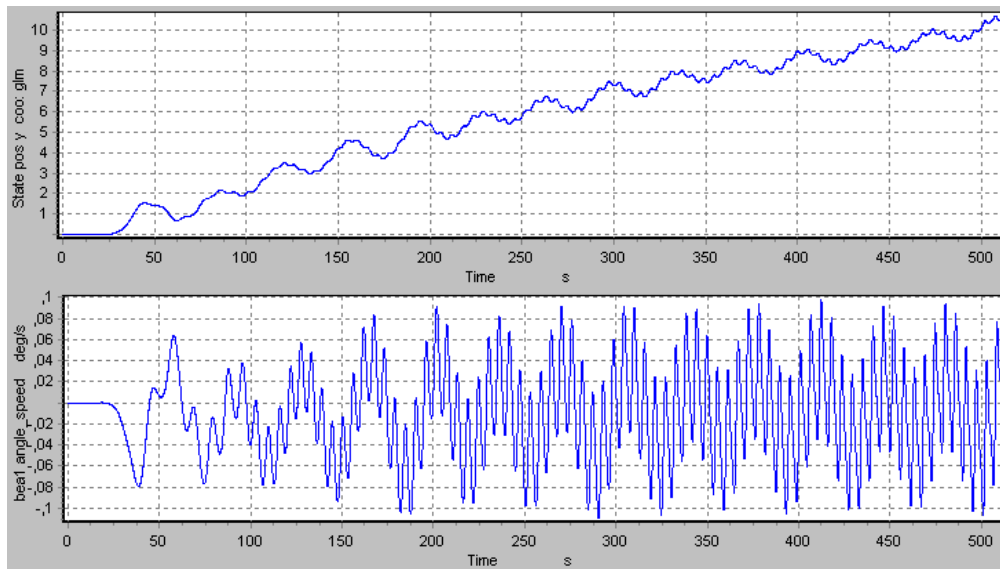


Figure 56 Turbine in still water, from top: 1.tilt angle measured at the bottom of the platform, 2.dx of the cross section at mean water level, 3.dy of the cross section at mean water level, 4.angular velocity of the structure measured at the bottom of the structure. The turbine is in still water and the wind speed varies linearly with time in the interval $5 < v_0 < 25$.

Figure 57 and Figure 58 report the moments M_x and M_y measured at the water surface (point5) and the forces F_x and F_y measured at the blade low root connection (point4), respectively. Both the moments and the forces are computed in the global reference system.

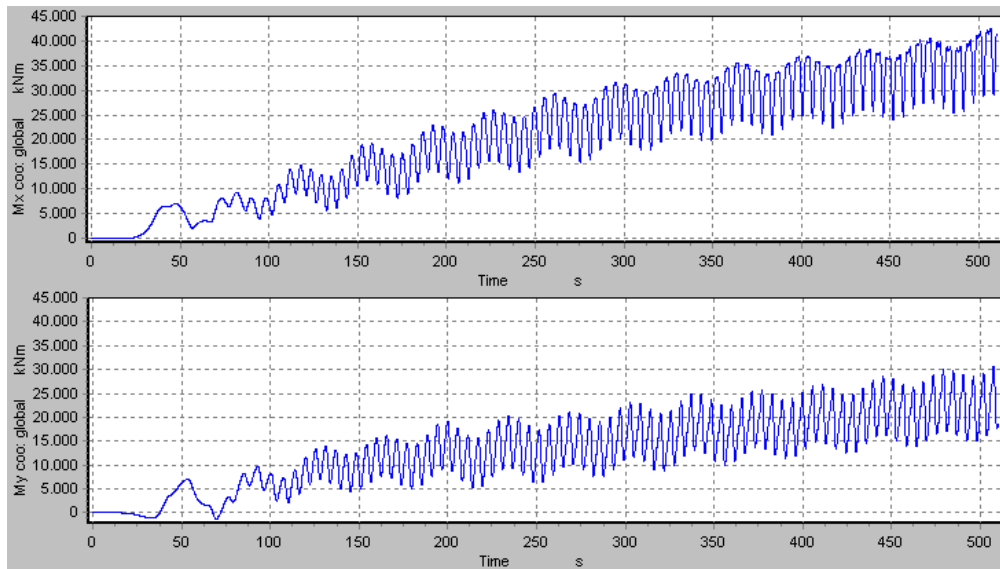


Figure 57 M_x (top) and M_y (bottom) at the water plane section. Turbine in still water and wind speed varying linearly with time in the interval $5 < v_0 < 25$.

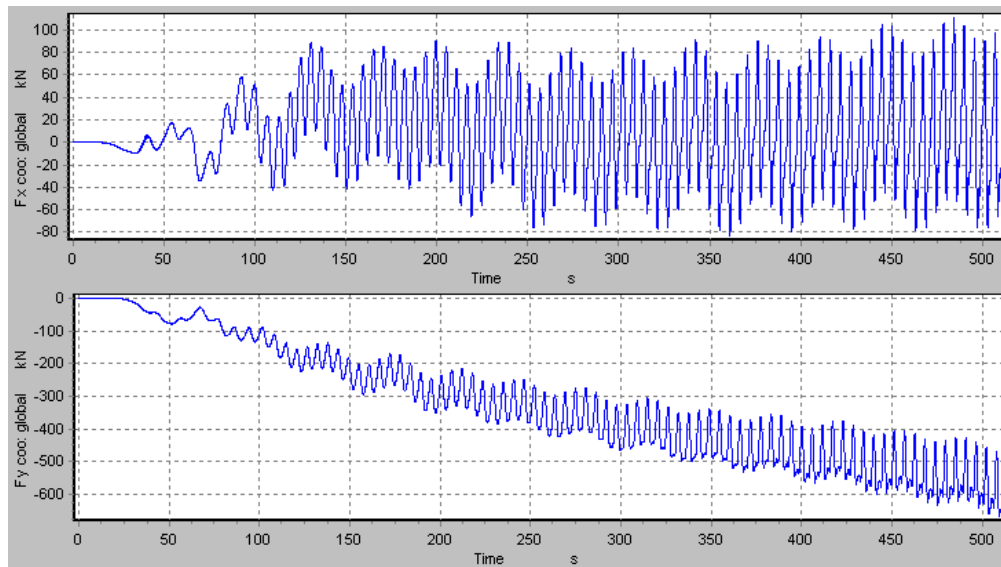


Figure 58 Aerodynamic forces F_x (top) and F_y (bottom) on the tower measured at the low root connection. Turbine in still water and wind speed varying linearly with time in the interval $5 < v_0 < 25$. The forces plotted are the reaction forces, therefore the sign is opposite to the sign of the aerodynamic forces.

The results from the simulations listed in Table 24 are grouped in the histograms of Figure 59 and Figure 60, reporting respectively:

- The minimum value of the SF, considering the total bending moment on the tower (M_b), measured at point 5 of Figure 27. Both the maximum value and the mean value of M_b were recorded. The design was carried out in order to achieve a minimum value of the SF equal to 2 for the maximum loads and to 4 for the mean value of the loads. The mean values were calculated at maximum wind speed and assuring the convergence of the value.
- The maximum values of the tilt angle ϕ measured at the bottom of the platform (point 7 of Figure 27) without including the effects of the deformation of the structure.

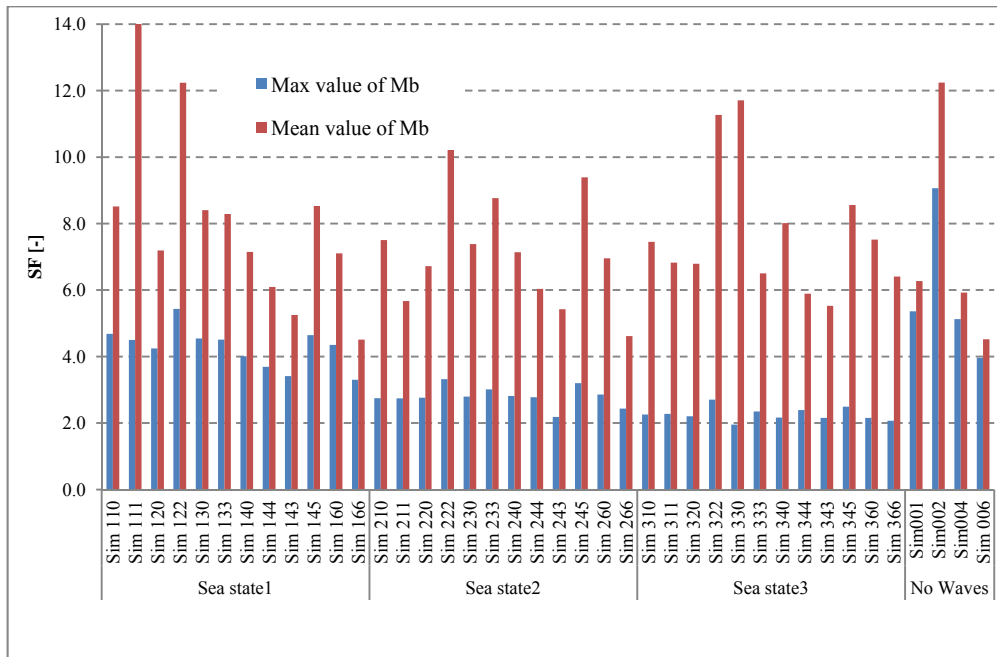


Figure 59 Minimum safety factor SF corresponding to the mean and maximum recorded values of the bending moment M_b at different environmental condition.

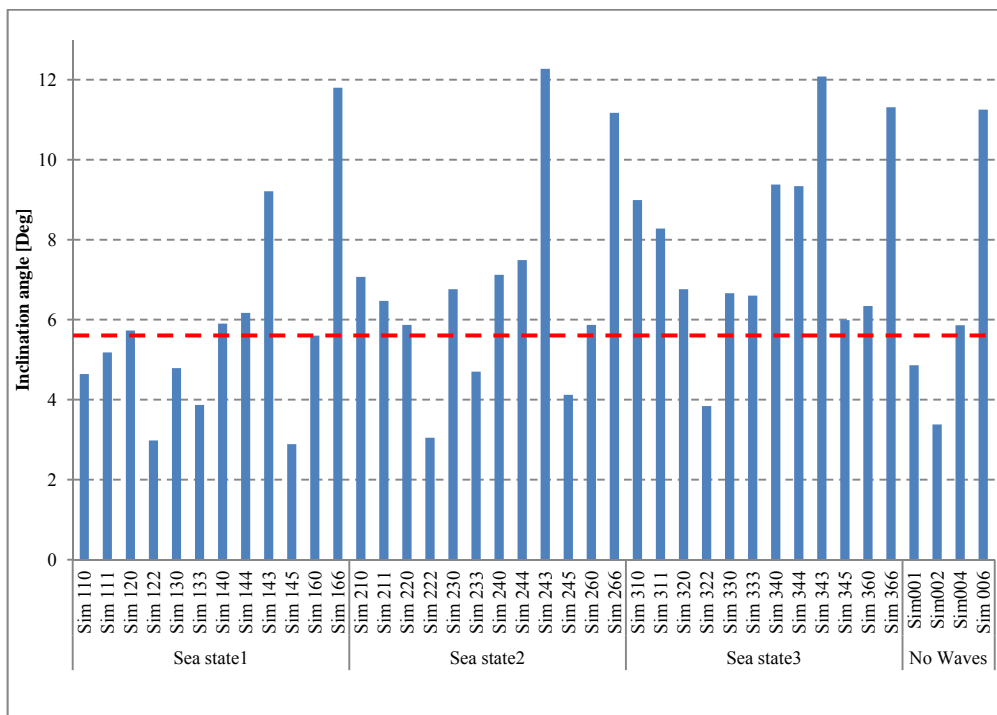


Figure 60 Maximum tilt angle for different sea states, the red dashed line states the value of the tilt angle in still water.

The effects of the wave intensity on the stability of the system are investigated in the next charts. Figure 61 shows the time series of the tilt angle for wind speed increasing linearly with time in the range $5\text{m/s} < v_0 < 25\text{m/s}$ and with wave direction $\beta_w = 90$ degrees. The wave characteristics (ζ_a and T_p) are dependent of the sea state and the currents are not included in the time series.

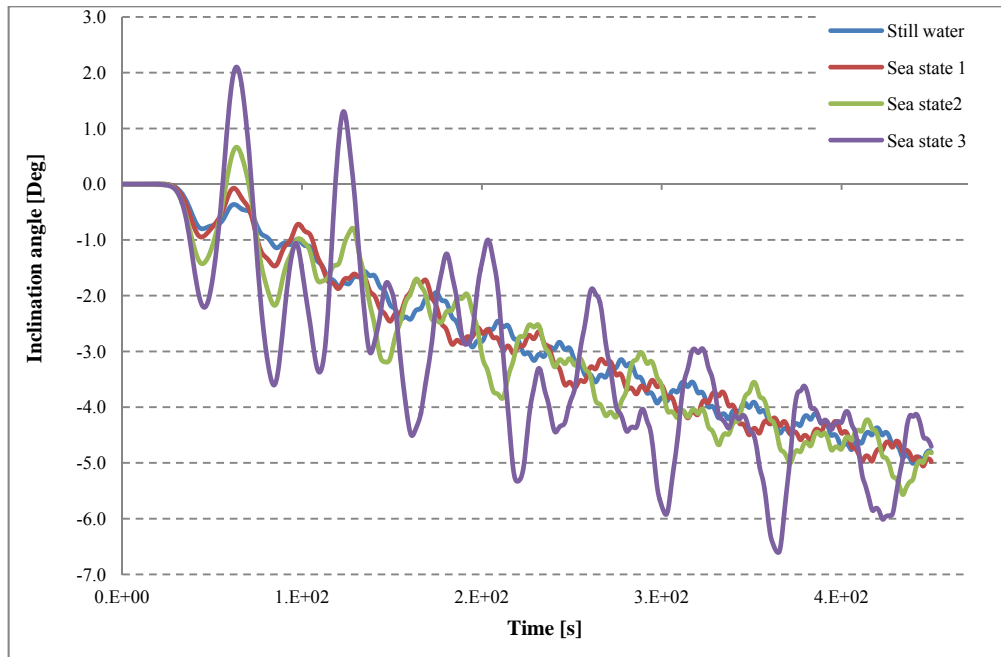


Figure 61 Tilt angle ϕ time series in still water and for the three sea states, with no currents and waves with $\beta_w=90$ degrees.

For the same external conditions the trajectory of the tower cross section at the mean water level is shown in Figure 62 for the turbine running in still water and in Figure 63 for the turbine operating in sea state 3 (most critical conditions).

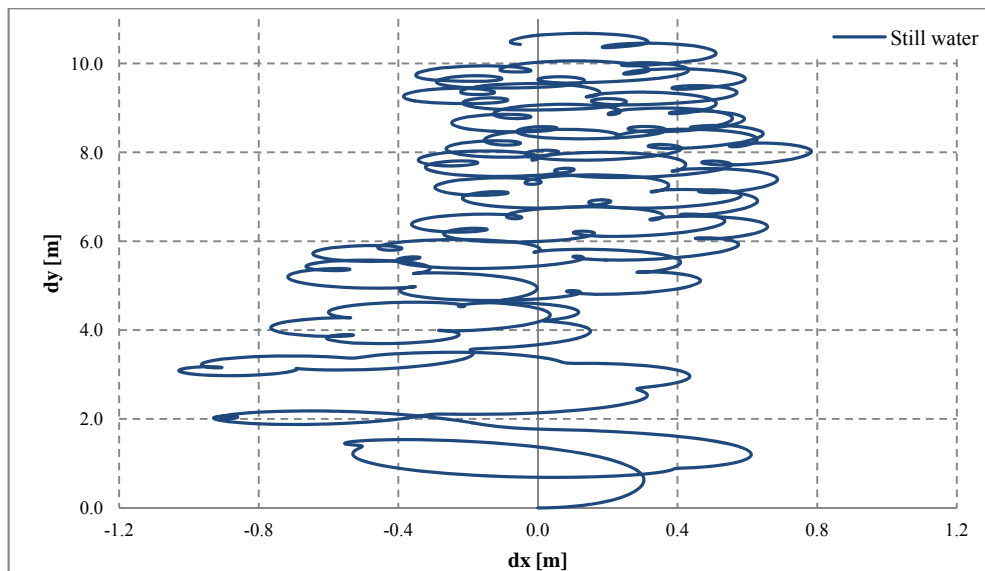


Figure 62 Trajectory of the cross section of the tower at the mean water level, still water conditions.

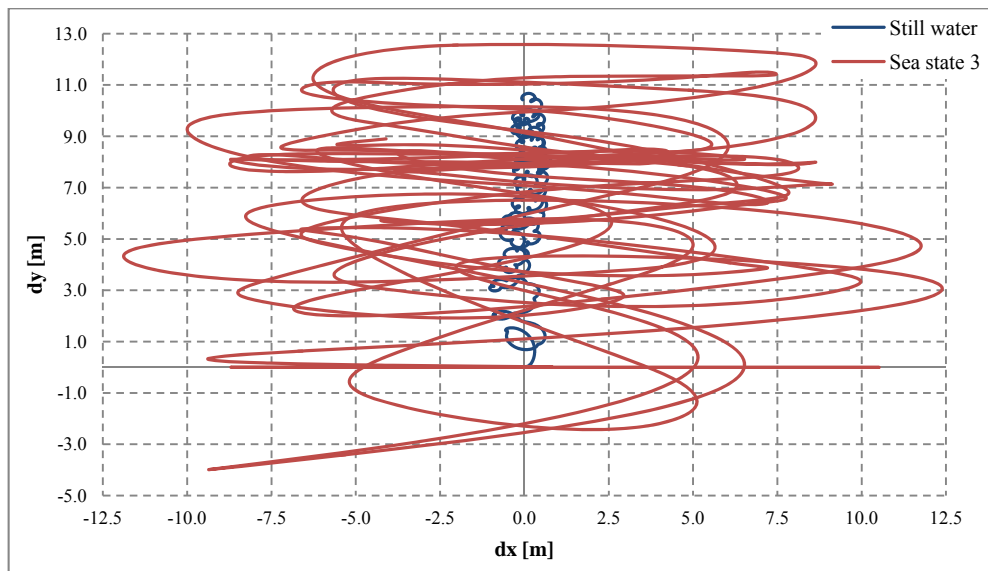


Figure 63 Trajectory of the cross section of the tower at the mean water level, still water and sea state 3 with no currents and waves with direction $\beta_w=90$ degrees.

8.3 Discussions of the results

The analysis of the floating VAWT in operative conditions shows a strong dependency of the dynamics of the system from the external conditions at the site. I have selected the maximum value of the tilt angle ϕ as the most important parameter to evaluate to stability of the floating wind turbine. In Figure 60 I compare the results from many different ocean external conditions with the maximum tilt angle that I recorded in still water. There are external conditions including severe values of the currents and the waves, which give values of ϕ_{\max} lower than in the case of still water. In some cases this is due to the damping effect that currents and waves have on the aerodynamic thrust, when their actions result in a load opposite to the aerodynamic moment. That is the case of currents with β_c equal to either 90 or 180 degrees and waves with $\beta_w=90$ degrees. Particular is the case of currents with $\beta_c=45$ degrees. Indeed, when $\beta_w=\beta_c=45$ degrees, the currents do not increase the value of ϕ and even act as a damper in the sea state 1 and 2. On the other hand when the same currents (with direction $\beta_c=45$) are added to waves acting on the wind direction ($\beta_w=0$ degrees), the turbine experiences a strong increase of the tilt angle, up to 12 degrees. Other critical situations for the control of the tilt angle seem to occur at currents from -90 degrees and waves on the same direction of the wind speed ($\beta_w=0$ degrees). Anyway, the currents are dominant in the determination of the maximum inclination of the turbine and the waves are mainly relevant for the calculations of the amplitude of the elliptic oscillations around the precession axis of the turbine. In Figure 61 to Figure 63, it is shown how the influence of the waves acts on the oscillations of the turbine around its equilibrium.

The moments M_x and M_y on the tower are also dependent of the currents, especially for the mean value, see **Error! Reference source not found.** and **Error! Reference source not found.**. From the plots, it is visible how the waves influence on the amplitude of the moment variation. The maximum mean values of the moments are

recorded for currents from 90 and -90 degrees, where sea state 3 shows the most challenging variations.

9 Downscaled model: 1kW

The design of a 1kW floating VAWT has been thought as a proof-of-principle for an experimental evaluation of the concept. Several configurations are possible for a 1kW demonstrator, depending on the DOF of the platform and the number of blades of the rotor. In my work I focus on the two bladed rotor anchored at the sea bottom, a configuration described in chapter 2.6.1 and investigated in the 5MW design.

9.1 Design

9.1.1 Site description

A 1kW turbine demonstrator (the configurations within the DeepWind project have not been decided yet) will be placed at Roskilde fjord, and I will use this site for my investigations. Due to the uncertainty on the water depth in a range of 4-5m, I selected a conservative value of 4m for the design.

The other characteristics at the location are:

- H_s , significant wave height, is 0.9m.
- T_P , peak period of the wave spectrum, is 3.2s, corresponding to $f_P=0.31$ Hz.
- The currents are expected to have a vertical averaged speed of 0.1m/s, as maximum value. The relative Re (on the tower diameter) of the free stream current is 1.2 104.

The values of the currents and the expected wave characteristics have been kindly supplied by DHI in a DeepWind internal report. In the same report it is also recommended the use of the formulas from the Shore Protection manual [82]:

$$\frac{gH_s}{U_A^2} = 0.283 \tanh \left(0.530 \left(\frac{gh}{U_A^2} \right)^{\frac{3}{4}} \right) \tanh \left(\frac{0.00565 \left(\frac{gF}{U_A^2} \right)^{0.5}}{\tanh \left(0.530 \left(\frac{gh}{U_A^2} \right)^{\frac{3}{4}} \right)} \right)$$

$$\frac{gT_P}{U_A} = 7.54 \tanh \left(0.833 \left(\frac{gh}{U_A^2} \right)^{\frac{3}{8}} \right) \tanh \left(\frac{0.0379 \left(\frac{gF}{U_A^2} \right)^{\frac{1}{3}}}{\tanh \left(0.833 \left(\frac{gh}{U_A^2} \right)^{\frac{3}{8}} \right)} \right)$$

U_A is the adjusted wind speed: $U_A = 0.71v_0^{1.23}$, H_s is the significant wave height, T_P is the wave peak period, h is the water depth, F is the fetch at which the wind speed is measured. Considering $F=6$ km and $v_0=20$ m/s, the results are very close to the values mentioned above, being $H_s=0.9$ m and $T_P=3.1$ s.

With known T_p and H_s it is possible to estimate the range of the most representative wave frequencies at the site:

$$1.05s < T_w < 4.25s,$$

Corresponding to:

$$0.23\text{Hz (1.47 radians/s)} < f_w < 0.95\text{Hz (5.98 radians/s)} \quad \text{Eq.10}$$

Other characteristic parameters are calculated using linear wave theory for finite water depth [41], [50]. A list of the wave characteristic numbers expected at Roskilde fjord is shown in the table below.

Table 25 Expected conditions at the Roskilde fjord at 4m water depth.

Roskilde Fjord			
ζ_a	(wave amplitude)	[m]	.45
λ_w	(wavelength)	[m]	14.92
T_p	(peak period)	[s]	3.2
f_p	(peak frequency)	[Hz]	0.31
ω_p	(peak rotational frequency)	[rad/sec]	1.96
K	(wave number)	[1/m]	0.42
H_s	(wave significant height)	[m]	0.9
h	(water depth)	[m]	4

9.1.2 Downscaling considerations

Applying the scale factors obtained in 5.2, fixed the power scale factor at 5000, the design values would be the ones in Table 26. A design using these values would not be feasible for several reasons. For example the conditions at Roskilde Fjord do not allow using neither a draft of the platform of 9.65m nor a rated wind speed of 4.15m/s.

Table 26 Design obtained applying the scale factors of Chapter 5.

		Scale factor	Baseline model	Downscaled model
Power	[kW]	5000	5000	1
Radius of the rotor	[m]	11.398	63.74	5.59
Height of the rotor	[m]	11.398	129.56	11.36
chord	[m]	11.398	7.45	0.65
Tower radius	[m]	11.398	4.15	0.28
Draft of the platform	[m]	11.398	108	9.65
Radius of the platform	[m]	11.398	3.15	0.38
Wind speed	[m/s]	3.376	14.0	4.15

Therefore, designing the 1kW turbine, I used a design scaling model, as described in Chapter 5.1, rather than a physical downscaling of the baseline model.

9.1.3 Rotor design

The selected configuration with two blades is supposed to be the most challenging because of the very high periodic loads on the tower (see section 3.2).

The aerodynamic design of small rotors is dominated by the effects of the Reynolds number. The typical local Re experienced by the blade elements of the demonstrator are plotted in Figure 64 for two elements and two operating conditions (starting and rated conditions). I define the local Reynolds number as $Re = cv_{local}/\nu$, with c the chord of the blade element, v_{local} the local velocity of the element (i.e. the vector summation of the wind speed and the relative velocity), ν the kinematic viscosity in air. For small rotors the local Re is commonly lower than 10^6 and in this range the characteristics of the aerodynamic airfoils are strongly dependent of the variation of Re [71]. For very low viscosity ($Re < 10^5$) the maximum values of the lift coefficient C_l drop and the stall happens at lower angle of attack. In designing small rotors this effect is taken into account avoiding low values of local Reynolds on the blades airfoils, in the most common range of operation of the turbine. This is achievable increasing the value of the blade chord, however other parameters have to be considered. Variations of the chord affect also the values of the solidity, which is another fundamental parameter for the design of a VAWT, $\sigma = cN/R$. Several numerical studies on the effect of the solidity at different Reynolds numbers have been carried out, for example by Strickland [36]. The maximum values of efficiency are generally reached for solidity values 0.2-0.25, while the most favorable control is achievable at lower solidity, in the range 0.1-0.2 [20]. However for small rotors, these studies are affected by the Reynolds number and higher values of efficiency are achieved at solidity values larger than 0.25.

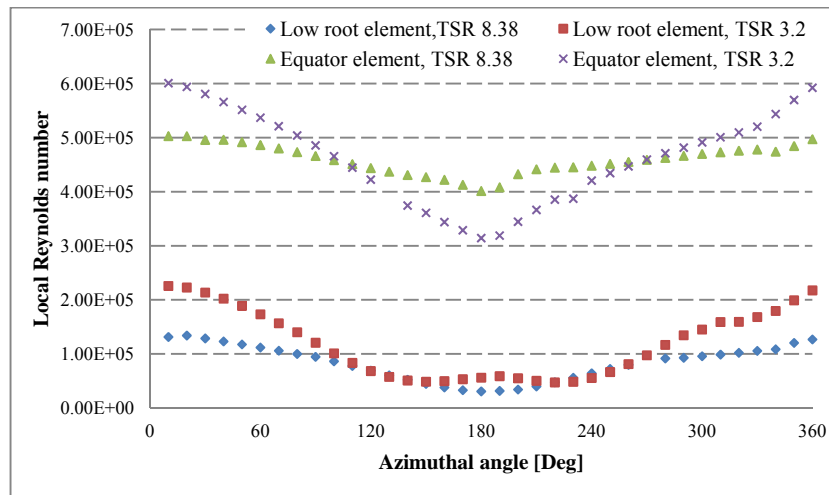


Figure 64 Local Reynolds number experienced by two elements of the blade at the start (tip speed ratio 8.38) and at rated conditions (Tip speed ratio 3.2). Chord=.172m

In the design of the demonstrator, other two issues to address are: the values of the rotor dimensions (radius and height) are limited by the water depth; the turbine has to be operative also at low wind speed, overcoming the power losses of the generator and the friction from the water. Based on these considerations, I have selected a rotor of 2m diameter and 2m height, with two blades of 0.172m chord ($\sigma=0.34$), also referring to the parametrical studies carried out by Trento University [83]. This

corresponds to a range of local Re included in the interval $0.5 \cdot 10^5 < Re < 6 \cdot 10^5$, as reported in Figure 64.

The rotor can reach a mechanical power close to 1.2kW at 13.2m/s and 440 rpm, as in Figure 65. A more detailed description of the aerodynamic performances and loads is available in [83] and [84].

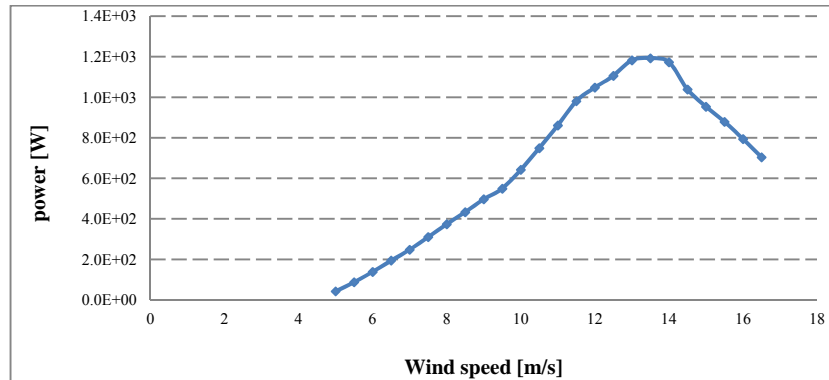


Figure 65 Power curve of the demonstrator.

The tower is a cylinder of 0.085m radius and 2mm wall thickness. The clearance of the blades from the mean water level is set at 0.5m. This value is very close to the wave amplitude, but the choice is supported by the following considerations:

- The turbine is supposed to be stopped in case of extreme conditions.
- The lower root of the blades has a low speed, due to the small value of the local radius. This may avoid major damages in case a wave would hit a blade.
- Design considerations require the rotor to be as light as possible.

Table 27 Rotor dimensions

Rotor characteristics		
Blade geometry	[-]	Troposkien
N, no of blades	[-]	2
H, rotor height	[m]	2.0
R, rotor radius	[m]	1.0
c, blade chord	[m]	0.172
σ, solidity	[-]	0.34
H₀, blade clearance	[m]	0.5
R_T, rotor tube radius	[m]	0.085
Th, tube wall thickness	[m]	0.002

The dimensions of the rotor are listed in Table 27, for a tower built in aluminum and blades in fiber glass. Due the high rotational speed, the centrifugal force acting on the blades of the demonstrator is larger than the gravity. Therefore a classic Troposkien shape has been selected for the blades of the demonstrator [9].

The properties are constant over the span of the blades and they are reported in Table 28.

Table 28 Blade Properties

Blade distributed properties			Blade undistributed properties		
Linear mass density	[kg/m]	1.34	Mass	[kg]	3.92
Cross sectional area	[m ²]	6.42 10 ⁻⁴	Length	[m]	2.93
I_x	[m ⁴]	8.44 10 ⁻⁹	Center of gravity (On the z axis)	[m]	0.99
I_y	[m ⁴]	1.47 10 ⁻⁷	I_{xx}	[m ⁴]	5.80
E	[N/ m ²]	1.6 10 ¹⁰	I_{yy}	[m ⁴]	4.92
			I_{zz}	[N/ m ²]	3.24

9.1.4 Platform design

Even though I will use only one configuration for my aero-elastic simulations, the design of the platform takes into account that the turbine has to run in the fjord under 3 possible configurations, as in section 2.6. In the second and third configuration the turbine is fixed to the bottom with an anchoring system and there is less available space to design the platform. Therefore I considered the third configuration in order to estimate the more restrictive design constraints.

Due to the wave height, in still water the elevation of the mooring lines needs to be at least 1m over the sea bed. Then the draft length of the platform in water is set to 3m.

The generator box is estimated to have a length of 0.3m, and then the length of the platform is reduced to 2.7m. The simulation of the first configuration needs a 1m extension from the bottom of the tower, which is then fixed at the sea bottom.

Also for the 1kW machine, the design has been finalized after an iterative process. The final dimensions are described in Table 29.

Table 29 Specification of the platform

1kW Demonstrator, platform specifications		
Length Mooring lines	[m]	1
Generator box diameter and height	[m]	0.3 x 0.3
H_P (draft)	[m]	2.7
H_{TOT} (included rotor)	[m]	5.2
R_P	[m]	.13
Radius distribution	[-]	Constant
Weight 1 blade	[kg]	3.92
Weight tower (H_{TOT})	[kg]	20.46
Ballast + Generator weight	[kg]	138
W_{TOT}	[kg]	166.3
Displacements	[kg]	164.55

The design is tailored for the Roskilde Fjord sea state described in Table 29, corresponding to the most critical conditions. The ratio D/λ_w is 0.017 which is much smaller than 0.2. Therefore the diffraction loads are not relevant in dimensioning the platform for a 1kW machine, and the structure can be studied as a slender body [48], [78]. The cyclical Reynolds number and the KC number of the platform are plotted over the water depth in Figure 66 and Figure 67. From $KC > 2$ the potential theory is not valid anymore because the fluid separates from the cylinder, the values of the inertial force drops and the drag force is dominant, [78]. However this theory does not consider the rotation of the platform that will delay the separation of the fluid and experimental data would be needed for a correct evaluation of the coefficients C_M and C_D . Even though not explicitly mentioned, the values recommended in the standards for C_M and C_D are applicable to larger structures and Reynolds numbers $> 10^6$. Thus they are not indicative for the 1kW design [78], [77]. I evaluate the drag force coefficient C_D considering the experimental results from [48]. For Re in a range of 10^4 C_D starts to increase for $KC > 0.3$ and it reaches an asymptotic value around $KC = 13$. In the range $0.3 < KC < 13$, an approximation for calculation of C_d is reported in [41]:

$$C_d = 0.2KC$$

The values of C_D and F_D , at different water depths, have been computed and they are reported in Figure 68.

The contribution in heave and pitch due to the wave-induced loads are calculated with the potential theory using the strip theory in [84].

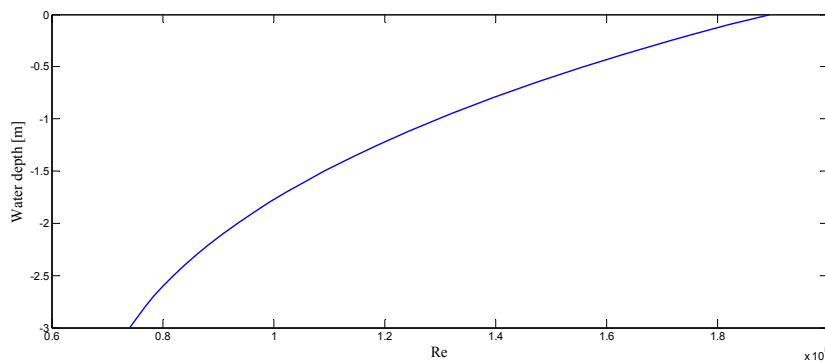


Figure 66 Range of oscillatory Reynolds numbers for the demonstrator.

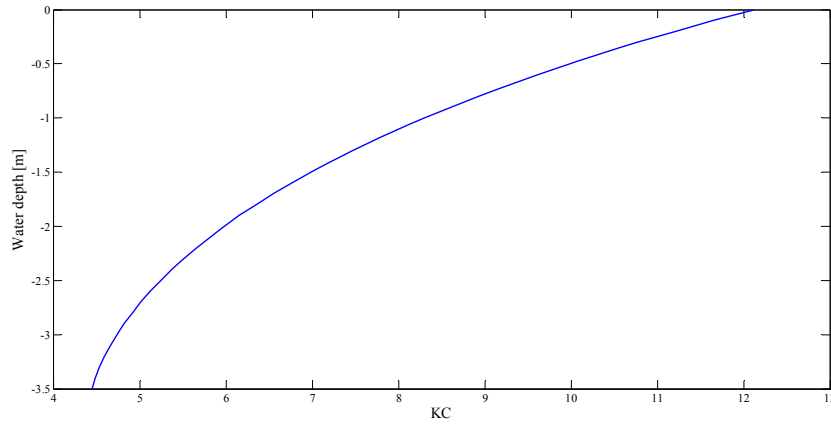


Figure 67 Range of KC numbers for the demonstrator.

The contribution of the lateral hydrodynamic force is computed, considering:

$$F_L(t) = \int_0^{H_P} .5\rho_w U(z, t)^2 D C_l(Re, \alpha) dz,$$

Where C_l is the 2D lift coefficient of a cylindrical section, rotating in a fluid stream of speed $U(z)$, at the local water depth z .

At the site, considering the maximum stream velocity ($U=0.1\text{m/s}$) and maximum angular speed ω (440rpm), the speed ratio α is 39.15. The free stream Reynolds number is equal to $1.2 \cdot 10^4$.

While there is a broad literature on C_l variation at the present range of Re , there is not any study, providing C_l on a cylinder for such high values of α , [56], [55], [53], [54], [52], [64]. However all these studies show that C_l reaches a maximum asymptotic value, at increased rotational speed, where Re is of the magnitude 10^4 . This is because the flow becomes fully attached to the cylinder.

Considering the asymptotic value $C_{l_{max}}=4\pi$, the force per length unit is:

$$F_l = .5\rho_w U^2 D C_l = 10.68\text{N/m}$$

Integrating on the cylinder, the total force and moment applied on the platform are:

$$F_L = 28.81\text{N}$$

$$M_x = 10.99\text{Nm}.$$

Therefore, for the downscaled model, the aerodynamic loads are dominant in the design and the effect of the currents is expected not to be significant.

The contributions of the aerodynamic and hydrodynamic loads to the pitch motion are reported in Table 30. I include also the contribution in heave, considering that in principle the design is supposed to work in all the three configurations.

Table 30 External loads on the platform.

LOAD	PITCH/ROLL [Nm]	HEAVE [N]	ω (frequency of the load) [rad/s]
Wave-induced	-523.97cos($\omega_w t$) -241.01 sin($\omega_w t$)	43.94sin($\omega_w t$)	1.96
Aerodynamic, longitudinal force	496.93 + 460.51cos($2\pi f_{2p} t$)	-	48.33
Aerodynamic, lateral constant term	-108.42 + 395.72cos($2\pi f_{2p} t$)	-	48.33
Hydrodynamic lateral force	10.99	-	-

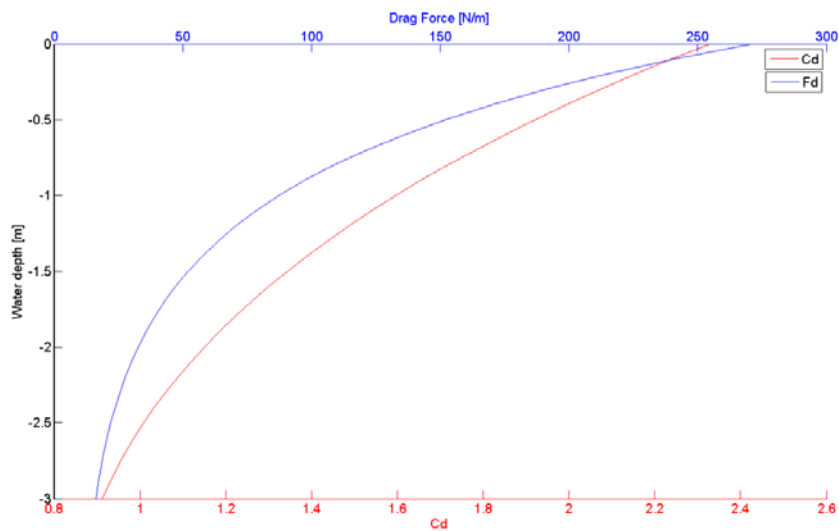


Figure 68 Cd and Fd for the platform of the 1kW turbine.

From the loads and using equations Eq.3 and Eq.4 in chapter 3, I calculate the most significant stability parameters which are shown in Table 31. The natural periods are calculated for an undamped and unmoored system, the displacement for the steady state of Table 24.

The natural periods are outside the range of the significant wave periods. The turbine has a large displacement in pitch, i.e. $\phi_{\max}=19.63 + 5.18\cos(1.96)$ deg.

However it should be noticed that these values have been obtained under conservative conditions. Moreover at maximum wave loads, the turbine is supposed not to be operative. Therefore, the two situations of max wave loads and max aerodynamic loads should not happen at the same time.

Table 31 Stability parameters of the platform of the 1kW turbine (positions in g.r.s.)

Platform stability		
Z_G	[m]	2.40
Z_B	[m]	1.54
Z_G-Z_B	[m]	0.86
C_{55}	[kg m ² /s ²]	1392.87
T_{n3}	[s]	6.41
ω_{n3}	[Hz]	0.15
T_{n5}	[s]	5.68
ω_{n4}	[Hz]	0.17
η_3 (from wave-induced loads)	[m]	.065 cos(1.69t)
η_4 (from wave-induced loads)	[deg]	5.18 sin(1.69t)
η_4 (from aerodynamic and hydrodynamic constant load)	[deg]	19.63
η_4 (from aerodynamic periodical terms)	[deg]	0.009 cos(48.33t)

The strong variation of the aerodynamic loads does not influence the equilibrium of the floating turbine. This effect is caused by the very high frequency of the aerodynamic loads. Indeed the equilibrium in pitch for an undamped floating body can be written as:

$$|\eta_4| = \frac{F_4}{C_{44} - (I_{44} + A_{44})\omega^2} = \frac{F_4}{C_{44}} - \frac{F_4}{(I_{44} + A_{44})\omega^2}$$

For large values of ω , the second term on the right hand side can be neglected and the equilibrium is depending on the mean values of the load F_4 and the restoring hydrodynamic coefficient C_{44} .

9.2 Results from numerical simulations

I carried out many simulations on the demonstrator. Here I report only the most significant results for the evaluation of the 1kW turbine. A more comprehensive study is available in [84].

The results are grouped in different sections:

1. Calculation of the eigen frequencies of the rotor.
2. Simulations on the turbine in on-land configuration to calculate power and comparison between the two airfoils.
3. Offshore simulations for different external conditions.

In most of the simulations, the turbine runs at constant wind speed and the rotational speed increases until a limit value, after which it is kept constant by the generator. However some simulations are carried out also at variable wind speed, with variable rotational speed. In these simulations, the rotational speed of the generator is adjusted as in Table 32 and Figure 69.

Table 32 Rotational speed and rotational frequency at different wind speeds

Wind speed [m/s]	ω_r rotor [rpm]	ω_n generator [rpm]	f_{1p} [Hz]
0 – 4	143.24	685.83	2.38
4 – 12.3	143.24 – 441.17	685.83 – 2112.36	2.38 – 7.35
12.3 – 14	441.17	2112.36	7.35
14 – 16	441.17 – 340.0	2112.36 – 1627	7.35 - 5.67

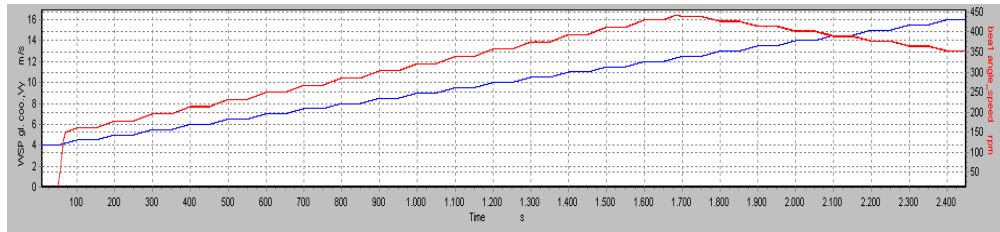


Figure 69 Sim.10, ω_r in red and ω_{sp} in blue

The reference systems used for the calculations is the one in Figure 26 and the measurement points are highlighted in Figure 27.

A specific issue in the code setup regards the time step for the numerical simulations of the 1kW turbine. During operations, the rotational speed is increased up to 440rpm, corresponding to a frequency of 7.33 Hz. Using a time step equal to 0.05s (20Hz) as for the 5MW, the code will compute the loads on the blades for maximum three azimuthal angles per revolution. In order to achieve an acceptable level of accuracy I run most of the simulations at 75Hz and 125Hz, corresponding to values of the time step of 0.013 and 0.008.

Another adjustment needed in the setup is the limit values of the residual forces. Indeed HAWC2 uses physical values given as convergence limits. Therefore a new set of values is needed for very small rotors. I used the following values: 1N as residual internal-external force, 0.001 as residual on the increment and $7 \cdot 10^{-7}$ as residual in the constraint equation. Further explanations on these parameters is available in [38].

9.2.1 Natural frequencies of the rotor

I performed some calculations with HAWC2, to verify the natural frequencies of the turbine. The constraints are considered rigid and no damping is included. The values seem to be consistent with the natural frequencies registered by Sandia for the 2m turbine [15]. The first nine natural modes and frequencies for the turbine standing on land are reported in Table 33 and drawn in Figure 70. The natural frequency modes are generally larger than the rotational frequencies of the rotor, apart from the first mode of the tower out of plane mode, which is close to f_{2p} for $\omega_r=441.17$ rpm.

Table 33 First nine natural frequency modes of the 1kW rotor

	Mode shape	Natural Frequency [Hz]
Mode1	1 st tower out of plane	15.79
Mode2	1 st tower in plane	16.75
Mode3	1 st blade flatwise symmetric	25.04
Mode4	1 st blade flatwise antisymmetric	25.61
Mode5	1 st rotor twist	26.83
Mode6	1 st blade edgewise	28.04
Mode7	2 nd rotor twist	35.52
Mode8	2 nd tower out of plane	36.51
Mode9	3 rd tower out of plane	38.84

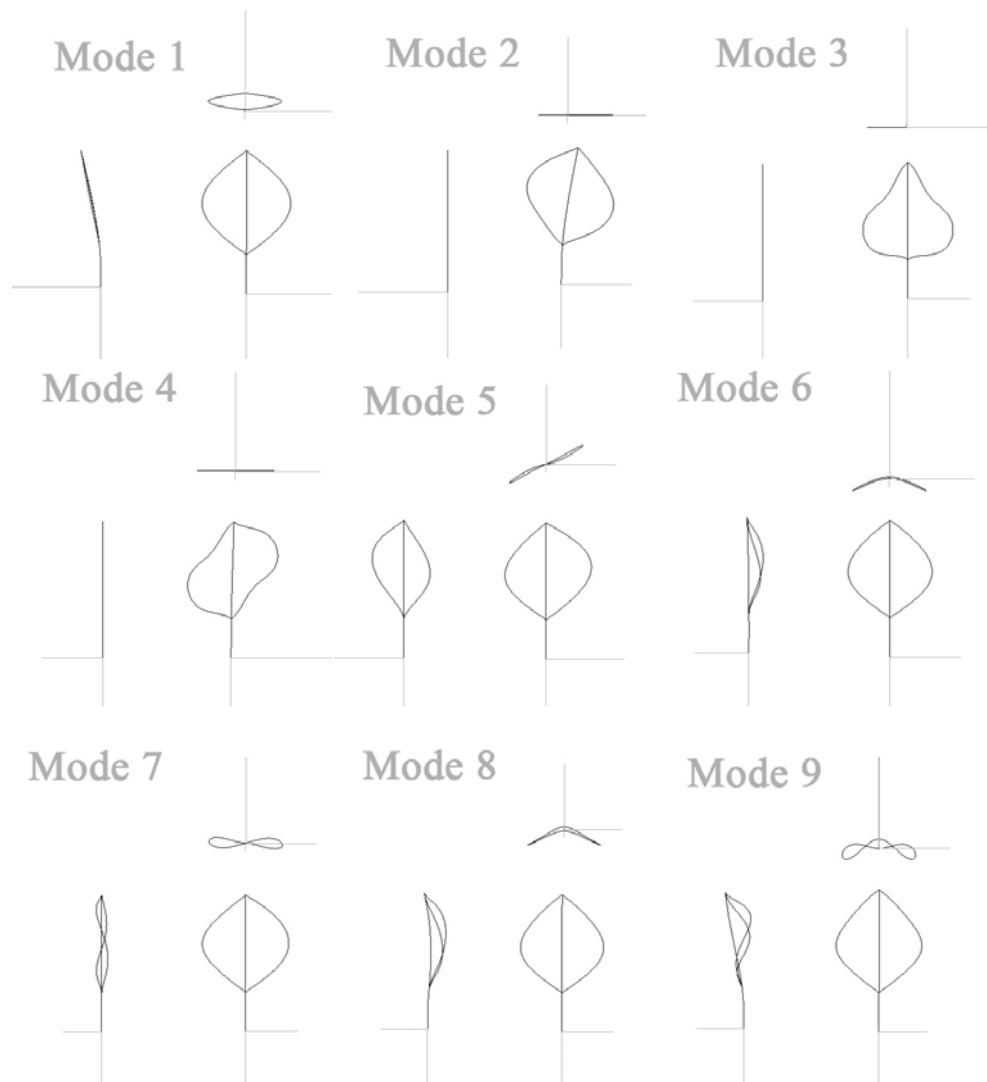


Figure 70 First nine natural modes of the rotor

9.2.2 On land configurations

Before running offshore simulations, I run some simulations of the turbine in on-land configuration, without using the hydro module. In this configuration, the rotor tower is directly fixed to the generator box, which is placed on the ground (there is no platform). I considered the same design described in 9.1.3 and I increased the stiffness of the tower to avoid structural problems. The goal of these simulations is to have a general understanding of the behavior of the rotor and to test the two different airfoils.

The simulations are listed in Table 34. In all the simulations the turbine it started from a standing vertical position and the spinning is supported from a motor for the first acceleration, see Figure 71.

Table 34 Simulations carried out for land configuration

Simulation N.	v_0 [m/s]	Profile	ω_r [rpm]	Frequency acquisition data [Hz]
0	No Aerodynamics	NACA 0018	0-500	75
1	7 constant	NACA 0018	251	75
2	7 constant	DU 06-W-200	251	75
3	10 constant	NACA 0018	358	75
4	10 constant	DU 06-W-200	358	125
5	12.3 constant	NACA 0018	440	125
6	12.3 constant	DU 06-W-200	440	125
7	16 constant	NACA 0018	410	75
8	16 constant	DU 06-W-200	410	75
9	4 – 16 variable	NACA 0018	Variable	20
10	4 – 16 variable	DU 06-W-200	Variable	20

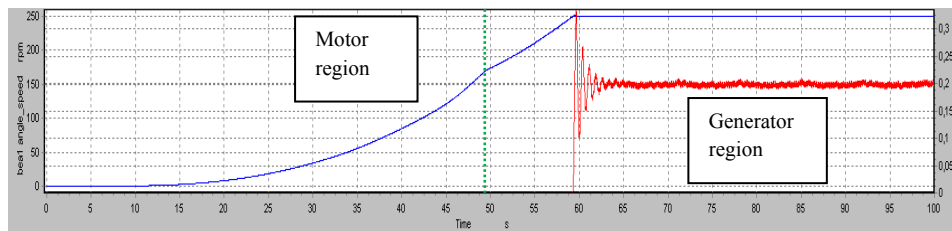


Figure 71 Sim.1- Rotational speed (blue) and electrical power (red). The green line defines the region where the generator acts as a motor

The simulations at constant wind speed give more reliable results, because of the lower value of the time step. I used these data to analyze the loads on the turbine in different operational points. In Figure 72 and Figure 73 I plot the forces and the moments on the tower, respectively, at the points 4 and 5 of Figure 27.

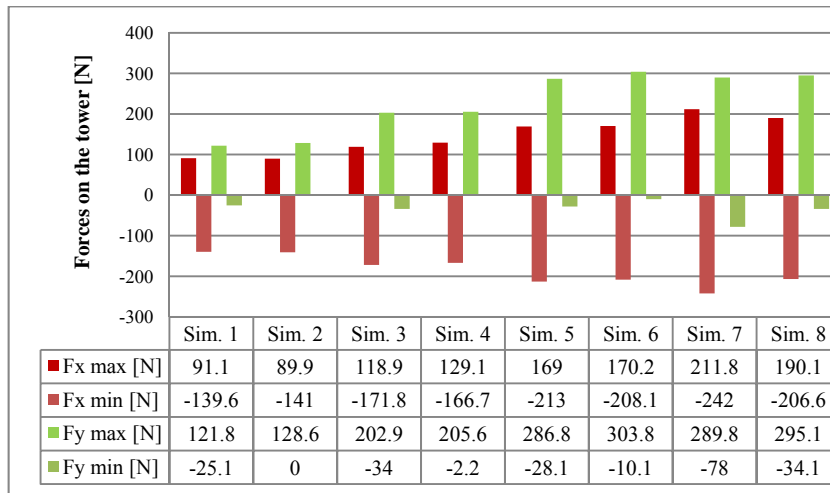


Figure 72 Forces on the tower, on land configuration point 4 of Figure 27

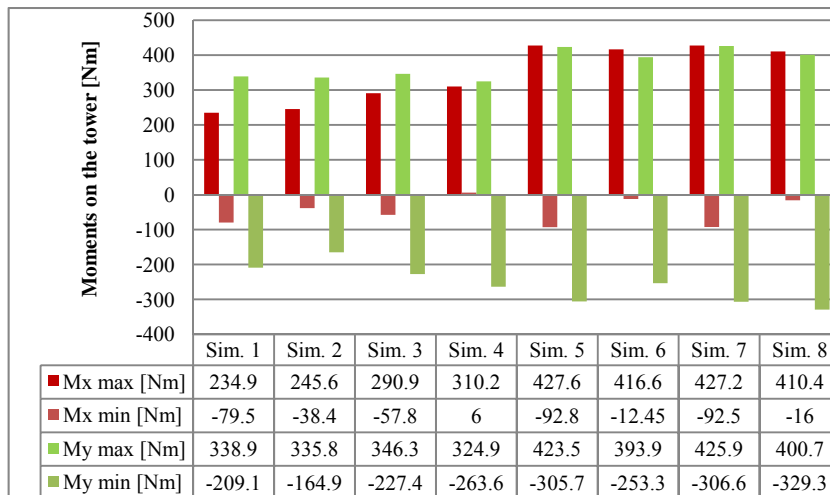


Figure 73 Moments on the tower, on land configuration, point 5 of Figure 27

A comparison on the power output with rotors mounting the two airfoils, is shown in Figure 74, considering four wind speeds.

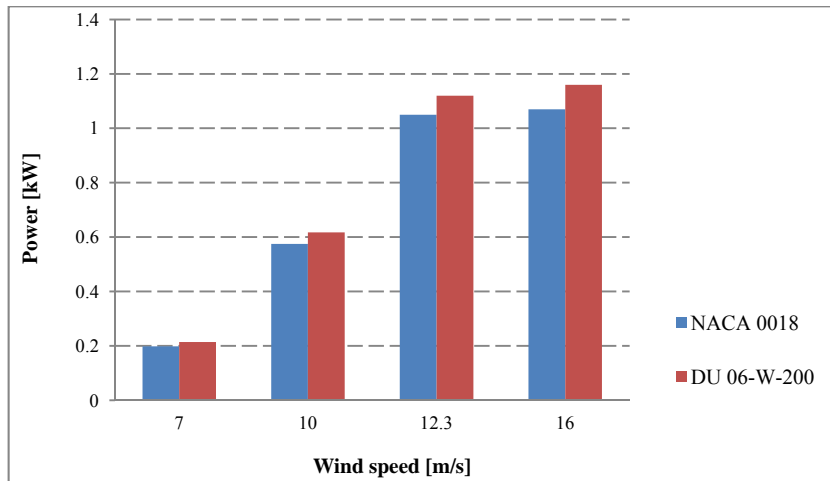


Figure 74 Maximum power output at four wind speeds, on land configuration

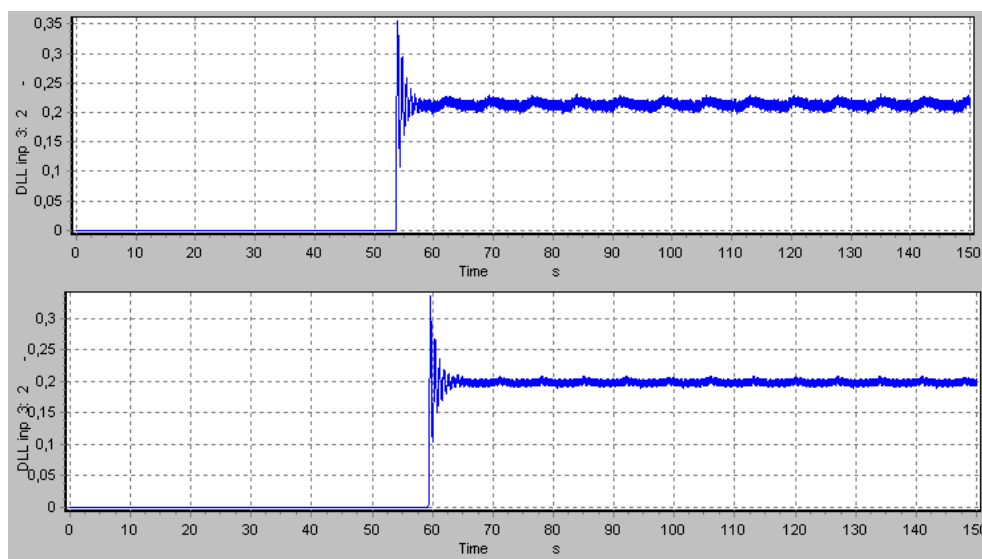


Figure 75 Power [kW] at 7m/s for 0018 (top) and Tu20 (bottom)

9.2.3 Discussion on the results of the on land configuration

As expected, F_y has a largely positive mean and the minimum value is around zero. F_x has a negative mean value, quite close to zero. The frequency of the loads is f_{2p} .

The highest loads are recorded at $v_0=12.3\text{m/s}$ and $v_0=16.0\text{m/s}$, corresponding to the maximum power output. There is not a large difference in the loads due to the different airfoils but at some wind speeds the NACA 0018 gives larger oscillations of both the forces and moments.

Figure 74 shows that the DU 06-W-200 performs better in all the operation conditions, with an improvement of the maximum power output around 6.6% at rated wind speed (12.3m/s). I have to stress that the available data for this profile were limited to $Re > 3 \cdot 10^5$ [72]. The data have been interpolated for lower Reynolds and an over estimation of the aerodynamic coefficient is possible to occur, partly justifying the increment in the power. The thicker airfoils has also better start characteristic, as shown in Figure 75, where the rotor with the DU 06-W-200 profile reaches

synchronous rotational speed of the generator faster than the rotor with a NACA 0018 profile.

Eventually, it should be stressed that at high wind speeds, the results are affected by an uncertainty, due to the dynamic stall contribution. Also turbulence might increase those values.

9.2.4 Offshore simulations

The rotor and aerodynamic set up is the same used for the on land calculations. In all the simulations I use the profile DU 06-W-200, since it performed better in the previous simulations.

This section includes results from 11 simulations, combining:

- Constant wind speed of 7m/s and 12.3 m/s
- Waves of amplitude .4m and period 2s. The wave characteristics have been reduced considering lower values of v_0 .
The wave directions, β_w , are 0 and 90 degrees, referred to the wind speed direction.
- Water current of maximum speed 0.1m/s. The current has a power law profile with coefficient 0.5.
The directions β_c of the current are 0 and 90 degrees, referred to the wind speed direction.

The complete list of the simulations is reported in Table 35.

Table 35 Simulations for the offshore configuration

Sim. N.	v_0 [m/s]	ϕ_0 [deg]	H_s [m]	T_P [s]	β_w [deg]	β_c [deg]	U [m/s]	ω_r [rpm]
11	No aerodynamics	5	-	-	-	-	-	0
12	No aerodynamics	5	-	-	-	-	-	0 - 350
13	7 constant	0	-	-	-	-	-	251
14	12.3 constant	0	-	-	-	-	-	440
15	7 constant	0	0.45	2	90	-	-	251
16	12.3 constant	0	0.45	2	90	-	-	251
17	7 constant	0	0.45	2	0	-	-	440
18	12.3 constant	0	0.45	2	0	-	-	440
19	7 constant	0	0.45	2	0	0	0.1	251
20	12.3 constant	0	0.45	2	0	0	0.1	440
21	12.3 constant	0	0.45	2	0	90	0.1	440

The first two offshore simulations, 11 and 12, do not include aerodynamic loads. I carried out these two runs to verify the dynamic response of the system in absence of aerodynamic loads and evaluated the natural periods in pitch and roll.

The results are shown in terms of dx, dy and dz, displacements of the cross sectional area of the tower at the mean water level. In simulation 11, the turbine is tilted 5 degrees around the x axis, and it is left free to oscillate in the water. In Figure 76 the time series of dx and dy are plotted.

The natural period in pitch and roll are equal and close to 6s, as expected. The roll mode consists only of a vibration mode at the natural frequency. The pitch motion, generated by the inclination of the tower, is larger and quite well damped.

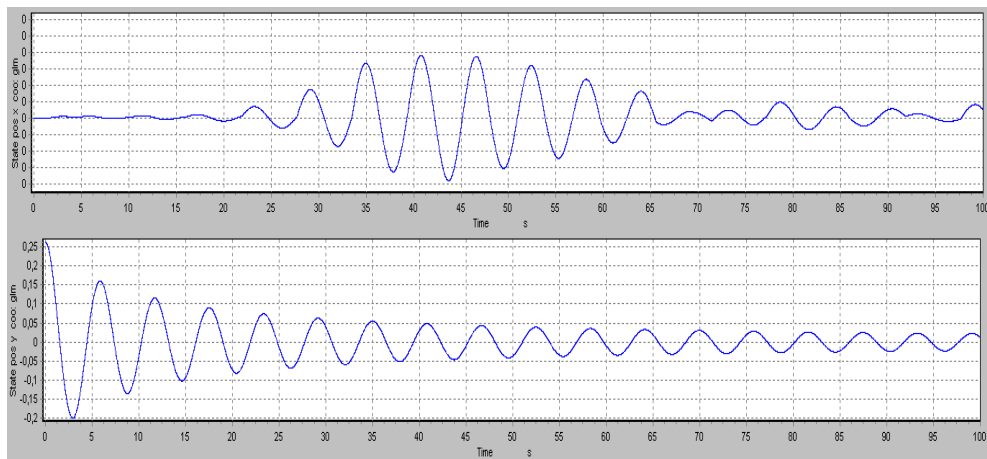
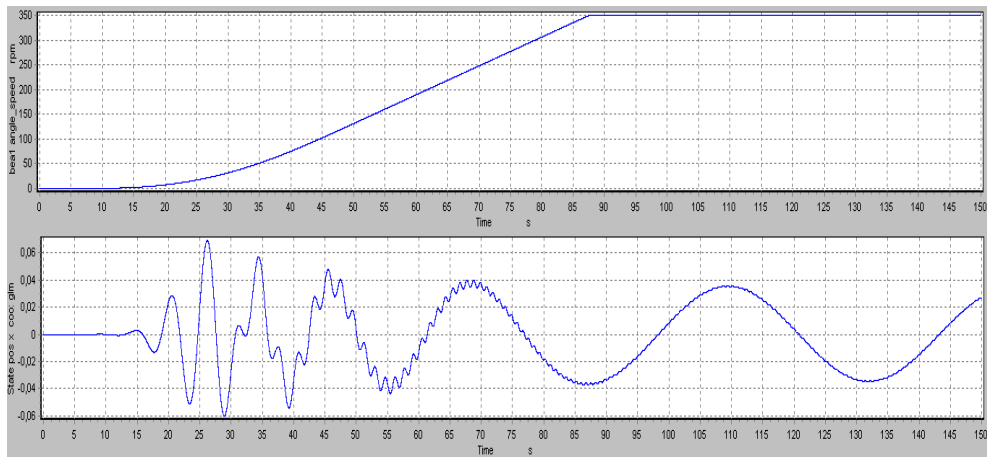


Figure 76 Sim11 From top: dx and dy, in meters



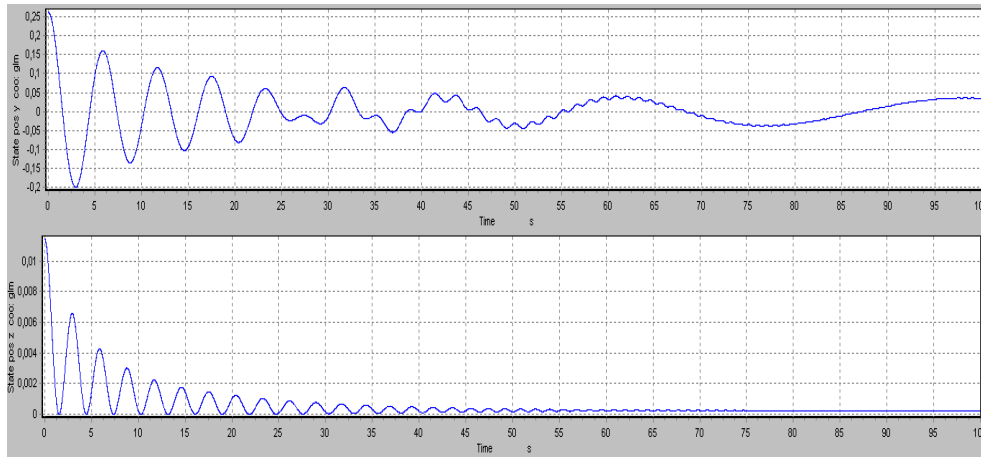


Figure 77 Sim12, from the top: 1. ω_r [rpm] 2. Dx [m], 3. dy [m], 4. dz [m]

In sim12, the turbine is also spinning up to 350rpm. In Figure 77, dx , dy and dz are plotted along with ω_r . The plots allow some observations:

- The natural periods are strongly affected by the rotational speed. At 350rpm, the period of the oscillations is greater than 40s. The same effect is present in both pitch and roll.
- dz , shows a very stiff behavior of the turbine
- As expected, at lower rotational speed some high frequency effects are visible. At high rotational speed, the inertia cancels those effects and the plot appears to be smoother.
- The roll motion generated by the pitch, has a low amplitude, but also a low damping.

The results of the other offshore simulations include:

- Parameters to evaluate the stability of the turbine: ϕ_{mean} , ϕ_{max} , see Figure 78. These values do not include the deflection of the tower.
- Loads in offshore environment: M_x and M_y on the mean water level cross section of the tower (point 5), Figure 79.

Time series of the tilt angle are plotted in Figure 80 - Figure 82.

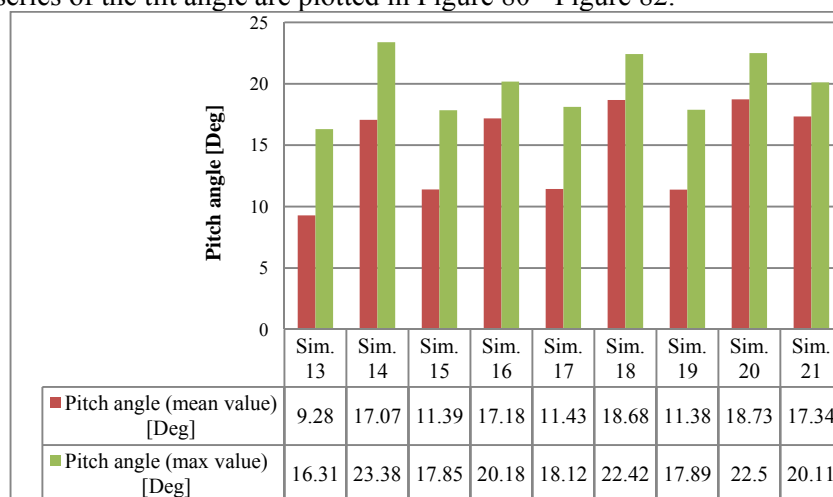


Figure 78 Maximum and mean value of the pitch angle for different offshore external conditions

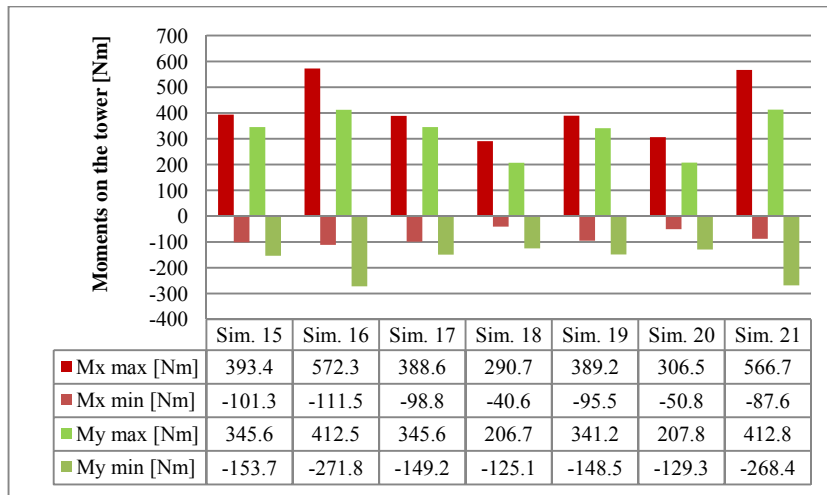


Figure 79 Moments on the tower, offshore configuration

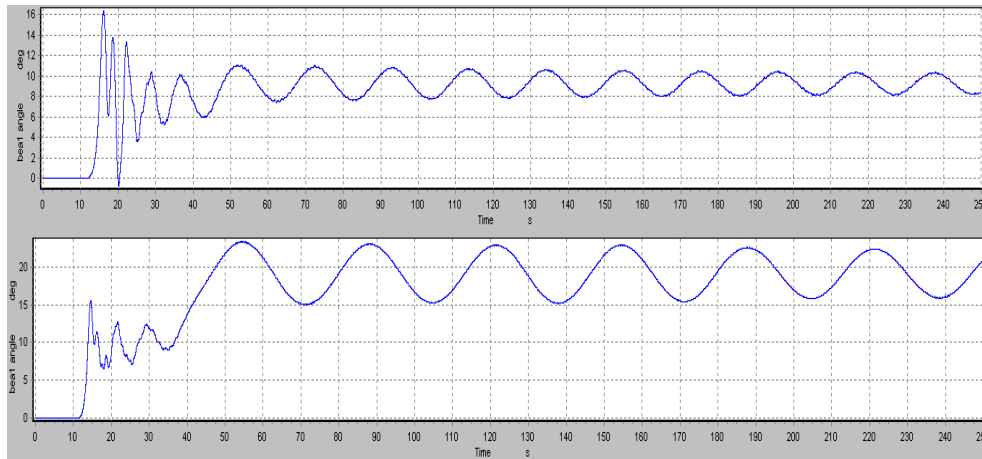


Figure 80 Tilt angle [Deg] time series, from top: Sim11 and Sim12

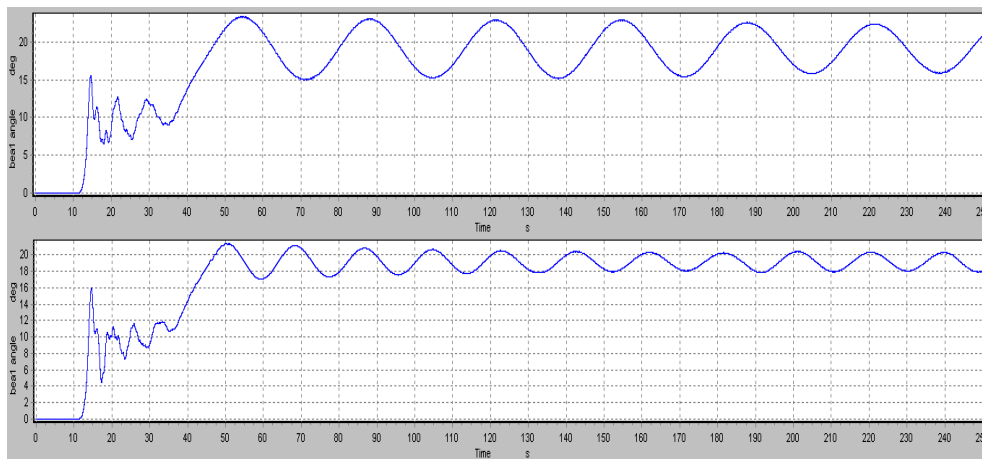


Figure 81 Tilt angle [Deg] time series, from top: Sim12 and Sim12 with reduced inertia of the tower

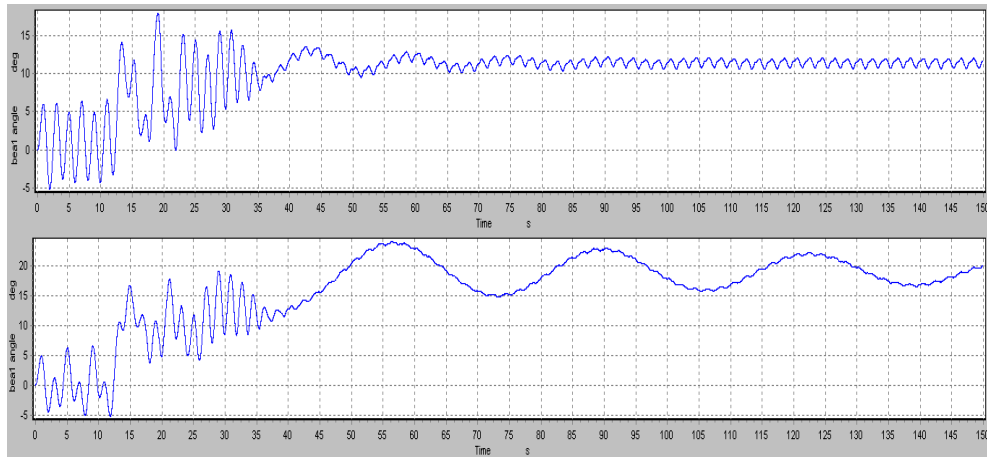


Figure 82 Tilt angle[Deg] time series. From top: sim17 and Sim18

9.2.5 Discussion on results and recommendations on the platform design

Among the performed simulations, the most challenging one for the equilibrium is at $v_0=12.3\text{m/s}$ and waves in the same direction as the wind (Sim18 in Figure 79). The water current do not seem to give significant changes (Sim20, in Figure 79).

On the other hand, the most critical loads on the tower, at the mean water level, are recorded for waves or currents perpendicular to the wind speed direction (Sim21 in Figure 79).

The maximum tilt angle do not correspond to the maximum external load, probably due to the strong contribution of the inertial loads.

At low wind speed (7m/s) and 251rpm, the most critical events seem to occur at the starting of the turbine (Figure 80 top). The frequency of the wave loads is still well distinguishable (Figure 82, top).

At $v_0=12.3\text{m/s}$ and $\omega_r=440\text{rpm}$, the periods of the motion in pitch increase strongly (Figure 80, bottom). The contributions of the high frequency loads are less visible (Figure 82, bottom). Meanwhile, the turbine has some larger oscillations, probably due to its inertia.

The loads in Figure 79 are much larger than the loads recorded in the on shore configuration and recorded in Figure 73. However, it is stressed that this may be due to the not scaled effects of the wave-induced loads on the structure, which have a larger relative importance in the downscaled model.

In Figure 81 is shown the importance of the inertia at high rotational speeds. The second plot in the figure is obtained by reducing the inertia of the tower. This causes a strong reduction in the amplitude of the platform oscillations.

9.3 Conclusions

The 1kW demonstrator design was first investigated with HAWC2 in on land configuration. The most significant results are:

- The 20% thick airfoil from TuDelft performs better than the NACA0018, based on a power output comparison (around 7% more production), as from Figure 74.
- Some simulations have been carried out at the same conditions investigated in the report from Trento Univeristy [83]. Results from HAWC2 seem quite consistent, as from Figure 75 (top).

Some conclusions have been presented on the loads in offshore configuration:

- Magnus effect seems not to be very relevant, at least in terms of maximum loads.
- The wave loads are quite large and need to be properly modeled. Some experimental results would be recommended to evaluate C_D and C_M at high rotational speed of the platform.

Aerodynamic loads are dominant for the stability of the platform. The mean value of the longitudinal force (thrust) is the most important parameter.

The periodical variation of the aerodynamic loads, do not affect the equilibrium at high rotational speed

The turbine has equilibrium in pitch, even though it operates at high tilt angles. In the worst condition, the turbine has a tilt angle of 19 degrees, plus fluctuations

The design has been verified with simulations in HAWC2:

- The inertial loads seem to be very important at high rotational speeds and the natural periods are larger than expected. (Figure 77, Figure 80, Figure 81).
- Due to the high frequencies, the periodical aerodynamic loads are not a problem for the stability (Figure 77).
- High rotational speeds and thrust give important values of the tilt angle.

Some limitations of this study should be mentioned:

- Aerodynamic load calculation may change with turbulence effects.
- Dynamic stall can also affects the results at high wind speeds.

Last, some recommendations for possible future work:

- A choice about the anchoring system should be made. Some considerations on this issue are:
 - To have a positive restoring contribution in pitch, the attachment of the mooring lines has to be above the centre of gravity. This would require a new modification of the design either the use of a bearing around the tower.

- In case the mooring lines are not taking any moment, the attachment could be placed at the bottom of the structure.
- In order to improve the stability of the platform, some new configurations for the offshore design could be considered, i.e. conical shaped tower. Other solutions found in the literature have also been mentioned.

10 Cost models for offshore floating wind turbines

The economics of wind-generated electricity can be studied from two different points of view: the cost to produce electricity and the value of the same electricity in the energy market. The first one addresses mainly technical and financial issues, while the second deals with social and political aspects. The two problems are obviously coupled, but in my dissertation I will consider the production cost (the first of the two mentioned approaches) of wind energy as an independent problem.

In this chapter I organize my research in two tasks:

- A survey of studies carried out in the past ten years
- A preliminary evaluation of the concept based on the present possibilities.

First, I introduce some terms which are commonly used in economical studies.

The levelized cost of energy (COE) is defined as:

$$COE = \frac{FCR \cdot ICC}{AEP} + AOE$$

Where

FCR is the fixed charge rate and depends on the currency in which the cost is calculated

ICC is the initial capital cost, corresponding to all the expenses at the moment of the wind farm installation. This term includes the cost of the turbine (rotor and tower), drive train and electrical components (generator, bearings, brakes transformer, cabling and electrical connection), balance of station (foundation, transportation, installation, permits). For offshore wind energy it will additionally include: anchoring and platform, harbour facilities and infrastructure, scour protection, marine operation, special additional permits, proper material treatment for marine environment, use of offshore technologies for installation and decommissioning.

AEP is the net annual energy production.

AOE is the annual operating expenses, mainly consisting of levelized O&M cost: $AOE = O\&M / AEP$. Additional annual expenses connected to permits, leasing and replacement of components can be added.

10.1 Cost analysis of wind energy

There are essentially two possible approaches to evaluate the cost effectiveness of wind turbine concepts: the first is based on statistical data and quotations from

manufactures; the other one is a design model where the data are acquired with an engineering numerical calculation, [85]. The last model has the advantage to be more accurate and adaptable to estimate cost effectiveness of new technological concepts. On the other hand it is usually quite complex and requires a team of expertise to be built and also to be run. The statistical model gives less flexibility in the design phase but it has the high advantage that, after compiled, it can be easily used also by not expert customers.

In the US, a project called WindPACT (Wind Partnership for Advanced Component Technology) was performed to predict cost projections for wind turbine upscaling. The results were grouped in several reports dealing with different terms of the cost of energy (such as composite blades for 80-120m rotors [66], base of station, alternative drive train, rotor and tower). WindINPACT project was not directly providing prices of the wind electricity production, but it was rather giving an estimation of the impact of new technologies on the mass and cost of wind turbine components. Cost functions were developed to scale the cost and the mass of the wind turbines. Starting from WindINPACT reports, NREL has developed a cost model to predict cost of wind-generated electricity [65]. The model essentially consists of a spreadsheet which predicts the COE of a wind farm using simple formulas to calculate each term of a wind farm cost. The formulas are obtained by analysis of statistical data (mainly for wind turbines up to 2MW) and using the upscaling functions from WindINPACT projects (for wind turbines larger than 2MW). One of the problems in developing this kind of model is to have a result durable in the time, which is not affected by financial variables. To overcome this limitation the cost models commonly include economic parameters, such as the inflation rate. NREL model uses the Produce Price Indexes (PPIs) rather than the inflation index. The PPI is released yearly from the US federal government and takes into account the prices of the materials from different industries in the U.S. The PPI is more accurate than the inflation index because it considers the variability of the cost linked to the production cost and to the availability of the rough materials. These indexes can be used only backwards in time to adjust the present prices on the older values, but it cannot be used to forecast future cost of the materials. Another limitation of the model is that, due to the statistical approach of the calculations and to the lack of offshore data, the model is mainly intended for onshore wind energy.

In Netherlands an advanced cost model had been developed specifically for offshore wind energy, within the DOWEC project (Dutch Offshore Wind Energy Converter), [74]. The project was carried out by a consortium and the model follows an approach similar to the one from NREL. All the relevant costs for the complete development of a wind farm were listed and the breakdown of the total cost was obtained. Then the data on the expected costs of each sub-component and sub-action were collected from different partners and reported in a spreadsheet. Finally all the costs are summed up again and used with the AEP and the financial parameters, to calculate the COE. DOWEC emphasizes particularly the importance of the coupling between a cost model and the design of the wind turbines, in order to estimate the cost effectiveness of a new concept design. The project included the design of a baseline 6MW HAWT, to use for evaluating the effect of new design concepts on the COE. The cost model is re-used at each design step, to integrate the cost analysis with the

technical improvements. An example of the application of this approach is given by Hendriks in the evaluation of different control strategies for HAWT (pitch and stall controls), [86].

Another study on the cost of offshore wind-generated electricity is available in a report from Garrad Hassan, [87]. The study aims at the calculation of the cost of energy production per installed MW but addresses that this value can be largely dependent to the technological concept. The major uncertainty results in the assessment of the O&M costs, which represents a considerable amount in the breakdown of the total cost for an offshore wind farm, i.e. 28% according to [45]. This is mostly due to the lack of available statistical data, which are essential for evaluation of O&M expenses. Another uncertainty in the estimation of the cost of the sub-components and sub-actions is due to the immature state of some technological elements. To overcome this limitation, in the report a progress ratio approach is used, estimating the future reduction in the cost due to technological upscaling, scale in the production and learning process. The report estimates a reduction in the cost of 15% in the short term. Using the same approach Juginger forecast a cost reduction up to 39% in 2020. The 80% of the improvement in cost effectiveness is supposed to come from mutual learning in the different technologies involved in the offshore wind energy [88].

An attempt to evaluate floating offshore wind turbine concepts has been carried out by Wayman [89]. She based her estimations on the capital cost of the considered concepts, disregarding O&M cost and the relevance of financial parameters.

As a conclusion of this overview on the wind energy cost models, I would like to quote Zaaijer from TUDelft: *“There is no such thing as ‘the one cost model for offshore wind energy’ [...] the cost model must match the target of the application”* [85].

10.2 DeepWind evaluation

So far, none of the described models is applicable to the DeepWind concept for limitations of the models (regarding both VAWTs and floating foundations) and for the limited development of the concept itself. At the current state of development an estimation of the COE would be pure speculation because the uncertainties in all aspects of parameter estimation would be extremely high. Therefore I have preferred to use a concept to concept comparison as evaluation method.

In my dissertation I consider neither financial nor socio-economic parameters, since I assume that these variables do not affect the value of a concept with respect to another one. I have also decided to not include the O&M costs because of their high variability. This is a strongest assumption, but I consider that in the evolution of new concepts, the ICC is still the most relevant parameter. Therefore I only focus at the capital cost ICC of the EOC formula (64% of the wind farm costs), and I consider the following shares [74]:

- Installation cost (17.2%), including assembly, transportation and installation.
- Hardware cost (82.8%), including, rotor, tower, platform and generator box.

I consider the hardware costs divided in:

- Rotor (20.1%), including hub, blades and pitch control system.
- Support structure (35.6%), consisting of tower and foundation (or platform). There is no reference on the breakdown of these costs between platform and tower. Here I consider the platform to be the 70% of the support structure costs (24.92% of the hardware costs) and the tower the 30% (10.68%)
- Nacelle (25.1%), including generator, gear box and all the sub-components housed in the nacelle.
- Other costs (19%), which are expenses not directly connected to the wind turbine concept, as the electric collection system and the transmission system to shore.

I have selected as a comparative model, OC3-Hywind 5MW design, as described in [44]. There are some clear advantages in this choice. First, Hywind is a good baseline model for a comparison, since it is a proven concept close to commercialization. Moreover the similarity between the two concepts allows some simplifications and reduces the uncertainties on the results. I consider the cost of a single wind turbine, since there are not sufficient data to evaluate the impact of the different concepts in a wind farm layout.

Table 36 Main characteristics of the two concepts. *the data are taken from [44], [28] and [43]

Parameter		OC3-Hywind*	DeepWind
Rated Power	[MW]	5	5
Rated rotational speed	[rpm]	12.1	5.26
Rated wind speed	[m/s]	11.4	15
Tower elevation	[m]	97.6	145
Tower weight	[kg]	$3.47 \cdot 10^5$	$4.45 \cdot 10^5$
Blades length	[m]	61.5	188.68
Weight of 1 blade	[kg]	$1.77 \cdot 10^4$	$1.58 \cdot 10^5$
Number of blades	[-]	3	2
Blade chord	[m]	4.65 – 1.42 (tapered)	7.45
Draft of the platform	[m]	120	110
Platform water displacements	[m ³]	8029	5940
Control systems	[-]	Pitch regulation + yaw system	Rotational speed regulation

In order to start, I had to make a further assumption, considering the costs breakdown above valid for both the two wind turbine concepts. I compare the cost of each sub-component in the two concepts.

When it is possible, I base the comparison on available data, such as the mass.

When detailed data are not available, I compare the sub-components using theoretical considerations. Then I rate each sub-component of the VAWT with respect to the respective HAWT component. When my comparison is based on a pure theoretical evaluation, I use 6 possible grades for the evaluations: highly unfavourable, unfavourable, slightly unfavourable, neutral, slightly favourable,

favourable, highly favourable. These correspond to a percentage variation in the cost, supposed to be respectively: -100%, -50%, -10%, 0%, 10%, 50%, 100%, see Table 38.

ROTOR

The blades for Deepwind are 3.07 times longer and even though only two blades are needed, the value of the weight ratio is larger. Indeed the weight of the two VAWT blades results in 5.95 times the total weight of the three HAWT blades (without including the hub). In his study on HAWTs blades, Cheney states the reduction in the cost due to pultrusion process to be up to 74%, [90]. In another investigation on pultruded blades for HAWTs, the cost of pultruded blades is indicated to be for the 97.74% linearly dependent from the mass, [46]. Therefore, supposing a unitary cost C_{blades_H} for the three HAWT blades, the relative cost C_{blades_V} of the VAWT blades is:

$$C_{blades_V} = C_{blades_H} (1 - 0.74)(0.0226 + 0.9774 \cdot 5.95) = 1.518 C_{blades_H}$$

Then I rated as unfavourable the production of VAWT blades.

However the breakdown of the cost of a HAWT rotor shows that the blades represent only 43% of the total rotor cost, with the other 57% consisting of the hub and pitch control system [74]. These two costs are not present in a VAWT design, therefore I consider the total relative cost of the rotor as:

$$C_{rotor_V} = C_{rotor_H} (0.43 \cdot 1.518) = 0.65 C_{rotor_H}$$

TOWER

Both the towers are built in steel and, considering the cost proportional to the weight of the structure, I obtain:

$$C_{tower_V} = C_{tower_H} \left(\frac{4.45}{3.47} \right) = 1.28 C_{tower_H}$$

I have to stress at least two possible sources of errors:

- The weights have been calculated using different properties for the steel. Indeed the Hywind OC3 is designed considering a density of 8500kg/m³, instead of the typical value of 7850kg/m³ used in my work. The reason of the higher values is to account for the weight of other parts, such as flanges and welds.
- I consider a more conservative value for the clearance of the blades from the water, i.e. 15m instead of 10m. This is mainly due to avoid any possible problems in the calculations but a lower value could be considered. Additionally, the VAWT tower can still be optimized reducing the radius of the height.

Both these two observations are valid also for the discussion on the platform, since the weight distribution has a strong influence on the design of the underwater structure.

GENERATOR BOX

Here I consider the elements housed in the generator box, which usually for a HAWT are grouped with the name “nacelle costs”. I considered some of the costs to be insensitive to the type of design, such as the computer, the sensors and the electrical converter. These costs make up to 38.5% of the total.

I considered as costly unfavourable for a VAWT, the following sub-components:

- The housing (originally the 2% of the cost), which has to deal with underwater pressure and corrosion. I applied an increasing ratio of 100%.
- The bearings, since they have to take a considerable axial load varying with the time. In HAWT breakdown this cost is set very close to zero, therefore I considered it as part of the generator costs.
- The generator, including gear system, makes up to 52% of the cost and it could in principle be the same for the two concepts. However, some distinctions have to be made. Placing the generator in the bottom, the VAWT has no limitation on the weight of the generator. A direct drive variable speed generator could be used saving the costs of the gear box. On the other hand, some limitations could occur in space. Indeed, the low rotational speed of the rotor makes the dimensioning of the generator to be challenging. Eventually also the cost of the bearings has to be included. An accurate prediction on these costs would require a deep investigation considering several aspects. Therefore, due to the large number of uncertainties, I have chosen a conservative approach, with an increase of 50% in the generator costs.
- The brake system has to be capable to stop the turbine without the support of aerodynamic brakes. Water brakes could solve this problem and cut the costs. Meanwhile I consider these costs to be doubled in a VAWT design. The original share of the brakes in the costs breakdown of a HAWT is 2.5%.

The yaw system, consisting of the 5% of the total cost, is not needed in a VAWT.

Table 37 Cost of the sub-components housed in the generator box.

Generator housing	Cost in percentage		Ratio
Housing	2	Highly unfavourable	2
Generator (included gear system and shaft)	52	Unfavourable	1.5
Yaw system	5	Not present	0
Bearings	<1	Highly unfavourable	-
Computer and sensors	26.5	Neutral	1
Electrical conversion	5	Neutral	1
Brake system	2.5	Highly unfavourable	2
Electrical cables	4.5	Neutral	1
miscellaneous	2.5	Neutral	1
TOTAL			1.219

The total cost of the components housed in the generator box is then:

$$\begin{aligned} C_{generator_V} &= C_{generator_H} (0.385 + .52 \cdot 1.5 + 0.02 \cdot 2 + .025 \cdot 2) \\ &= 1.219 C_{generator_H} \end{aligned}$$

PLATFORM AND ANCHORING

I considered as unchanged the costs for mooring lines and anchors. A best evaluation would require a tailored design of DeepWind according to the 3rd configuration of 2.6.3.

For the platform I considered the same approach used for the tower, considering the cost to be directly proportional to the water displacements. Then it is:

$$C_{platform_V} = C_{platform_H} \left(\frac{5940}{8029} \right) = 0.74 C_{platform_H}$$

INSTALLATION

As described in 2.3.1, DeepWind allows some better possibilities for installation procedure, especially at sites where the turbine has to be tilted up with the rotor already mounted. Meanwhile, no VAWT has ever been installed offshore and an additional cost connected to the learning process should be considered in the first years. Eventually I rated as slightly favourable DeepWind configuration for the installation.

Table 38 Cost comparison of different sub-components of the capital costs.

Sub-component	From OC3Hywind to DeepWind	Cost ratio DeepWind/OC3Hywind
ROTOR		0.65
Blades	Unfavourable	1.518
Hub and Pitch control	Not present	-
TOWER		1.28
Tower structure	Unfavourable	1.28
GENERATOR BOX		1.219
Housing	Unfavourable	2.0
Generator	Unfavourable	1.5
Yaw system	Not present	-
Bearings	Highly unfavourable	(included in the generator)
Computer and sensors	Neutral	1.0
Electrical conversion	Neutral	1.0
Break coupling system	Highly unfavourable	2.0
Electrical cables	Neutral	1.0
miscellaneous	Neutral	1.0
OFFSHORE STRUCTURES		0.74
Platform	Favourable	0.74
INSTALLATION		0.9
Transportation	Slightly favourable	0.9
Installation	Slightly favourable	0.9

Summing up the values in Table 39, I obtain a relative cost factor of 0.93, meaning a 7% reduction of the capital costs in using DeepWind concept. This preliminary study allows considering DeepWind as a possible competitive concept in a market where Hywind is close to become commercial. Nevertheless, particular care is recommended in use of these values as a demonstration of possible concept superiority. There are still too many uncertainties, which don't allow any further and definitive conclusion. Among these uncertainties, the most relevant are:

- The analysis of different offshore concepts is very dependent from the site and a cost analysis should be made considering different sites with a considerable number of available data
- The turbines are designed for different rated wind speeds and with a different control system. Thus the AEP is very different (higher for the HAWT design). Also the design of the rotor should be tailored on the site to maximize the AEP.
- The VAWT design has not been optimized, as the HAWT. Some additional iteration in the design process, which would include more detailed descriptions of the components, could reduce the gap in the AEP. A better study on the control possibilities would also better clarify which control strategy can be applied to increase the energy efficiency.

10. Cost models for floating offshore wind turbines

- The properties used to describe the materials are not the same, as I have mentioned for the steel. And also the safety factors applied on the structure seem to be different.
- The design of the VAWT is mainly thought to use the technologies available on the market nowadays. These technologies have been mostly meant to work on HAWTs and in the future more tailored product for VAWTs could be available.

Table 39 Summation of the sub-components costs

	Original share in offshore HAWT wind farm	DeepWind adaptation factor	Final weight compared to OC3Hywind
Rotor	0.17	0.65	0.11
Generator box	0.21	1.22	0.25
Tower	0.09	1.28	0.11
Platform	0.21	0.74	0.15
Other costs	0.16	1.00	0.16
Installation	0.17	0.90	0.15
TOTAL	1.00		0.93

11 Conclusions

My work aimed at investigating the feasibility and the potential of a new offshore floating vertical axis wind turbine concept. Driven by this goal, the study has gone through a broad range of disciplines and technological problems. At the end of my dissertation, the state of the knowledge on this new concept is increased thank to new results and meantime additional questions emerged during the study, addressing the need for further investigations.

The most relevant conclusions for the concept evaluations are:

1. The new concept has its greater favourable characteristic in its simplicity. This allows different possible configurations, for example for the rotor and the anchoring system. In the selection of the first configuration to study I followed the approach used by Hendriks to design a baseline HAWT turbine [45]. Since this first design has possibly to be a reference for future calculations and modifications, it has to be based as much as possible on known and proven technology. Following this criteria, the first design decisions have been taken in Chapter 2.
2. From the analysis of the loads, it is emerged the preponderance of the hydrodynamic loads for the stability of the system. This result is extendable to other floating wind turbine concepts and it is consistent with the previous studies. It also means that both the feasible and the optimal design of floating wind turbines are strongly dependent from the site.
3. The coupling between the design and the external conditions is even more evident in DeepWind concept because the rotation of the platform generates new loads, such as a lateral force (Magnus effect), a drag force and a friction moment. The forces and the moment generated by a water stream passing the rotating platform have been numerically computed in Chapter 4. To my knowledge this study has two novelties: the application of these loads to the platform of a wind turbine and the large values of the Reynolds number ($>10^6$) combined to the large number of α (>2), where α is the ratio of the peripheral speed and the velocity of the water stream. The results show values of the lateral force very close to the value found at lower Reynolds numbers ($Re \sim 10^4$) by other authors. These results were expected at high rotational speed, since in both cases Re is larger enough to avoid the separation of the boundary layer. It was unexpected to me the presence of a negative drag (thrust) at large values of α . This result needs further investigation and it could affect the platform stability. The friction seems to represent a minor problem in the design, but marine growth could make it worst. Therefore, even though the friction doesn't represent a significant limit in power production, it could result in an undesired increase in O&M costs.
4. The concept has been tested using the numerical code HAWC2, developed at Risø DTU and capable in handling very different concepts, such as

floating VAWTs. To achieve an acceptable accuracy in my simulations, I added some DLLs to the code, simulating the VAWT aerodynamics and the hydrodynamic loads on the rotating structures. A first 2MW design has been used as a test model to verify the proper functionality of the software and the correct coupling of all hydro and aero- dynamics.

5. A 5MW concept has been designed and tested with HAWC2. The design addressed some challenges, for example in dimensioning of very large blades with constant properties over the length (hypothesis due to the pultrusion process). The large dimensions of the platform results mainly in a regime dominated by inertial forces, apart for the most critical sea states, which generates large KC numbers and significant viscous effects. The turbine has been designed to run with a tilt angle ϕ lower than 10 degrees, in most of the operative conditions, to avoid major structural problems. I carried out simulations at three sea states and for different directions of the currents and of the waves propagation. The turbine operates with a tilt angle ϕ depending on the external conditions. When the turbine is in equilibrium (in absence of large variations of the external conditions) the platform oscillates around the equilibrium value of ϕ and describes an elliptical motion, due to the precession mode of the turbine. The motion of the turbine in the mean water plane is strongly coupled in the x and y axes. Indeed the turbine is subjected to gyroscopic effects generated by the rotation and to the hydrodynamic lateral force generated by the relative motion of the platform respect to the water.

From the simulations, the turbine exceeds the inclination of 10degrees (≈ 12 degrees) only for two particular combinations of wave, wind and currents directions. However I didn't register any significant deformation of the tower due to the high tilt angle. The greater values of ϕ are due to the currents acting perpendicularly to the wind, resulting in a hydrodynamic force on the same direction of the hydrodynamic thrust. The hydrodynamic loads of the currents and the aerodynamic loads have the same magnitude order and when they act on the same direction, the turbine operates close to the vertical position. The dynamic contribution of the waves results in larger amplitudes of the motion of the turbine and in increased loads on the structure.

6. I designed also a 1kW model for experimental investigations. The typical scale factors applied in offshore modelling are described in Chapter 5. However these scale factors cannot be applied without to adjust the rotor design. I eventually decided to design the 1kW floating VAWT, as a small version of the concept rather than as a downscaled model of a 5MW turbine. This is also due to practical reasons in manufacture the small turbine and to the real conditions at the site, which cannot be scaled as a downscaled model would require. A small model, even though not reproducing exactly a larger design, can give important clarifications on the feasibility of the concept (such as the possibility of using the water as a roller bearing) and can possibly address new relevant aspects to investigate. The design of the turbine has been conditioned by the limited depth of the Roskilde fjord. For such shallow waters, the draft of the platform cannot exceed 2.7m and the

turbine is designed to operate at high tilt angle ϕ . The numerical simulations confirm this data and show a strong influence of the rotor inertia on the dynamics of the platform. The natural periods of the pitch and roll modes are much larger than expected and I believe this is due to the high rotational speeds. Due to the high rotational speed the stability of the platform is not affected by the strong periodic variation of the aerodynamic loads. Another peculiarity of the small model is that the aerodynamic loads are dominant over the other loads and the turbine is constantly tilted in the wind direction. The Magnus effect doesn't give significant contribution, due to the low speed of the currents at the site.

7. From my investigation it emerges that there is a large numbers of variables to consider in the study of DeepWind concept and the design space is very narrow. However, I did not find any serious issue, which could invalidate the feasibility of the concept and from a first outlook there are good economical potentials.

The need for further work emerged during this study and I grouped some of the most urgent key aspects, which should be developed first:

1. Due to the novelty of the concept I experienced a lack of appropriated standards. Nothing is specified about the characterization of the vertical water current profile and only small attention is dedicated to turbulence of the water stream and the direction of the currents with respect to the waves. Other limits regard the rotor standards, since VAWTs are not included in the wind turbine standards [49], [76].
2. Other improvements can come from a more precise characterization of the met-ocean conditions at the site. A correct evaluation of DeepWind concept would require a joint of wind, waves and currents data. Additionally, the vertical variation of the currents should be measured, including the velocity and the currents direction.
3. The implementation of the aerodynamic code in a DLL offered some advantages during the development process. However, for further investigations, the integration of the aerodynamic routine in the main code is recommended to decrease the computation time, reduce the number of input files and allow the use of all the features included in the main program (as turbulence, dynamic stall and tower shadow effects).
4. Possible design variations to the concept could be tested: straight blades can allow pitch control and lower the weight, 3 blades to reduce the periodic loads, longer rotor to reduce the cost and the gyroscopic effects. Investigation of the second and third configurations should come parallel to the new design concepts.
5. The rotation in water of the rotor affects the natural frequencies of the system. This can be an important issue to investigate, especially for the demonstrator.
6. The design of the blades for large rotors is resulted to be challenging. Here, I proposed to use to different sections over the blade, even though without changing the chord. Other designs are possible and some further studies are

needed, taking three variables into account: the structural strength of the blade, the manufacture feasibility and the costs.

7. The design of the generator for the 5MW DeepWind concept has to deal with some particular constraints, such as the placement in deep water and the very low rotational speed. The weight is not a limitation in the design, but the dimensions could create problems in dimensioning the platform. An option could be to use more than one generator, for example two 2.5MW generators.
8. Beyond the evaluation of this concept, there is need for new cost models capable to evaluate floating wind turbine concepts. I would distinguish between two possible models.

A specific simplified cost model could be useful in the design process of DeepWind concept, to evaluate the possible technological solutions and modifications applicable to the baseline model.

Another model could be used to evaluate different floating wind turbine concepts. As learnt from literature a cost model with this potential cannot be exclusively based on statistical data, but it needs an engineering model and a baseline design to use as reference [45], [85]. Both the tasks are challenging due to the many differences among the floating wind turbine concepts describe in Table 2.

Bibliography

- [1] L. Vita, U. S. Paulsen, T. F. Pedersen, H. A. Madsen, and F. Rasmussen, "A novel floating offshore wind turbine concept," in *Proceedings of the European Wind Energy Conference (EWEC)*, Marseille, France, 2009.
- [2] U. S. Paulsen, T. F. Pedersen, and L. Vita, "Existing VAWT technologies," Risø DTU (Technical University of Denmark), Roskilde, Denmark, I-2613(EN), 2008.
- [3] U. S. Paulsen, T. F. Pedersen, L. Vita, H. A. Madsen, and F. Rasmussen, "Recommendations for floating VAWT technology demonstration and development," Risø DTU (Technical University of Denmark), Roskilde, Denmark, I-2616(EN), 2008.
- [4] A. Zervos and C. Kjaer, "Pure Power - Wind Energy scenarios up to 2030," European Wind Energy Association (EWEA), 2008.
- [5] N. Fichaux and J. Wilkes, "Oceans of opportunity," European Wind Energy Association (EWEA), Brussels, Belgium, 2009.
- [6] S. Krohn, P. Morthorst, and S. Awerbuch, "The economics of wind energy," European Wind Energy Association (EWEA), Brussels, Belgium, 2009.
- [7] G. J.M. Darrieus, "Turbine having its rotating shaft transverse to the flow of the current," 1835018, 1926.
- [8] D. Coiro, F. Nicolosi, A. De Marco, S. Melone, and F. Montella, "Dynamic behaviour of patented Kobold tidal current turbine: numerical and experimental aspects," in *Proceeding of the 4th International Conference on Advanced Engineering Design*, Glasgow, UK, 2004.
- [9] T. D. Ashwill and T. M. Leonard, "Developments in blade shape design for a Darrieus vertical axis wind turbine," Sandia National Laboratories, Albuquerque, New Mexico (US), SAND86- 1085, 1986.
- [10] R. E. Sheldal, "Comparison of field and wind tunnel Darrieus wind turbine data," Sandia National Laboratory, Albuquerque, New Mexico (US), SAND80-2469, 1981.
- [11] B. F. Blackwell, Robert E. Sheldahl, and Louis V. Feltz, "Wind tunnel performance data for the Darrieus wind turbine with NACA 0012 blades," Sandia National Laboratory, Albuquerque, New Mexico (US), SAND76-0130, 1977.
- [12] R. E. Sheldal, P. C. Klimas, and L. V. Feltz, "Aerodynamic performance of a

- 5-metre-diameter turbine with extruded aluminum NACA 0015 blades," Sandia National Laboratories, Albuquerque, New Mexico (US), SAND80-0179, 1980.
- [13] T. D. Ashwill, "Measured data for the Sandia 34-meter vertical axis wind turbine," Sandia National Laboratories, Albuquerque, New Mexico (US), SAND91-222, 1992.
- [14] T. D. Ashwill, "Initial structure response measurements and model validation for the Sandia 34-Meter VAWT test bed," Sandia National Laboratories, Albuquerque, New Mexico (US), SAND88-0633, 1990.
- [15] T. G. Carne and A. R. Nord, "Modal testing of rotating wind turbine," Sandia National Laboratories, Albuquerque, New Mexico (US), SAND82-0631, 1983.
- [16] D. E. Berg, "Structural design of the Sandia 34-meter vertical axis wind turbine," Sandia National Laboratories, Albuquerque, New Mexico (US), SAND84-1287, 1985.
- [17] M. E. Ralph, "Design and Control of the variable speed generator on the Sandia 34-meter vertical axis wind turbine," in *Proceedings of the Windpower Conference*, San Francisco, California (US), 1989, pp. 55-59.
- [18] FloWind Corporation, "Final project report: high energy rotor development, test and evaluation," Flowind Corporation, Sandia Contract AB-7292, San Rafael, California (US), SAND96-2205, 1996.
- [19] P. W. Carlin, A. S. Laxson, and E. B. Muljadi, "The history and state of the art of variable speed wind turbine technology," *Wind Energy*, vol. 6, pp. 129-159, 2003.
- [20] I. Paravischivoiu, *Wind turbine design, with emphasis on Darrieus concept.*: Polytechnic International Pres, 2002.
- [21] C. Beller, "Urban wind energy - state of the art 2009," Risø DTU (Technical University of Denmark), Roskilde, Denmark, Risø-R-1668(EN), 2009.
- [22] Renewable Energy 2010 target Team Business Development Unit, "The world offshore renewable energy report 2004-2008," London (UK), 2008.
- [23] A. R. Henderson and David Witch, "Floating offshore wind energy - A review of the current status and an assessment of the prospects," *Wind Engineering*, vol. 34, no. 1, pp. 1-16, 2010.
- [24] W. Musial and B. Ram, "Large-scale offshore wind power in the United States - Assessment of opportunities and barriers," National Renewable Energy Laboratory, Golden, Colorado (US), NREL/TP-500-40745, 2010.

- [25] W. Musial and C. Butterfield, "Future for offshore wind energy in the United States," in *Proceedings of the Energy Ocean Conference*, Palm Beach, FL, 2004.
- [26] W. Stoddard, "The life and work of Bill Heronemus, wind energy pioneer," *Wind Engineering*, vol. 26, no. 5, pp. 335-341, 2002.
- [27] O. M. Faltinsen, *Sea loads on ships and offshore structures.*: Cambridge University Press, 1990.
- [28] J. Jonkman and D. Matha, "Dynamics of offshore floating wind turbines - analysis of three concepts," *Wind Energy*, vol. 14, no. 4, pp. 557-569, 2011.
- [29] PrinciplePowerInc., "Column-Stabilized Offshore Platform with Water-Entrapment," WO2009131826.
- [30] B. Skaare et al., "Integrated dynamic analysis of floating offshore wind turbines," in *Proceedings of the Euorpean Wind Energy Conference (EWEC)*, Milan, Italy, 2007.
- [31] J. Jonkman, "Dynamics modelling and load analysis of an offshore floating wind turbine," National Renewable Energy Laboratory, Golden, Colorado (US), Ph.D. Dissertation NREL/TP-500-41958, 2007.
- [32] I. Ushiyama, K. Zechi, and H. Miura, "A feasibility study for floating offshore windfarms in Japanese waters," *Wind Engineering*, vol. 28, no. 4, pp. 383-398, 2004.
- [33] T. J. Larsen and T. D. Hanson, "A method to avoid negative damped low frequent tower vibrations for a floating, pitch controlled wind turbine," in *Proceedings of the Conference The science of making torque from the wind*, Copenhagen, Denmark, 2007.
- [34] J. E. Withee, "Fully coupled analysis of a floating wind turbine system," MIT (Massachussets Institute of Technology), Cambridge, Massachussets (US), PhD Thesis 2004.
- [35] K. H. Lee and P. Sclavounos, "Floating wind turbines," in *Proceedings of the 20th Workshop on Water Waves and Floating Bodies*, Spitsbergen, Norway, 2005.
- [36] J. H. Strickland, "The Darrieus turbine: a performance prediction model using multiple streamtubes," Sandia National Laboratories, Albuquerque, New Mexico (US), SAND75-0431, 1975.
- [37] H. A. Madsen, "On the ideal and real energy conversion in a straight bladed vertical axis wind turbine," Aalborg University Centre, Aalborg, Denmark, Ph.D. Report ISBN: 87-87681-06-4, 1983.

- [38] T. J. Larsen and A. M. Hansen, "How 2 Hawc2, the user's manual," Wind Energy, Risø DTU (Technical University of Denmark), Roskilde, Denmark, Risø-R-1597, 2009.
- [39] J. Jonkman et al., "Offshore code comparison collaboration within IEA wind task 23: Phase IV results regarding floating wind turbine modelling," in *Proceedings of the European Wind Energy Conference (EWEC)*, Warsaw, Poland, 2010.
- [40] L. Vita, U. S. Paulsen, T. F. Pedersen, H. A. Madsen, and F. Rasmussen, "DeepWind: a novel floating offshore wind turbine concept," *WindTech*, vol. 6, no. 4, 2010.
- [41] J. N. Newman, *Marine Hydrodynamics*.: Massachusetts Institute of Technology, 1977.
- [42] L. Vita et al., "A novel concept for floating offshore wind turbines: recent developments in the concept and investigations on fluid interaction with the rotating foundation," in *Proceedings of the International Conference on Ocean Offshore and Arctic Engineering (OMAE)*, Shanghai, China, 2010.
- [43] J. Jonkman, S. Butterfield, W. Musial, and G. Scott, "Definition of a 5-MW reference wind turbine for offshore system development," National Renewable Energy Laboratory, Golden, Colorado (US), Technical Report NREL/TP-500-38060, 2009.
- [44] J. Jonkman, "Definition of the floating system for phase IV of OC3," National Renewable Energy Laboratory, Golden, Colorado (US), Technical report NREL/TP-500-47535, 2010.
- [45] H. B. Hendriks and alt., "Cost modelling aspects in the design of an offshore wind turbine," in *Proceedings of the Offshore wind energy special topic conference*, Brussels, Belgium, 2001.
- [46] P. G. Migliore and M. C. Cheney, "Feasibility study of pultruded blades for wind turbine rotors," in *Proceedings of the ASME/AIAA Wind Energy Symposium*, Reno, Nevada (US), 2000.
- [47] B. F. Blackwell, "The Vertical Axis Wind Turbine, "how it works"," Sandia National Laboratories, Albuquerque, New Mexico (US), Patent Caution SLA-74-0160, 1974.
- [48] B. M. Sumer and J. Fredsøe, *Hydrodynamics around cylindrical structures*.: World Scientific, 2006.
- [49] IEC 61400 – 3 Ed.1, "IEC 61400 – 3 Ed.1: Wind turbines – Part3: Design requirements for offshore wind turbines," 2008.

- [50] B. M. Sumer and J. Fredsøe, *Hydrodynamics around cylindrical structures.*: World Scientific, 2006.
- [51] R. Monti and R. Savino, *Aerodinamica*. Napoli: Liguori Editore, 1999.
- [52] L. Prandtl, "Die Naturwissenschaften (Application of the Magnus effect to the wind propulsion of ships," NACA, Tech Mem. 387, vol.13, 1926.
- [53] S. Mittal and B. Kumar, "Flow past a rotating cylinder," *Journal of fluid mechanics*, vol. 476, pp. 303-334, 2003.
- [54] J. C. Padrino and D. D. Joseph, "Numerical study of the steady-state uniform flow past a rotating cylinder," *Journal of fluid mechanics*, vol. 557, pp. 191-223, 2006.
- [55] M. B. Glauert, "The flow past a rapidly rotating cylinder," *Proceedings of the Royal Society of London*, vol. 242, pp. 108-115, 1957.
- [56] Y. T. Chew, M. Cheng, and S. C. Luo, "A numerical study of flow past a rotating circular cylinder using a hybrid vortex scheme," *Journal of fluid mechanics*, vol. 299, pp. 35-71, 1995.
- [57] P. T. Tokumaru and P. E. Dimotakis, "The lift of a cylinder executing rotary motions in an uniform flow," *Journal of fluid mechanics*, vol. 255, pp. 1-10, 1993.
- [58] C. C. Chang and R. L. Chern, "Vortex shedding from an impulsively started rotating and traslating circular cylinder," *Journal of fluid mechanics*, vol. 233, pp. 265-298, 1991.
- [59] J. Wang and D. D. Joseph, "Boundary layer analysis for effect of viscosity on the irrotational flow induced by a rapidly rotating cylinder in a uniform stream," *Journal of fluid mechanics*, vol. 557, pp. 167-190, 2006.
- [60] T. Theodorsen and A. Regier, "Experiments on drag of revolving disks, cylinders and streamline rods at high speeds," National Advisory Committee for Aeronautics, Langley Field, Virginia (US), 793, 1946.
- [61] J. A. Michelsen, "Basis 3D - A platform for the development of multiblock PDE solvers," Technical University of Denmark (DTU), Lyngby, Denmark, Technical report AFM 92-05, 1992.
- [62] J. A. Michelsen, "Block structured multigrid solution of 2D and 3D elliptic PDE's," Technical University of Denmark (DTU), Lyngby, Denmark, Technical report AFM-94-06, 1994.
- [63] N. N. Sørensen, "General purpose flow solver applied to flow over hills," Risø DTU (Technical University of Denmark), Roskilde, Denmark, R-827-(EN),

1995.

- [64] E. G. Reid, "Test of rotating cylinders," NACA, Tech. note 209 1925.
- [65] L. Fingersh, M. Hand, and A. Laxson, "Wind turbine design cost and scaling model," National Renewable Energy Laboratory, Golden, Colorado (US), NREL/TP-500-40566, 2006.
- [66] Dayton A. Griffin, "WindPACT turbine design scaling studies technical area 1 - composite blades for 80 - to 120 - meter rotor," National Renewable Energy Laboratory, Golden, Colorado (US), NREL/SR-500-29492, 2001.
- [67] E. G. Kadlec, "Characteristics of future vertical axis wind turbines," Sandia National Laboratories, Albuquerque, New Mexico (US), Sand79-1068, 1982.
- [68] U. S. Paulsen, J. Nørkær, and J. E. Nielsen, "Aerodynamisk og svingningsteoretisk undersøgelse af en Darrieusrotor," Risø National Laboratory, Roskilde, Denmark, Risø-M-2451, 1985.
- [69] O. de Vries, "Fluid dynamic aspects of wind energy conversion," Brussels, Belgium, AGARDograph 243, 1979.
- [70] J. H. Strickland, T. B. Webster, and T. Nguyen, "A vortex model of the Darrieus turbine: an analytical and experimental study," Texas Tech University, Lubbock, Texas (US), SAND79-7058, 1980.
- [71] R. E. Sheldahl and P. C. Klimas, "Aerodynamic characteristics of seven symmetric airfoil sections through 180-degree angle of attack for use in aerodynamic analysis of vertical axis wind turbines," Sandia National Laboratories, Albuquerque, New Mexico (US), SAND80-2114, 1981.
- [72] M. C. Classens, "The design and testing of airfoils for application in small vertical axis wind turbine," TUDelft (Delft University of Technology), Delft, Netherlands, M.Sc. Dissertation 2006.
- [73] T. J. Larsen, "Slip generator model implemented in HAWC2 as an external dll," Wind Energy, Risø-DTU (Technical University of Denmark), Roskilde, Denmark, 2005-12-05 J.nr.200500523, 2005.
- [74] S. A. Herman, "DOWEC cost model - Implementation," ECN, Petten, Netherlands, DOWEC-F1W2-SH-03-087/00-C, 2003.
- [75] U. S. Paulsen, T. F. Pedersen, and L. Vita, "Floating VAWT wind farm concepts," Risø DTU (Technical University of Denmark), Roskilde, Denmark, I-2615(EN), 2008.
- [76] Bureau Veritas NI 572 DT R00 E, "Certification and classification of floating offshore wind turbines," 2010.

- [77] DNV-RP-C205, "Environmental conditions and environmental loads, Recommended practice ," 2010.
- [78] Norsok standard N-003 Ed.2, "Actions and action effects," 2007.
- [79] S. Carstensen, "DeepWind test plan (Milestone 11)," DHI (Danish Hydraulic Institute), 256769-Deepwind, 2011.
- [80] T. S. Hopkins, "The GIN (Greenland, Inland and Norway) Sea - A synthesis of its physical oceanography and literature reaview 1972-1985," *Earth-Science reviews*, vol. 30, pp. 175-318, 1991.
- [81] L Otto and Al., "review of the physical oceanography of the North Sea," *Netherlands journal of sea research*, vol. 26, pp. 161-238, 1990.
- [82] Coastal Engineering Research Center (U.S.), *Shore protection manual*. Vicksburg, Missisipi, US: Department of the army, US Army Corps of Engineers, 1984, vol. 1.
- [83] L. Battisti, L. Zanne, and A. Brighenti, "Aerodynamic design of the 2m diameter Darrieus wind turbine," Trento (Italy), 2011.
- [84] L. Vita, "Design and aero-elastic simulation of a 1kw floating vertical axis wind turbine," Risø DTU (Technical University of Denmark), Roskilde, Denmark, Risø-I-3204, 2011.
- [85] M. B. Zaaier and alt., "How to benefit from cost modelling of offshore wind farms?," in *Proceedings of the European Wind Energy Conference (EWEC)*, Madrid, Spain, 2003.
- [86] H. B. Hendriks and alt., "Application of an advanced cost model in the different design phases of an offshore wind turbine," in *Proceedings of the European Wind Energy Conference (EWEC)*, Copenhagen, Denmark, 2001.
- [87] C. A. Morgan, M. H. Snodin, and N. C. Scott, "Offshore wind. Economies of scale, engineering resource and load factors," Garrard Hassan, Bristol (UK), 3914/BR/01, 2003.
- [88] M. Junginger, A. Faaij, and W. C. Turkenburg, "Cost reduction prospects for offshore wind farms," *Wind engineering*, vol. 28, no. 1, pp. 97-118, 2004.
- [89] E. Wayman, "Coupled dynamics and economic analysis of floating wind turbine systems," MIT (Massachusetts Institute of Technology), Cambridge, Massachusetts (US), MSc Thesis 2006.
- [90] M. C. Cheney, T. Olsen, G. Quandt, and A. Arcidiacono, "Analysis and test of pultruded blades for wind turbine rotors," National Renewable Energy Laboratory, Golden, Colorado (US), NREL/SR-500-25949, 1999.

- [91] Z. Z. Chen, N. J. Tarp-Johansen, and J. J. Jensen, "Mechanical characteristics of some deepwater floater design for offshore wind turbines," *Wind Engineering*, vol. 30, no. 5, pp. 417-430, 2006.
- [92] D. O. Hodgins and B. N. Lea, "A spar buoy design for oceanographic data telemetry," *Atmosphere-Ocean journal*, vol. 19, no. 2, pp. 158-171, 1981.
- [93] Z. Jingrui, T. Yougang, and S. Wenjun, "A study of the combination resonance response of a classic SPAR platform," *Journal of vibration and control*, vol. 0, no. 0, pp. 1-25, 2010.
- [94] W. A. Timmer, "Two dimensional low-Reynolds number wind tunnel results for airfoil NACA 0018," *Wind Engineering*, vol. 32, 2008.
- [95] M. J. Tucker, "The heave response of a spar buoy," *Ocean engineering journal*, vol. 9, no. 3, pp. 259-270, 1982.
- [96] T. R. Camp et al., "Design methods for offshore wind turbines at exposed sites," Garrard Hassan and Partners, Bristol, UK, Final report of the OWTES Project, EU Joule III Project JOR3-CT98-0284 2317/BR/22D, 2004.
- [97] J. Cohen et al., "Technology improvement opportunities for low wind speed turbines and implications for cost of energy reduction," National Renewable Energy Laboratory, Golden, Colorado (US), Technical Report NREL/TP-500-41036, 2008.
- [98] D. E. Dodd, D. E. Borg, and T. D. Ashwill, "The status of the U.S. VAWT program," Sandia National Laboratories, Albuquerque, New Mexico (US), SAND-91-23860, 1991.
- [99] A. R. Henderson, "Hydrodynamic loading on offshore wind turbines," Delft University of Technology, Section Wind Energy, Delft, Netherlands, OWTES Task 4.2 Duwind 2003.025, 2003.
- [100] B. van Hees and et al., "Study to feasibility of and boundary conditions for floating offshore wind turbines (Drijfwind)," TNO-Bouw, Delft, Netherlands, 2002-CMC-R43, 2002.
- [101] F. G. Nielsen, T. D. Hanson, and B. Skaare, "Integrated dynamic analysis of floating offshore wind turbines," in *Proceedings of the European Wind Energy Conference (EWEC)*, Athens, Greece, 2006.
- [102] A. R. Henderson, G. M. Watson, M. H. Patel, and J. A. Helliday, "Floating offshore wind farm - an option?," in *Proceedings of the Conference of the Offshore wind energy in the Mediterranean and other European seas*, Siracusa, Italy, 2000.
- [103] D. Matha, "Model development and load analysis of an offshore wind turbine on a tension leg platform, with a comparison to other floating turbine

concepts," University of Colorado, Boulder, Colorado (US), MSc Thesis NREL/SR-500-45891, 2010.

- [104] U. S. Paulsen, T. F. Pedersen, and L. Vita, "Floating VAWT concepts," Risø DTU (Technical University of Denmark), Roskilde, Denmark, I-2614(EN), 2008.
- [105] F. L. Ponta and P. M. Jacovkis, "A vortex model for Darrieus turbine using finite element techniques," *Renewable energy*, vol. 24, pp. 1-18, 2001.
- [106] L. Vita, U. S. Paulsen, and T. F. Pedersen, "A novel floating wind turbine concept: new development," in *Proceedings of the European Wind Energy Conference (EWEC)*, Warsaw, Poland, 2010.

Appendix A - Structural input for the numerical calculations

5MW

Tower

r	m	x c g	y c g	rix	riy	x s	y s	E	G	Ix	Iy	K	k x	k y	A	thet a_z	x e	y e
0	1.01 E+0 4	0	0	2.91 6869	2.91 6869	0	0	2.10 E+1 1	8.10 E+1 0	11.025 73849	11.025 73849	22.051 47697	0 .	0 .	1.2959 0697	0	0	0
0.02	1.01 E+0 4	0	0	2.91 6869	2.91 6869	0	0	2.10 E+1 1	8.10 E+1 0	11.025 73849	11.025 73849	22.051 47697	0 .	0 .	1.2959 0697	0	0	0
0.04	1.01 E+0 4	0	0	2.91 6869	2.91 6869	0	0	2.10 E+1 1	8.10 E+1 0	11.025 73849	11.025 73849	22.051 47697	0 .	0 .	1.2959 0697	0	0	0
5	1.01 E+0 4	0	0	2.91 6869	2.91 6869	0	0	2.10 E+1 1	8.10 E+1 0	11.025 73849	11.025 73849	22.051 47697	0 .	0 .	1.2959 0697	0	0	0
10	1.01 E+0 4	0	0	2.91 6869	2.91 6869	0	0	2.10 E+1 1	8.10 E+1 0	11.025 73849	11.025 73849	22.051 47697	0 .	0 .	1.2959 0697	0	0	0
20	1.01 E+0 4	0	0	2.91 6869	2.91 6869	0	0	2.10 E+1 1	8.10 E+1 0	11.025 73849	11.025 73849	22.051 47697	0 .	0 .	1.2959 0697	0	0	0
30	1.01 E+0 4	0	0	2.91 6869	2.91 6869	0	0	2.10 E+1 1	8.10 E+1 0	11.025 73849	11.025 73849	22.051 47697	0 .	0 .	1.2959 0697	0	0	0
40	1.01 E+0 4	0	0	2.91 6869	2.91 6869	0	0	2.10 E+1 1	8.10 E+1 0	11.025 73849	11.025 73849	22.051 47697	0 .	0 .	1.2959 0697	0	0	0
50	1.01 E+0 4	0	0	2.91 6869	2.91 6869	0	0	2.10 E+1 1	8.10 E+1 0	11.025 73849	11.025 73849	22.051 47697	0 .	0 .	1.2959 0697	0	0	0
60	1.01 E+0 4	0	0	2.91 6869	2.91 6869	0	0	2.10 E+1 1	8.10 E+1 0	11.025 73849	11.025 73849	22.051 47697	0 .	0 .	1.2959 0697	0	0	0
65	1.01 E+0 4	0	0	2.91 6869	2.91 6869	0	0	2.10 E+1 1	8.10 E+1 0	11.025 73849	11.025 73849	22.051 47697	0 .	0 .	1.2959 0697	0	0	0
70	1.01 E+0 4	0	0	2.91 6869	2.91 6869	0	0	2.10 E+1 1	8.10 E+1 0	11.025 73849	11.025 73849	22.051 47697	0 .	0 .	1.2959 0697	0	0	0
80	1.01 E+0 4	0	0	2.91 6869	2.91 6869	0	0	2.10 E+1 1	8.10 E+1 0	11.025 73849	11.025 73849	22.051 47697	0 .	0 .	1.2959 0697	0	0	0
87	1.01 E+0 4	0	0	2.91 6869	2.91 6869	0	0	2.10 E+1 1	8.10 E+1 0	11.025 73849	11.025 73849	22.051 47697	0 .	0 .	1.2959 0697	0	0	0
91	1.01 E+0 4	0	0	2.91 6869	2.91 6869	0	0	2.10 E+1 1	8.10 E+1 0	11.025 73849	11.025 73849	22.051 47697	0 .	0 .	1.2959 0697	0	0	0
93	1.01 E+0 4	0	0	2.91 6869	2.91 6869	0	0	2.10 E+1 1	8.10 E+1 0	11.025 73849	11.025 73849	22.051 47697	0 .	0 .	1.2959 0697	0	0	0
94	8.08 E+0 3	0	0	2.74 2732	2.74 2732	0	0	2.10 E+1 1	8.10 E+1 0	7.7916 09951	7.7916 09951	15.583 2199	0 .	0 .	1.0357 63463	0	0	0
96	5.79 E+0 3	0	0	2.56 9475	2.56 9475	0	0	2.10 E+1 1	8.10 E+1 0	4.8989 95642	4.8989 95642	9.7979 91285	0 .	0 .	0.7420 2455	0	0	0
102	3.74 E+0 3	0	0	2.39 6221	2.39 6221	0	0	2.10 E+1 1	8.10 E+1 0	2.7507 79436	2.7507 79436	5.5015 58871	0 .	0 .	0.4790 73245	0	0	0
103	3.08 E+0 3	0	0	2.22 0327	2.22 0327	0	0	2.10 E+1 1	8.10 E+1 0	1.9452 40116	1.9452 40116	3.8904 80232	0 .	0 .	0.3945 84037	0	0	0
106	3.08 E+0 3	0	0	2.22 0327	2.22 0327	0	0	2.10 E+1 1	8.10 E+1 0	1.9452 40116	1.9452 40116	3.8904 80232	0 .	0 .	0.3945 84037	0	0	0
108	3.08 E+0 3	0	0	2.22 0327	2.22 0327	0	0	2.10 E+1 1	8.10 E+1 0	1.9452 40116	1.9452 40116	3.8904 80232	0 .	0 .	0.3945 84037	0	0	0
108. 1	3.08 E+0 3	0	0	2.22 0327	2.22 0327	0	0	2.10 E+1 1	8.10 E+1 0	1.9452 40116	1.9452 40116	3.8904 80232	0 .	0 .	0.3945 84037	0	0	0
113	3.08 E+0 3	0	0	2.22 0327	2.22 0327	0	0	2.10 E+1 1	8.10 E+1 0	1.9452 40116	1.9452 40116	3.8904 80232	0 .	0 .	0.3945 84037	0	0	0
120	3.08 E+0 3	0	0	2.22 0327	2.22 0327	0	0	2.10 E+1 1	8.10 E+1 0	1.9452 40116	1.9452 40116	3.8904 80232	0 .	0 .	0.3945 84037	0	0	0
121	3.08 E+0 3	0	0	2.22 0327	2.22 0327	0	0	2.10 E+1 1	8.10 E+1 0	1.9452 40116	1.9452 40116	3.8904 80232	0 .	0 .	0.3945 84037	0	0	0
122. 999	3.08 E+0	0	0	2.22 0327	2.22 0327	0	0	2.10 E+1	8.10 E+1	1.9452 40116	1.9452 40116	3.8904 80232	0 .	0 .	0.3945 84037	0	0	0

Appendix A

	3							1	0					9	9				
123	3.08	0	0	2.22	2.22	0	0	2.10	8.10	1.9452	1.9452	3.8904	0	0	0.3945	0	0	0	0
	E+0			0327	0327			E+1	E+1	40116	40116	80232	.	.	84037				
	3							1	0				9	9					
123.001	3.08	0	0	2.22	2.22	0	0	2.10	8.10	1.9452	1.9452	3.8904	0	0	0.3945	0	0	0	0
	E+0			0327	0327			E+1	E+1	40116	40116	80232	.	.	84037				
	3							1	0				9	9					
130	3.08	0	0	2.22	2.22	0	0	2.10	8.10	1.9452	1.9452	3.8904	0	0	0.3945	0	0	0	0
	E+0			0327	0327			E+1	E+1	40116	40116	80232	.	.	84037				
	3							1	0				9	9					
140	3.08	0	0	2.22	2.22	0	0	2.10	8.10	1.9452	1.9452	3.8904	0	0	0.3945	0	0	0	0
	E+0			0327	0327			E+1	E+1	40116	40116	80232	.	.	84037				
	3							1	0				9	9					
150	3.08	0	0	2.22	2.22	0	0	2.10	8.10	1.9452	1.9452	3.8904	0	0	0.3945	0	0	0	0
	E+0			0327	0327			E+1	E+1	40116	40116	80232	.	.	84037				
	3							1	0				9	9					
160	3.08	0	0	2.22	2.22	0	0	2.10	8.10	1.9452	1.9452	3.8904	0	0	0.3945	0	0	0	0
	E+0			0327	0327			E+1	E+1	40116	40116	80232	.	.	84037				
	3							1	0				9	9					
170	3.08	0	0	2.22	2.22	0	0	2.10	8.10	1.9452	1.9452	3.8904	0	0	0.3945	0	0	0	0
	E+0			0327	0327			E+1	E+1	40116	40116	80232	.	.	84037				
	3							1	0				9	9					
180	3.08	0	0	2.22	2.22	0	0	2.10	8.10	1.9452	1.9452	3.8904	0	0	0.3945	0	0	0	0
	E+0			0327	0327			E+1	E+1	40116	40116	80232	.	.	84037				
	3							1	0				9	9					
190	3.08	0	0	2.22	2.22	0	0	2.10	8.10	1.9452	1.9452	3.8904	0	0	0.3945	0	0	0	0
	E+0			0327	0327			E+1	E+1	40116	40116	80232	.	.	84037				
	3							1	0				9	9					
200	3.08	0	0	2.22	2.22	0	0	2.10	8.10	1.9452	1.9452	3.8904	0	0	0.3945	0	0	0	0
	E+0			0327	0327			E+1	E+1	40116	40116	80232	.	.	84037				
	3							1	0				9	9					
210	3.08	0	0	2.22	2.22	0	0	2.10	8.10	1.9452	1.9452	3.8904	0	0	0.3945	0	0	0	0
	E+0			0327	0327			E+1	E+1	40116	40116	80232	.	.	84037				
	3							1	0				9	9					
220	3.08	0	0	2.22	2.22	0	0	2.10	8.10	1.9452	1.9452	3.8904	0	0	0.3945	0	0	0	0
	E+0			0327	0327			E+1	E+1	40116	40116	80232	.	.	84037				
	3							1	0				9	9					
230	3.08	0	0	2.22	2.22	0	0	2.10	8.10	1.9452	1.9452	3.8904	0	0	0.3945	0	0	0	0
	E+0			0327	0327			E+1	E+1	40116	40116	80232	.	.	84037				
	3							1	0				9	9					
240	3.08	0	0	2.22	2.22	0	0	2.10	8.10	1.9452	1.9452	3.8904	0	0	0.3945	0	0	0	0
	E+0			0327	0327			E+1	E+1	40116	40116	80232	.	.	84037				
	3							1	0				9	9					
252.56	3.08	0	0	2.22	2.22	0	0	2.10	8.10	1.9452	1.9452	3.8904	0	0	0.3945	0	0	0	0
	E+0			0327	0327			E+1	E+1	40116	40116	80232	.	.	84037				
	3							1	0				9	9					
253	3.08	0	0	2.22	2.22	0	0	2.10	8.10	1.9452	1.9452	3.8904	0	0	0.3945	0	0	0	0
	E+0			0327	0327			E+1	E+1	40116	40116	80232	.	.	84037				
	3							1	0				9	9					

Blades

r	m	x c g	y c g	rix	riy	x s	y s	E	G	Ix	Iy	K	k x	k y	A	thet a_z	x e	y e
0	1.01E+03	0	0	2.00E+00	3.00E+00	0	0	2.07E+10	7.58E+09	2.44E-01	2.62E+00	2.16E+00	5	5	5.61E-01	0	0	0
6.86744705	1.01E+03	0	0	2.00E+00	3.00E+00	0	0	2.07E+10	7.58E+09	2.44E-01	2.62E+00	2.16E+00	5	5	5.61E-01	0	0	0
13.67875216	1.01E+03	0	0	2.00E+00	3.00E+00	0	0	2.07E+10	7.58E+09	2.44E-01	2.62E+00	2.16E+00	5	5	5.61E-01	0	0	0
20.3781815	1.01E+03	0	0	2.00E+00	3.00E+00	0	0	2.07E+10	7.58E+09	2.44E-01	2.62E+00	2.16E+00	5	5	5.61E-01	0	0	0
26.96630227	1.01E+03	0	0	2.00E+00	3.00E+00	0	0	2.07E+10	7.58E+09	2.44E-01	2.62E+00	2.16E+00	5	5	5.61E-01	0	0	0
32.95377077	1.01E+03	0	0	2.00E+00	3.00E+00	0	0	2.07E+10	7.58E+09	2.44E-01	2.62E+00	2.16E+00	5	5	5.61E-01	0	0	0
39.54189155	1.01E+03	0	0	2.00E+00	3.00E+00	0	0	2.07E+10	7.58E+09	2.44E-01	2.62E+00	2.16E+00	5	5	5.61E-01	0	0	0
45.47584899	1.01E+03	0	0	2.00E+00	3.00E+00	0	0	2.07E+10	7.58E+09	2.44E-01	2.62E+00	2.16E+00	5	5	5.61E-01	0	0	0
51.04126859	6.97E+02	0	0	2.00E+00	3.00E+00	0	0	2.07E+10	7.58E+09	1.10E-02	1.19E-01	5.55E-01	5	5	3.87E-01	0	0	0
56.35074865	6.97E+02	0	0	2.00E+00	3.00E+00	0	0	2.07E+10	7.58E+09	1.10E-02	1.19E-01	5.55E-01	5	5	3.87E-01	0	0	0
61.3141393	6.97E+02	0	0	2.00E+00	3.00E+00	0	0	2.07E+10	7.58E+09	1.10E-02	1.19E-01	5.55E-01	5	5	3.87E-01	0	0	0
65.90321314	6.97E+02	0	0	2.00E+00	3.00E+00	0	0	2.07E+10	7.58E+09	1.10E-02	1.19E-01	5.55E-01	5	5	3.87E-01	0	0	0
70.1877839	6.97E+02	0	0	2.00E+00	3.00E+00	0	0	2.07E+10	7.58E+09	1.10E-02	1.19E-01	5.55E-01	5	5	3.87E-01	0	0	0

Appendix A

74.157 30217	6.97E +02	0	0	2.00E +00	3.00E +00	0	0	2.07E +10	7.58E +09	1.1 0E- 02	1.19E -01	5.55E -01	5	5	3.8 7E- 01	0	0	0
77.795 69038	6.97E +02	0	0	2.00E +00	3.00E +00	0	0	2.07E +10	7.58E +09	1.1 0E- 02	1.19E -01	5.55E -01	5	5	3.8 7E- 01	0	0	0
81.253 71717	6.97E +02	0	0	2.00E +00	3.00E +00	0	0	2.07E +10	7.58E +09	1.1 0E- 02	1.19E -01	5.55E -01	5	5	3.8 7E- 01	0	0	0
84.543 13097	6.97E +02	0	0	2.00E +00	3.00E +00	0	0	2.07E +10	7.58E +09	1.1 0E- 02	1.19E -01	5.55E -01	5	5	3.8 7E- 01	0	0	0
87.782 13097	6.97E +02	0	0	2.00E +00	3.00E +00	0	0	2.07E +10	7.58E +09	1.1 0E- 02	1.19E -01	5.55E -01	5	5	3.8 7E- 01	0	0	0
91.031 15125	6.97E +02	0	0	2.00E +00	3.00E +00	0	0	2.07E +10	7.58E +09	1.1 0E- 02	1.19E -01	5.55E -01	5	5	3.8 7E- 01	0	0	0
94.408 33191	6.97E +02	0	0	2.00E +00	3.00E +00	0	0	2.07E +10	7.58E +09	1.1 0E- 02	1.19E -01	5.55E -01	5	5	3.8 7E- 01	0	0	0
97.677 92203	6.97E +02	0	0	2.00E +00	3.00E +00	0	0	2.07E +10	7.58E +09	1.1 0E- 02	1.19E -01	5.55E -01	5	5	3.8 7E- 01	0	0	0
101.11 41423	6.97E +02	0	0	2.00E +00	3.00E +00	0	0	2.07E +10	7.58E +09	1.1 0E- 02	1.19E -01	5.55E -01	5	5	3.8 7E- 01	0	0	0
104.61 88546	6.97E +02	0	0	2.00E +00	3.00E +00	0	0	2.07E +10	7.58E +09	1.1 0E- 02	1.19E -01	5.55E -01	5	5	3.8 7E- 01	0	0	0
108.28 67177	6.97E +02	0	0	2.00E +00	3.00E +00	0	0	2.07E +10	7.58E +09	1.1 0E- 02	1.19E -01	5.55E -01	5	5	3.8 7E- 01	0	0	0
112.04 81049	6.97E +02	0	0	2.00E +00	3.00E +00	0	0	2.07E +10	7.58E +09	1.1 0E- 02	1.19E -01	5.55E -01	5	5	3.8 7E- 01	0	0	0
115.94 53119	6.97E +02	0	0	2.00E +00	3.00E +00	0	0	2.07E +10	7.58E +09	1.1 0E- 02	1.19E -01	5.55E -01	5	5	3.8 7E- 01	0	0	0
119.95 20177	6.97E +02	0	0	2.00E +00	3.00E +00	0	0	2.07E +10	7.58E +09	1.1 0E- 02	1.19E -01	5.55E -01	5	5	3.8 7E- 01	0	0	0
123.99 65739	6.97E +02	0	0	2.00E +00	3.00E +00	0	0	2.07E +10	7.58E +09	1.1 0E- 02	1.19E -01	5.55E -01	5	5	3.8 7E- 01	0	0	0
128.49 62351	6.97E +02	0	0	2.00E +00	3.00E +00	0	0	2.07E +10	7.58E +09	1.1 0E- 02	1.19E -01	5.55E -01	5	5	3.8 7E- 01	0	0	0
132.95 18852	6.97E +02	0	0	2.00E +00	3.00E +00	0	0	2.07E +10	7.58E +09	1.1 0E- 02	1.19E -01	5.55E -01	5	5	3.8 7E- 01	0	0	0
137.54 0959	6.97E +02	0	0	2.00E +00	3.00E +00	0	0	2.07E +10	7.58E +09	1.1 0E- 02	1.19E -01	5.55E -01	5	5	3.8 7E- 01	0	0	0
142.55 28222	6.97E +02	0	0	2.00E +00	3.00E +00	0	0	2.07E +10	7.58E +09	1.1 0E- 02	1.19E -01	5.55E -01	5	5	3.8 7E- 01	0	0	0
147.09 69625	6.97E +02	0	0	2.00E +00	3.00E +00	0	0	2.07E +10	7.58E +09	1.1 0E- 02	1.19E -01	5.55E -01	5	5	3.8 7E- 01	0	0	0
152.06 03532	1.01E +03	0	0	2.00E +00	3.00E +00	0	0	2.07E +10	7.58E +09	2.4 4E- 01	2.62E +00	2.16E +00	5	5	5.6 1E- 01	0	0	0
157.07 22163	1.01E +03	0	0	2.00E +00	3.00E +00	0	0	2.07E +10	7.58E +09	2.4 4E- 01	2.62E +00	2.16E +00	5	5	5.6 1E- 01	0	0	0
162.33 13317	1.01E +03	0	0	2.00E +00	3.00E +00	0	0	2.07E +10	7.58E +09	2.4 4E- 01	2.62E +00	2.16E +00	5	5	5.6 1E- 01	0	0	0
167.44 11459	1.01E +03	0	0	2.00E +00	3.00E +00	0	0	2.07E +10	7.58E +09	2.4 4E- 01	2.62E +00	2.16E +00	5	5	5.6 1E- 01	0	0	0
172.70 02613	1.01E +03	0	0	2.00E +00	3.00E +00	0	0	2.07E +10	7.58E +09	2.4 4E- 01	2.62E +00	2.16E +00	5	5	5.6 1E- 01	0	0	0
178.00 97413	1.01E +03	0	0	2.00E +00	3.00E +00	0	0	2.07E +10	7.58E +09	2.4 4E- 01	2.62E +00	2.16E +00	5	5	5.6 1E- 01	0	0	0
183.31 92214	1.01E +03	0	0	2.00E +00	3.00E +00	0	0	2.07E +10	7.58E +09	2.4 4E- 01	2.62E +00	2.16E +00	5	5	5.6 1E- 01	0	0	0
188.67 9351	1.01E +03	0	0	2.00E +00	3.00E +00	0	0	2.07E +10	7.58E +09	2.4 4E- 01	2.62E +00	2.16E +00	5	5	5.6 1E- 01	0	0	0

1kW

Tower

r	m	x c g	y c g	rix	riy	x s	y s	E	G	Ix	Iy	K	k x	k y	A	thet a_z	x e	y e
0	2.8500 52855	0	0	0.0594 01	0.0594 01	0	0	2.10 E+11	8.10 E+11	3.7 2E- 06	3.7 2E- 06	7.4 5E- 06	0 9	0 9	0.0010 55575	0	0	0
0.0 01	2.8500 52855	0	0	0.0594 01	0.0594 01	0	0	2.10 E+11	8.10 E+11	3.7 2E- 06	3.7 2E- 06	7.4 5E- 06	0 9	0 9	0.0010 55575	0	0	0
0.5	2.8500 52855	0	0	0.0594 01	0.0594 01	0	0	2.10 E+11	8.10 E+11	3.7 2E- 06	3.7 2E- 06	7.4 5E- 06	0 9	0 9	0.0010 55575	0	0	0
1	2.8500 52855	0	0	0.0594 01178	0.0594 01178	0	0	2.10 E+11	8.10 E+11	3.7 2E- 06	3.7 2E- 06	7.4 5E- 06	2	2	0.0010 55575	0	0	0
1.5	2.8500 52855	0	0	0.0594 01178	0.0594 01178	0	0	2.10 E+11	8.10 E+11	3.7 2E- 06	3.7 2E- 06	7.4 5E- 06	2	2	0.0010 55575	0	0	0
2	2.8500 52855	0	0	0.0594 01178	0.0594 01178	0	0	2.10 E+11	8.10 E+11	3.7 2E- 06	3.7 2E- 06	7.4 5E- 06	2	2	0.0010 55575	0	0	0
2.6 99	2.8500 52855	0	0	0.0594 01178	0.0594 01178	0	0	2.10 E+11	8.10 E+11	3.7 2E- 06	3.7 2E- 06	7.4 5E- 06	2	2	0.0010 55575	0	0	0
2.7 001	2.8500 52855	0	0	0.0594 01178	0.0594 01178	0	0	2.10 E+11	8.10 E+11	3.7 2E- 06	3.7 2E- 06	7.4 5E- 06	2	2	0.0010 55575	0	0	0
2.8	2.8500 52855	0	0	0.0594 01178	0.0594 01178	0	0	2.10 E+11	8.10 E+11	3.7 2E- 06	3.7 2E- 06	7.4 5E- 06	2	2	0.0010 55575	0	0	0
3	2.8500 52855	0	0	0.0594 01178	0.0594 01178	0	0	2.10 E+11	8.10 E+11	3.7 2E- 06	3.7 2E- 06	7.4 5E- 06	2	2	0.0010 55575	0	0	0
3.1 99	2.8500 52855	0	0	0.0594 01178	0.0594 01178	0	0	2.10 E+11	8.10 E+11	3.7 2E- 06	3.7 2E- 06	7.4 5E- 06	2	2	0.0010 55575	0	0	0
3.2 001	2.8500 52855	0	0	0.0594 01178	0.0594 01178	0	0	2.10 E+11	8.10 E+11	3.7 2E- 06	3.7 2E- 06	7.4 5E- 06	2	2	0.0010 55575	0	0	0
3.3	2.8500 52855	0	0	0.0594 01178	0.0594 01178	0	0	2.10 E+11	8.10 E+11	3.7 2E- 06	3.7 2E- 06	7.4 5E- 06	2	2	0.0010 55575	0	0	0
4	2.8500 52855	0	0	0.0594 01178	0.0594 01178	0	0	2.10 E+11	8.10 E+11	3.7 2E- 06	3.7 2E- 06	7.4 5E- 06	2	2	0.0010 55575	0	0	0
5	2.8500 52855	0	0	0.0594 01178	0.0594 01178	0	0	2.10 E+11	8.10 E+11	3.7 2E- 06	3.7 2E- 06	7.4 5E- 06	2	2	0.0010 55575	0	0	0
5.1 99	2.8500 52855	0	0	0.0594 01178	0.0594 01178	0	0	2.10 E+11	8.10 E+11	3.7 2E- 06	3.7 2E- 06	7.4 5E- 06	2	2	0.0010 55575	0	0	0
5.2	2.8500 52855	0	0	0.0594 01178	0.0594 01178	0	0	2.10 E+11	8.10 E+11	3.7 2E- 06	3.7 2E- 06	7.4 5E- 06	2	2	0.0010 55575	0	0	0
5.2 001	2.8500 52855	0	0	0.0594 01178	0.0594 01178	0	0	2.10 E+11	8.10 E+11	3.7 2E- 06	3.7 2E- 06	7.4 5E- 06	2	2	0.0010 55575	0	0	0

Blades

r	m	x c g	y c g	rix	riy	x s	y s	E	G	Ix	Iy	K	k x	k y	A	thet a_z	x e	y e
0.08602 3253	2.2365 504	0	0	1.03E +00	3.8 9E- 01	0	0	1.00E +10	1.20E +09	1.9 2E- 06	9.2 6E- 08	1.3 4E- 05	5 0	5 0	3.2 0E- 03	0	0	0
0.18550 1894	2.2365 504	0	0	1.03E +00	3.8 9E- 01	0	0	1.00E +10	1.20E +09	1.9 2E- 06	9.2 6E- 08	1.3 4E- 05	5 0	5 0	3.2 0E- 03	0	0	0
0.27731 1479	2.2365 504	0	0	1.03E +00	3.8 9E- 01	0	0	1.00E +10	1.20E +09	1.9 2E- 06	9.2 6E- 08	1.3 4E- 05	5 0	5 0	3.2 0E- 03	0	0	0
0.36828 4002	1.3046 544	0	0	1.03E +00	3.8 9E- 01	0	0	1.00E +10	1.20E +09	1.9 2E- 06	9.2 6E- 08	1.3 4E- 05	5 0	5 0	1.8 6E- 03	0	0	0
0.45759 2457	1.3046 544	0	0	1.03E +00	3.8 9E- 01	0	0	1.00E +10	1.20E +09	1.9 2E- 06	9.2 6E- 08	1.3 4E- 05	5 0	5 0	1.8 6E- 03	0	0	0
0.54443 1388	1.3046 544	0	0	1.03E +00	3.8 9E- 01	0	0	1.00E +10	1.20E +09	1.9 2E- 06	9.2 6E- 08	1.3 4E- 05	5 0	5 0	1.8 6E- 03	0	0	0
0.62883 5179	1.3046 544	0	0	1.03E +00	3.8 9E- 01	0	0	1.00E +10	1.20E +09	1.9 2E- 06	9.2 6E- 08	1.3 4E- 05	5 0	5 0	1.8 6E- 03	0	0	0
0.71163 6146	1.3046 544	0	0	1.03E +00	3.8 9E- 01	0	0	1.00E +10	1.20E +09	1.9 2E- 06	9.2 6E- 08	1.3 4E- 05	5 0	5 0	1.8 6E- 03	0	0	0
0.79050 9462	1.3046 544	0	0	1.03E +00	3.8 9E- 01	0	0	1.00E +10	1.20E +09	1.9 2E- 06	9.2 6E- 08	1.3 4E- 05	5 0	5 0	1.8 6E- 03	0	0	0
0.86708 6221	1.3046 544	0	0	7.00E -01	1.1 9E- 01	0	0	1.00E +10	1.20E +09	1.9 2E- 06	9.2 6E- 08	1.3 4E- 05	5 0	5 0	1.8 6E- 03	0	0	0
0.93994 9106	1.3046 544	0	0	7.00E -01	1.1 9E- 01	0	0	1.00E +10	1.20E +09	1.9 2E- 06	9.2 6E- 08	1.3 4E- 05	5 0	5 0	1.8 6E- 03	0	0	0
1.00995 6248	0.2982 672	0	0	7.00E -01	1.1 9E- 01	0	0	1.00E +10	1.20E +09	1.9 2E- 06	9.2 6E- 08	1.3 4E- 05	5 0	5 0	4.2 6E- 04	0	0	0
1.07655 9551	0.2982 672	0	0	7.00E -01	1.1 9E- 01	0	0	1.00E +10	1.20E +09	1.9 2E- 06	9.2 6E- 08	1.3 4E- 05	5 0	5 0	4.2 6E- 04	0	0	0
1.13936 0825	0.2982 672	0	0	7.00E -01	1.1 9E- 01	0	0	1.00E +10	1.20E +09	1.9 2E- 06	9.2 6E- 08	1.3 4E- 05	5 0	5 0	4.2 6E- 04	0	0	0
1.19926 9088	0.2982 672	0	0	7.00E -01	1.1 9E- 01	0	0	1.00E +10	1.20E +09	1.9 2E- 06	9.2 6E- 08	1.3 4E- 05	5 0	5 0	4.2 6E- 04	0	0	0
1.25609 3379	0.2982 672	0	0	7.00E -01	1.1 9E- 01	0	0	1.00E +10	1.20E +09	1.9 2E- 06	9.2 6E- 08	1.3 4E- 05	5 0	5 0	4.2 6E- 04	0	0	0
1.31032 4366	0.2982 672	0	0	7.00E -01	1.1 9E- 01	0	0	1.00E +10	1.20E +09	1.9 2E- 06	9.2 6E- 08	1.3 4E- 05	5 0	5 0	4.2 6E- 04	0	0	0
1.36282 1985	0.2982 672	0	0	7.00E -01	1.1 9E- 01	0	0	1.00E +10	1.20E +09	1.9 2E- 06	9.2 6E- 08	1.3 4E- 05	5 0	5 0	4.2 6E- 04	0	0	0
1.41362 5529	0.2982 672	0	0	7.00E -01	1.1 9E- 01	0	0	1.00E +10	1.20E +09	1.9 2E- 06	9.2 6E- 08	1.3 4E- 05	5 0	5 0	4.2 6E- 04	0	0	0
1.46371 5448	0.2982 672	0	0	7.00E -01	1.1 9E- 01	0	0	1.00E +10	1.20E +09	1.9 2E- 06	9.2 6E- 08	1.3 4E- 05	5 0	5 0	4.2 6E- 04	0	0	0
1.51380 5367	0.2982 672	0	0	7.00E -01	1.1 9E- 01	0	0	1.00E +10	1.20E +09	1.9 2E- 06	9.2 6E- 08	1.3 4E- 05	5 0	5 0	4.2 6E- 04	0	0	0
1.56460 891	0.2982 672	0	0	7.00E -01	1.1 9E- 01	0	0	1.00E +10	1.20E +09	1.9 2E- 06	9.2 6E- 08	1.3 4E- 05	5 0	5 0	4.2 6E- 04	0	0	0
1.61710 6529	0.2982 672	0	0	7.00E -01	1.1 9E- 01	0	0	1.00E +10	1.20E +09	1.9 2E- 06	9.2 6E- 08	1.3 4E- 05	5 0	5 0	4.2 6E- 04	0	0	0
1.67133 7517	0.2982 672	0	0	7.00E -01	1.1 9E- 01	0	0	1.00E +10	1.20E +09	1.9 2E- 06	9.2 6E- 08	1.3 4E- 05	5 0	5 0	4.2 6E- 04	0	0	0
1.72816 1807	0.2982 672	0	0	7.00E -01	1.1 9E- 01	0	0	1.00E +10	1.20E +09	1.9 2E- 06	9.2 6E- 08	1.3 4E- 05	5 0	5 0	4.2 6E- 04	0	0	0
1.78807 007	0.2982 672	0	0	7.00E -01	1.1 9E- 01	0	0	1.00E +10	1.20E +09	1.9 2E- 06	9.2 6E- 08	1.3 4E- 05	5 0	5 0	4.2 6E- 04	0	0	0
1.85087 1344	0.2982 672	0	0	7.00E -01	1.1 9E- 01	0	0	1.00E +10	1.20E +09	1.9 2E- 06	9.2 6E- 08	1.3 4E- 05	5 0	5 0	4.2 6E- 04	0	0	0
1.91747 4647	0.2982 672	0	0	7.00E -01	1.1 9E- 01	0	0	1.00E +10	1.20E +09	1.9 2E- 06	9.2 6E- 08	1.3 4E- 05	5 0	5 0	4.2 6E- 04	0	0	0
1.98748 179	0.2982 672	0	0	7.00E -01	1.1 9E- 01	0	0	1.00E +10	1.20E +09	1.9 2E- 06	9.2 6E- 08	1.3 4E- 05	5 0	5 0	4.2 6E- 04	0	0	0
2.06034 4675	0.2982 672	0	0	7.00E -01	1.1 9E- 01	0	0	1.00E +10	1.20E +09	1.9 2E- 06	9.2 6E- 08	1.3 4E- 05	5 0	5 0	4.2 6E- 04	0	0	0
2.13692	1.3046	0	0	7.00E	1.1	0	0	1.00E	1.20E	1.9	9.2	1.3	5	5	1.8	0	0	0

Appendix A

1434	544			-01	9E-01			+10	+09	2E-06	6E-08	4E-05	0	0	6E-03			
2.21579	1.3046	0	0	1.03E+00	3.89E-01	0	0	1.00E+10	1.20E+09	1.92E-06	9.26E-08	1.34E-05	5	5	1.86E-03	0	0	0
475	544																	
2.29859	1.3046	0	0	1.03E+00	3.89E-01	0	0	1.00E+10	1.20E+09	1.92E-06	9.26E-08	1.34E-05	5	5	1.86E-03	0	0	0
5716	544																	
2.38299	1.3046	0	0	1.03E+00	3.89E-01	0	0	1.00E+10	1.20E+09	1.92E-06	9.26E-08	1.34E-05	5	5	1.86E-03	0	0	0
9507	544																	
2.46983	1.3046	0	0	1.03E+00	3.89E-01	0	0	1.00E+10	1.20E+09	1.92E-06	9.26E-08	1.34E-05	5	5	1.86E-03	0	0	0
8439	544																	
2.55914	1.3046	0	0	1.03E+00	3.89E-01	0	0	1.00E+10	1.20E+09	1.92E-06	9.26E-08	1.34E-05	5	5	1.86E-03	0	0	0
6893	544																	
2.65011	1.3046	0	0	1.03E+00	3.89E-01	0	0	1.00E+10	1.20E+09	1.92E-06	9.26E-08	1.34E-05	5	5	1.86E-03	0	0	0
9416	544																	
2.74192	1.3046	0	0	1.03E+00	3.89E-01	0	0	1.00E+10	1.20E+09	1.92E-06	9.26E-08	1.34E-05	5	5	1.86E-03	0	0	0
9002	544																	
2.84140	2.2365	0	0	1.03E+00	3.89E-01	0	0	1.00E+10	1.20E+09	1.92E-06	9.26E-08	1.34E-05	5	5	3.20E-03	0	0	0
7643	504																	
2.92743	2.2365	0	0	1.03E+00	3.89E-01	0	0	1.00E+10	1.20E+09	1.92E-06	9.26E-08	1.34E-05	5	5	3.20E-03	0	0	0
0895	504																	

Appendix B – Attached papers

A Novel Floating Offshore Wind Turbine Concept

L. Vita, U.S.Paulsen, T.F.Pedersen, H.A.Madsen, F.Rasmussen
Risø-DTU Technical University of Denmark, Roskilde, Denmark
luca.vita@risoe.dk

Abstract:

This paper will present a novel concept of a floating offshore wind turbine. The new concept is intended for vertical-axis wind turbine technology. The main purpose is to increase simplicity and to reduce total costs of an installed offshore wind farm. The concept is intended for deep water and large size turbines.

Keywords: **offshore, floating, vertical-axis wind turbine, novel concept.**

1. Introduction

Wind energy is more needed than ever. The offshore sector is in focus for development of larger and more cost effective projects. Horizontal-axis "state of the art" wind turbines have been erected on seabed foundations in shallow water wind farms. Up-scaling of the wind turbines and positioning at deeper waters are in progress, and floating concepts at deep waters, like HyWind [1], Sway [2] and BlueH[3], are investigated. New ideas and innovative concepts may lead the way for further development of floating offshore wind turbines. Vertical-axis concepts are re-vitalized in offshore environments (eurowind [4] and NOVA [5]) and some of them are floating, like Ecopower [6] and SELSAM [7].

This paper deals with ideas of a novel floating offshore wind turbine concept which may point to future very large wind turbines in very large wind farms at deep waters. The basic ideas of the concept are described, and technical details of subcomponents and procedures for operation and maintenance are discussed. A vision regarding a future

utilization of the novel concept is presented, and finally a status of the work done on the concept is made.

2. A novel floating offshore concept

In search of a simple and novel concept offering cost reduction potential in comparison to present horizontal-axis wind turbine applications, we have adapted technology elements known from vertical-axis wind turbines, floating offshore platforms, pultrusion, generators, power controls and wind turbine safety philosophy.

In particular, we suggest a vertical-axis concept consisting of a Darrieus rotor as the energy capturing device, and a long vertical rotating tube transitioning into a submerged buoy-like part which is connected to the sea bed (Figure 83).

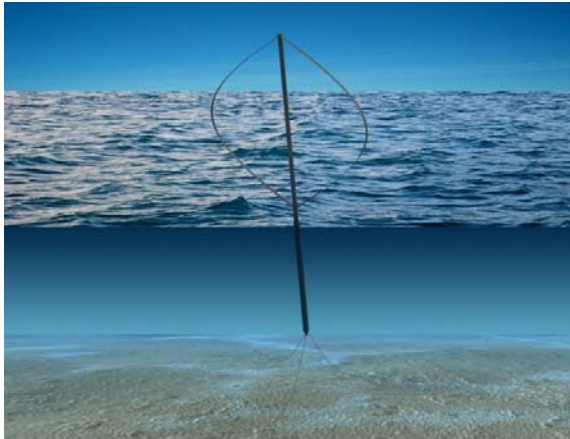


Figure 83 Artistic view of the concept

The concept combines:

- a 2 or 3 bladed Darrieus wind turbine rotor which does not need a yawing mechanism, neither a top-mounted heavy nacelle;
- an innovative offshore rotating foundation for deep-sea which does not need a main bearing;
- new technology in blade manufacture for large rotors;
- simple controls;
- simple safety philosophy.

3. Description of the basic components

Some specific technological solutions are proposed for the components of the turbine.

3.1 Rotor

The rotor is a vertical-axis wind turbine. Many different technical solutions have been proposed during the last 40 years, but we have chosen the Darrieus rotor. The main reasons are: simplicity of the concept, reasonable efficiency, good economy, and a long record of research and development in the past.

3.2 Blades

The blades are characterized by a simple design (constant geometry along the length). The pultrusion process of GRP seems quite promising for large blade profiles, and the material strength of pultruded GRP is much better than for hand layed-up GRP for horizontal-axis wind turbines. It seems possible to design the rotor at a cost comparable to horizontal-axis wind turbines.

3.3 Transmission System

Many generator configurations are possible with the generator placed in the bottom of the submerged structure. The generator must in this case also be able to start the Darrieus rotor.

We see five potential configurations:

- The generator is mounted inside the submerged foundation at the bottom and rotate with the rotor. The shaft is extended through the foundation bottom and fixed to the torque arms, Figure 84a.
- The generator is mounted outside the foundation and fixed to the torque arms. The shaft is fixed to the torque arms, Figure 84b.
- The generator is fixed on the sea bed and the shaft is fixed to the rotating structure Figure 84c.
- Two generators are placed in two turbine gondolas, fixed to the tubular structure. The turbine gondolas each consist of a turbine and a generator and through the rotation in the water they convert the rotor power into electricity, Figure 85
- The conversion of the power can be obtained by a drag device, rotating slowly at the bottom of the structure, Figure 86. The configurations in Figure 3 and 4 both absorb the rotor torque in the water and torque arms are thus not necessary.

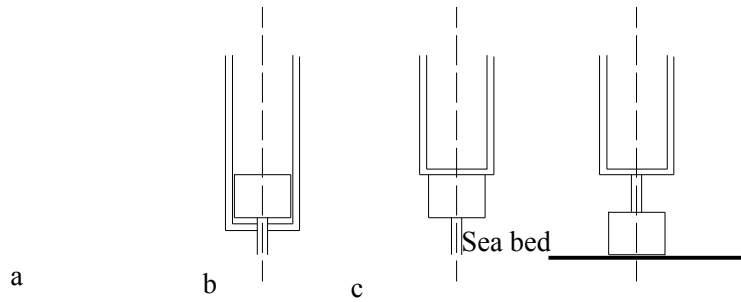


Figure 84 Different configurations for the placement of the generators

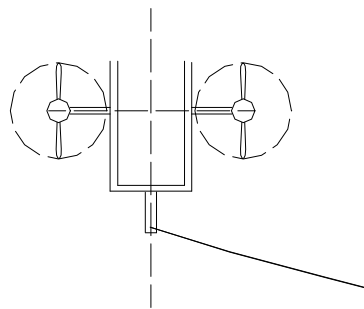


Figure 85 Configuration with two gondolas with turbines and generators

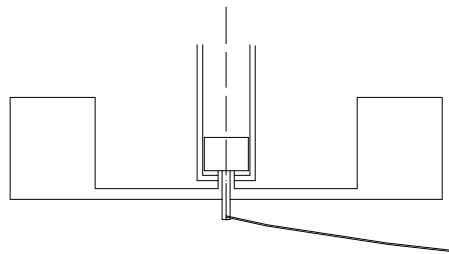


Figure 86 Drag device for torque absorption in the water

3.4 Safety System

Instead of air brakes we propose water brakes for overspeeding protection. The system consists of drag devices, that in overspeeding conditions are deployed from the rotating submerged foundation (Figure 87).

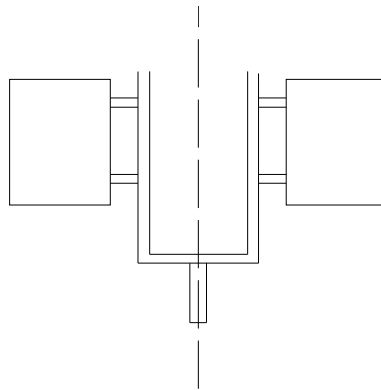


Figure 87 The safety system consisting of drag devices

3.5 Control System

The turbine does not need a pitch neither a yaw control system. The power control is obtained by rpm control of the rotor speed.

3.6 Anchoring Part

The torque and the thrust are transmitted through the foundation to the bottom of the structure. The foundation is anchored to the sea bed with tensioned wires. The forces are transferred through these wires. To take the torque two or more rigid arms are necessary (Figure 88).

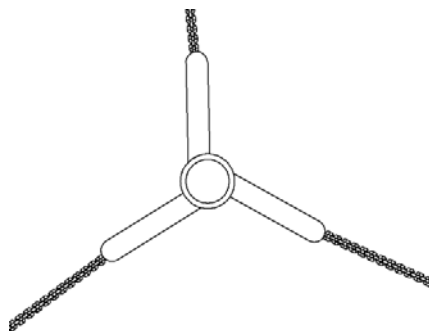


Figure 88 Torque arms and anchoring wires

3.7 Installation

The rotor and the foundation can be towed to the site. In case of a two-bladed rotor, the whole structure, without counterweight, can float and lay horizontally on the water line. Counterweight can be gradually added, to tilt down the turbine. In case that the generator is mounted inside the foundation, it can be inserted from the top of the structure.

3.8 O&M

Some specific solutions are available for the maintenance of the turbine. Moving the counterweight from the bottom of the foundation upwards is possible to tilt up the submerged part for service. An outside generator can be serviced and marine growths on the rotor can be removed. It is possible to place a lift inside the tubular structure to have easy access from the top of the turbine to the submerged part.

4. Advantages and challenges

The novel floating offshore wind turbine concept has some evident technical advantages, but on the other hand, some severe challenges are foreseen.

4.1 Advantages

The most obvious advantage of the concept is its simple design. The whole construction is simply a rotor, embedded in and supported by the water itself. The simple design is exemplified in the rotor tube which in principle can be made as one long tube like a wind turbine tower is made today. Another example of the simple concept is the blades. Rather large blade sections can be pultruded in GRP by production facilities that are indeed rather small. In principle, a production facility can be put on a ship, and the blades can be produced offshore in lengths of kilometres. The simplicity of the concept is underlined by the balancing of the forces in the water. The rotor is allowed to tilt, which makes it possible to transfer the rotor thrust to the shaft in the bottom from where it is further transferred to the seabed by anchor chains.

Another advantage of the concept is the simple way it can be regulated by the generator. The generator can start the rotor from stand still, regulate power by stall, and stop the rotor as a brake. It needs no yawing system to position the rotor into the wind, and it is not sensitive to inclined flow due to the tilting of the rotor, and no pitching of blades is necessary to regulate power. The Darrieus rotor is stall-regulated at high wind speeds, or the power can be down-regulated by reducing the rotor speed. Overspeeding of Darrieus wind turbines is a problem, but in this case the overspeed protection can be made with water brakes rather than with air brakes. Water brakes are much more efficient than air brake, which means that overspeeding protection can be made very and small.

An advantage of the concept is that the rotor may be tilted by moving the ballast in the tube. During installation and maintenance (3.7, 3.8)

The vertical-axis wind turbine concept seems to have an advantage for very large systems. The gravitational blade loads are the dominant fatigue loads for horizontal-axis wind turbines. They increase significantly with the increasing sizes, while the gravitational of vertical-axis turbines are constant during rotation.

4.2 Specific challenges

A number of challenges of the novel floating offshore design should be mentioned. First of all, the fundamental question whether the concept works properly according to the idea must be verified. The rotating foundation will have a certain friction with the water which will reduce the net amount of power. This friction will increase as marine growths build up on the surface. It is an open question whether this friction will increase to a significant amount or whether the friction can be kept low by reducing the biomass build up with ordinary bottom ship painting. At present, a silicone based paint, which significantly reduces the build up, is on the market.

The shaft sealing in the bottom of the rotor is also a challenge since the pressure difference over the bearings put high requirements to the sealing. Meanwhile, this technical problem is similar to the sealing problem of propeller shafts on sea vessels. It is therefore anticipated that solutions from shipbuilding or submarine construction technology building can be transferred to this wind turbine design.

The advantage that the generator with a high mass may be put in the bottom of the rotor tube generates another challenge. The positioning of the generator in the bottom makes maintenance and exchange of the component very complicated. Methods for lifting up the generator through the tube, eventually in smaller parts, must be developed. In case the generator is mounted outside the rotor, methods to tilt up the generator must be found.

Even though the Darrieus rotor was developed significantly during the 70's and 80's it is still considered a challenge to make blades for this design in a cost-efficient way. The most promising method seems to be pultrusion of GRP in full blade length sections that are bent into the blade shape and glued together. A substantial development work is needed to make such blades commercial compared to the horizontal wind turbine blades of today.

The most significant foundation difference compared to the horizontal-axis wind turbine is that the rotor torque must be absorbed in the sub-sea systems. This may be through the use of torque arms connected to the anchoring system or through drag elements in the water, either with turbine gondolas or drag plates. The torque of the Darrieus rotor varies

with the position on the rotation and this varying torque will also have to be absorbed through the anchoring system. This additional dynamic effect has to be considered in the design.

5. Status of development

The concept emerged from a brain storming in 2007. A PhD study was initiated in August 2008.

5.1 Present status

First part of the PhD study has been to develop a vertical-axis rotor code. A double stream tube code has been implemented (in Fortran language) to provide some preliminary results. Some rough dimensions for two specific sizes have been determined, see Table 1.

Table 40 Dimensions and characteristics of 2 MW and 20 MW rotors

Size	2MW	20M W
Rotor Radius (m)	40	120
Rotor Height (m)	80	240
Chord (m)	2.5	11
Torque at rated power (N*m)	$5 \cdot 10^7$	$1.4 \cdot 10^6$
Thrust at rated power (N)	$2.5 \cdot 10^6$	$2 \cdot 10^5$
Rotational speed at rated power (rpm)	4.1	13.3

The submerged structure needs to be dimensioned for each of the two sizes. The submerged part has:

- To ensure the buoyancy to float
- To balance the weight of the structure and the vertical component of the thrust force.
- To ensure, with the counterweight, the equilibrium of the structure.

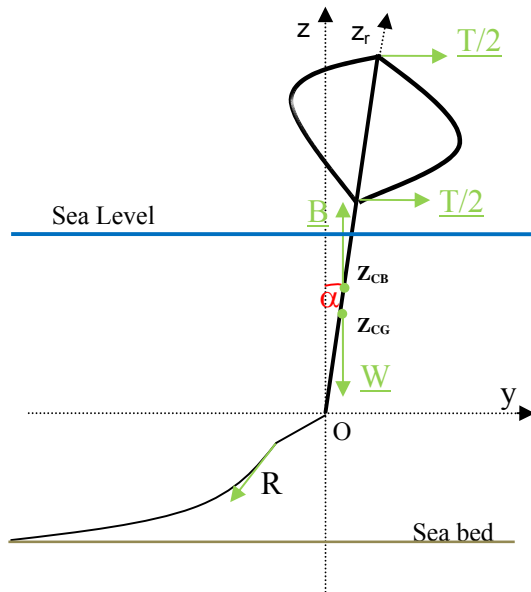


Figure 89 Schematic view of the forces

Particularly important is the position of the center of gravity with respect to the center of the buoyancy force. At equilibrium it is necessary that the center of gravity (z_{CG}) on the vertical-axis is below the center of buoyancy (z_{CB}). Figure 89 shows the forces, the external forces apply a moment on the structure. This moment has to be balanced from the moment due to the buoyancy:

$$M = (B - W) (z_{CG} - z_{CB}) \sin(\alpha) \quad (1)$$

where T is the thrust, B the buoyancy, W the weight and α the tilt angle.

A basic routine has been implemented to calculate the dimensions of the submerged part. The routine consider:

- The bending moment due to maximum value of the thrust and the tubular structure is dimensioned to a safety factor greater than 2.
- Different materials (steel, aluminum, concrete) in order to optimize the total weight of the structure.
- The equilibrium between buoyancy force and weight.
- The equilibrium of the moment of the thrust and the moment due to buoyancy M (equation 1)
- A very simple design consisting of a slender tubular structure

Several design configurations are possible for the 2MW and 20MW sizes, see Table 41.

Table 41 Dimensions of the structure for 2MW and 20MW sizes

Size	2MW	20MW
Radius of the rotor structure (m)	2	3
Radius of the submerged part (m)	6	6.5
Thickness (m)	0.03	0.03
Total weight (tons)	2300	13000
Rotor length (m)	80	240
Total length (m)	161	345

5.2 Next Development

The next step in the technological development is the implementation of an aeroelastic and hydrodynamic coupled code. At Risø DTU a code has been developed for horizontal-axis floating turbines, HAWC2 [8]. The PhD project is ongoing to implement an aerodynamic subroutine for VAWT to HAWC2 . Indeed the equilibrium and the loads on a floating HAWC have been studied [9,10]. The influence of the rotation of the structure and of the cycling loads of a VAWT rotor is now being investigated.

Another subroutine to add is a subroutine to calculate the friction force around the rotating foundation. Preliminary studies indicate that this drag is insignificant (around 1% of the power). A more detailed analysis is needed, that includes other variables: influence of marine growths, change of roughness, current and waves.

In the meantime some future developments have been planned. In 2010 a kW size prototype will be built and tested in Roskilde fjord. This will be a concept test to verify the feasibility of the concept. A one year friction experiment will explore on friction and marine growths around a rotating cylindrical structure.

Looking forward (2011-2015), also an upscaling phase has been planned. A first demonstration project is planned with a turbine size in the order of 100kW. In the meantime feasibility studies of a MW scale turbine will go on a parallel track.

6. Commercial perspectives

Large scale wind energy systems at highly potent wind resource areas are key candidates for significant contributions to the energy supply. The most potent wind resource areas

on the earth are deep sea offshore sites, and the potentially most interesting wind energy system for deployment at such sites are floating multi-MW size wind turbines. The primary markets are at deep sea offshore sites along the coasts of for example Norway, France, Spain, the Pacific and Atlantic Ocean (USA) and Asia (China and Japan) and close to big cities. Along with development, optimized floating concepts could be commercialized for places like the North Sea or coastal shallow seas. On the long term exploitation of the wind resources in the "roaring forties" on the southern planet can be made possible with this concept combined with battery or hydrogen tankers that supports energy to coastal cities.

New business opportunities might enter the market in the marine operations and shipping sector, and in the shipyard industry. They will develop sea vessels accordingly with handling, manufacturing and operation of these large wind systems in mind:

- Ships with towing capacity and with pultrusion factory on board
- Shipping companies might trade electricity with battery ships gathering electricity from remote offshore wind farms.
- Floating factories might be developed for very large concepts (support structure for instance made with concrete composites)

The new concept contributes significantly with added value of technology to the wind industry if the concept is developed and demonstrated under real conditions. Within this perspective, the new concept may become an interesting competitor to concepts like HYWIND[1], SWAY[2], BLUEH[3] and NOVA[5], presently being closer to demonstration.

References

1. *Hywind Floating wind power production*. Alexandra Bech Gjørnv Oil & Energy 2006-05-24
2. sway.no
3. www.bluehgroup.com
4. *A needed change in orientation*. Pierce, WindTech international October 2007
5. www.nova-project.co.uk
6. www.ecopowerusa.com
7. www.selsam.com
8. *How 2 HAWC2*, The user's manual, T.J. Larsen and A.M. Hansen. Risø-R-1597, 2008

9. *Responses of Floating Wind Turbines to Wind and Wave Excitation, Master thesis in Ocean Engineering*, K. H. Lee, Massachusetts Institute of Technology, 2005

10. *Loads Analysis of Floating Offshore Wind Turbine Using Fully Coupled Simulation*, Wind power 2007; J.M. Jonkman, M.L. Buhl, Los Angeles, California, 2007

Proceedings of the ASME 2010 29th International Conference on Ocean,
Offshore and Arctic Engineering
OMAE2010
June 6-11, 2010, Shanghai, China

OMAE2010-20357

**A Novel concept for floating offshore wind turbines:
Recent developments in the Concept and investigation on fluid
Interaction with the rotating foundation**

Luca Vita
Risø DTU

Frederik Zahle
Risø DTU

Uwe S. Paulsen
Risø DTU

Troels F. Pedersen
Risø DTU

Helge A. Madsen
Risø DTU

Flemming Rasmussen
Risø DTU

vita@risoe.dtu.dk

Risø National Laboratory for Sustainable Energy

DTU, Technical University of Denmark

Roskilde 4000 Denmark

ABSTRACT

This paper describes the recent developments regarding a new concept for deep sea offshore vertical axis wind turbines. The concept utilizes a cylindrical foundation rotating in the water. The 2D Navier-Stokes solver EllipSys2D has been used to investigate the interaction between the rotating foundation and a water flow stream passing the turbine. Lift and drag forces, and the friction moment on the rotating foundation of the turbine have been computed. The calculations are repeated for different operating conditions of the wind turbine on a range of rotational speeds. The Reynolds number, based on the diameter of the foundation, is 5×10^6 .

Keywords: Vertical Axis Wind Turbine, Floating, Offshore, deep sea, rotating cylinder, lift, friction.

1. Introduction

The fast growth of the wind energy market has increased the strategic importance of offshore wind energy. The European annual report [2] predicts a growth in the European wind energy production from 119 TWh (2007) to 935 TWh (expected in 2030). The electricity production from offshore wind energy is expected to increase from 4 TWh (2007) to 469 TWh (expected in 2030). Thus the share of the offshore production will increase from 3% to 50%. On the other hand, the economic wind energy report from EU [3] (2009) addresses an important cost issue: in average, the cost of offshore wind energy is 2400 Euro/kW versus the 1250 Euro/kW of the on shore (data 2008), with a quite different cost break down in the two cases.

This scenario defines the border lines of a new market, distinct from the ongoing onshore wind energy. If we consider offshore wind energy as a new independent market, it is not reasonable to produce offshore wind energy just moving wind energy technology from onshore out into shallow waters. New specific offshore concepts are needed in order to reduce the cost (to be competitive with the onshore market) and to exploit the considerable offshore wind energy resources.

One of the key challenges is the possibility to optimize wind energy systems for deep water sites with floating wind turbines. This new technology becomes attractive for water deeper than 50 m, and it pushes the limit of the water depth to several hundred meters.

The authors presented in [1] a new concept for floating offshore wind turbines (Figure 90), that is suitable for deep water. The concept has an extremely simple design which simplifies its up-scaling. The main characteristic is that the floating foundation is rotating in the water.

In [1], the most important challenges have been pinpointed, which need to be investigated in order to validate the feasibility of the concept. These challenges consist of: the investigation of the hydrodynamic forces acting on the rotating structure in a water flow stream; the torque absorption at the bottom of the rotor and the dynamic loads on the shaft; the control system; the maintenance strategy for the underwater components.

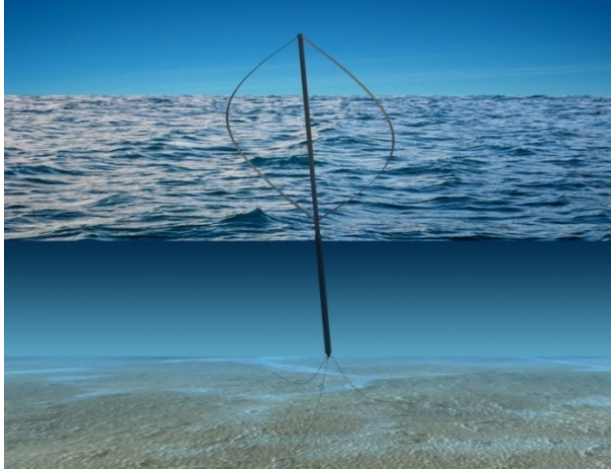


Figure 90 Artistic view of the concept.

This paper deals with the hydrodynamic forces generated by a water stream passing the rotating foundation. These forces occur due to the water currents and due to the motion of the foundation. A cylindrical structure rotating in a fluid experiences two forces (lift and drag) and one moment (friction). The two non-dimensional parameters governing the physics of the problem are: the Reynolds number ($Re = Dv/U$) and the ratio of peripheral speed and the freestream speed ($\alpha = \omega R/U$). The first studies on a rotating cylinder were carried out by Prandtl [16]. He found that the C_L (lift coefficient) increased linearly with α until an asymptotic value, i.e. $C_{L\text{Max}} = 4\pi$. In the last 50 years many numerical, theoretical and experimental studies have been carried out, as well summarized by Mittal [7] and Padrino[5].

Unfortunately most of the studies are numerical at low Re (<1000) and low α . The typical values for our floating foundation are in order of $Re = 10^6$. The first numerical study was made by Glauert [6], who solved the two dimensional Navier-Stokes equations. Glauert's results show that the lift increases linearly and indefinitely with α , exceeding the limit of Prandtl. Other studies show different results: Chew [8] confirms in his numerical studies the results of Prandtl; however the experiments by Tokumaru [4] and the numerical model by Mittal [7] show a value of the lift higher than the limit of Prandtl, even if an asymptotic value is observed as well. The value of α when the vortex shedding ceases and the lift tends to an asymptotic value is called α limit (α_L). The value of α_L depends on Re . For very low Re ($Re < 160$) this value is a logarithmic function of Re , for $Re > 1000$ it seems to be constant, i.e. $\alpha_L = 2$ [7].

Some numerical results at higher Re ($10^4 < Re < 10^6$) are presented by Chang [9]. The stopping of vortex shedding is shown and the lift seems to decrease at high Re . Unfortunately, the numerical simulation at high Re are very limited in time because of convergence problems and it is not possible to predict a fully developed regime.

The boundary layer around a rotating cylinder is described by Padrino [5] and Wang [11] for $Re < 1000$. The friction torque coefficient is reported and it seems to decrease by the Re number. Another possibility to calculate the friction of a rotating cylinder at high Reynolds numbers is shown in [10] by Theodorsen.

In the present paper the forces and the friction moment on the rotating structure are calculated by numerical simulation, using the code EllipSys2D developed in collaboration between DTU and Risø DTU. The simulation is repeated for different operating conditions of the wind turbine at different rotational speeds. The results show a steady solution for $\alpha > 2$ and the maximum lift coefficient achieved is 10.4 (for $\alpha = 5.2$).

The results are used to calculate the force acting on the structure at different operating conditions and the friction losses in terms of percentage of the nominal power.

2. Concept description

The concept consists of a Darrieus rotor whose tower is extended underwater, in order to act as a spar buoy. The whole system is rotating and generates power with a generator placed at the tower bottom and fixed at the anchoring system.

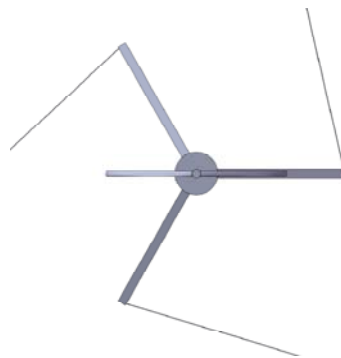


Figure 91 Darrieus rotor, torque arms and mooring system, top-view.



Figure 92 Darrieus rotor, floating foundation and torque arms, trimetric-view.

Three rigid torque arms connect the generator to the mooring system and absorb the torque (Figure 91 and Figure 92).

Due to its simplicity many solutions are available for the design. Some specific solutions have been selected and they are described below.

ROTOR

A 2 bladed Darrieus rotor has been selected. The choice of 2 blades is to facilitate the installation procedure and to minimize the production costs [12].

BLADES

The blades have a constant geometry along the length. They can be realized in GRP (reinforced glass fibers) by a pultrusion process. Their cost is expected to be comparable to the blades for horizontal axis wind turbines.

SAFETY SYSTEM

Since the whole system is rotating, it is possible to use water brakes as safety system. They consist of drag devices deploying from the rotating foundation in over-speeding conditions (Figure 93).

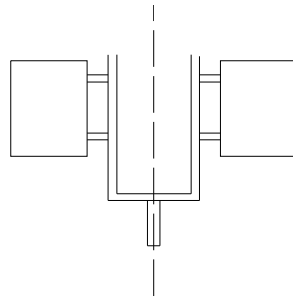


Figure 93 Water brakes (safety system).

CONTROL SYSTEM

The control system is achieved by controlling the rotational speed of the generator. At cut-out the turbine is stopped by the generator and the safety system.

No yaw system is needed for VAWTs.

GENERATOR

The generator has several functions:

- To generate power.
- To start the turbine, since the VAWTs are not self starting.
- To control the system by varying the rotational speed.
- To act as a brake in over-speeding condition.
- To stop the turbine.

In order to control the turbine, the generator has to be a variable speed generator. Due to its placement in the bottom of the structure, it acts as a counterweight. Therefore the generator has no restrictions due to the weight.

The multi-pole permanent magnet generators seem to fit these prerequisites.

ANCHORING SYSTEM

As mentioned, torque arms are necessary to absorb the torque at the bottom of the structure. The dimension of the anchoring system is the most critical since it has to absorb the reaction forces (torque, thrust and hydrodynamic forces) at the bottom of the structure.

Specific procedures for installation and O&M are suggested as well.

INSTALLATION

Using a two bladed rotor, the turbine and the foundation can be towed to the site by a ship. The structure, without counterweight, can float horizontally in the water. Ballast can be gradually added to tilt up the turbine.

O&M

Moving the counterweight in the bottom of the foundation is possible to tilt up the submerged part for service, in particular build up of marine growths. It is possible to place a lift inside the tubular structure for easy access from the top of the turbine to the submerged part.

3. Sizes and performances

The design of the Darrieus rotor and of the rotating foundation are coupled

The design of the underwater part is a compromise between several issues:

- Balancing the forces and the moments due to the weigh, the buoyancy and the aerodynamic thrust. This objective is achieved by varying the volumes of the submerged foundation and the values of the counterweight.
- Reducing the radius and the rotational speed to avoid critical hydrodynamic forces and friction losses
- Reducing the total length, in order to reduce forces and moments and to reduce the production costs.

In Table 42, the dimensions of the concept are shown for 2 MW and 20 MW. The simple concept design facilitates up-scaling.

Table 42 Dimensions of the rotor and of the rotating foundation, for 2 MW and 20 MW

Size	2MW	20MW
Rotor Diameter (m)	67	120
Rotor Height (m)	75	240
Chord (m)	3.2	11
Torque at rated power (N×m)	1.4×10^6	5×10^7
Thrust at rated power (N)	2.4×10^5	2.5×10^6
Rotational speed at rated power (rpm)	15.0	4.1
Radius of the rotor tower above the water level (m)	2	3
Radius of the submerged part of the tower (m)	2.5	6.5
Total weight (tons)	2300	13000
Total length (m)	160	345

However a full study of a 20 MW machine requires more in depth knowledge of the concept, the different materials and deep water site conditions.

A more detailed investigation has been carried out on the 2MW size.

The solidity of the rotor ($\sigma=Nc/R$), is equal to 0.19. This value is a compromise between the optimization of the rotor performances (higher values of σ) and the reduction of the cost (0.1 is the optimum σ value), [12].

The aspect ratio of the rotor, defined as ratio between height and diameter of the rotor, is 1.12. Also this value is a compromise between the optimum, discussed by Paraschivoiu to be around 1.3 [12], and the reduction of the costs, obtained by reducing the height. It is useful to stress that a taller rotor in turn also requires a deeper foundation. This means higher costs in terms of: longer structure, larger forces on the submerged part and larger values of the frictional losses to the nominal power.

Numerical simulations have been performed using a multiple stream tube model, developed at Risø-DTU. The airfoil used for the simulation is a NACA 0018.

In Figure 94, power coefficient C_p and the power are plotted versus the tip speed ratio ($\lambda = \omega R / v_{sp}$).

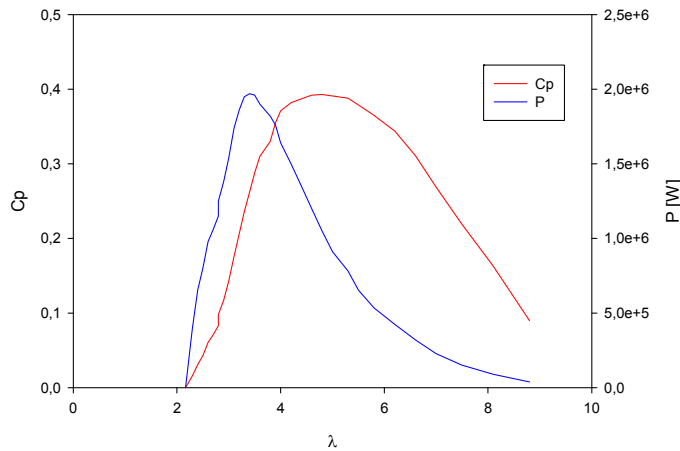


Figure 94 Power and C_p versus the tip speed ratio.

In the next charts the thrust and the power versus the wind speed (

Figure 95) are reported, and the power versus the rotational speed (

Figure 96). The turbine has a cut-in wind speed of 5.5 m/s, a cut-out wind speed of 28 m/s and the rated power is achieved at 15m/s, consistent to offshore environment and high wind resources.

At wind speeds higher than 15m/s, the power is kept constant by increasing the rotational speed. This possibility is risky because a negative variation in the wind speed can cause a positive variation of the power. Therefore it would require a very fast and accured rotational speed control system.

An alternative solution could be to keep constant the rotational speed at wind speeds higher than 15m/s. In this case the power would decrease as in Figure 94 and no instability could occur.

On figure 6 and figure 7, four operational points correspond to four rotational speeds. They are representative of four operational conditions of the turbine:

- 5.5rpm (starting of the rotor)
- 11rpm (corresponding to the peak of the C_p)
- 15rpm (corresponding to the peak of P)
- 20rpm (rotor constant power at high wind speed, corresponding to the maximum value of the thrust)

The forces acting on the submerged foundation at these four operating points are analysed. The flow around the cylinder is computed: the lift, the drag and the friction moment are calculated.

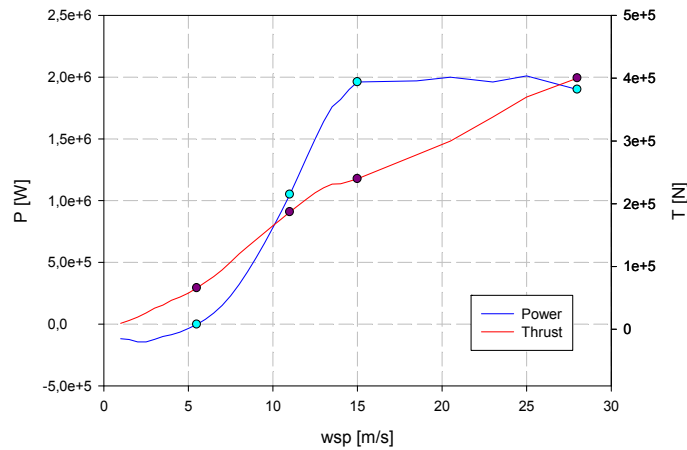


Figure 95 Thrust and Power versus the wind speed. The red dots refer to operating points (rotational speeds) and are selected for further investigation.

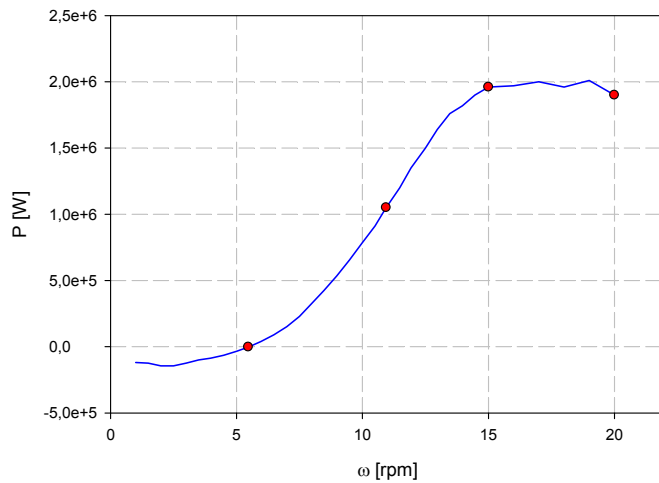


Figure 96 Power curve versus the rotational speed. The red dots refer to operating points (rotational speeds) and are chosen to investigate the hydrodynamic forces.

4. CFD COMPUTATIONAL TOOL

For all computations, the EllipSys2D pressure based incompressible Reynolds averaged Navier-Stokes flow solver written by Michelsen [13,14] and Sørensen[15] is used. The code uses the finite volume method, solving for the primitive variables u , v , w , and p , in general curvilinear coordinates. The variables are stored in a collocated grid arrangement, and odd/even pressure decoupling is avoided using the Rhie-Chow interpolation.

The iterative PISO algorithm is used to advance the solution in time using a second-order accurate scheme. The convective terms are discretized using the Quadratic Upstream Interpolation for Convective Kinematics Scheme, QUICK, and the viscous terms are discretized using central differencing. The momentum equations are solved decoupled from each other using a red/black Gauss-Seidel point solver. To accelerate the convergence of the pressure-correction equation, a multi-grid solution

strategy is implemented combined with the additive Schwarz method, where each sub-domain is solved for simultaneously. To further accelerate the convergence of the solution, grid and time step sequencing is used.

The simulations were carried out using a combination of steady state and unsteady simulations. Due to the low freestream velocity, convergence was very slow, and as such the unsteady simulations were started from an initial steady state guess. The time step used in the unsteady simulations was set to $\Delta t=0.01$ s. Fully turbulent flow was assumed over the cylinder using the $k-\omega$ SST turbulence model. The mesh which was used was a curvilinear mesh using an O-type grid with a first cell height corresponding to a y^+ of less than two. The outer boundary was placed 100 cylinder diameters away from the cylinder. The rotational speed was prescribed on the cylinder surface to account for the rotation.

5. RESULTS

The numerical simulations have been carried out at an inflow velocity of 1m/s corresponding to $Re= 5 \times 10^6$.

The calculations are repeated at four operating conditions, corresponding to different rotational speeds. The speed ratios α and the corresponding rotational speeds are listed in Table 5.

Table 43 speed ratios α corresponding to the selected rotational speeds

α [-]	1.4	2.9	3.9	5.2
ω [rpm]	5.5	11	15	20

Due to the variation of α (from 1.4 to 5.2) different flow regimes are expected around the cylinder at different operating conditions.

The results and the analysis of the flow regime are reported for the different speed ratios.

$\alpha=1.4$

At the lowest speed ratio the separated shear layer becomes unstable in the wake which gives rise to some unsteadiness in the lift and drag on the cylinder due to beginning vortex shedding (Figure 17). The lift coefficient was found to be equal to 3.99, the C_D to 0.180 and the C_M to 0.0307.

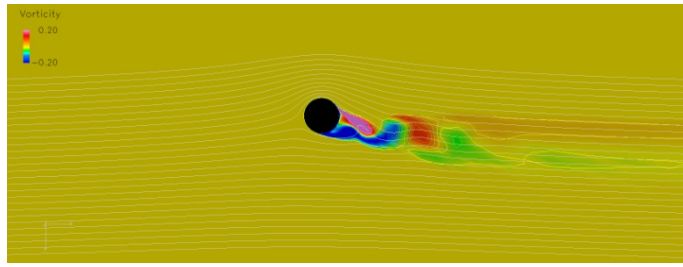


Figure 97 Vorticity contours around the cylinder at $\alpha=1.4$, $U=1\text{m/s}$.

$\alpha=2.9$

The increased rotation delays separation of the shear layer which causes the flow to be steady in the wake of the cylinder. An approximately linear increase of lift is measured compared to α 1.4 resulting in a C_L of 9.5.

$\alpha=3.9$

This speed ratio is representative of rated power conditions ($\omega=15$). Due to the relatively high rotational speed, the flow is highly influenced downstream and upstream. The high rotational speed causes the flow to be entirely steady around the cylinder, eliminating vortex shedding which would otherwise be present on a cylinder in this Reynolds number range. This is illustrated in Figure 18 and Figure 19, where the vorticity magnitude and pressure coefficient contours are plotted.

The resulting forces on the cylinder are considerable with a lift coefficient C_L of 10.1, corresponding to a total force of 25.2 kN/m, and a drag coefficient $C_D=-0.016$ (40N/m). The drag force changes its direction, respect to the lower rotational speed and it acts as a thrust.

The friction moment coefficient is equal to 0.013, corresponding to a friction moment of 324 Nm/m.

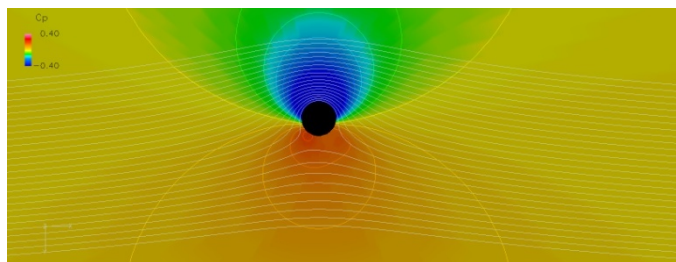


Figure 98 Pressure coefficient contours around the cylinder at $\alpha=3.9$, $U=1\text{m/s}$.

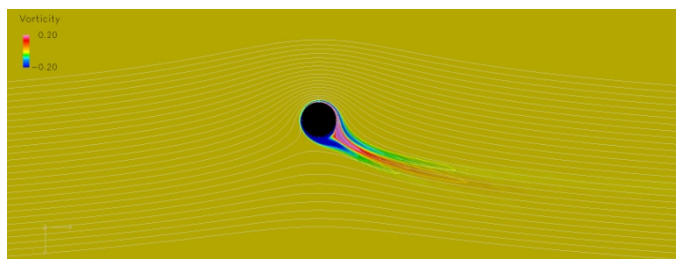


Figure 99 Vorticity contours around the cylinder at $\alpha=3.9$, $U=1\text{m/s}$.

$\alpha=5.2$

At the highest rotational speed, the flow bears the same characteristics as for $\alpha=3.9$ with a slightly increased C_L , the drag is still acting as a thrust and the C_M is the double than in the previous conditions.

6. DISCUSSION

The force coefficients calculated for the different rotational speeds are summarized in Table 44.

Table 44 Forces and moment coefficients at different α

α	C_L	C_D	C_M
1.4 (5.5rpm)	3.99	0.180	0.0307
2.9 (11rpm)	9.50	0.0009	0.06914
3.9 (15rpm)	10.1	-0.016	0.12973
5.2 (20rpm)	10.4	-0.043	0.2493

The values of C_L are surprisingly close to the values reported by Tokumaru in [4]. Tokumaru compares his experimental data with the experimental data from Prandtl [16] and Reid [17]. The data of Tokumaru show a C_L around 10.0 at $Re\ 3.8 \times 10^3$. In the experiment of Reid, C_L achieves a value between 9.0 and 10.0 at $Re\ 4.7 \times 10^4$. The data from Prandtl under estimate the C_L , but that is probably due to the low ratio of the cylinder span and the diameter used in Prandtl's experiment. Numerical computations for $Re < 10^3$ report C_L greater than 10 [5,6].

In

Figure 100, the data obtained by using EllipSys2D at $Re\ 5 \times 10^6$ are plotted with the data reported by Tokumaru. The C_L seems to be insensitive to the increasing of the Reynolds number for values of α between 3 and 4. At higher values of α Tokumaru achieves higher values of C_L than EllipSys2D and this can be due to 3D effects.

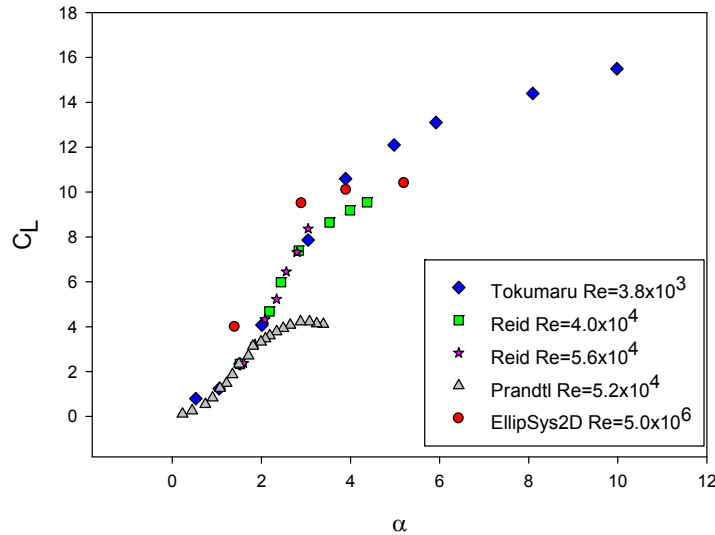


Figure 100 Values C_L from EllipSys2D at $Re 5 \times 10^6$ (○), from Reid at $Re 4 \times 10^4$ (□) and 5.6×10^4 (☆) [17], from Prandtl at $Re 5.2 \times 10^4$ (▲) [16], from Tokumaru at $Re 3.8 \times 10^3$ (◇) [4]. Data from [4].

In Table 45, the lift, the drag and the friction moment are reported for length of unity.

At rated power conditions, a lift of 2.52×10^4 N/m acts on the submerged foundation. The total force, integrated over the whole structure is 2.14×10^6 N, being much larger than the value of the aerodynamic force.

Table 45 Forces and moment per length at different α

α	Lift (N/m)	Drag (N/m)	Friction moment (N×m/m)
1.4 (5.5rpm)	9950	450	76.5
2.9 (11rpm)	23720	2.2	172.5
3.9 (15rpm)	25148	-41	323.7
5.2 (20rpm)	25860	-106	622

At rated power conditions the friction moment per length corresponds to a power of 508W/m. The total power consumption from friction is 43.2kW, corresponding to a friction to the nominal power ratio of 2.2%. The same analysis has been carried out with the data suggested by Theodorsen in [10]. In his data, Theodorsen suggests to

compute the friction moment per length unit on revolving cylinders using the formula $M_F = C_F \rho \pi D^4 \omega^2 / 16$, C_F is the skin friction factor that Theodorsen calculates with an empirical logarithmical formula. The C_F results to be 2.22×10^{-3} at $Re = 5 \times 10^6$ and $M_F = 644 \text{ Nm/m}$. The ratio of friction to nominal power is 4.3%.

In

Figure 101, the data from Theodorsen and from EllipSys2D are compared at the four rotational speeds.

Both the data seem to follow an exponential fit curve, but the Theodorsen's formula overestimates the friction moment for higher rotational speeds.

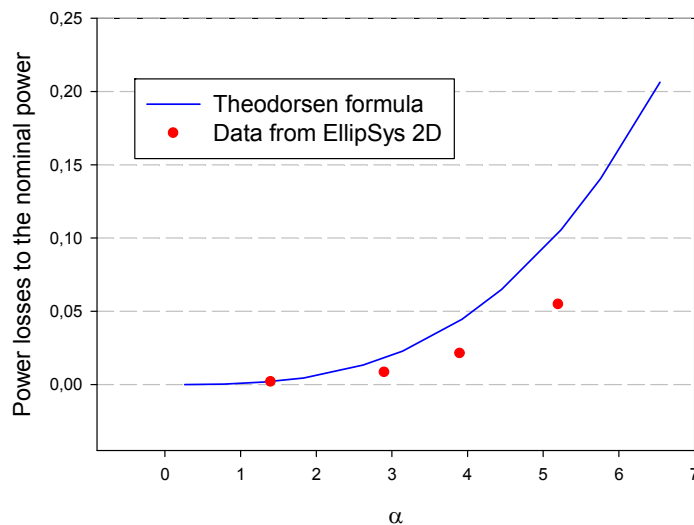


Figure 101 Power losses to the nominal power versus α . The blue line is obtained by using the formula reported in [10] by Theodorsen and the red dots are the values achieved by EllipSys2D.

In Table 8, the forces and the friction moment acting on the turbine at the four operating conditions are summarized ($U=1\text{m/s}$ is considered). In all the conditions, the thrust is small compared to the lift force acting on the underwater foundation. The power friction is compared to the power production at the same rotational speed and not to the nominal power. The power friction has a maximum of 5.6% during operational conditions.

Table 46 Forces acting on the turbine, power production and power friction at the four operating conditions

α	Lift [kN]	Thrust [kN]	Friction power [kW]	Power [kW]	Friction /power
1.4	845.7	65.81	3.71	0.00	/
2.9	2016.2	186.85	16.69	1050	0.012
3.9	2137.6	239.65	43.20	1960	0.022
5.2	2198.1	400.00	109.49	1900	0.056

7. CONCLUSIONS

A concept for floating offshore wind turbines has been presented, including the dimensions and the characteristic curves of the rotor. The main challenge for the concept development is the study of the hydrodynamic forces on the rotating foundation. Four operation conditions have been selected and the forces have been investigated for each of them.

The investigations, carried out in EllipSys2D, show force coefficients consistent with other results at lower Re [4]. At nominal power conditions (at $\alpha=3.9$) a C_L of 10.1 is achieved when the solution of the flow appears steady.

Vortex shedding was observed only for the lowest rotational speed (at $\alpha=1.4$).

The force coefficients calculated by numerical simulations are used to calculate the forces acting on the rotating foundation. For rated power conditions ($\alpha=3.9$, $\omega=15$ rpm) a force of 2.52×10^4 N/m is achieved. The total force on the submerged foundation is of 2.14×10^6 N that is almost 10 times larger than the thrust at the same conditions. It has to be stressed that from these studies, the hydrodynamic forces are the most important parameters in the design of the concept. Therefore it is important to know the ocean currents before this concept can be applied.

Further investigations have to concern the variation of the forces in both time and space domain. Indeed the results of this paper concern the forces for a 1D inflow stream at $U=1$ m/s. In steady water conditions, the thrust is the larger force acting on the structure. In a 3D flow, the different sections of the submerged foundation may additionally be loaded with forces in different directions.

The friction moment, acting in the direction opposite to the foundation rotation, is used to calculate the total friction on the foundation, in terms of power losses. At rated power conditions, the friction to nominal power ratio is 2.2%, a higher value (4.3%) was achieved by using the literature [10].

However it is stressed that experimental results would be needed to fully validate the numerical results. Unfortunately, to reproduce the flow regimes investigated in this paper correctly, it would require a quite complex experimental set up. It should reflect the high Re and the high distortion of the flow around the cylinder, which is expected from numerical simulation. Also, the ratio of the cylinder span to the diameter should be correctly reproduced, as described by Tokumaru in his experimental set up and results [4].

NOMENCLATURE

C_p = Power coefficient of the rotor

C_{pMAX} = Max value of the power coefficient of the rotor

C_D = Drag coefficient of the cylinder (rotating foundation)

C_F = Skin friction coefficient of the cylinder (rotating foundation)

C_L = Lift coefficient of the cylinder (rotating foundation)

C_{LMAX} = Maximum value the lift coefficient of the cylinder (rotating foundation)

C_M = Friction moment coefficient of the cylinder (rotating foundation)

D = Diameter of the submerged foundation

L = length of the submerged foundation

M_F = Friction Moment

N = Number of blades

P = Power of the rotor

P_{MAX} = Max value of the power

R = Radius of the rotor

U = Water stream flow velocity

c = Chord length

p = Pressure

u, v, w = Components of the velocity U

wsp = Wind speed

α = speed ratio of peripheral speed and the stream speed

α_L = speed ratio limit

λ = Tip speed ratio

ν = Kinematic viscosity of the water

ρ = Density of the water

σ = Solidity of the rotor

ω = Rotational speed of the rotor

REFERENCES

1. Vita L., Paulsen U.S., Pedersen T.P., Madsen H.A., Rasmussen F., (2009). "A Novel Floating Offshore Wind Turbine Concept" EWEC2009, Marseille, France

2. “Pure Power-Wind Energy Scenarios up to 2030” (2008) European Wind Energy association
3. S. Krohn, P. Morthorst, S.Awerbuch (2009) “The Economics of Wind Energy” European Wind Energy Association
4. P.T. Tokumaru, P.E.Dimotakis (1993) “The lift of a cylinder executing rotary motions in an uniform flow” J. Fluid Mechanics, vol.255
5. J.C. Padrino, D.D. Joseph (2006) “ Numerical study of the steady-state uniform flow past a rotating cylinder“, J. Fluid Mechanics, vol. 557
6. M.B. Glauert (1957) “The flow past a rapidly rotating cylinder” Proceedings of the Royal Society of London, vol.242
7. S. Mittal, B. Kumar (2003) “Flow past a rotating cylinder”, J. Fluid Mechanics, vol.476
8. Y.T. Chew, M. Cheng, S.C. Luo (1995) “A numerical study of flow past a rotating circular cylinder using a hybrid vortex scheme”, J. Fluid Mechanics, vol. 299
9. C.C. Chang, R.L. Chern (1991) “Vortex shedding from an impulsively started rotating and translating circular cylinder”, J. Fluid Mechanics, vol.233
10. T. Theodorsen, A. Regier (1946) “Experiments on drag of revolving disks, cylinders and streamline rods at high speeds”
11. J.Wang, D.D. Joseph “Boundary layer analysis for effect of viscosity on the irrotational flow induced by a rapidly rotating cylinder in a uniform stream”, J. Fluid Mechanics, vol.557
12. I. Paravischivoiu (2002) “Wind Turbine Design, with emphasis on Darrieus concept”, Polytechinc International Pres
13. Michelsen JA (1992) “Basis3D - a Platform for Development of Multiblock PDE Solvers.”, Technical Report AFM 92-05, Technical University of Denmark
14. Michelsen JA (1994) “Block structured Multigrid solution of 2D and 3D elliptic PDE's.” Technical Report AFM 94-06, Technical University of Denmark
15. Sørensen NN (1995) “General Purpose Flow Solver Applied to Flow over Hills.” Risø-R-827-(EN), Risø National Laboratory, Roskilde, Denmark
16. L. Prandtl (1925) *Die Naturwissenschaften*, vol. 13, pp. 93-108. (English transl: Application of the “Magnus Effect” to the wind propulsion of ships. *NACA Tech. Mem.* 387, June 1926.)
17. Reid E.G. (1925) “Test of rotating cylinders”, NACA Tech. Note 209

Risø DTU is the National Laboratory for Sustainable Energy. Our research focuses on development of energy technologies and systems with minimal effect on climate, and contributes to innovation, education and policy. Risø has large experimental facilities and interdisciplinary research environments, and includes the national centre for nuclear technologies.

Risø DTU
National Laboratory for Sustainable Energy
Technical University of Denmark

Frederiksborgvej 399
PO Box 49
DK-4000 Roskilde
Denmark
Phone +45 4677 4677
Fax +45 4677 5688

www.risoe.dtu.dk